

**CARTILAGE TISSUE ENGINEERING WITH
HETEROGENEOUS AND CLONAL MESENCHYMAL
STEM CELL POPULATIONS: MULTI-SCALE ANALYSIS
OF MATURATION, STABILITY, AND RESPONSE TO
ENVIRONMENTAL STRESSORS**

Megan J. Farrell

A DISSERTATION in Bioengineering

Presented to the Faculties of the University of Pennsylvania in Partial Fulfillment of the Requirements for the Degree of Doctor of Philosophy, 2013

Supervisor of Dissertation

Robert L. Mauck
Associate Professor of Orthopaedic Surgery and Bioengineering
University of Pennsylvania

Graduate Group Chairperson

Jason A. Burdick
Professor of Bioengineering
University of Pennsylvania

Dissertation Committee

Jason A. Burdick, Professor of Bioengineering, University of Pennsylvania

Kurt D. Hankenson, Associate Professor of Musculoskeletal Research and Orthopaedic Surgery, University of Pennsylvania

Arjun Raj, Assistant Professor of Bioengineering, University of Pennsylvania

CARTILAGE TISSUE ENGINEERING WITH HETEROGENEOUS AND CLONAL
MESENCHYMAL STEM CELL POPULATIONS: MULTI-SCALE ANALYSIS OF
MATURATION, STABILITY, AND RESPONSE TO ENVIRONMENTAL
STRESSORS

COPYRIGHT

2013

Megan Jean Farrell

ACKNOWLEDGEMENTS

I must first acknowledge and thank Dr. Robert Mauck. As a dissertation advisor, Rob has an uncanny ability to adjust his degree of management to best suit the personality and professional development of his students. As a scientist, he bears a higher level of understanding, an impeccable memory, and a never faltering ambition; yet he remains personable, and therefore able to engage and excite others in his scientific endeavors. It was not until writing this dissertation that I became aware of how his assignments, although at times seeming menial or fruitless, led to incremental steps of personal and scientific growth. I thank him for his foresight, his mentorship, and the chance he took by providing me with this opportunity.

I would also like to thank my committee members, Drs. Burdick, Hankenson, and Raj. Their guidance and scientific expertise were instrumental in developing many of the protocols used throughout this dissertation. Furthermore, their capacity to casually converse about brilliant science is unparalleled.

Next, I must thank members of the Raj lab, particularly Margaret Dunagin and Patrick McClanahan, for the design of the cow FISH probes and the countless hours of imaging and spot counting.

I would like to thank the staff, students, and faculty of the biology and bioengineering labs in the McKay Orthopaedic Laboratories, as well as members of the Elliott Lab, for their assistance, guidance, and friendship throughout the years.

The hypoxia studies would not have been possible without the assistance of the Smith Lab, including Dr. Lachlan Smith, Debora Gorth, and Joseph Chiaro, with additional thanks to Joe for his continued work on the RAR studies.

I would like to acknowledge all of my colleagues in the Mauck Lab, both past and present, in addition to Smith Lab members, for contributing greatly to my science and my sanity these past few years. A special thanks to my co-authors and members of the CarTE group, Minwook Kim and Drs. Alice Huang, Isaac Erickson, and Matthew Fisher, whose science, collectively, created the framework from which this dissertation was developed. I would further like to thank Alice for her patience when I started in lab and her continued mentorship, and Matt for being an ideal officemate in addition to answering numerous questions daily.

I would like to thank the following undergraduate students and volunteers who have contributed greatly to MATLAB programming, data acquisition, and data analysis throughout the years: Jeffrey Perreira, Eric Comeau, Chieh Hou, Kimberly Farrell, and John Shin.

Finally, I must thank and acknowledge my family for their continued support. My sisters and best friends, Jessica, Christina, and Kimberly. Whenever things get difficult, they are always there to pick me up. My parents, Brenda and Joe, who have made many sacrifices to provide me with the means to take advantage of any opportunity I come across,

therefore allowing me to make the decisions that guide my life. One last thank you must go to my Uncle Bob. My uncle contributed greatly to my education throughout my life and introduced me to biomedical engineering while looking for undergraduate programs. It was through the loss of my uncle that I realized illness is indiscriminate, inflicting even the most brilliant individuals, and we must therefore use the short time we have to positively impact those around us.

ABSTRACT

CARTILAGE TISSUE ENGINEERING WITH HETEROGENEOUS AND CLONAL MESENCHYMAL STEM CELL POPULATIONS: MULTI-SCALE ANALYSIS OF MATURATION, STABILITY, AND RESPONSE TO ENVIRONMENTAL STRESSORS

Megan J. Farrell

Robert L. Mauck

Osteoarthritis is a disease of high incidence with significant clinical impact. Unfortunately, joint arthroplasty remains the gold standard treatment as there has been limited success in long term cartilage repair with biological treatments. While advances have been made in cartilage tissue engineering, resulting in the *in vitro* development of a mechanically viable tissue, much of this progress has been restricted to chondrocyte-based engineered tissues, and these cells are limited in their availability. Mesenchymal stem cells are one possible alternative cell source for cartilage repair strategies; however, they have yet to produce a mechanically stable tissue comparable to chondrocytes cultured identically. Thus, the objective of this dissertation was to use a multi-scale approach to better characterize, between these two cell types, where differences in matrix production and construct mechanics arise, the time scales during which chondrocytes and MSCs diverge in their production of a mechanically stable tissue, and the environmental factors that may be impacting MSC health. Furthermore, we assessed if there are clonal subpopulations with a greater propensity for chondrogenic differentiation. Through assessment of regional mechanical properties of cell-laden constructs, we found that MSCs are in fact capable of producing mechanically functional matrix equivalent to that

produced by chondrocytes. However, due to nutritional stress, the health and viability of these cells is severely impacted in regions of constructs that are nutrient deprived. By modulating nutrient (glucose) and metabolic (oxygen) concentrations in the growth media, we found that glucose concentration had a greater impact on cell health than low oxygen tension. However, with increased culture time, regardless of nutrient provision, MSC-based constructs underwent mechanical failure (with loss of GAG content) , suggesting innate instability of this stem cell population. Probing subpopulations of heterogeneous MSC isolates for chondrogenic potential revealed that both inter- and intra- colony heterogeneity exists, with a small fraction of colony subpopulations showing greater chondrogenic potential. Collectively, this work highlights potential pitfalls that are encountered when developing a stem cell based cartilage *in vitro*, which may further be exacerbated *in vivo*, but also provides future directions that may result in a clinically successful stem cell based cartilage replacement.

TABLE OF CONTENTS

ACKNOWLEDGEMENTS	iii
ABSTRACT.....	vi
LIST OF TABLES	xiii
LIST OF FIGURES	xiv
CHAPTER 1: INTRODUCTION.....	1
CHAPTER 2: BACKGROUND	7
2.1 Cartilage and the Knee.....	7
2.1.1 Cartilage.....	7
2.1.2 The Knee	8
2.1.3 Articular Cartilage Structure.....	9
2.1.4 Synovial Fluid and Articular Cartilage Nutrition	12
2.1.5 Articular Cartilage Function	13
2.2 Osteoarthritis and Clinical Repair Strategies	15
2.2.1 Osteoarthritis.....	15
2.2.2 Clinical Repair of Cartilage	16
2.3 Cartilage Tissue Engineering.....	20
2.3.1 Cells	21
2.3.2 Growth Factors.....	22
2.3.3 Materials	23
2.3.4 Chondrocyte and Stem Cell Cartilage Tissue Engineering – Current Successes and Limitations	26
2.4 The Origin of Chondrocytes and MSCs – Implications in Stem Cell Stability and Heterogeneity	30
2.4.1 Chondrogenesis and Chondrocytes.....	30
2.4.2 Mesenchymal Stem Cells and Heterogeneity	32
2.5 Summary.....	35
CHAPTER 3: MESENCHYMAL STEM CELLS PRODUCE FUNCTIONAL CARTILAGE MATRIX IN THREE-DIMENSIONAL CULTURE IN REGIONS OF OPTIMAL NUTRIENT SUPPLY	36

3.1	Introduction.....	36
3.2	Materials and Methods.....	38
3.2.1	Cell Isolation and 3D Encapsulation.....	38
3.2.2	Hydrogel Construct Culture.....	39
3.2.3	Mechanical Analysis of Bulk Properties.....	40
3.2.4	Mechanical Analysis of Local Properties.....	41
3.2.5	Histological Analysis.....	42
3.2.6	Biochemical Analysis.....	42
3.2.7	Quantification of Viability.....	43
3.2.8	Statistical Analysis.....	43
3.3	Results.....	44
3.3.1	Bulk Mechanical Properties Depend on Culture Conditions.....	44
3.3.2	Depth-Dependent Local Mechanical Properties.....	45
3.3.3	Regional Matrix Distribution And Content.....	50
3.3.4	Overall and Regional Chondrocyte and MSC Viability.....	56
3.4	Discussion.....	59
CHAPTER 4: FUNCTIONAL PROPERTIES OF MSC-BASED ENGINEERED		
CARTILAGE ARE UNSTABLE WITH VERY LONG TERM IN VITRO		
CULTURE.....		
4.1	Introduction.....	67
4.2	Materials and Methods.....	69
4.2.1	Study 1: Long-Term Culture of Cell-Seeded Agarose Hydrogels.....	69
4.2.2	Study 1: Mechanical Analysis of Bulk Properties.....	70
4.2.3	Study 1: Histological Analysis.....	71
4.2.4	Study 1: Biochemical Analysis.....	72
4.2.5	Study 1: Quantification of Viability.....	72
4.2.6	Study 2: Long-Term Culture of Cell-Seeded Hyaluronic Acid Hydrogels: Hyaluronic Acid Hydrogel Formation and Cell Encapsulation.....	73
4.2.7	Study 2: Mechanical, Biochemical, and Histological Analyses.....	73
4.2.8	Statistical Analysis.....	73
4.3	Results.....	74

4.3.1 Study 1: Long-Term Agarose Biomechanical and Biochemical Analyses.....	74
4.3.2 Study 1: Histology and Immunohistochemistry	78
4.3.3 Study 1: Cell Viability	81
4.3.4 Study 2: Long-Term Culture of MSC-Seeded Hyaluronic Acid Hydrogels: Biomechanical, Biochemical, and Histological Analyses	84
4.4 Discussion.....	85
CHAPTER 5: FUNCTIONAL CONSEQUENCES OF GLUCOSE AND OXYGEN DEPRIVATION ON ENGINEERED MESENCHYMAL STEM CELL-BASED CARTILAGE CONSTRUCTS	91
5.1 Introduction.....	91
5.2 Materials and Methods.....	93
5.2.1 MSC Isolation and Hydrogel Culture	93
5.2.2 Quantification of Cell Viability	95
5.2.3 Construct Mechanical Properties and Biochemical Content.....	95
5.2.4 Histology and Immunohistochemistry	96
5.2.5 Statistics	97
5.3 Results	97
5.3.1 Impact of Oxygen and Glucose on Construct Mechanics and Matrix Content	97
5.3.2 Matrix Distribution and Cell Viability in Thick Constructs	100
5.3.3 Evaluation of Viability and Glucose Utilization in Thin Constructs	101
5.4 Discussion.....	105
CHAPTER 6: VARIATION IN FUNCTIONAL CHONDROGENESIS AND RESPONSE TO ENVIRONMENTAL STRESSORS IN CLONAL MESENCHYMAL STEM CELL POPULATIONS	109
6.1 Introduction.....	109
6.2 Materials and Methods.....	111
6.2.1 Micromechanics	111
6.2.1.1 Study 1: Agarose Culture of Chondrocytes and MSCs	111
6.2.1.2 Study 2: Agarose Culture of Mixed Parent and Clonal MSC Populations.....	112

6.2.1.3 Study 3: HA Culture of Mixed Parent and Clonal MSC Populations – 2 and 3-Dimensional	114
6.2.1.4 Micromechanical Testing.....	114
6.2.1.5 Histological Assessment of Pericellular Matrix Accumulation.....	117
6.2.1.6 Statistics	117
6.2.2 Analysis of Single Cell Gene Expression - Fluorescence In-Situ Hybridization (FISH)	117
6.2.3 Pellet Culture, Viability, and Biochemical Analysis of Clonal MSC Subpopulations.....	119
6.3 Results	120
6.3.1 Micromechanics	120
6.3.1.1 Study 1: CH vs. MSC – 2-Dimensional.....	122
6.3.1.2 Study 2: Agarose – MSC Mixed Parent Populations vs. Colony Subpopulations – 2-Dimensional.....	124
6.3.1.3 Study 3: HA – MSC Mixed Parent Populations vs. Colony Subpopulations – 2 and 3-Dimensional	126
6.3.2 Single Cell Gene Expression in Clonal Colonies.....	130
6.3.3 Clone Dependent Response to Stressors.....	134
6.4 Discussion.....	136
CHAPTER 7: TUNABLE AND DEPTH-DEPENDENT MECHANICS OF AGAROSE/POLY(ETHYLENE GLYCOL) DIACRYLATE INTERPENETRATING NETWORKS	143
7.1 Introduction.....	143
7.2 Materials and Methods.....	145
7.2.1 PEG-DA Hydrogel Fabrication.....	145
7.2.2 Agarose Hydrogel Fabrication.....	146
7.2.3 Agarose/PEG-DA Interpenetrating Network Fabrication.....	146
7.2.4 Bulk Mechanical Testing	147
7.2.5 Local Mechanical Testing.....	147
7.2.6 Statistics	148
7.2.7 Cell Viability.....	148

7.3 Results	148
7.3.1 IPN Formation in the Presence and Absence of Nitrogen	148
7.3.2 Bulk and Local Mechanical Properties	149
7.3.3 Cell Viability.....	153
7.4 Discussion.....	153
CHAPTER 8: RAR INVERSE ACTIVATION FOR STEM CELL BASED CARTILAGE ENGINEERING	155
8.1 Introduction.....	155
8.2 Materials and Methods.....	157
8.2.1 Pellet Culture	157
8.2.2 Hydrogel Culture	157
8.2.3 Statistics	158
8.3 Results	158
8.3.1 Pellets.....	158
8.3.2 Hydrogels.....	159
8.4 Discussion.....	161
CHAPTER 9: SUMMARY AND FUTURE DIRECTIONS.....	163
9.1 Summary.....	163
9.2 Limitations.....	169
9.2.1 Bovine vs. Human Cell Populations	169
9.2.2 Micromechanical Assessments of Matrix Properties.....	169
9.2.3 Stem Cell Stability and Hypertrophy	170
9.3 Conclusions.....	170
APPENDIX 1: CELL VIABILITY QUANTIFICATION MATLAB CODE	172
APPENDIX 2: STRESS RELAXATION CURVE FIT MATLAB CODE	176
APPENDIX 3: 2-DIMENSIONAL CELL DEFORMATION ANALYSIS MATLAB CODE.....	183
APPENDIX 4: 3-DIMENSIONAL CELL DEFORMATION ANALYSIS MATLAB CODE.....	190
BIBLIOGRAPHY	202

LIST OF TABLES

<i>Table 3-1: Statistical comparison of local strain.</i>	47
<i>Table 5-1: Culture conditions and abbreviations.</i>	95
<i>Table 6-1: Descriptive statistics of mRNA counts in populations shown in Figure 6-12.</i>	131
<i>Table 6-2: Descriptive statistics of mRNA counts in populations shown in Figure 6-13.</i>	132

LIST OF FIGURES

<i>Figure 2-1: Schematic of basic knee anatomy, adapted with permission from (Makris et al., 2011).</i>	9
<i>Figure 2-2: Depth-dependent histological staining of adult bovine cartilage from the femoral condyle. Alcian Blue (proteoglycans, left), Picrosirius Red (collagens, center), and Alizarin Red (calcium deposits, right).</i>	10
<i>Figure 2-3: Cartilage organization as a function of depth. Left) Polarized light imaging of adult bovine cartilage from the femoral condyle. Right) Alignment map generated from quantitative polarized light microscopy analysis (extinction angles with 5° rotation increments of polarizer) as in (Thomopoulos et al., 2003).</i>	11
<i>Figure 2-4: Clinical signs and current treatments of osteoarthritis. A) Radiograph showing joint space narrowing of an osteoarthritic knee. B) Gross appearance of osteoarthritic cartilage. C) Radiograph of total knee arthroplasty. D) Radiograph of partial knee arthroplasty. Images adapted from (Carr et al., 2012) with permission.</i>	17
<i>Figure 2-5: (Left) Mosaicplasty of the medial femoral chondyl. (Right) Donor site. Adapted from (Hangody et al., 2008) with permission.</i>	18
<i>Figure 2-6: Toluidine blue staining of repair tissue from from ACI, microfracture, and periosteal transplant shows decrease in staining intensity and increased levels of fibrous tissue in repair techniques compared to cartilage control. Adapted from (LaPrade et al., 2008) with permission.</i>	20
<i>Figure 2-7: A) Anatomically correct porous osteo- and chondro-inductive implant fabricated via computer aided design and bioprinting. B) Nanofibrous hollow microspheres that support the chondrogenic phenotype and foster tissue repair in vivo. Images adapted from (Lee et al., 2010) and (Liu et al., 2011) with permission.</i>	25
<i>Figure 2-8: Events of chondrogenesis during bone development. Adapted from (Goldring et al., 2006) with permission.</i>	31

Figure 3-1: Study design schematic. (A) Construct orientation (4 mm diameter, 2.25 mm thick) was maintained throughout the culture period. Construct tops (Region 1) were stained after removal from the tissue culture well plate to maintain orientation through mechanical testing. (B) Following bulk testing, constructs were cored and halved through the transverse plane for biochemical assessment. (C) Prior to local mechanical property assessment, constructs were halved through the median plane. Half of the construct was stained and tested in a custom microscope-based uniaxial compression device. The remaining half was preserved for histology or regional viability assessment.....40

*Figure 3-2: Gross appearance and bulk assessment of unconfined compressive properties of constructs cultured in free swelling (FS) or orbital shaking (Dyn) conditions, with (+) or without (-) TGF- β 3. (A) Gross appearance of chondrocyte-laden (top) and MSC-laden (bottom) constructs on Day 63. (B) Bulk construct equilibrium modulus was evaluated through Day 63. Dotted lines denote Day 1 equilibrium modulus values. (# vs. all lower within culture condition and cell type; ** vs. FS(+TGF β -3) within day and cell type; ∇ vs. CH cultured identically, $p < 0.05$). $n = 3$ 45*

Figure 3-3: Assessment of local compressive strain and equilibrium modulus. (A) Schematic of microscopic strain application and region of analysis with overlay of Vic2D Exx strain contour plot. (B) Compressive Lagrangian strain (Exx) through the depth of constructs as a function of time, cell type, and culture condition. Unique strain plot profiles developed as early as Day 21 and persisted through Day 63. (C) Day 63 local equilibrium modulus profiles as a function of cell type and culture condition. Dynamic culture reduced depth dependency in chondrocyte-laden constructs, but not for MSC-laden constructs, especially in the central regions. (cross vs. Region 2; L vs. Region 9, $p < 0.05$). $n = 5$49

Figure 3-4: Scale adjustment for local equilibrium modulus in Regions 5 and 6 (Figure 3-3). (red circle vs. all lower within region and cell type; blue circle vs. MSCs cultured identically, $p < 0.05$).....50

Figure 3-5: (Top) Day 63 Alcian Blue staining of proteoglycans (PGs) as a function of cell type and culture condition. Dotted rectangle indicates area of intensity plot profiles. Scale bar = 500 μ m. (Bottom) Stain intensity profiles of free swelling and dynamically cultured constructs in the presence of TGF- β 3. PG staining intensity mirrors local equilibrium modulus profiles with the exception of chondrocyte-laden FS(+TGF- β 3) constructs.52

Figure 3-6: (Top) Day 63 Picrosirius Red staining of collagen as a function of cell type and culture condition. Dotted rectangle indicates area of intensity plot profiles. Scale bar = 500 μ m. (Bottom) Stain intensity profiles of free swelling and dynamically cultured constructs in the presence of TGF- β 3.53

*Figure 3-7: Glycosaminoglycan (GAG) content (normalized by wet weight) as a function of region, time, cell type, and culture condition. Chondrocyte-laden constructs had a relatively homogenous GAG distribution. GAG content of MSC-laden constructs was highly dependent on region; GAG content regionality was relieved with dynamic culture. (# vs. top of the same group; * vs. annulus of the same group; \boxtimes vs. chondrocyte of the same region cultured identically, $p < 0.05$). $n = 3$ 55*

Figure 3-8: Collagen quantification (normalized to wet weight) in Day 63 constructs indicated low levels of collagen regardless of cell type, culture condition, and region. $n = 3$56

Figure 3-9: Assessment of cell viability. (A) Central images of bisected constructs of both viable (green, left column) and dead (red, right column) cells. Scale bar = 100 μ m. (B) Quantification of aggregate viability (from all five regions) as a function of time showed that chondrocyte viability remained relatively stable, while MSC viability declined significantly from Day 1 values. Dotted line denotes mean Day 1 viability. (# vs. FS(-TGF- β 3); \boxtimes vs. FS(+TGF- β 3), $p < 0.05$). (C) Analysis of viability through the depth of the constructs on Day 63 revealed a significantly lower percentage of viable cells in the center and bottom regions of MSC FS(+TGF- β 3) constructs compared to the top region. (vs. Top, $p < 0.05$). $n = 3$ 58*

Figure 3-10: TUNEL staining (green) in Day 21 MSC-laden free swelling constructs (central region of the construct) suggests an increase in the number of apoptotic cells at this early time point. DAPI counterstain (blue). Scale = 100 μ m.....59

Figure 4-1: Mechanical properties of chondrocyte (CH) and mesenchymal stem cell (MSC)-laden agarose hydrogels cultured under free swelling (FS) or dynamic (Dyn) conditions in the absence or presence of TGF- β (-/+). (A) Equilibrium modulus through 112 days (D112) demonstrating a progressive increase and/or stability in properties in CH-laden constructs, and an overall lower and unstable mechanical growth trajectory for MSC-laden constructs in CM(+) conditions. (B) Dynamic modulus of constructs showing a similar growth trajectory (with a particular instability in this measure for MSC-laden Dyn(+) constructs). Significance established with $p < 0.05$. () vs. previous time point of same group; (#) Dyn(-) vs. FS(-) or Dyn(+) vs. FS(+) within cell type and time point. (Ø) FS(-) vs. FS(+) and Dyn(-) vs. Dyn(+) within cell type and time point.76*

Figure 4-2: Biochemical content of CH and MSC-laden agarose constructs on Day 56 (D56) and Day 112 (D112). (A) Glycosaminoglycan (GAG) content from D56 to D112 differs with cell type and culture condition, with increases in GAG content apparent in CH-based constructs and loss of GAG content in MSC-based constructs. (B) Collagen content per construct similarly differs with cell type and culture condition. Significance established with $p < 0.05$. () vs. previous time point of same group; (#) Dyn(-) vs. FS(-) or Dyn(+) vs. FS(+) within cell type and time point. (Ø) FS(-) vs. FS(+) and Dyn(-) vs. Dyn(+) within cell type and time point.77*

Figure 4-3: Histological analysis reveals differences in matrix formation and retention between groups on D56 and D112. (A) Alcian Blue staining showing differences in proteoglycan accumulation and distribution; most notably a lighter, more diffuse staining in MSC FS(+) and Dyn(+) groups in D112 compared to D56 constructs. Scale = 1mm. (B) No marked differences in collagen staining are apparent via Picrosirius Red staining. Scale = 1mm78

Figure 4-4: Immunohistochemical analysis on D56 and D112. (A) CH-laden hydrogels stain intensely for type II collagen, with little or no staining of type I collagen, indicative of a stable chondrogenic phenotype. Scale = 1mm. (B) Although MSC-laden hydrogels stain less intensely for type II than their CH counterparts, staining is relatively stable from D56 and D112. Positive type I collagen staining is apparent only in MSC FS(-) and Dyn(-) conditions, and increases from D56 to D112. Scale = 1 mm80

Figure 4-5: (A) Higher magnification of type I collagen staining illustrates pockets of intense deposition in MSC FS(-) conditions at D112. Scale = 200 μ m. (B) Positive Alizarin Red staining for MSC FS(-) and Dyn(-) conditions at D112 indicates that these constructs are heavily calcified, despite the absence of specific pro-hypertrophic signals. Scale = 1mm81

Figure 4-6: Short and long-term viability in CH and MSC-laden constructs. (A) Marked differences in viability between groups are observed as early as D28. MSC-based cultures continue to decline through D112. Nuclei of dead cells are labeled in red, cytoplasm of live cells are labeled in green. Scale = 100 μ m. (B) Quantification of percent viability in the center of constructs shows a marked decline in MSC viability at early time points, reaching an extremely low level by D112, compared with much smaller changes in CH-based construct viability over the same time course. Significance established with $p < 0.05$. Markers indicating significance included in box above plots. (Line) vs. Day 1 with line style and color corresponding to respective group. (Circle and square) vs. previous time point with marker style and color corresponding to respective group.....83

Figure 4-7: Mechanical, biochemical, and histological assessment of MSCs cultured in a hyaluronic acid (HA) hydrogel over long-term in vitro culture. (A) Equilibrium modulus and (B) dynamic modulus show instability in construct properties similar to that of agarose constructs, with marked declines occurring by D126. (C) Glycosaminoglycan (GAG) content per construct declines similarly while (D) collagen per construct is stable. Significance established with $p < 0.05$. (*) vs. previous time point. Histological staining

of (E) proteoglycans (Alcian Blue) and (F) collagens (Picrosirius Red) confirm biochemical assays. Scale = 200 μm85

Figure 5-1: Schematic illustration of culture conditions and their combinations. Gray boxes indicate control conditions.94

Figure 5-2: Biomechanical and biochemical findings illustrate that low glucose conditions have a greater impact than low oxygen on limiting functional maturation. Biomechanical properties: (A) equilibrium modulus and (B) dynamic modulus. Biochemical constituents: (C) DNA content, (D) glycosaminoglycan content, and (E) collagen content all reported as a percent wet weight (% ww). * indicates significant difference of Norm vs. Hyp ($p < 0.05$) in same TGF and glucose condition. # indicates significant difference of LG vs. HG ($p < 0.05$) in same TGF and oxygen condition. \emptyset indicates significant difference of (-) vs. (+) ($p < 0.05$) in same glucose and oxygen condition.99

Figure 5-3: Matrix distribution in engineered constructs as a function of low-glucose and hypoxic culture conditions. (A) Immunohistochemical staining for type II collagen reveals punctuate homogeneous staining in both LG and HG CM(-) conditions, with relatively homogenous staining in HG(+) conditions. Regional differences are marked with transition to LG+ conditions, where matrix deposition is limited to the construct boundary. No obvious differences were noted between Norm and Hyp conditions. (B) Alcian Blue staining showed similar proteoglycan deposition, with the exception of slightly lighter staining apparent in Hyp HG+ conditions compared to Norm HG+. Scale = 500 μm 101

Figure 5-4: Distribution of viability in engineered constructs as a function of low-glucose and hypoxic culture conditions. (A) Live/dead staining of thick constructs (mid-plane, B) shows viable cells restricted to the periphery in LG+ conditions, with few differences between Hyp and Norm conditions. Scale = 500 μm . (B, bottom, and C) Example image of thin Norm LG+ construct showing marked differences in viability on the top and bottom of the same construct. (D) Percent viability calculated from the top and bottom of thin constructs (where maximum viability occurs at the top of the construct

with maximal nutrient exchange). Normoxic, high glucose conditions maintain a high level of viability, while low glucose conditions promote loss of viability, especially in the context of TGF- β and hypoxia. # indicates significant difference from Norm HG+ ($p < 0.05$) on Day 28.103

Figure 5-5: Glucose concentration in media as a function of low-glucose and hypoxic culture conditions. (A) Measured media glucose levels 3 days after feeding. The initial high glucose media concentration was ~25 mM whereas the initial low glucose media concentration was ~5 mM. (B) Media glucose values for the LG groups only (note change in scale). # indicates significant difference for CM⁻ vs. CM⁺ of same oxygen level and starting glucose concentration on Day 28 ($p < 0.05$).104

Figure 6-1: Gross assessment of colony heterogeneity. (A) Crystal violet staining of an MSC marrow isolate after 14 days in culture showing colonies of varying sizes and densities. Scale = 10 mm. (B) Phase contrast images of cell colonies after 11 days of culture show varying cell densities and cell morphologies. Scale = 500 μ m110

Figure 6-2: Isolation of colonies. (A) Edge of colony outlined under 4X magnification. Cell colony is apparent on the right side of marker line with relatively few cells located on the left side of the line. Scale = 500 μ m. (B) Image of plate with trypsin droplets over identified colonies. Representative of typical spacing between colonies.113

Figure 6-3: Micromechanical testing apparatus and protocol. (A) Custom device equipped with linear stage, micrometer, and load cell for uniaxial compression testing during confocal imaging. (B) Underside of device showing capacity for imaging via inverted microscope through a coverglass bottomed PBS bath. (C) Schematic showing geometry of halved constructs and direction of uniaxial compression. (D) Representative three-dimensional reconstruction of MSCs (green) compressed to 40% grip-to-grip applied strain on Day 1. (E) Two-dimensional image slice of MSC-laden (MSC=green) construct, under 40% axial strain, stained for matrix components (unfixed; anti-chondroitin sulfate; red), demonstrates compression of both dense pericellular matrix (negative space) and cell. Scale = 50 μ m116

Figure 6-4: Identification of single mRNA molecules (small dots) labeled with a series of oligonucleotide sequences for three distinct genes (COMP=Pink; Aggrecan=Yellow; GAPDH=Cyan) using fluorescence in-situ hybridization.119

Figure 6-5: FE analysis of a deformable spherical inclusion within a deformable cylindrical construct subjected to axial compression (purple arrow). By varying the modulus of the spherical inclusion, compression applied to the cylindrical construct (which has a constant modulus) results in differing (A) levels of deformation of the inclusion (aspect ratio; AR) and (B) strain fields in and around the inclusion, depending on the properties of the inclusion. (C) Schematic representation of expected results of cell deformation for a heterogeneous population that has deposited matrix of varying stiffness.....121

Figure 6-6: Two-dimensional assessment of bounding box ratio in 2% agarose at 0% and 30% applied strain for donor matched chondrocytes (CH) and mesenchymal stem cells (MSCs) after 1 day of culture in CM⁻ or 8 days of culture in CM⁺. (A) Average of image mean bounding box aspect ratio (Y/X) from a 2D z-projection of a single construct (n=3 constructs). \$ indicates significance at p<0.05, ¢ indicates trend at p<0.10 for MSC vs. donor matched CH at same day and same applied strain. Solid line indicates significance within group; dotted line indicates trend. (B) Percent increase in mean bounding box aspect ratio from 0% to 30% strain of 3 images from each donor (gray) with average of n=3 images from each donor indicated with blue dot. (C) Standard deviation of bounding box aspect ratio calculated from each image processed (n=3 images from each donor). * indicates significance at p<0.05 MSC vs. donor matched CH. (D) Alcian Blue staining of proteoglycans in the pericellular regions of Donor 3 constructs, showing more consistent matrix formation around chondrocytes. Scale = 100 µm.....123

Figure 6-7: Conservation of cell area in the X-Y direction of 2D projected stacks with the application of 30% strain (A) and changes in area for MSCs with time in culture (B). * indicates significance for MSC vs. donor matched CH (p<0.05). # indicates significance for MSC Day 1 vs. Day 8 (p<0.05).....124

Figure 6-8: Two-dimensional assessment of bounding box ratio in 2% agarose at 0% and 30% applied strain for donor matched MSC parent population (Het1) and MSC colony subpopulations (C1-C11) and an additional non-donor matched parent population (Het2) after 1 day of culture in CM⁻ or 8 days of culture in CM⁺. (A) Average of mean bounding box aspect ratio (Y/X) from a 2D z-projection of a single construct (n=3 constructs). (B) Difference in bounding box aspect ratio at 30% applied strain from Day 8 to Day 1, with the more negative number indicating less deformation on Day 8. Significance was calculated from comparisons of Day 1 vs. Day 8 (see A for raw values and error bars) with \$ indicating significance at p<0.05 and ¢ indicating trend at p<0.10. (C) Alcian Blue staining of proteoglycans in pericellular region of select groups. Scale = 100 µm.....125

Figure 6-9: Two-dimensional assessment of bounding box ratio in 1% HA at 0% and 40% applied strain for a donor matched MSC parent population (Het1) and MSC colony subpopulations (C1-C8) after 1 day of culture in CM⁻ or 7 days of culture in CM⁺. (A) Average of mean bounding box aspect ratio (Y/X) from a 2D z-projection of a single construct (n=3 constructs). (B) Difference in bounding box aspect ratio at 40% applied strain from Day 7 to Day 1 with a more negative number indicating less deformation at Day 7. Significance was calculated from comparison of Day 1 vs. Day 7 (see A for raw values and error bars) with \$ indicating significance at p<0.05 and ¢ indicating trend at p<0.10. (C) Standard deviation of bounding box aspect ratio calculated from each image processed (n=3 images from each donor).127

Figure 6-10: Quantification of cell area illustrates conservation of area in the X-Y direction of 2D projected stacks with the application of 40% strain (A) and moderate changes in area for some colony subpopulations with time (B). \$ indicates significance Day 1 vs. Day 7 (p<0.05.....128

Figure 6-11: (A) Three-dimensional assessment of cell deformation in 1% HA at 0% and 40% applied strain for donor matched MSC parent population (Het1) and MSC colony subpopulations (C1-C8) after 1 day of culture in CM⁻ or 7 days of culture in CM⁺. Significance of D1 40% vs. D7 40% indicated with \$ (p<0.05) with trend indicated with ¢

($p < 0.10$). (B) Ratio of z-bounding box length (object length through the depth in the z-stack) at 40% deformation to 0% deformation shows no overall trend of z-elongation with compression (ratio > 1 with 1 indicated by red line). ϕ indicates trend z-length at 0% strain vs. z-length at 40% strain with $p < 0.10$. (C) 3D quantification of cell volume follows 2D quantification of cell area, with overall conservation of volume with compression. ϕ indicates trend at 0% strain vs 40% strain with $p < 0.10$129

Figure 6-12: Single cell RNA quantification. (A) Boxplots of single cell mRNA counts of cartilage oligomeric matrix protein (COMP) and aggrecan (AGG) showing median, quartiles, and outliers (asterisks) for a heterogeneous MSC population and colony derived subpopulations from the same donor. Blue dot indicates mean mRNA count within the population. Cells were cultured in monolayer in chemically defined media without TGF- β (CM-) or chemically defined media with TGF- β (CM+) for 7 days. (B) Fold increase of mean mRNA values (CM+/CM-) for each population.131

Figure 6-13: Repeated study of single cell RNA quantification shown in Figure 6-12 with different mixed parent and clonal populations. (A) Boxplots. Blue dot indicates mean mRNA count within the population. Cells were cultured in monolayer in basal media (BM), chemically defined media without TGF- β (CM-), or chemically defined media with TGF- β (CM+) for 7 days. (B) Fold increase of mean mRNA values (CM+/CM-) for each population.....132

Figure 6-14: Heat maps of single cell mRNA counts in an un-passaged MSC bone marrow colony in monolayer culture (11 days in basal media followed by CM+ for 4 days). Phase contrast image (A), note slightly different image frame and scale. Variable induction is present in this single, unpassaged colony. Signal intensity for COMP (B) and Aggrecan (C), showing isolated regions of high expression (red), with a few (but not all) of these hot spots highlighted with arrows. Conversely, more consistent levels of GAPDH expression (D) are observed across the colony.....133

Figure 6-15: Impact of low glucose and hypoxic culture conditions on differentiation and viability of MSC clonal populations cultured as micro-pellets. (A) 3D reconstruction of partial pellet volume (Left) with visualization of cell nuclei (Right) identified as non-

viable by ethidium homodimer staining. (B and C) Quantification of cell death (Top), glycosaminoglycan content per pellet (Middle), and glycosaminoglycan content per DNA (Bottom) showing variable responses of clonal subpopulations (C1-C6 from Donor 1; C1-C9 from Donor 2) compared to the heterogeneous parent population (Het) after 14 days of culture. $n=1-3$ per clonal population. (D) Select z-projections of Live/Dead stacks from Donor 2. Scale = 200 μm 135

Figure 7-1: Aspect ratio quantification from a finite element model of spherical inclusions with varying moduli situated within cylindrical hydrogel constructs that also have varying moduli and are subjected to compression. These data demonstrate that one cannot discriminate between mechanical properties of spheres with high moduli (50 and 100 kPa) in hydrogels of a low modulus (1 kPa).....144

Figure 7-2: Schematic demonstrating the use of a secondary polymer network to increase the mechanical properties of the interstitial space after matrix has been deposited around cells.144

Figure 7-3: Schematic of IPN formation. Agarose constructs are soaked in a PEG-DA/photoinitiator solution for 24 hours, after which the secondary PEG-DA network is crosslinked with UV light.....147

Figure 7-4: (A) Gross appearance of Agarose/IPN construct balanced on its side. Polymerization without the nitrogen gas flooding resulted in localized IPN formation in the bottom center of the construct. (B) Rhodamine incorporation confirmed region dependent polymerization without the use of nitrogen gas flooding (top view of construct). (C) Demonstration of UV polymerization under nitrogen gas flooding. (D) Rhodamine incorporation showing a more uniform polymerization of the secondary PEG-DA network in the presence of nitrogen. (E) Construct bisection showing non-uniform pattern of rhodamine incorporation when gels were not flipped. (F) More uniform intensity patterns were achieved by flipping constructs midway through polymerization duration.....149

*Figure 7-5: Bulk modulus of PEG-DA and IPN gels (all flipped). 2.5% and 5% PEG-DA failed to produce gels that could be mechanically assessed. * indicates $p < 0.05$ for PEG vs. IPN and PEG & IPN vs. Ag, $n = 5/\text{group}$ 151*

*Figure 7-6: (A) Bulk modulus of gels tested via microscope testing device. * indicates $p < 0.05$ vs. 20% IPN. (B) Local strain (Left) per region and local modulus (Right) per region through the depth of agarose constructs and IPNs. Bar indicates significance ($p < 0.05$).152*

Figure 7-7: Dramatic loss of viability of cells cultured in basal media with PEG-DA for 3 hours compared to basal media alone.153

Figure 8-1: Dose response of MSC pellets with addition of RA, α , β , and γ antagonists, and IA relative to CM^- and CM^+ with controls (in red). Bar indicates significance vs. CM^- or CM^+ control ($p < 0.05$). (Inset) Staining of D21 pellets with 5 μM treatment. Scale = 100 μm 159

Figure 8-2: GAG content and equilibrium modulus of MSC-seeded hydrogels after 21 days of culture in CM^+ without or with IA exposure. Significance established at $p < 0.05$, star = GAG and eq. mod vs. CM^+ ; triangle = GAG only vs. CM^+ 160

Figure 8-3: Pericellular proteoglycan deposition increased in both CM^- and CM^+ conditions with IA supplementation. Scale = 100 μm 160

Figure 8-4: RT-PCR plate array findings depicting highest fold changes of $CM^+/2\mu\text{M}$ IA compared to CM^+ after 7 days of culture.161

CHAPTER 1: INTRODUCTION

Osteoarthritis affects upwards of 30 million adults in the United States. This progressive degeneration of articular cartilage results in extensive pain and disability that arise from direct bone on bone contact, osteophyte formation, and the activation of an inflammatory cascade, exciting nociceptors in the synovial capsule. As cartilage is avascular, the propensity for intrinsic healing is limited. Surgical repair strategies are therefore often necessary for the treatment of cartilage damage, ranging from small focal defects to chronic osteoarthritis of an entire joint. Although total joint arthroplasty remains the gold standard treatment for osteoarthritis, the biological repair of cartilage has been the focus of much basic science and clinical research over the past two decades.

Tissue engineering is a repair approach in which researchers combine cells, scaffolding materials, and soluble and/or mechanical cues to mimic various conditions cells experience in the native tissue microenvironment. Although the use of a native cell type would be most ideal for engineering a particular tissue, as it has been preconditioned through development and tissue maintenance, the use of chondrocytes, the native cell type in cartilage, has limitations. Namely, cartilage is a tissue of low cell density. To develop cartilaginous tissues with sufficient matrix and mechanical properties, many researchers rely on high cell density techniques. As such, cell expansion is required, resulting in dedifferentiation and altered activity of chondrocytes. Furthermore, osteoarthritis is generally a slowly progressing disease, characterized by aging cells that are exposed to both metabolic and inflammatory stressors over a long duration. Cell aging reduces the regenerative capacity of cells, while long periods of exposure to

inflammatory cytokines and challenging metabolic conditions can alter baseline cellular anabolic and catabolic activities. Finally, from a practical perspective, most patients with osteoarthritis progress to a point where very little cartilage remains before they see a physician, making it necessary to regenerate large joint surface areas. Taken together, the lack of sufficient availability of healthy, fully differentiated, autologous chondrocytes is a limitation in the clinical application of engineered cartilage based on native tissue cells.

Adult derived stem cells are a possible alternative source to fully differentiated cells in musculoskeletal tissue engineering applications. These cells can be isolated from a range of tissues including adipose tissue, synovium, or bone marrow and are able to readily proliferate in monolayer culture while maintaining their differentiation capacity. While only multipotent in their differentiation potential, they retain the propensity to differentiate into cells of musculoskeletal lineages, and are therefore a suitable and less controversial cell source than embryonic stem cells for many applications. For cartilage tissue engineering, the differentiation of adult derived stem cells is most often carried out in a three-dimensional culture system such as micromasses, pellets, or within hydrogels, and in the presence of soluble growth factors such as bone morphogenetic proteins or transforming growth factor proteins. However, chondrogenic differentiation of these stem cells often results in a phenotype that is distinct from that of a fully differentiated chondrocyte. These differences are most notable and clinically significant in the functionality and stability of the tissue engineered construct. For example, when cultured under identical conditions, chondrocytes produce tissue of increasing mechanical function with extended time in culture, whereas tissue produced by bone marrow derived

mesenchymal stem cells plateau at levels of markedly lower mechanical function. Furthermore, tissue developed by mesenchymal stem cells can progress to a hypertrophic state, becoming vascularized and mineralized when exposed to subcutaneous *in vivo* environments.

Given these current limitations in the application of MSCs for cartilage tissue engineering and regenerative medicine applications, the overall objectives of this work were to first use a multi-scale approach to determine where, when, and why differences arise in MSC-laden constructs compared to chondrocyte-laden constructs, and then to use this understanding to characterize the heterogeneity of these stem cell populations to determine if there are clonal subpopulations more conducive to robust and stable chondrogenic differentiation.

In Chapter 2, the pitfalls and limitations of current cartilage repair and tissue engineering strategies are discussed, thus defining the objectives of the work to follow. In doing so, the synovial joint, cartilage structure and function, and disease pathology are reviewed, providing the set of benchmark characteristics against which the repair tissue must compare. This review of the current literature highlights advances now occurring in cartilage tissue engineering, while bringing forth a discussion of issues that remain to be resolved, preventing these tissues from reaching clinical application. The chapter concludes with a deeper look into cartilage development, chondrocyte origin, and a perspective on the use of adult stem cells to improve outcomes.

In Chapter 3, the focus turns towards the determination of where stem cell based constructs fail to achieve mechanical success by conducting a multi-scale comparison of the performance of chondrocytes and mesenchymal stem cells in a standard three-dimensional agarose hydrogel culture system. Specifically, a texture correlation approach is used to compare local (microscale) construct mechanics to bulk (macroscale) mechanical properties derived from standard mechanical testing modalities. In addition to regional assessment of mechanics, a comprehensive assessment of regional matrix accumulation and cell viability and the impact of media agitation are explored. These studies begin to investigate how the fundamental differences in the performance of these cells arise on a matrix production basis.

Chapter 4 focuses on the long-term assessment of chondrocyte and MSC-laden construct maturation and stability and evaluates when differences in cell health and matrix production become apparent in these two cell populations. Time profiles of cell viability, construct mechanical properties, and matrix elaboration and stability illustrate when and in what manner the performance of these two cell types diverge.

Motivated by the knowledge gained in the previous chapters, the role of environmental stressors in MSC-laden construct maturation is carefully explored in Chapter 5. The functionality of constructs cultured in lower oxygen tension and glucose concentration is investigated. Furthermore, construct size is decreased in an attempt to limit diffusional constraints, and spent glucose concentration and cell viability are measured in environmentally stressed conditions.

By their very nature, bone marrow derived mesenchymal stem cell populations are heterogeneous, comprised of cells of varying characteristics including differentiation potential. As such, in Chapter 6, colony isolation techniques are employed to isolate subpopulations from a heterogeneous parent population. Here, the goal is to investigate the differential chondrogenic induction capacity of these colony subpopulations, and to determine whether clonal sub-populations are more homogenous than their heterogeneous parent populations. To enable these studies, a novel single cell gene expression technique, quantitative fluorescence in-situ hybridization, is employed. To investigate variation in the functional chondrogenic capacity of these subpopulations, histological and micromechanical techniques are used to determine if these subpopulations produce significantly different amounts of extracellular matrix and if the mechanical integrity of this extracellular matrix is colony dependent. Finally, colony dependent response to environmental stressors, assessed in bulk constructs in Chapter 5, is investigated in low glucose and low oxygen conditions.

In Chapter 7, studies providing the groundwork for future investigation into micromechanical heterogeneity at later time points are presented. The use of a secondary interpenetrating hydrogel network potentially provides increased mechanical properties following the deposition of pericellular matrix in an agarose hydrogel, allowing for the assessment of pericellular matrix of higher mechanical function than the surrounding hydrogel without disturbing growth conditions. Characterization of the synergistic response in both bulk and local mechanical properties of these gels are explored.

As all previous studies used TGF- β supplementation for chondrogenic induction, and therefore the results regarding cell health and stability may be dependent on targeting this specific pathway, Chapter 8 investigates the use of a synthetic inverse agonist of the retinoic acid receptor for the use in stem cell based cartilage tissue engineering applications. Chondrogenic induction capacity of this molecule is compared to that of agonists and antagonist of retinoic acid receptors in the absence and presence of TGF- β . Furthermore, its impact on the functional development of tissue engineered constructs is assessed. The chapter concludes with the possible targets and downstream effects of the retinoic acid receptor inverse agonist.

A summary of significant findings and their scientific and clinical impact is discussed in Chapter 9. Progress gained, as well as limitations and future directions necessary to achieve clinical realization of stem cell-based tissues, complete the discussion.

CHAPTER 2: BACKGROUND

2.1 Cartilage and the Knee

In the mature adult, cartilage is an avascular tissue with a slow rate of matrix turnover. As the tissue lacks the quality of intrinsic repair, unbalanced catabolic activity as well as mechanical insult or dysfunction results in severe tissue damage and loss of function. Before a discussion of disease pathology, clinical repair strategies, and functional cartilage tissue engineering can commence, it is necessary to develop a firm understanding of healthy cartilage composition, structure, and function as a means of establishing the metrics against which successful repair can be defined.

2.1.1 Cartilage

Cartilage is a collagenous, proteoglycan rich, and water saturated soft connective tissue. A single cell type, the chondrocyte, is responsible for cartilage tissue maintenance and homeostasis. The tissue is aneural and avascular in the adult (Hunter, 1743; Leidy, 1849; Toynebee, 1837) and relies on diffusion for nutrient and waste exchange (Brodin, 1955; Strangeways, 1920). Based on structure and function, cartilaginous tissues are categorized as elastic cartilage, fibrocartilage, or hyaline cartilage (Gray and Goss, 1973).

Elastic cartilage is a flexible cartilage with elastin as a main component of the extracellular matrix. In addition to auricular cartilage, elastic cartilage can be found in the Eustachian tube, the epiglottis, and portions of the larynx.

Fibrocartilages, in the broadest terms, contain both type I and type II collagen. Some fibrocartilages, such as the meniscus or annulus fibrosus of the intervertebral disc, have highly organized hierarchical designs that lend themselves to specific load transmission and load dispersion. However, when referring to cartilage repair, particularly as it relates to articular cartilage repair (hyaline cartilage), the term ‘fibrocartilage’ often refers to a fibrous, disorganized, scar tissue with inappropriate matrix constituents and inadequate mechanical properties.

Hyaline cartilage includes articular cartilage, costal cartilage, and cartilage found in the trachea and some portions of the larynx. It is the most common type of cartilage found within the body and is referenced as having a glistening white or bluish tint (Gray and Goss, 1973). Specifics of articular cartilage, the cartilage lining the joint surfaces of bones, will be the focus of sections to follow.

2.1.2 The Knee

The knee is a diarthrodial joint enclosed in a synovial membrane and bathed in synovial fluid, an ultrafiltrate of blood plasma (Ropes et al., 1939), that supports the nutritional demands of cartilage and lowers friction in the joint (Ogston and Stanier, 1953; Reimann, 1976; Swann et al., 1985). Ligaments and menisci (**Figure 2-1**) stabilize the knee (Flandry and Hommel, 2011), with the menisci playing an additional role in load transmission and distribution (Jones et al., 1996)). Articular cartilage covers the joint surfaces of the femur, tibia, and patella, transferring load at three articulating surfaces:

two femoral condyles contacting menisci and adjacent tibial surfaces and the patella contacting the trochlear groove of the femur (Gray and Goss, 1973).

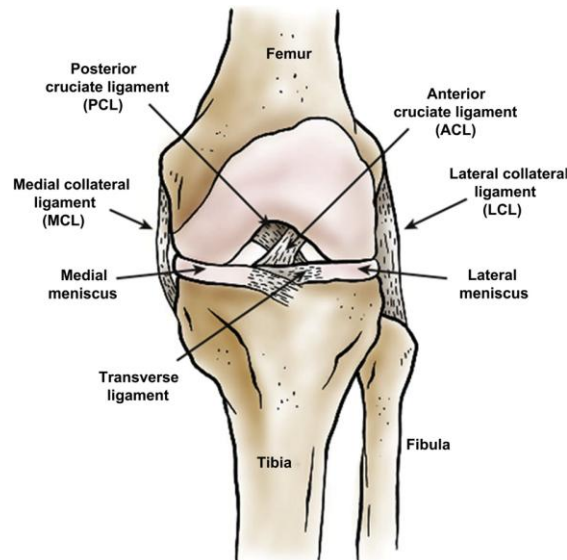


Figure 2-1: Schematic of basic knee anatomy, adapted with permission from (Makris et al., 2011).

2.1.3 Articular Cartilage Structure

Articular cartilage lines the joint surfaces of bones, transmits load across the joint, and provides a low friction surface crucial for joint motion. Water comprises approximately 60-85% of the wet weight of cartilage, and is important not only for nutrient and waste exchange, but also lends itself to the high load bearing function of the tissue. The primary structural macromolecule of cartilage is type II collagen (15-22% wet weight); however, types VI, IX, X, XI, and XIV collagen are also present in articular cartilage (summarized in (Mow and Huiskes, 2005)), with type VI collagen involved in pericellular signaling and mechanotransduction (Choi et al., 2007; Guilak et al., 2006) and type X collagen produced by hypertrophic chondrocytes (Kielty et al., 1985). Although type II collagen is the primary component responsible for tensile properties,

secondary interactions of collagen with water and proteoglycans (**Figure 2-2**) contribute to the resistive compressive properties. Proteoglycans, in particular aggrecan (4-7% wet weight), play a large role in the compressive mechanical function of the tissue (Mow and Huijskes, 2005). Aggrecan, so named for its characteristic aggregation on hyaluronic acid chains, is densely packed with sulfated glycosaminoglycans (sGAG), giving cartilage a high fixed charged density, ultimately creating a swelling pressure through electrochemical interactions with water due to the Donnan effect (Buschmann and Grodzinsky, 1995).

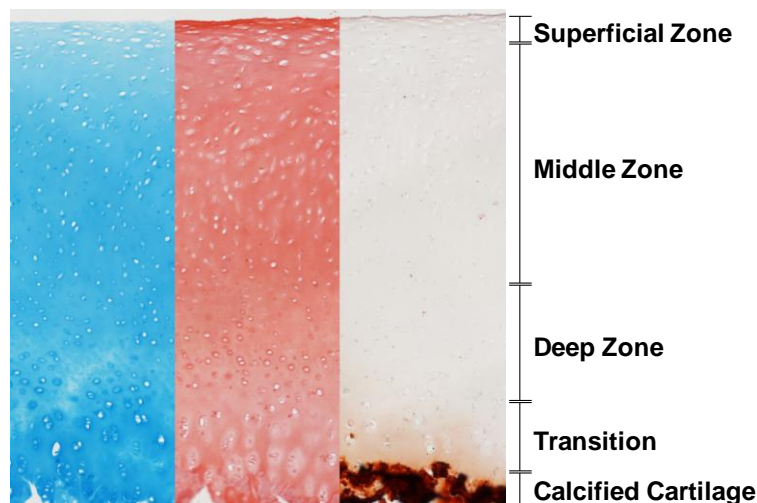


Figure 2-2: Depth-dependent histological staining of adult bovine cartilage from the femoral condyle. Alcian Blue (proteoglycans, left), Picrosirius Red (collagens, center), and Alizarin Red (calcium deposits, right).

Articular cartilage has a graded distribution of matrix (**Figure 2-2**), organization, and mechanical properties through its depth (Freeman, 1979; Huang et al., 2005; Schinagl et al., 1997), and is segregated into the following zones: superficial zone, middle zone, deep zone, and calcified cartilage. Although cartilage has one primary cell type, chondrocyte

phenotype changes through the tissue depth to play specific roles in each of these regions (Klein et al., 2007; Youn et al., 2006).

Within the superficial (tangential) zone, collagen content is high (Muir et al., 1970) and fibers are oriented tangentially to the articulating surface (**Figure 2-3**), while proteoglycan content is lower than in the deeper zones (Muir et al., 1970). In this most superficial zone, chondrocytes are ellipsoidal in morphology and synthesize molecules such as proteoglycan 4 (Schumacher et al., 1994), previously referred to as lubricin or superficial zone protein, that help to maintain a low friction coefficient between the two articulating surfaces (Swann et al., 1985).

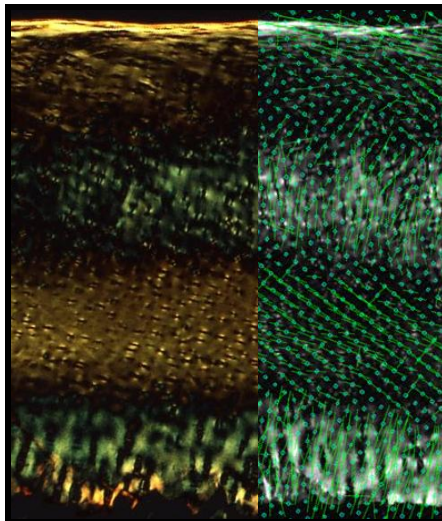


Figure 2-3: Cartilage organization as a function of depth. Left) Polarized light imaging of adult bovine cartilage from the femoral condyle. Right) Alignment map generated from quantitative polarized light microscopy analysis (extinction angles with 5° rotation increments of polarizer) as in (Thomopoulos et al., 2003).

Progressing further through the depth to the middle (transitional) zone, collagen content decreases and proteoglycan content increases compared to the superficial zone. In this zone, which comprises the majority of the cartilage thickness, collagen fibrils have a less dense, random orientation, and chondrocytes adopt a more rounded morphology.

The deep zone is marked by a shift in collagen fiber orientation with larger bundles that run perpendicular to the articular surface. Chondrocytes within this zone appear in columnar arrangements. The deep zone is separated from the underlying calcified cartilage by a tidemark (Redler et al., 1975). This calcified cartilage, the result of hypertrophic differentiation of chondrocytes, contains matrix specific markers such as type X collagen, and forms a transition between the cartilage and subchondral bone.

2.1.4 Synovial Fluid and Articular Cartilage Nutrition

While the role of the subchondral bone in the nutrition of articular cartilage is still debated (Hodge and McKibbin, 1969; Imhof et al., 1999; Malinin and Ouellette, 2000; Wang et al., 2013), the most common thinking on this topic is that since cartilage is mostly avascular in the adult, diffusion of molecules from the synovial fluid, either passively or actively with cyclic compression (O'Hara et al., 1990), is the primary source of cartilage nutrition. Synovial fluid is a dialysate of blood plasma, with the synovium acting as a semi-permeable membrane, allowing cross-membrane transport of small molecules such as glucose and waste products while retaining high synovial fluid concentrations of larger molecules produced by synoviocytes and chondrocytes, such as hyaluronic acid and lubricin (PRG4) (Hui et al., 2012). These large molecules contribute

to the viscous, low friction characteristics of the synovial fluid. Additionally, synovial fluid includes many cytokines (pro- and anti- inflammatory of the interleukin families) and growth factors (transforming growth factor and insulin-like growth factor) (Hui et al., 2012). Glucose levels in the synovial fluid approximate those of blood plasma levels (~ 5.5 mM, 1 g/L [0.07 – 1.40 g/L blood glucose range from US Center for Disease Control]) (Dechant et al., 2011; Tumram et al., 2011), with large differences in serum-synovial fluid glucose levels indicative of a septic joint (Dechant et al., 2011; Thompson et al., 1978). Given the lack of blood supply in the adult, cells within articular cartilage experience low oxygen tension. Direct measurements and theoretical models have approximated this oxygen tension in the tissue to range from 7% in the superficial zone to 1% in the deep zone of cartilage (Silver, 1975; Zhou et al., 2004). Due to these low oxygen tensions, chondrocyte metabolism is largely anaerobic (Lane et al., 1977; Marcus, 1973; Otte, 1991). While chondrocytes are able to survive near anoxic conditions (Grimshaw and Mason, 2000), altered oxygen tensions (hypoxic and hyperoxic) can impact cell activity and/or cell health.

2.1.5 Articular Cartilage Function

Articular cartilage is an important component in the musculoskeletal system, contributing largely to the repetitive locomotive and load transmission needs of articulating joints. Articular cartilage exhibits anisotropic, viscoelastic, and depth dependent mechanical properties (Huang et al., 2005; Schinagl et al., 1997). Due to its high water content, which interacts with the solid matrix, cartilage is often modeled as a biphasic or triphasic material (with the third ‘phase’ consisting of dissolved ions and other solutes) (Ateshian

et al., 2004; Lai et al., 1991; Mow et al., 1980). Compressive loads exerted on a joint can be many times that of body weight (D'Lima et al., 2012). Fluid pressurization at high strain rates with high loads allows for immediate support and load transfer across the joint, while the viscoelastic nature of the tissue and fluid dissipation allow for lower load transfer to the solid matrix of cartilage with longer static loading durations. Cartilage withstands high physiological compressive loads, and therefore, cartilage is most commonly tested in compression. However, due to the complex loading in a joint and the mechanical role of osmotic swelling and the collagen network, cartilage matrix does experience tension, shear, and torsional loading as well.

Compressive mechanical properties can vary with species, age, tissue location, and tissue health (Armstrong and Mow, 1982; Athanasiou et al., 1991; Treppo et al., 2000; Williamson et al., 2001). For example, bovine articular cartilage has an aggregate compressive modulus of 0.079 MPa in the superficial zone, 1.14 MPa in the middle zone, and 2.10 MPa in the deepest zone, with a full thickness modulus of 0.38 MPa (Schinagl et al., 1997). As it relates to location, the equilibrium aggregate modulus of bovine cartilage is on the order of 0.89 MPa in the lateral condyle and 0.47 MPa in the patellar groove (Athanasiou et al., 1991). Cartilage tissue engineering strategies currently strive to achieve compressive equilibrium modulus values on the order of magnitude of 0.5-1 MPa (Erickson et al., 2012; Kim et al., 2012; Lima et al., 2007), such that constructs can function in compression in a similar fashion to the native tissue.

2.2 Osteoarthritis and Clinical Repair Strategies

“... we shall find, that an ulcerated Cartilage is universally allowed to be a very troublesome Disease; that it admits of a Cure with more difficulty than a carious Bone; and that, when destroyed, it is never recovered.” These words written by William Hunter in 1743 (Hunter, 1743) describe what remains a perplexing task in the 21st century. How can we repair a tissue with limited intrinsic healing capacity when it affected by a progressive degenerative disease? The sections to follow describe the impact of osteoarthritis and current clinical repair strategies.

2.2.1 Osteoarthritis

Osteoarthritis is a disease of high prevalence with a large economic burden. Although advances in molecular biology have led to a more complete characterization of the role of inflammatory cytokines in osteoarthritis, the disease remains elusive. Clinically characterized by joint pain, immobility, joint space narrowing, cartilage fissuring, and osteophyte formation and subchondral bone sclerosis, osteoarthritis etiology is not always apparent (Berenbaum, 2013; Goldring and Goldring, 2006; Haviv et al., 2013). The disease is linked to aging, post-traumatic cartilage damage, disease such as diabetes, and in some instances can be idiopathic. In cases of osteoarthrosis, cartilage degeneration is present without signs of inflammation.

Many times, osteoarthritis progresses to a chronic state with irreversible loss of cartilage. The disease is associated with extensive pain, due not to the direct degeneration of the cartilage itself (cartilage lacks a nerve supply), but rather to the exposure and contact of

the highly innervated bone and the activation of nociceptors in the synovial capsule by inflammatory molecules (Mease et al., 2011). While osteoarthritis poses the most difficult scenario for clinical cartilage repair (involving as it does the whole joint surface), additional conditions must be addressed as well. For instance, trauma induced focal defects can be painful and impact quality of life (Heir et al., 2010), and if left untreated, can alter tissue deformation and stress concentrations locally, and ultimately progress to joint-wide osteoarthritis (Guettler et al., 2004; Lefkoe et al., 1993).

2.2.2 Clinical Repair of Cartilage

Severe joint damage caused by chronic osteoarthritis (**Figure 2-4A , B**) cannot be treated with conservative methods and requires joint arthroplasty (**Figure 2-4C**) or joint resurfacing to alleviate pain. This technique is highly invasive and involves the surgical removal of the diseased cartilage and the underlying bone, followed by the implantation of a prosthetic articular surface with a stem that is cemented or press fit into the intermedullary canal. Implants can be comprised of ceramics, metals, and ultra high molecular weight polymers with the primary goal of providing a stable, low friction surface with good wear properties that will maintain joint stability and restore some aspects of normal joint motion (Wong et al., 2011). While joint arthroplasty is one of the more successful long term osteoarthritis treatments, the invasiveness leaves little room for additional surgical procedures if implant failure occurs. Joint arthroplasty is a particularly unattractive option for younger individuals (Li et al., 2012) as implant failure can occur during the lifespan of the patient (Mulhall et al., 2006). To allow for additional future joint arthroplasty surgeries, less invasive, yet similar repair techniques have been

used as a first line of treatment, including partial joint replacement (i.e. unicompartmental knee replacement (**Figure 2-4D**)) or joint resurfacing.

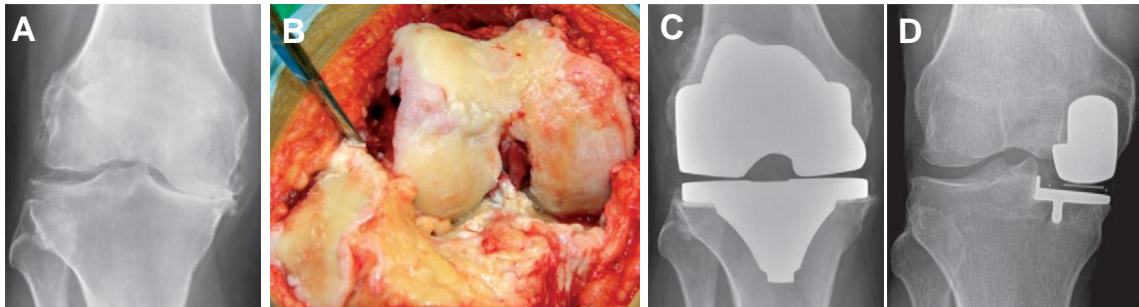


Figure 2-4: Clinical signs and current treatments of osteoarthritis. A) Radiograph showing joint space narrowing of an osteoarthritic knee. B) Gross appearance of osteoarthritic cartilage. C) Radiograph of total knee arthroplasty. D) Radiograph of partial knee arthroplasty. Images adapted from (Carr et al., 2012) with permission.

In instances where damage or osteoarthritic tissue is localized to smaller lesion sites, biological based cartilage repair techniques are clinically available. One such treatment, microfracture, induces *de novo* tissue formation from a bone marrow clot in the lesion site (Gomoll, 2012; Gomoll and Minas, 2011). Microfracture is a marrow stimulation technique that involves first debridement of the lesion followed by the perforation of the subchondral bone using an awl. The microfracture perforations allow for the flooding of the lesion site by blood and bone marrow, which in turn results in the formation of a clot and the development of tissue by cells within the clotted marrow. Limitations of this procedure include long recovery periods, inadequate tissue development (often fibrocartilaginous and disorganized), and short term efficacy (LaPrade et al., 2008; Mithoefer et al., 2009).

Alternatively, living osteochondral tissue can be grafted into a defect site (a procedure termed osteochondral allografting (Gomoll and Minas, 2011) when donor tissue is used

or osteochondral autograft transfer (OAT) when the patient's own tissue is used). When numerous osteochondral plugs are used to fill a single, large defect, the procedure may be referred to as mosaicplasty (**Figure 2-5**), given the resemblance of the repair site to a mosaic. To conduct OAT procedures, osteochondral plugs are harvested from non-load-bearing sites of the joint, such as the trochlear ridge or the intercondylar notch, using a sharp harvest tool. This tissue is then typically press fit into the defect site. Limitations associated with such techniques can be tissue availability, chondrocyte viability at the plug harvest interface (Huntley et al., 2005), decreased cell viability or tissue degeneration during storage (Fening et al., 2011; Pallante et al., 2009), donor site morbidity (Matricali et al., 2010), poor lateral tissue integration, and donor to patient disease transmission in the case of allografts.

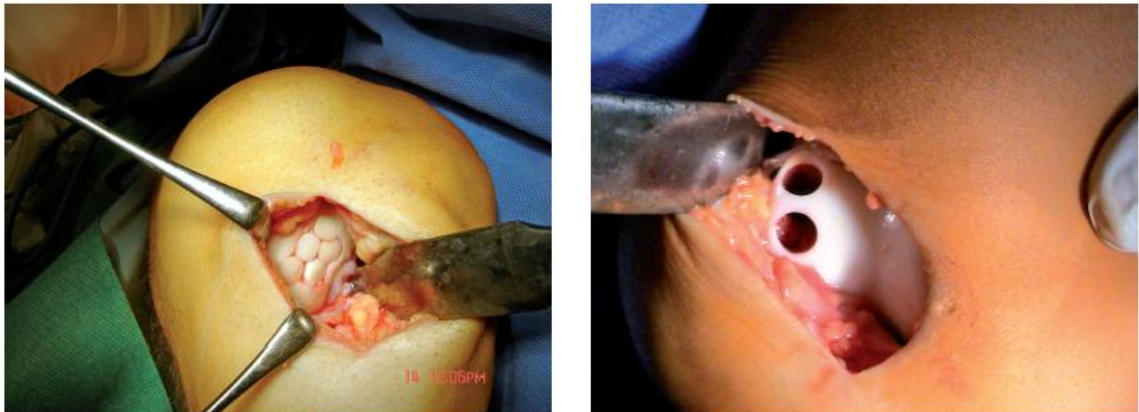


Figure 2-5: (Left) Mosaicplasty of the medial femoral condyl. (Right) Donor site. Adapted from (Hangody et al., 2008) with permission.

Finally, autologous chondrocyte implantation (ACI) (Minas, 2001, 2011) is a cell based therapy for cartilage repair that uses transplanted chondrocytes to form *de novo* cartilage within the defect site. ACI, also referred to as ACT (autologous chondrocyte

transplantation) is a two-stage surgical procedure which first involves the harvesting of cartilage from a non-load bearing donor site of the patient. This harvested cartilage is then shipped to a laboratory and digested to isolate the chondrocytes within, which are subsequently expanded in a tissue culture facility to obtain a sufficient number for re-implantation. The cells are returned to the surgeon and injected under a covering (typically a periosteal or collagen-based flap) fixed over the cartilage defect with sutures and fibrin glue. The primary indication for use of ACI, as suggested by Genzyme©, provider of Carticel® autologous cultured chondrocytes, is for cartilage lesions that have been treated unsuccessfully with other methods, and is not suggested for the treatment of generalized osteoarthritis. A high rate of subsequent surgical procedures is amongst the limitations associated with this procedure. Additionally, there remains a vigorous debate in the field as to whether the cartilage formed is true hyaline cartilage and not fibrous (**Figure 2-6**), as well as ongoing considerations as to the cost/benefit ratio relative to simpler microfracture procedures (Nehrer et al., 1999; Van Assche et al., 2010).

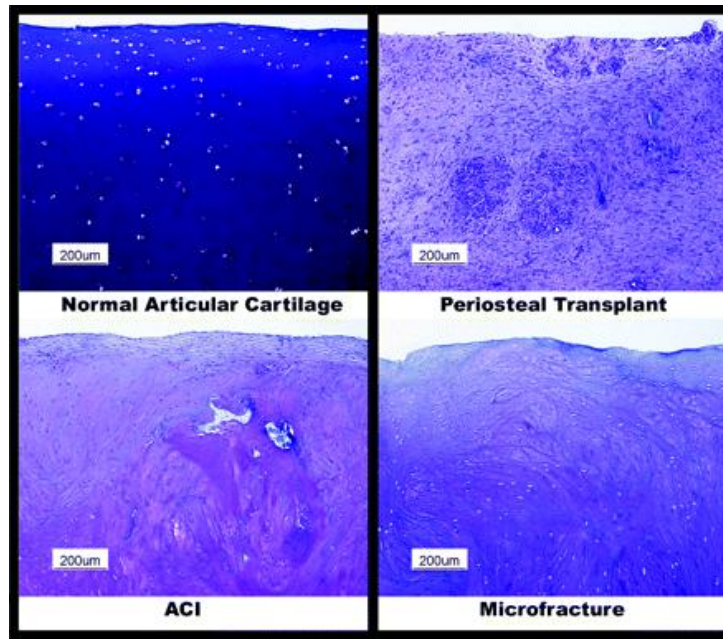


Figure 2-6: Toluidine blue staining of repair tissue from from ACI, microfracture, and periosteal transplant shows decrease in staining intensity and increased levels of fibrous tissue in repair techniques compared to cartilage control. Adapted from (LaPrade et al., 2008) with permission.

2.3 Cartilage Tissue Engineering

Due to the inability of cartilage to heal even minor defects, and the limitations of the aforementioned cartilage repair strategies, the biological repair of this tissue has been the primary focus of decades of basic science and pre-clinical research. This research focused on cartilage repair has witnessed marked advances via developments in biomaterials science as well as in tissue engineering methodologies. The sections to follow will discuss some of the more prevalent cell types, growth factors, and materials that have been used to address these challenges.

2.3.1 Cells

Chondrocytes are the sole cell type in cartilage, and are therefore the primary cells of interest for cartilage regeneration and engineering. Chondrocytes isolated from articular cartilage produce tissue rich in proteoglycans (aggrecan, biglycan, decorin) and type II collagen. Important considerations for the use of chondrocytes for tissue engineering purposes include cell health and matrix producing capacity as a function of zonal location (Hu and Athanasiou, 2006; Kim et al., 2003; Ng et al., 2009), patient age (Skaalure et al., 2012; Tran-Khanh et al., 2005), disease state of the isolated tissue (Dorotka et al., 2005; Hsieh-Bonassera et al., 2009), and phenotypic and metabolic changes as a result of expansion conditions (Benya and Shaffer, 1982; Heywood and Lee, 2010; Schiltz et al., 1973).

One alternative to chondrocytes for cartilage tissue engineering applications is the use of chondrocyte progenitor cells such as embryonic stem cells (Toh et al., 2011), adipose derived stem cells (Estes et al., 2010), synovium derived stem cells (Jones and Pei, 2012), or bone marrow derived mesenchymal stem cells (Johnstone et al., 1998; Mauck et al., 2006; Pittenger et al., 1999) (MSCs). Stem cell differentiation capacity is impacted by factors including tissue source (El Tamer and Reis, 2009), growth factor supplementation (Freyria and Mallein-Gerin, 2012), and oxygen tension (Adesida et al., 2012; Malda et al., 2003). Although chondrogenic stem cells hold promise for cartilage regeneration and tissue engineering applications, *in vivo* hypertrophic terminal differentiation, marked by cell enlargement, production of types I and X collagen, increased alkaline phosphatase activity, cell apoptosis, and tissue mineralization (Pelttari et al., 2006), remains a

significant challenge to overcome before this cell type reaches clinical application. A more comprehensive review comparing chondrocytes and mesenchymal stem cells will conclude Chapter 2.

2.3.2 Growth Factors

The role of growth factors in cartilage regeneration and tissue engineering is to enhance matrix production and promote chondrogenesis, reduce inflammatory responses and catabolic matrix degradation, and prevent hypertrophic differentiation. As such, media cocktails including one or more of the following growth factors have been used:

TGF- β Superfamily: Members of the transforming growth factor-beta (TGF- β) superfamily include TGF- β and bone morphogenetic proteins (BMP). These factors are morphogens that activate SMAD signaling pathways and ultimately alter expression of cartilage-related genes (Watanabe et al., 2001). TGF- β has been shown to initiate the expression of chondrogenic markers including SRY (sex determining region Y)-box 9 (SOX9), cartilage oligomeric matrix protein (COMP), aggrecan, and type II collagen (Denker et al., 1995; Johnstone et al., 1998; Mauck et al., 2006). The most frequently used isoforms for chondrogenic differentiation are TGF- β 1 (Cals et al., 2012; Estes et al., 2010; Johnstone et al., 1998) and -3 (Buckley et al., 2012; Cals et al., 2012; Huang et al., 2010a), although TGF- β 2 (Barry et al., 2001; Cals et al., 2012; Kim and Im, 2009) has also been used. BMPs can induce chondrogenic and osteogenic differentiation, depending on the context in which they are applied. BMPs used for cartilage tissue engineering include BMP-2, -4, -6, and -7 (Weiss et al., 2010).

Fibroblast growth factor (FGF): FGF is categorized as a mitogen. FGF isoforms that have been used to enhance proliferation, chondrogenesis, and osteogenesis include FGF-18 (Davidson et al., 2005) and FGF-2 (Hellingman et al., 2010; Hsieh-Bonassera et al., 2009) (also referred to as basic fibroblast growth factor [bFGF]).

Parathyroid hormone-related protein (PTH-rP): PTH-rP is a protein that is used to promote chondrocyte proliferation and suppress terminal hypertrophic differentiation (Bian et al., 2011b; Harrington et al., 2004; Weiss et al., 2010).

Insulin-like growth factor (IGF): IGF is a chondrogenic anabolic factor that has been used to reduce chondrocyte apoptosis and increase matrix synthesis, particularly proteoglycans (Guenther et al., 1982; Starkman et al., 2005).

Dexamethasone: Dexamethasone is an anti-inflammatory steroidal hormone commonly used in chemically defined media culture of tissue engineered cartilage (Johnstone et al., 1998; Mauck et al., 2006; Ng et al., 2009). Although dexamethasone has been shown to enhance chondrogenesis, it has also been linked to increased alkaline phosphatase activity (Johnstone et al., 1998).

2.3.3 Materials

Biomaterials, or three-dimensional scaffolds, serve to provide immediate mechanical function in the cartilage lesion, guide or enhance cell matrix deposition, or act as a

delivery vehicle for controlled drug release. In the section to follow, examples of natural and synthetic materials used for cartilage regeneration and tissue engineering will be provided.

Scaffold Free Materials: Cartilage formation during development occurs via condensation of cells of the mesenchyme into high density masses in the limb bud. Scaffold-free, or self-assembling, tissue replacements attempt to emulate this developmental process by aggregating cells into micromasses or high density monolayer-type aggregates, supporting the chondrogenic phenotype and the production of *de novo* cartilaginous matrix *in vitro* (Kim et al., 2011; Natoli et al., 2009; Solorio et al., 2012). The result is the development of a dense, cartilaginous tissue. This method has been used with both chondrocytes and MSCs, and is similar to clinical cell-based cartilage repair techniques such as ACI and microfracture, though in this formulation the initial tissue formation and condensation would be carried out prior to implantation.

Metals and Ceramics: Although less common, metals have been implanted *in vivo* into chondral defects in animal models. Such metals include oxidized zirconium (Custers et al., 2010), cobalt-chromium (Custers et al., 2010; Custers et al., 2009), porous tantalum (Mardones et al., 2005; Mrosek et al., 2010), and titanium (Karagianes et al., 1975). While some success has been achieved in using metal implants to enhance bone integration as part of an osteochondral repair with cartilage overgrowth, the implantation of metals into cartilage lesions to prevent osteoarthritis progression has not been successful. The primary use of ceramics in cartilage tissue engineering applications is

within composite osteochondral grafts, where bone integration may contribute to implant success. Some examples include bioactive glasses (Jiang et al., 2010), hydroxyapatite (Schek et al., 2004; Tampieri et al., 2008), and calcium-phosphate (Guo et al., 2004; Kandel et al., 2006; Tanaka et al., 2005).

Polymer Hydrogels: Polymer hydrogels are the most widely used materials for cartilage tissue engineering and regeneration. The versatility of polymers, such as tunable mechanical and degradative properties, possibility for hierarchical structure, and controllable geometry (**Figure 2-7**), is instrumental for recreating the complex structure and function of cartilage.

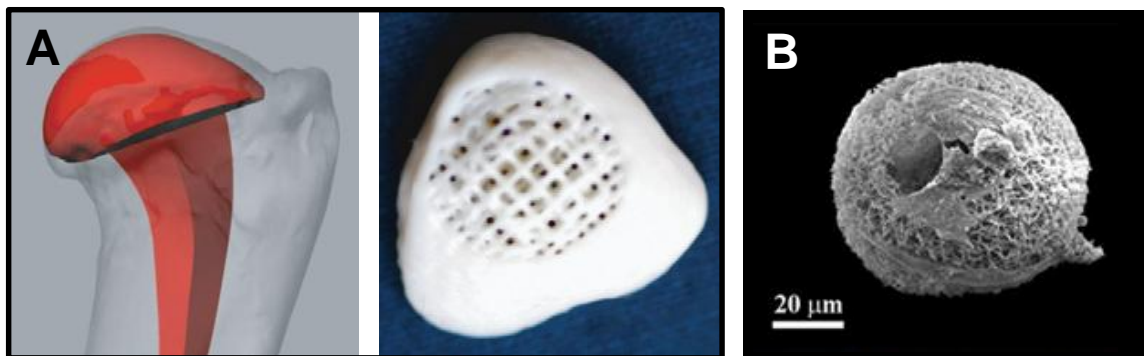


Figure 2-7: A) Anatomically correct porous osteo- and chondro-inductive implant fabricated via computer aided design and bioprinting. B) Nanofibrous hollow microspheres that support the chondrogenic phenotype and foster tissue repair in vivo. Images adapted from (Lee et al., 2010) and (Liu et al., 2011) with permission.

Hydrogels are hydrophilic polymer networks that, dependent on the polymer, may be formed through physical or chemical crosslinks. They are porous and water retentive, an important factor when attempting to regenerate or engineer a viscoelastic tissue with a high water content such as cartilage. Hydrogels used for cartilage tissue engineering

include combinations of synthetic polymers created from polyethylene-glycol (PEG) and polyethylene-glycol diacrylate (PEG-DA) (Hwang et al., 2011; Johnstone et al., 1998; Nguyen et al., 2012), polyglycolic acid (PGA) (Shahin and Doran, 2011; Terada et al., 2005), and poly(lactic-co-glycolic acid) (PLGA) (Chang et al., 2012; Spiller et al., 2011; Spiller et al., 2009). Naturally occurring polymers include those derived from mammalian species (type I collagen (Schulz et al., 2008; Yuan et al., 2010), type II collagen (Jurgens et al., 2012), and hyaluronic acid (Chung et al., 2008; Erickson et al., 2012; Toh et al., 2012)), polymers derived from plants and fungi (e.g. agarose (Buckley et al., 2012; Farrell et al., 2012; Lima et al., 2007), alginate (Coates et al., 2012; Degala et al., 2012; Estes et al., 2010), and chitosan (Bhardwaj et al., 2011; Lahiji et al., 2000; Sechriest et al., 2000)), and commercially available engineered proteins and composites (e.g. Puramatrix (Dickhut et al., 2008; Erickson et al., 2009a; Maher et al., 2010) and Matrigel (Basic et al., 1996; Bradham et al., 1995; Dickhut et al., 2008)). Hydrogels are particularly beneficial for cartilage tissue engineering in that polymerization processes are often conducive to cell encapsulation.

2.3.4 Chondrocyte and Stem Cell Cartilage Tissue Engineering – Current Successes and Limitations

Engineered tissues rich in type II collagen and aggrecan (markers of mature cartilage) with mechanical properties comparable to native tissue have been fabricated from a number of starting biomaterials (Chung and Burdick, 2008). Improvements in culture methods, including tailored biochemical and mechanical stimulation, have further improved the *in vitro* development of these constructs (Hung *et al.*, 2004). Recent

studies have shown that chondrocytes encapsulated in agarose can produce cartilage-like materials with near-native mechanical properties (Byers *et al.*, 2008; Lima *et al.*, 2007). Despite this progress, limitations in the use of chondrocytes include the requirement of invasive harvest from non-diseased, non-load bearing sites within the joint, as well as the limited activity and health of these cells when derived from adults. Therefore, interest has focused on the use of adult-derived mesenchymal stem cells (MSCs) for cartilage tissue engineering applications.

As with chondrocytes, steady improvements in chondrogenic growth conditions, three-dimensional scaffold design, and mechanical loading regimens have significantly enhanced construct formation using MSCs (Huang *et al.*, 2010a). The use of adult derived progenitor or stem cells for the clinical repair of cartilage defects has been investigated since the early 1990s. Purified isolations of bone marrow derived MSCs were first described by Friedenstein in the 1970s as colony forming fibroblast-like cells (Friedenstein *et al.*, 1970). Since then, both the self-renewing and multipotent nature of these cells has been demonstrated (Pittenger *et al.*, 1999). Importantly, these cells can undergo chondrogenic differentiation in defined culture conditions, suggesting that they may serve as a suitable alternate cell source for cartilage repair techniques (Johnstone *et al.*, 1998; Mauck *et al.*, 2006; Pittenger *et al.*, 1999), overcoming the limitation of insufficient chondrocyte numbers needed for such repair strategies (Johnstone *et al.*, 2013).

Like chondrocytes, MSCs can be readily encapsulated and differentiate in a number of different three-dimensional systems (Huang et al., 2010b). However, limitations in MSC potential become apparent with long-term culture in these three-dimensional contexts. Namely, when cultured identically, MSCs produce matrix of a lower modulus when compared to chondrocytes (Erickson et al., 2009a; Farrell et al., 2012; Huang et al., 2010a; Lima et al., 2007; Mauck et al., 2006). On a molecular level, direct comparisons between differentiated MSCs and chondrocytes revealed many hundreds of genes that remain differentially regulated between the two cell types (Boeuf et al., 2008; Huang et al., 2010c). Likewise, while mechanical pre-conditioning has been shown to improve the mechanical properties of MSC-based constructs (Huang *et al.*, 2010a; Meyer *et al.*, 2011), these improvements are small in comparison to the same stimulus applied to chondrocyte-based constructs (Lima *et al.*, 2007).

One potential reason for the lack of mechanical equivalence between engineered cartilage constructs formed from MSCs and chondrocytes may simply be that a lag exists during which MSCs differentiate to the chondrogenic state. Chondrocytes, and the tissue they produce, are exposed to a number of soluble and mechanical factors through development, which culminates over a period of years in a tissue with refined properties (Koyama et al., 2008; Williamson et al., 2001). Conversely, engineered tissues based on MSCs are forced to undergo both differentiation and maturation within an abbreviated time scale. Notably, MSC-based constructs appear to respond negatively to dynamic loading early in culture (Thorpe et al., 2008), but respond in a positive fashion after a brief period (1-3 weeks) of differentiation (Huang et al., 2010a; Mouw et al., 2007).

Supporting this notion, whole genome profiling revealed that many genes remain differentially regulated between MSCs and chondrocytes cultured in agarose after 28 days (Huang et al., 2010c). However, gene expression remained dynamic through day 56, suggesting that MSCs may have the capacity to continue towards a more chondrogenic state with prolonged culture. Thus the disparity in mechanical properties might be a function of insufficient time to achieve the chondrogenic state, rather than an innate limitation in cartilage-forming potential by MSCs.

An alternative explanation for the disjunction between chondrocyte and MSC-based engineered cartilage may lie in the completeness of phenotypic conversion. It may well be that the best conditions for chondrogenesis of MSCs *in vitro* simply prolongs their residence in that state, but does not eliminate the possibility of differentiation towards alternative lineages. For example, it has been shown that MSCs committed to one lineage (e.g., adipogenesis) can be recovered and forced down another lineage (e.g. osteogenesis), suggesting a somewhat tenuous hold on the differentiated phenotype (Song and Tuan, 2004). Recent studies have shown that transient application of pro-chondrogenic factors, including transforming growth factor beta (TGF- β), in a defined serum free medium, is sufficient to induce and sustain the chondrogenic state, without evidence of type X collagen or mineral deposition (Kim et al., 2012). However, a number of other studies have reported transition from the chondrogenic to the hypertrophic phenotype (with expression of type X collagen, bone markers, and eventual mineralization) when constructs were transferred to environments that presented conflicting signals (Studer et al., 2012). For example subcutaneous implantation of

chondrogenic pellets and hydrogels commonly results in formation of a mineralized tissue (Bian et al., 2011b; Pelttari et al., 2006; Vinardell et al., 2012), and challenge with pro-hypertrophic conditions (i.e., removal of TGF and addition of thyroid hormone T3) can result in *in vitro* mineralization (Mueller et al., 2010; Mueller and Tuan, 2008).

2.4 The Origin of Chondrocytes and MSCs – Implications in Stem Cell Stability and Heterogeneity

Discrepancies in the performance of chondrogenically induced mesenchymal stem cells and chondrocytes may arise from the innate biologic differences of these cell types. Complicating matters is inter-colony population heterogeneity of stem cell function and differentiation capacity. To provide the foundation necessary for the investigation into stem cell heterogeneity, the sections to follow will summarize chondrocyte and mesenchymal stem cell biology.

2.4.1 Chondrogenesis and Chondrocytes

Endochondral ossification, and thus chondrogenesis, is the driving mechanism of the development of the axial skeleton and limbs. Although discoveries in molecular and developmental biology have improved our understanding of the many factors involved in skeletogenesis, a complete understanding of the formation of synovial joints has yet to be attained (Pacifci et al., 2005). Limbs form from the lateral plate of the mesoderm (Tickle and Munsterberg, 2001), with the limb buds of the appendicular skeleton apparent at around 4 weeks gestation during human development. During skeletal development, precursor mesenchymal cells of the skeletal blastema divide and transition to

chondrogenic and myogenic lineages, with the epithelium influencing chondrogenesis by regulating mesenchymal cell recruitment, proliferation, and condensation (Fell, 1925; Hinchliffe, 1994; Holder, 1977; Mitrovic, 1978). Prechondrogenic cells produce matrix high in hyaluronan and type I collagen. Subsequent hyaluronidase activity is coupled with increased cell condensation, after which neural cadherin (N-cadherin) and neural cell adhesion molecule (N-CAM) are increased and regulated by transforming growth factor- β through fibronectin production. Transition to a fully committed chondrocyte phenotype involves the interaction of tenascins and thrombospondins (such as cartilage oligomeric protein) with adhesion molecules. Spatial control of the developing tissue is driven by fibroblast growth factor (FGF), hedgehog, bone morphogenetic protein (BMP), and Wnt pathways (**Figure 2-8**) (Goldring et al., 2006; Tuan, 2003). Joint initiation of an uninterrupted mesenchymal condensation occurs at interzones (Pacifici et al., 2006), with Hox genes identified as key players in the determination of the site of joint formation (Koyama et al., 2010; Villavicencio-Lorini et al., 2010).

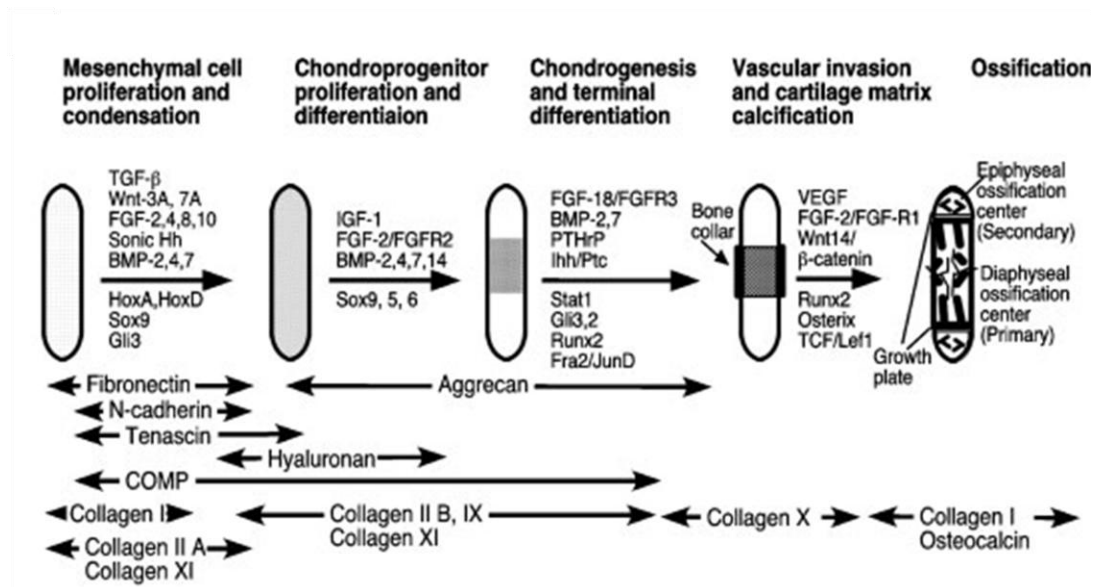


Figure 2-8: Events of chondrogenesis during bone development. Adapted from (Goldring et al., 2006) with permission.

Although questions remain regarding the distinguishing factors between permanent articular and transient chondrocytes, an understanding of what is known of terminal differentiation and endochondral ossification is imperative for the use of bone marrow derived stem cell repair of cartilage, as these cells can be phenotypically unstable and are prone to hypertrophy, much like transient chondrocytes of the developing skeleton (Mueller and Tuan, 2008; Pelttari et al., 2006; Studer et al., 2012). Chondrogenic differentiation (summarized in (Goldring et al., 2006; Studer et al., 2012)) is marked by the production of type II collagen and aggrecan. Sox9 is an early nuclear transcription factor expressed during the condensation phase, controlling cartilage protein expression including type II collagen expression. Terminal differentiation commences with an altered balance of BMP, FGF, and parathyroid hormone-related protein (PTHrP) in the developing bone. Endochondral ossification is characterized by chondrocyte hypertrophic differentiation, mineralization of the cartilagenous template, vascular invasion, and finally ossification. Indian hedgehog signaling is required for endochondral bone formation and can be regulated by Runx2 which plays a part in the progression of a prehypertrophic chondrocyte to a hypertrophic state, with matrix metalloproteinase-13 as one of its downstream targets. Hypertrophic chondrocytes begin to express type X collagen and become apoptotic, followed by mineralization and vascular invasion of the tissue.

2.4.2 Mesenchymal Stem Cells and Heterogeneity

Although the use of mesenchymal stem cells in tissue engineering and regenerative medicine research has rapidly increased in the past decade, definitive characteristics of

the cell type remain elusive and a debate continues as to whether the term "stem cell" should be applied to this cell type (Bianco et al., 2013; Dominici et al., 2006). By definition, a stem cell is a cell capable of multi-lineage differentiation potential and self-renewal, i.e. the cell should be capable of symmetric division with both daughter cells maintaining the stemness of the parent cell. However, inconsistencies in cell isolation and expansion techniques and population characterization have led to an all inclusive use of this term to describe progenitor or stromal cell populations of the musculoskeletal system that have been isolated from a number of different tissues. Regardless of the overarching lack of consistency in the MSC literature, the consensus is that the bone marrow does contain a plastic-adherent multipotent stem cell population, fulfilling the more stringent definition of a mesenchymal stem cell, a single cell with the *in vivo* capacity to autonomously generate heterotopic bone and a bone marrow cavity (Bianco et al., 2013). It is also a highly accepted notion that in addition to donor-to-donor variability, there is inter-colony population heterogeneity in these stem cell isolations, with different colony forming units (CFUs) derived from the same isolated population having differing characteristics (Pevsner-Fischer et al., 2011; Phinney, 2002).

Since MSCs were first described by Friedenstein in the 1970s, it was noted that differences in colony behavior exist, with cells in a single population adopting different morphologies and producing colonies of different sizes (Friedenstein et al., 1970; Friedenstein et al., 1974; Friedenstein et al., 1976; Friedenstein et al., 1982). It was not until 1999, however, that the true heterogeneity of these different colonies was verified (Pittenger et al., 1999). Using techniques to isolate populations derived from single

human MSCs, Pittenger showed that within the heterogeneous stem cell population there existed cells capable of tri-potential differentiation (osteogenic, adipogenic, and chondrogenic differentiation), and that different colonies had different differentiation capacities *in vitro*. Specifically, of six colonies isolated via a clonal ring technique, all were capable of osteogenesis; however, only five underwent adipogenesis, and only two underwent chondrogenic differentiation. In the years that followed, this assessment of heterogeneity in MSC differentiation capacity gained interest. Multiple studies have come to the conclusion that the osteogenic pathway may be intrinsically dominant in these populations, given that most colonies are capable of differentiation into some combination of the osteo-lineage (i.e., they are either tri-, bi-, or uni-potent) (Gronthos et al., 2003; Halleux et al., 2001; Okamoto et al., 2002), with Okamoto et al. finding no colonies with chondro-adipo bi-potentiality. In 2010, Russell et al. further showed that within a population, there exists colonies that reside in all eight niches of the MSC differentiation hierarchy; however, colonies with differentiation potential that excluded osteogenesis were a small fraction of the population (Russell et al., 2010). Complicating matters is the fact that population enrichment for chondrogenic potential via antigen surface marker selection with current MSC markers is not feasible or reliable. Of relevance is the finding that although heterogeneous in differentiation capacity, where some clonal subpopulations are not able to undergo chondrogenesis, most cells within a heterogeneous isolate continue to express cell surface markers characteristic of MSCs, including CD29, CD44, CD73, CD90, CD105, and CD166 (Mareddy et al., 2007). It is therefore necessary to acknowledge that while the development of consistent definitions, culture conditions, and characterization of MSCs remains a pressing research question, it

is well documented that when isolated from bone marrow, MSC populations are heterogeneous and require functional assays to further characterize the differences in chondrogenic potential of colony subpopulations.

2.5 Summary

Osteoarthritis is a debilitating disease of high incidence. To date, there has been limited success in the long-term clinical repair of cartilage defects and the door remains open for the development of a successful, biologically-based repair technique. It is likely that the future of cartilage repair will involve the delivery of chondrocytes, chondro-progenitor cells, or stem cells, in combination with a biocompatible scaffold and growth factors. Although *in vitro* success has been achieved in developing mechanically viable chondrocyte-laden constructs, limitations in chondrocyte availability and health have researchers searching for alternative cell sources, including the clinically available MSC. While MSCs have the capacity to undergo chondrogenesis in three-dimensional culture, they often underperform in the functionality of the tissue they produce when compared directly to chondrocytes, hampering their clinical use. Furthermore, the chondrogenic phenotype of MSCs can be unstable, progressing to a hypertrophic state. The heterogeneous nature of the MSC isolates itself adds to the increased complexity in determining the underlying differences leading to discrepancies in the performance of chondrocytes and chondrogenically induced MSCs. A more rigorous investigation into where, when, and why MSC-laden tissue engineered cartilage fails, and the implications of stem cell heterogeneity on this process, is therefore necessary and is the subject of this thesis.

CHAPTER 3: MESENCHYMAL STEM CELLS PRODUCE FUNCTIONAL CARTILAGE MATRIX IN THREE-DIMENSIONAL CULTURE IN REGIONS OF OPTIMAL NUTRIENT SUPPLY

3.1 Introduction

As with chondrocytes, steady improvements in chondrogenic growth conditions, three-dimensional scaffold design, and mechanical loading regimens have significantly enhanced construct formation using MSCs (Huang et al., 2010b). However, limitations in MSC potential ensue with long-term culture. Namely, when cultured identically, MSCs produce matrix of a lower modulus when compared to chondrocytes (Erickson et al., 2009a; Huang et al., 2010a; Lima et al., 2007; Mauck et al., 2006). In Chapter 2, we discussed how, on a molecular level, direct comparisons between differentiated MSCs and chondrocytes revealed many hundreds of genes that remain differentially regulated between the two cell types (Boeuf et al., 2008; Huang et al., 2010c). Furthermore, while mechanical pre-conditioning has been shown to improve the mechanical properties of MSC-based constructs (Huang et al., 2010a; Meyer et al., 2011), these improvements are small in comparison to the same stimuli applied to chondrocyte-based constructs (Lima et al., 2007).

Together, these data suggest that, on a bulk level, MSCs do not fully replicate the properties or potential of native tissue chondrocytes. However, a significant limitation of this previous work was the fact that all analyses were performed on whole constructs that perforce contain a potentially heterogeneous population of cells (Halleux et al., 2001; Mareddy et al., 2007; Okamoto et al., 2002; Pittenger et al., 1999; Russell et al., 2010),

and are of sufficient size as to allow for the development of diffusional gradients across the construct expanse (Buckley et al., 2012; Zhou et al., 2008). In such conditions, nutrient and growth factor utilization at the periphery may limit MSC differentiation and matrix production away from these sources. Bulk analysis of molecular expression and mechanical properties would therefore blur any variations that arise from these gradients, and so fail to identify differential chondrogenic efficacy as a function of the changing microenvironment. Furthermore, oxygen consumption by MSCs in chondrogenic pellet culture is nearly 10-fold higher than that of freshly isolated chondrocytes (i.e. 12.3 fmol/h/cell (Pattappa et al., 2011) vs. 1.34 fmol/h/cell (Heywood and Lee, 2008)). This differential utilization of metabolites (due to persistent differences in cell metabolism) would exacerbate nutritional gradients throughout the construct, and would likely impact the development of functional properties in regions away from the construct periphery.

To address these issues, this study sought to determine whether the differences in macroscopic properties observed in MSC-based constructs result from inadequate chondrogenic induction throughout the construct or from spatially varying matrix production and properties. For this, we used fluorescence microscopy and digital image correlation to investigate the mechanical properties of matrix produced by MSCs and chondrocytes on a microscopic scale. Similar techniques have been used for the investigation of the depth-dependent mechanical properties of native cartilage (Schinagl et al., 1997; Wang et al., 2001) and tissue engineered chondrocyte-laden constructs (Kelly et al., 2006; Klein et al., 2007; Klein and Sah, 2007). Our objective was to identify where mechanical properties in MSC-laden constructs are lowest and to

determine mechanistically why these differences arise relative to chondrocyte-based constructs. Based on histological staining patterns, we hypothesized that MSC-laden constructs would develop depth-dependent mechanical properties resultant of nutrient and waste gradients, compared to more homogeneous profiles for chondrocyte-laden constructs. Furthermore, we hypothesized that dynamic culture and improved solute transport would reduce the depth-dependency of MSC-laden constructs and result in a significant increase in macroscopic mechanical properties compared to free-swelling conditions.

3.2 Materials and Methods

3.2.1 Cell Isolation and 3D Encapsulation

Unless otherwise stated, reagents were purchased from Sigma-Aldrich (St. Louis, MO, USA). Juvenile bovine MSCs were isolated from marrow from the femur and tibia of three donor calves (Research 87, Boylston, MA, USA) (Mauck *et al.*, 2006). MSCs were expanded through passage 2 in medium consisting of high glucose Dulbecco's Modified Eagle Medium (DMEM; Gibco, Invitrogen Life Sciences, Carlsbad, CA, USA), 10% fetal bovine serum (FBS, Gibco), and 1% Antibiotic-Antimycotic (PSF; Gibco). Donor-matched primary chondrocytes were isolated from the carpometacarpal cartilage of the three donors. Diced cartilage was subjected to pronase digestion (2.5 mg/mL, 1 h, 37°C; Calbiochem/EMD Chemicals, Gibbstown, NJ, USA) followed by collagenase digestion (0.5 mg/mL, 6 h, 37°C) (Mauck *et al.*, 2003b). After expansion (MSCs) or digestion (chondrocytes), cells were encapsulated in 2% agarose. Briefly, cells were suspended in a chemically defined media (CM) at a density of 40 million cells/mL. The

cell suspension was then mixed with molten 4% w/v agarose (type VII, 49°C) in phosphate-buffered saline (PBS) at a 1:1 ratio and cast between two parallel plates separated by 2.25 mm spacers (Mauck et al., 2003b; Mauck et al., 2006). Using a biopsy punch, 2% agarose constructs (4 mm in diameter, 2.25 mm in depth) were extracted with an initial cell density of 20 million cells/mL. CM consisted of high glucose DMEM, 1% PSF, 0.1 µM dexamethasone, 50 µg/mL ascorbate 2-phosphate, 40 µg/mL insulin, 6.25 µg/mL transferrin, 6.25 ng/mL selenous acid, 1.25 mg/mL bovine serum albumin, and 5.35 µg/mL linoleic acid.

3.2.2 Hydrogel Construct Culture

Constructs were cultured under free swelling or dynamic conditions over 9 weeks. For free swelling conditions, constructs were cultured in CM with (FS (+TGF-β3)) or without (FS (-TGF-β3)) the addition of 10 ng/mL transforming growth factor-beta 3 (TGF-β3; R&D Systems, Minneapolis, MN, USA). Dynamically cultured constructs were cultured in CM with TGF-β3 (Dyn (+TGF-β3)) while being subjected to continuous orbital shaking at 1.2 Hz (115V – 25x25 Orbital Shaker, BellCo Glass Inc, Vineland, NJ, USA). These conditions were chosen to provide continuous agitation of the medium, while ensuring that constructs did not tumble. For all culture conditions, care was taken to ensure constructs did not flip during handling and feeding. Constructs were fed twice weekly with 1 mL of medium per construct. Immediately upon removal from the well plate, the top surface of each construct was stained with a solution consisting of 50% v/v PBS, 25% v/v hematoxylin solution (2.5% w/v hematoxylin (Thermo Fisher Scientific, Hampton, New Hampshire) in 95% ethanol), 12.5% v/v aqueous ferric chloride (10% w/v

ferric chloride (Fisher) in distilled water), and 12.5% Wiegert's iodine (Fisher) to maintain orientation throughout testing (**Figure 3-1A**).

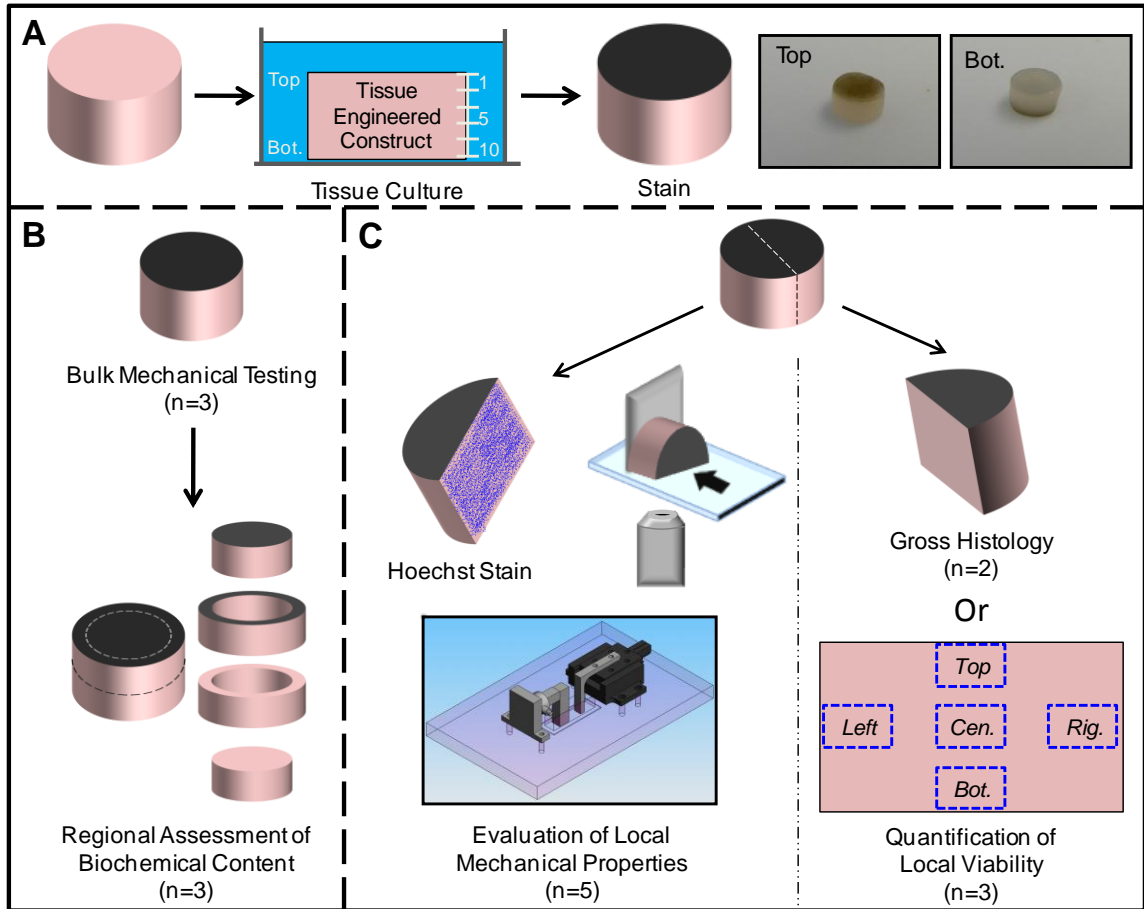


Figure 3-1: Study design schematic. (A) Construct orientation (4 mm diameter, 2.25 mm thick) was maintained throughout the culture period. Construct tops (Region 1) were stained after removal from the tissue culture well plate to maintain orientation through mechanical testing. (B) Following bulk testing, constructs were cored and halved through the transverse plane for biochemical assessment. (C) Prior to local mechanical property assessment, constructs were halved through the median plane. Half of the construct was stained and tested in a custom microscope-based uniaxial compression device. The remaining half was preserved for histology or regional viability assessment.

3.2.3 Mechanical Analysis of Bulk Properties

Constructs (n=3) were tested in uniaxial unconfined compression for the assessment of bulk properties as in (Mauck et al., 2000). Constructs were first equilibrated under a 0.02

N static load for 5 min, followed by evaluation of equilibrium stress (1000 s stress relaxation) following application of 10% strain (at a rate of 0.05%/s). Equilibrium modulus was calculated from the equilibrium stress and sample geometry. Following mechanical testing, constructs were cored with a 3 mm biopsy punch and bisected through the transverse plane, resulting in 4 sections of roughly equal volume including: top annulus, top core, bottom annulus, and bottom core. Construct regions were frozen separately at -20°C for regional assessment of biochemical content (**Figure 3-1B**).

3.2.4 Mechanical Analysis of Local Properties

Constructs (n=5) were halved diametrically for local assessment of compressive strain via digital image correlation. The construct half was stained with 80 $\mu\text{g}/\text{mL}$ Hoechst 33342 (Molecular Probes, Invitrogen) to label cell nuclei as fiducial markers; the remaining half was reserved for histology (n=2) or assessment of viability (n=3). Stained construct halves were placed in PBS in a custom unconfined compression tester (modified after (Knight et al., 1998)) situated on the stage of a Nikon Eclipse TE2000-U inverted microscope (Nikon Instruments Inc, Melville, NY, USA). Uniaxial compression was applied in 4% platen-to-platen strain increments through 12% strain, with a 7 min relaxation period following each compressive step (**Figure 3-1C**). Images were acquired at 0% strain and at equilibrium for each strain increment with 3X magnification. Load at equilibrium was recorded for each increment. Sequential images were analyzed using Vic2D (Correlated Solutions, Columbia, SC, USA), and Lagrangian strain (E_{xx}) was calculated with X defined as the direction of loading. Lagrangian strain values at 12% platen-to-platen engineering strain were binned into ten regions of equal size through the

depth of the construct using a custom MATLAB script (The MathWorks Inc, Natick, MA, USA) and averaged to obtain average strain values through the depth. These values, coupled with the equilibrium boundary stresses, were used to calculate local modulus through the depth. Region of analysis was restricted to the inner 80% of the construct (Region 2 to Region 9) due to edge effects of the testing modality.

3.2.5 Histological Analysis

Construct halves (n=2) were fixed in 4% paraformaldehyde (FD NeuroTechnologies Inc, Ellicott City, MD, USA), dehydrated with a series of ethanol washes, and paraffin embedded (**Figure 3-1C**). Sections (8 μm) were rehydrated and stained for proteoglycans (Alcian Blue, Rowley Biochemical Inc, Danvers, MA, USA). Additional sections were rehydrated, incubated in hyaluronidase (1 mg/mL) for 2 h at 37°C to remove proteoglycans, and stained for collagens (Picrosirius Red) as in (Melrose et al., 2004). Stain intensity through the depth of the construct was assessed using the plot profile function of Image J (NIH). Additional sections were stained for apoptotic markers using the FragEL DNA Fragmentation Detection Kit (Calbiotech, Spring Valley, CA, USA) according to manufacturer's instructions. Cells positive for apoptosis were indicated by co-localization of DAPI and TUNEL stains.

3.2.6 Biochemical Analysis

Samples were papain digested as in (Mauck et al., 2006) at 60°C for 24 h. The supernatant was assessed for sulfated glycosaminoglycan (GAG) content with the 1,9-dimethylmethylene blue dye-binding assay (Farndale et al., 1986) and collagen content

with the orthohydroxyproline assay (Stegemann and Stalder, 1967) and a OHP:collagen correction factor ratio of 7.14. GAG and collagen content is presented as percent of construct wet weight.

3.2.7 Quantification of Viability

Construct halves (n=3) were stained with the LIVE/DEAD Cell Viability Assay Kit for mammalian cells (Molecular Probes, Invitrogen, Life Sciences) for 30 min in PBS. Stained construct halves were imaged under 10X magnification, with calcein and ethidium-homodimer-1 signal acquired in the same focal plane in 5 regions of the bisected face including: center, top, bottom, left, and right (**Figure 3-1C**). Constructs were aligned and centered under 4X magnification to ensure consistency of regional assessment. A custom MATLAB (The MathWorks, Inc.) script was used to automate counting of cells in each image (**Appendix 1**). Local percent viability was calculated in each region, as well as aggregate viability as the percent ratio of live cells to the total number of cells within all five regions. Total cell count per area was recorded to ensure any change in percent viability was the result of cell death rather than a change of cell number.

3.2.8 Statistical Analysis

The statistical software SYSTAT (Systat Software, Inc., Chicago, IL, USA) was used to carry out ANOVA with Tukey's *post-hoc* testing to enable pairwise comparisons between groups. Data are presented as the mean and the standard deviation, with significance set at $p < 0.05$. Three-way ANOVA was conducted for bulk equilibrium

modulus, aggregate viability, aggregate cell count, and central cell count, with cell type, day, and culture condition as independent variables. Additional three-way ANOVA was conducted for local modulus, local cell count, and collagen content with cell type, region, and culture condition as independent variables. Four-way ANOVA was conducted for GAG content with cell type, region, culture condition, and day as independent variables. Two-way ANOVA was conducted for local modulus with cell type and culture condition as independent variables. One-way ANOVA was conducted for local strain and local Day 63 viability, with region as the independent variable.

3.3 Results

3.3.1 Bulk Mechanical Properties Depend on Culture Conditions

Consistent with previous findings for MSC- and chondrocyte-seeded constructs (Erickson et al., 2009a; Huang et al., 2010a; Mauck et al., 2006), construct opacity (**Figure 3-2A**) and equilibrium modulus increased with time for all free swelling groups (Day 1 vs. Day 63, $p < 0.001$), with the exception of MSC FS(-TGF- β 3) (**Figure 3-2B**). Whereas chondrocyte-laden FS(+TGF- β 3) construct equilibrium modulus increased from Day 42 to Day 63 ($p = 0.001$), MSC-laden FS(+TGF- β 3) constructs plateaued over this same time period, reaching 129 and 122 kPa on Day 42 and Day 63, respectively. Conversely, when cultured with continual agitation (Dyn), the equilibrium modulus of Day 63 MSC Dyn(+TGF- β 3) constructs increased compared to Day 42 ($p < 0.001$) and was ~3-fold higher than Day 63 MSC FS(+TGF- β 3) ($p < 0.001$). Indeed, under these conditions, the equilibrium modulus of Day 63 MSC Dyn(+TGF- β 3) constructs approached Day 63 chondrocyte Dyn(+TGF- β 3) levels (~20% lower, $p < 0.01$).

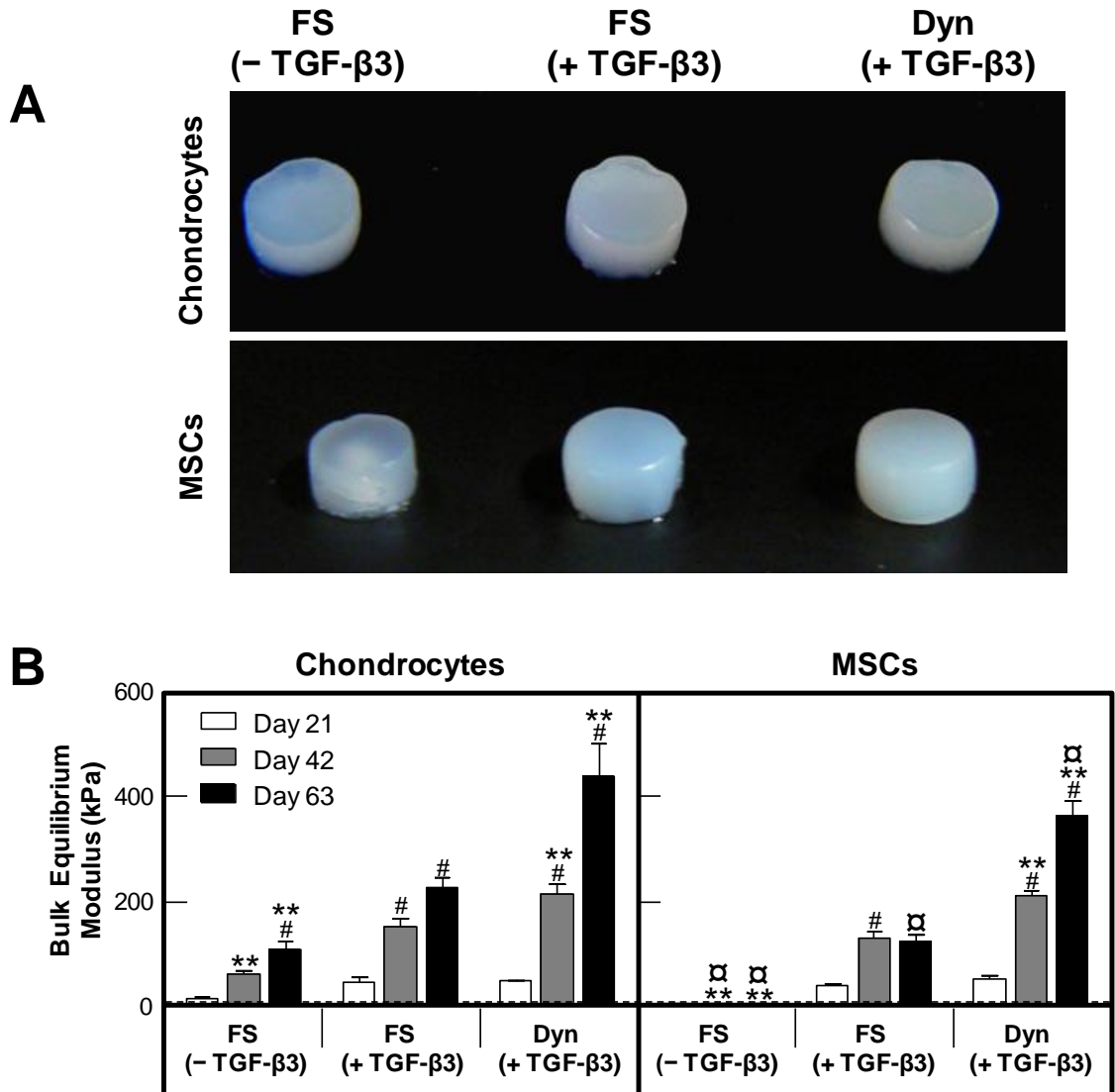


Figure 3-2: Gross appearance and bulk assessment of unconfined compressive properties of constructs cultured in free swelling (FS) or orbital shaking (Dyn) conditions, with (+) or without (-) TGF- β 3. (A) Gross appearance of chondrocyte-laden (top) and MSC-laden (bottom) constructs on Day 63. (B) Bulk construct equilibrium modulus was evaluated through Day 63. Dotted lines denote Day 1 equilibrium modulus values. (# vs. all lower within culture condition and cell type; ** vs. FS(+TGF β -3) within day and cell type; α vs. CH cultured identically, $p < 0.05$). $n = 3$

3.3.2 Depth-Dependent Local Mechanical Properties

To ascertain the origin of the differences in bulk mechanical properties, we next analyzed the local strain profiles within constructs during compressive deformation (**Figure 3-3A**). This analysis showed that in the absence of TGF- β 3 (FS(-TGF- β 3)), both chondrocyte-

laden constructs and MSC-laden constructs had uniform strain profiles with time in culture, with little variation from the superficial zone (Region 2) to the deep zone (Region 9) (**Table 3-1; Figure 3-3B**). However, when cultured in the presence of TGF- β 3 (FS(+TGF- β 3)), both free swelling chondrocyte-laden and MSC-laden constructs developed depth-dependent strain profiles by Day 21. In these constructs, an ~2.5-fold increase in compressive strain was observed comparing superficial regions (Region 2) to middle regions (Regions 5 and 6) for chondrocyte-laden constructs. For MSC-laden constructs, this difference was even more marked, with an ~6-fold increase in strain in the center of the construct compared to the top surface. Once established, these depth dependent profiles were consistent through Day 63 for both cell types.

When cultured in dynamic conditions with TGF- β 3, a shift in strain profiles for both cell types was observed. For chondrocyte-laden constructs, the central regions of the construct deformed least. An ~2-fold increase in compressive strain from Regions 5 and 6 to Regions 2 and 9 at Day 21 persisted through Day 63 with a 2-fold increase in strain from Regions 5 and 6 to Region 9. Conversely, for MSC-laden constructs cultured in dynamic conditions, the central regions remained highest in compressive strain (Regions 5 and 6). Although Regions 2 and 9 were no longer different for MSC-laden Dyn(+TGF- β 3) constructs at any time point, the central portion of the construct continued to show substantial deformation. MSC-laden Dyn(+TGF- β 3) constructs showed a 1.6-fold difference in center-to-edge strain at Day 21, which progressed to a 4.6-fold difference by Day 63 (Region 9 vs. 5).

Table 3-1: Statistical comparison of local strain.

	Chondrocytes		MSCs	
	5, 6, 9 vs. Region 2	5, 6 vs. Region 9	5, 6, 9 vs. Region 2	5, 6 vs. Region 9
D1 FS(-TGF-β3)	9 (p=0.12)	none	6 (p=0.025)	none
D21 FS(-TGF-β3)	none	none	none	none
D21 FS(+TGF-β3)	5, 6, 9 (p<0.000)	none	5, 6, 9 (p<0.000)	none
D21 Dyn(+TGF-β3)	5, 6 (p<0.000)	5, 6 (p<0.000)	5 (p=0.024), 6 (p=0.004)	none
D42 FS(-TGF-β3)	none	none	none	none
D42 FS(+TGF-β3)	5 (p=0.002), 6 (p<0.000), 9 (p<0.000)	5 (p=0.001)	5, 6, 9 (p<0.000)	none
D42 Dyn(+TGF-β3)	5, 6 (p<0.000)	5, 6 (p<0.000)	none	none
D63 FS(-TGF-β3)	none	none	5 (p=0.021), 6 (p=0.021)	none
D63 FS(+TGF-β3)	6 (p=0.002), 9 (p<0.000)	none	6 (p=0.009), 9 (p=0.005)	none
D63 Dyn(+TGF-β3)	none	5 (p=0.009), 6 (p=0.014)	5 (p=0.001), 6 (p<0.000)	5 (p=0.033), 6 (p=0.010)

To better understand the implications depth-dependent strain profiles had on compressive properties, we calculated the local modulus through the depth on Day 63 (**Figure 3-3C**). Both chondrocyte and MSC-laden constructs cultured in the presence of TGF-β3 in free swelling conditions (FS(+TGF-β3)) had depth dependent moduli. In each case, the most superficial zone (Region 2) was stiffer than center and bottom regions (5, 6, and 9, p<0.001). However, between cell types, the extent to which the local moduli values decreased was strikingly different. While there was an ~3.5-fold decline in modulus from Region 2 to Region 5 for chondrocyte-laden constructs, MSC-laden constructs showed an ~11.5-fold decrease in modulus. Furthermore, the lowest local modulus value for free swelling MSC-laden constructs cultured with TGF-β3 was 141 kPa, whereas the lowest value for chondrocyte-laden constructs was 341 kPa, both in Region 7. Of note, however, in the most superficial zone, MSC-laden and chondrocyte-laden constructs had moduli that were not different from one another (p=0.877).

Dynamic culture resulted in a shift in this depth dependency, where the deepest region (Region 9) was no longer different from the most superficial region (Region 2) for MSC-laden constructs. However, under these dynamic conditions, the differences between MSC-laden constructs and chondrocyte-laden constructs within the central regions were further accentuated (**Figure 3-3C**). In Regions 5 and 6, moduli for MSC-laden constructs increased compared to free swelling conditions (from 217 and 153 kPa to 399 and 397 kPa in Regions 5 and 6, respectively) (**Figure 3-4**). However, central regions of chondrocyte-laden constructs remained significantly higher ($p < 0.01$) than MSC-laden constructs cultured identically, achieving 519 and 341 kPa in free swelling conditions and 1553 and 1478 kPa in dynamic culture conditions (Regions 5 and 6, respectively).

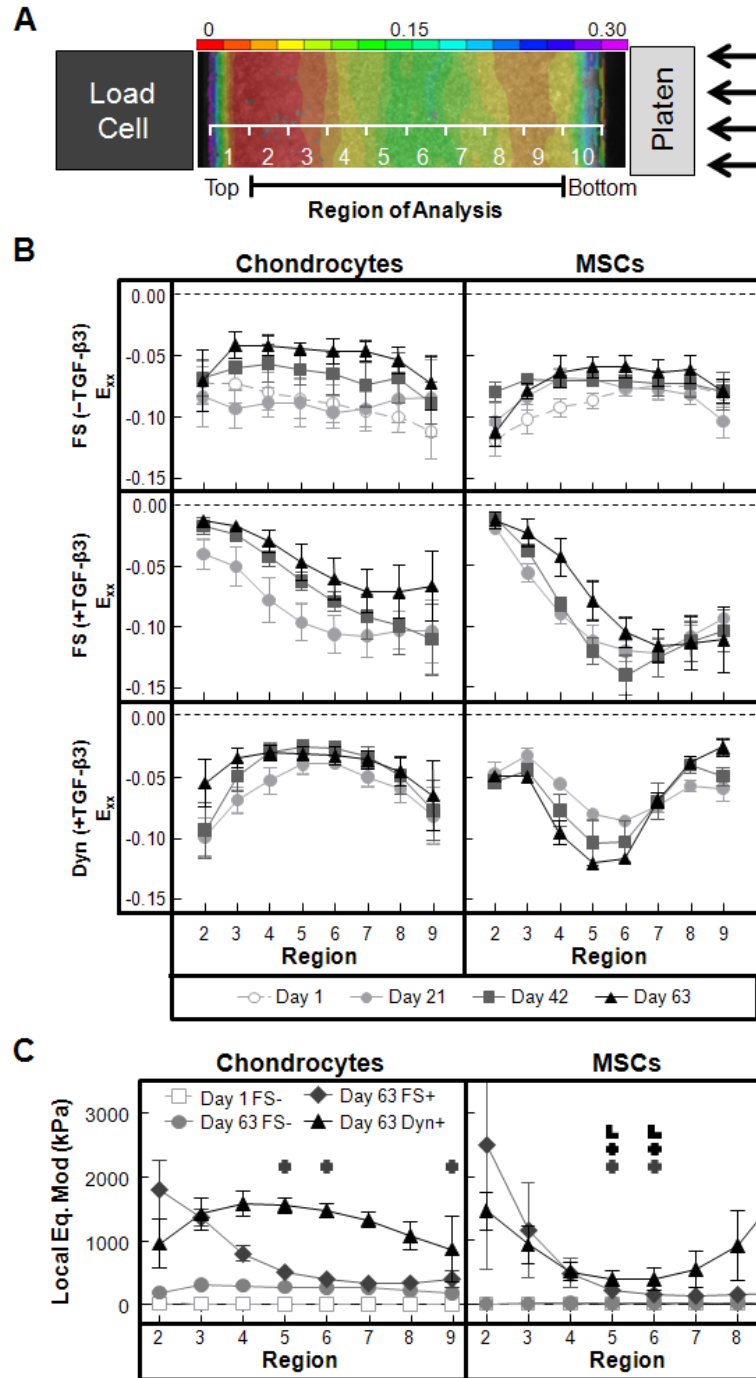


Figure 3-3: Assessment of local compressive strain and equilibrium modulus. (A) Schematic of microscopic strain application and region of analysis with overlay of Vic2D E_{xx} strain contour plot. (B) Compressive Lagrangian strain (E_{xx}) through the depth of constructs as a function of time, cell type, and culture condition. Unique strain plot profiles developed as early as Day 21 and persisted through Day 63. (C) Day 63 local equilibrium modulus profiles as a function of cell type and culture condition. Dynamic culture reduced depth dependency in chondrocyte-laden constructs, but not for MSC-laden constructs, especially in the central regions. (■ vs. Region 2; ■ vs. Region 9, $p < 0.05$). $n = 5$

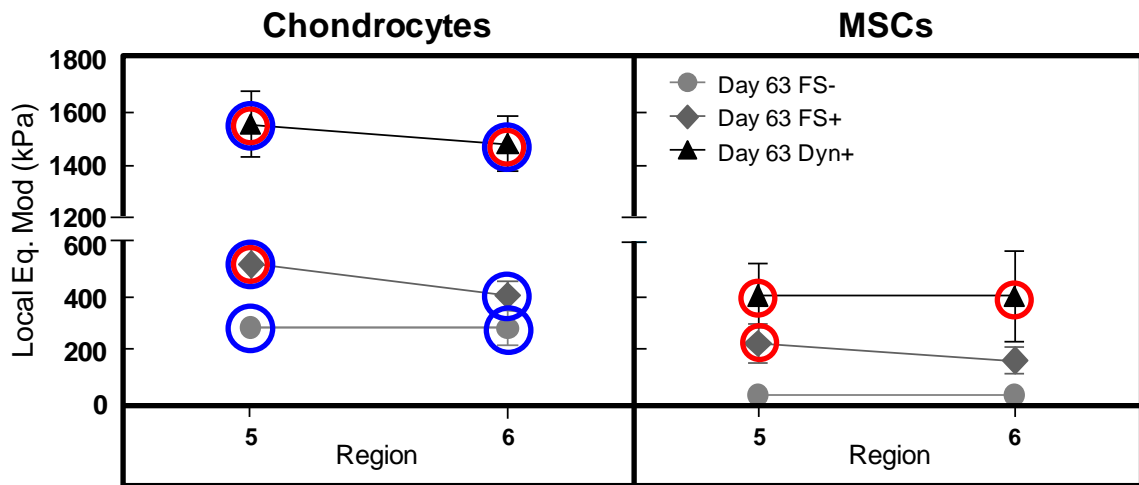


Figure 3-4: Scale adjustment for local equilibrium modulus in Regions 5 and 6 (Figure 3-3). (red circle vs. all lower within region and cell type; blue circle vs. MSCs cultured identically, $p < 0.05$)

3.3.3 Regional Matrix Distribution And Content

To determine the compositional basis of these depth dependent mechanical properties, the distribution of the principal cartilage extracellular matrix elements (i.e. proteoglycans and collagens) was assessed. Histological analysis showed that, after 63 days of culture, punctate pericellular accumulations of proteoglycans were present in both chondrocyte- and MSC-laden constructs in FS(-TGF- β 3) conditions, with less overall staining in the MSC-laden constructs (**Figure 3-5**). There was a marked increase in overall staining intensity for MSC-laden FS(+TGF- β 3) constructs compared to constructs cultured without TGF- β 3. Quantification of staining intensity through the depth yielded a profile that mirrored that of the local equilibrium modulus, with the most intense staining near the top surface of the construct. Interestingly, depth dependence in staining intensity was not observed in chondrocyte-laden FS(+TGF- β 3) constructs, despite the measured depth-dependent mechanical profiles in these constructs. This finding may reflect limitations in

the range over which Alcian Blue staining can effectively discriminate between proteoglycan levels. Nevertheless, Alcian Blue staining intensity for both cell types in dynamic culture mirrored the measured mechanical profiles. Both MSC- and chondrocyte-laden Dyn(+TGF- β 3) constructs had the least intense staining right at the periphery of the constructs, indicating potential proteoglycan loss and/or dedifferentiation at this border. While chondrocyte-laden Dyn(+TGF- β 3) displayed the most intense staining in the central regions, the central-most regions of MSC-laden Dyn(+TGF- β 3) constructs had lower staining intensity compared to regions closer to the construct border.

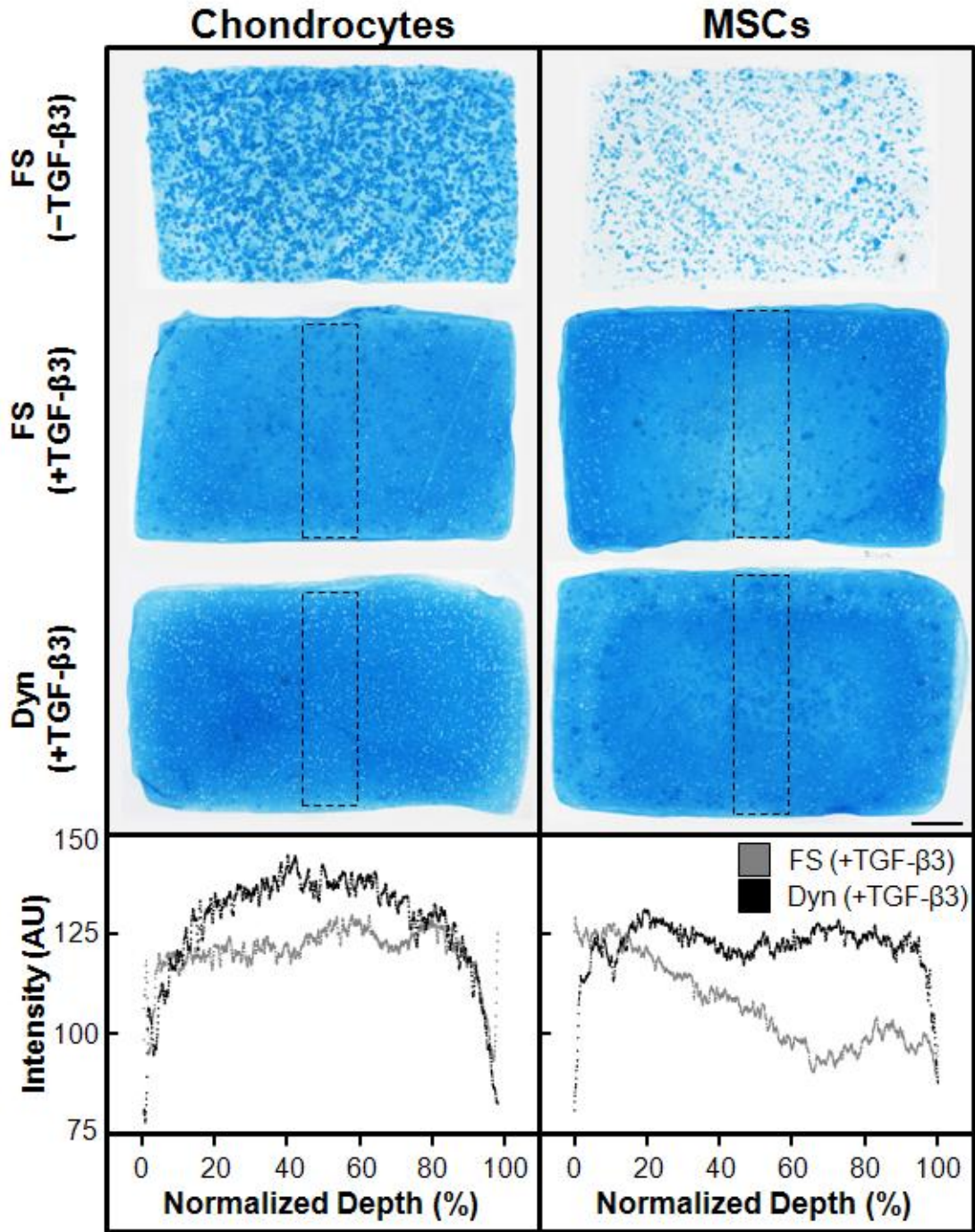


Figure 3-5: (Top) Day 63 Alcian Blue staining of proteoglycans (PGs) as a function of cell type and culture condition. Dotted rectangle indicates area of intensity plot profiles. Scale bar = 500 μm . (Bottom) Stain intensity profiles of free swelling and dynamically cultured constructs in the presence of TGF- β 3. PG staining intensity mirrors local equilibrium modulus profiles with the exception of chondrocyte-laden FS(+TGF- β 3) constructs.

Similarly, inhomogeneous staining of collagens was observed, with the most intense staining occurring at the periphery of MSC-laden Dyn(+TGF- β 3) constructs (**Figure 3-6**). Immunohistochemical staining of these sections (data not shown) revealed intense type II collagen staining and very low, cell-associated, type I collagen staining for all constructs cultured in the presence of TGF- β 3.

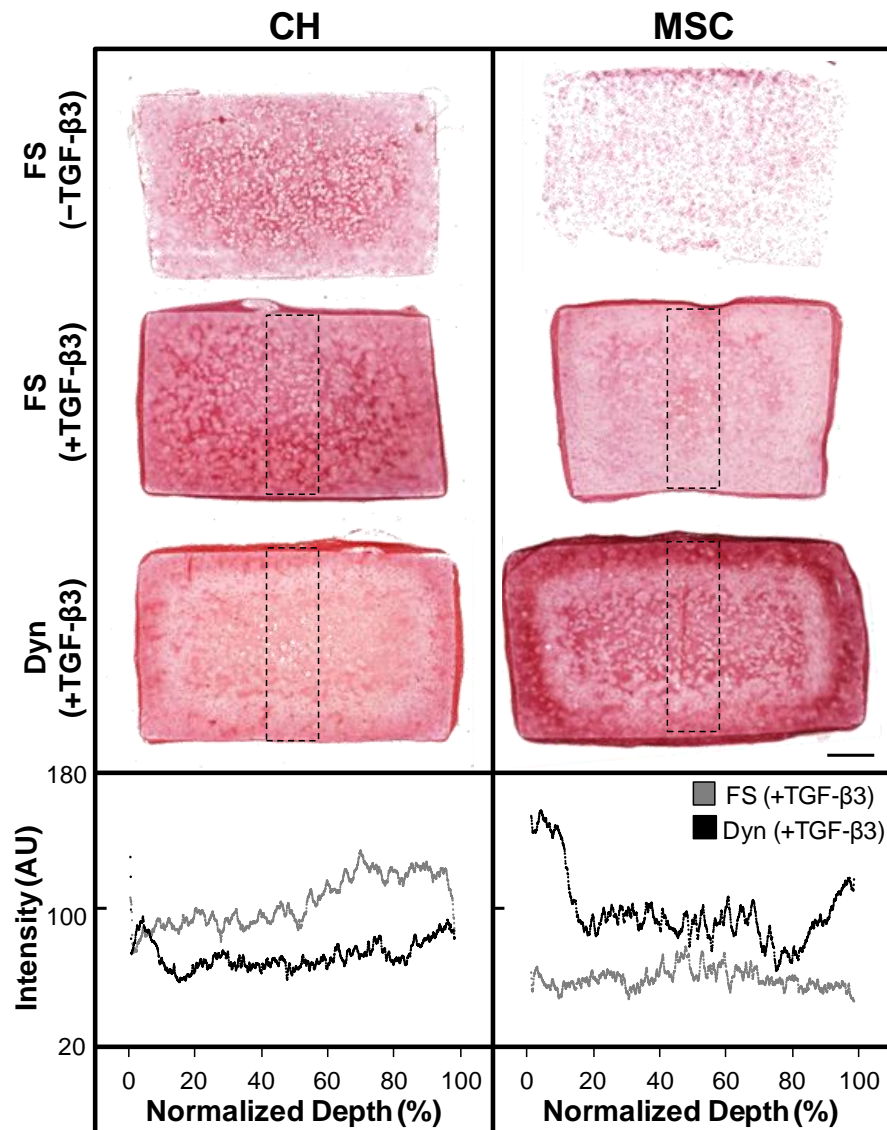


Figure 3-6: (Top) Day 63 Picrosirius Red staining of collagen as a function of cell type and culture condition. Dotted rectangle indicates area of intensity plot profiles. Scale bar = 500 μ m. (Bottom) Stain intensity profiles of free swelling and dynamically cultured constructs in the presence of TGF- β 3.

Regional quantification of glycosaminoglycan (GAG) and collagen content supported these histological findings. GAG content in chondrocyte-laden constructs was relatively uniform in the four regions of the construct assayed, regardless of culture condition and time, with the exception of chondrocyte-laden Dyn(+TGF- β 3) constructs, where GAG levels were ~5.2% in the core regions, but only ~3.5% in the annulus regions (**Figure 3-7**). MSCs in free swelling culture without TGF- β 3 failed to produce appreciable amounts of GAG. Free swelling culture in the presence of TGF- β 3 resulted in inhomogeneous GAG production by Day 63, with the bottom core region of the construct having significantly lower GAG content (1.8%) than the remaining three portions of the construct (top annulus = 4.4%; top core = 3.3%; bottom annulus = 3.6%; $p < 0.05$). Of note, in the top annulus region, FS(+TGF- β 3) MSC-laden constructs had significantly higher GAG content than this same region in chondrocyte-laden constructs at Day 63. Dynamic culture reduced this region dependency in GAG content in these MSC-laden constructs. Day 63 assessment of collagen content showed relatively low levels of collagen (<1%) and little region dependency, regardless of cell type and culture condition (**Figure 3-8**).

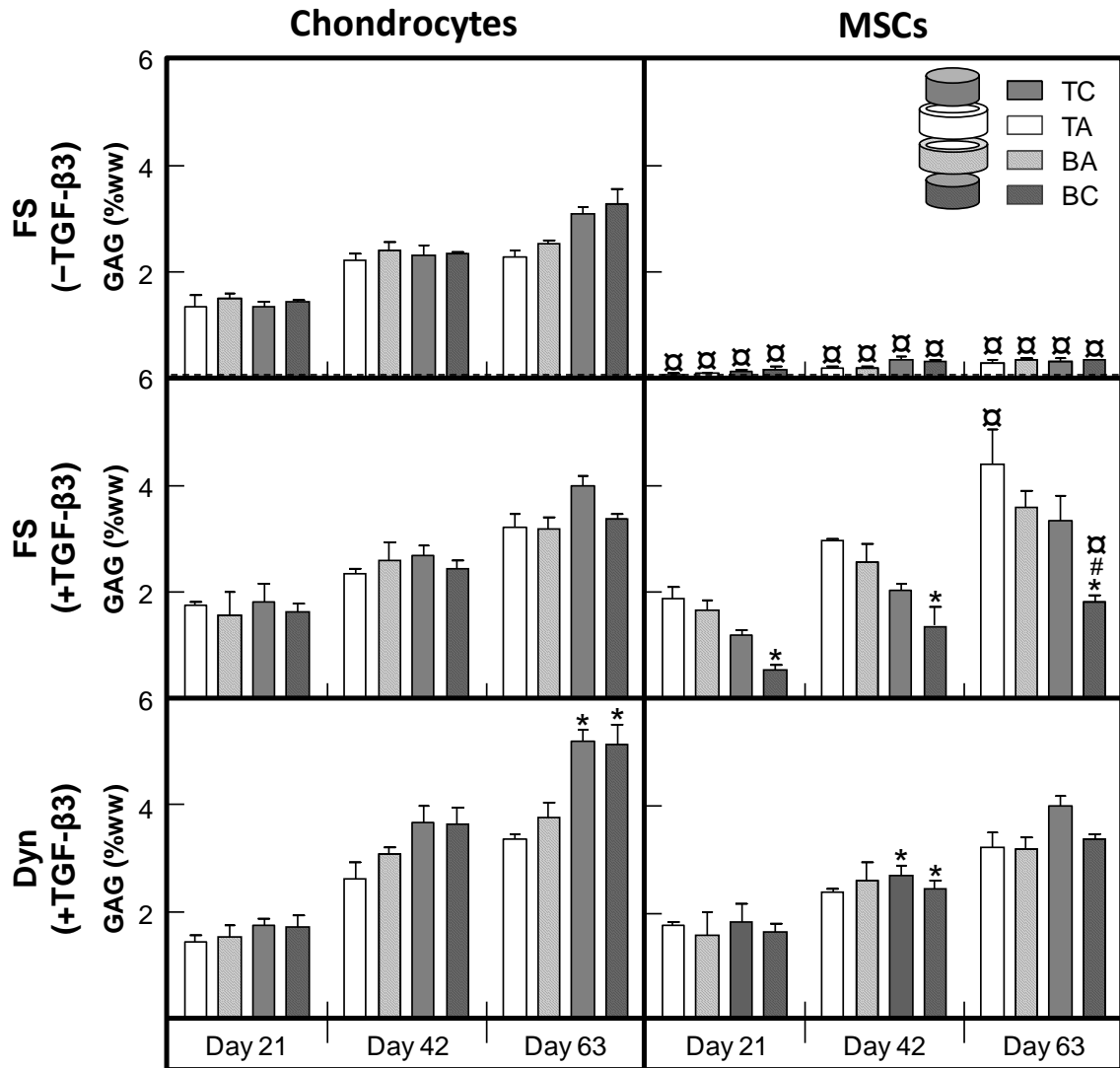


Figure 3-7: Glycosaminoglycan (GAG) content (normalized by wet weight) as a function of region, time, cell type, and culture condition. Chondrocyte-laden constructs had a relatively homogenous GAG distribution. GAG content of MSC-laden constructs was highly dependent on region; GAG content regionality was relieved with dynamic culture. (# vs. top of the same group; * vs. annulus of the same group; □ vs. chondrocyte of the same region cultured identically, $p < 0.05$). $n = 3$

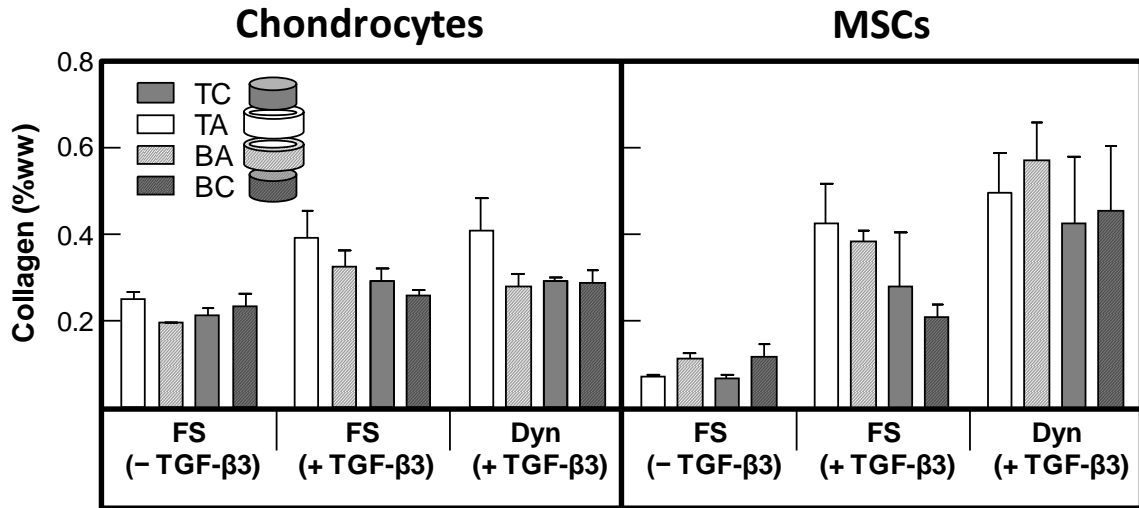


Figure 3-8: Collagen quantification (normalized to wet weight) in Day 63 constructs indicated low levels of collagen regardless of cell type, culture condition, and region. n = 3.

3.3.4 Overall and Regional Chondrocyte and MSC Viability

To identify the underlying cellular mechanisms responsible for the establishment of these gradients in matrix deposition and depth-dependent mechanical properties, we next quantified cell viability as a function of time, location, cell type, and culture condition. Day 1 aggregate viability (the percent cell viability in all five regions) for chondrocyte-laden and MSC-laden constructs was high (88% and 82%, respectively, **Figure 3-9A**). With increased culture duration, viability in chondrocyte-laden constructs did not significantly change from Day 1 values in any culture condition. Conversely, there were marked decreases in viability for all culture conditions in MSC-laden constructs. As early as Day 21, viability declined to 40% in FS(-TGF-β3) conditions, 41% in FS(+TGF-β3) conditions, and 67% in Dyn(+TGF-β3) conditions. Although viability in MSC-laden Dyn(+TGF-β3) conditions on Day 21 was ~1.5-fold higher than FS(+TGF-β3), these values declined with time such that differences were no longer significant by Day 63

(**Figure 3-9A, B**). Regional assessment of viability on Day 63 showed a depth-dependent decline in viability in MSC-laden FS(+TGF- β 3) constructs from the top surface to the central and bottom regions (**Figure 3-9C**). Dynamic culture maintained an equivalent viability through the depth, though levels were markedly lower than Day 1 in every region. TUNEL staining for apoptosis on Day 21 (**Figure 3-10**) revealed a low percentage of apoptotic chondrocytes within the center of the constructs, regardless of culture condition. Conversely, a marked increase in TUNEL-positive cells was observed in MSC-laden constructs under free swelling conditions. In Dyn(+TGF- β 3) conditions, fewer TUNEL-positive MSCs were observed in the center of constructs.

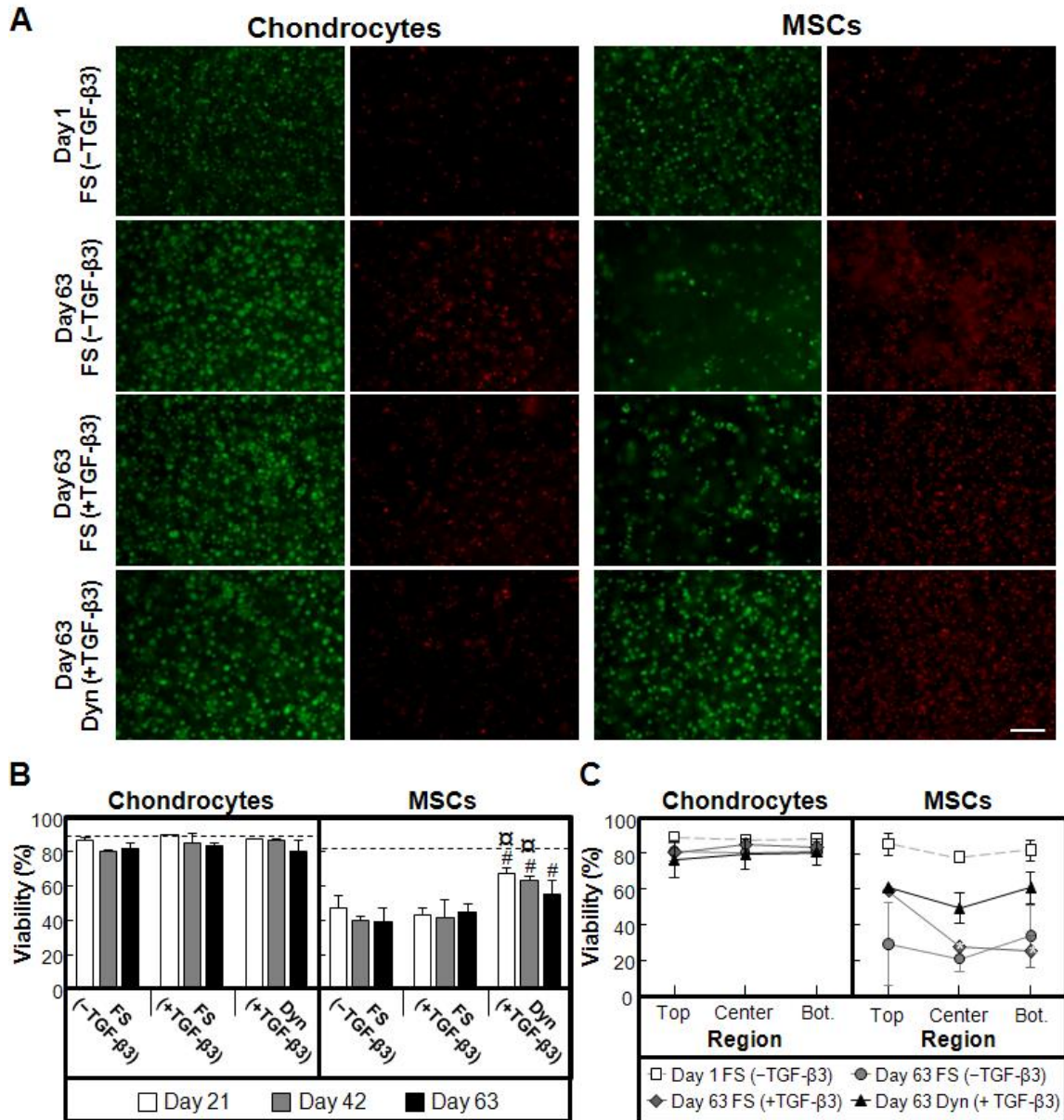


Figure 3-9: Assessment of cell viability. (A) Central images of bisected constructs of both viable (green, left column) and dead (red, right column) cells. Scale bar = 100 μ m. (B) Quantification of aggregate viability (from all five regions) as a function of time showed that chondrocyte viability remained relatively stable, while MSC viability declined significantly from Day 1 values. Dotted line denotes mean Day 1 viability. (# vs. FS(-TGF- β 3); \square vs. FS(+TGF- β 3), $p < 0.05$). (C) Analysis of viability through the depth of the constructs on Day 63 revealed a significantly lower percentage of viable cells in the center and bottom regions of MSC FS(+TGF- β 3) constructs compared to the top region. (* vs. Top, $p < 0.05$). $n = 3$

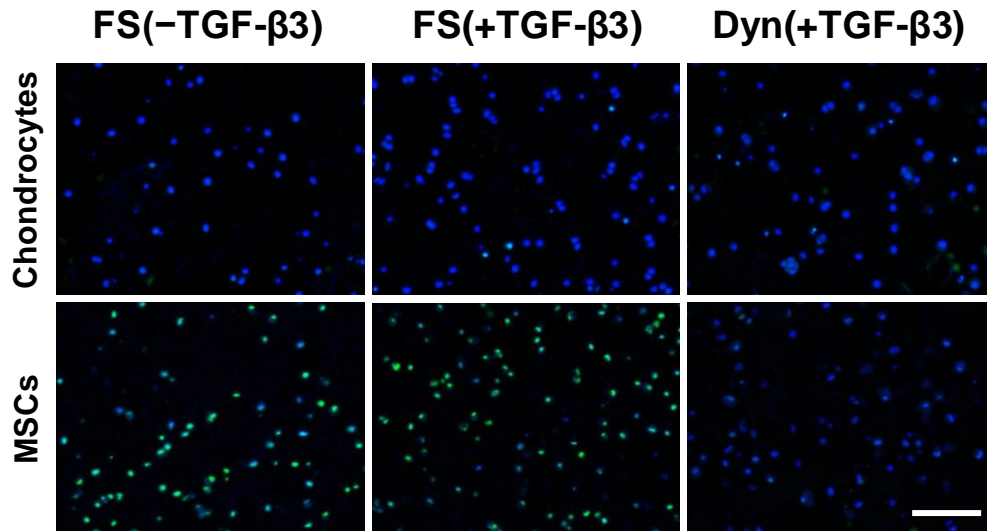


Figure 3-10: TUNEL staining (green) in Day 21 MSC-laden free swelling constructs (central region of the construct) suggests an increase in the number of apoptotic cells at this early time point. DAPI counterstain (blue). Scale = 100 μ m

3.4 Discussion

It is widely accepted that adult-derived MSCs hold promise for regenerative medicine and tissue engineering applications. Their utility has been proven in instances where the demands placed on the engineered system, whether mechanical or metabolic, are modest or supplemental in nature. For example, recent reports show that MSCs can successfully generate tissue-like mimics that reconstitute (or supplement) *in vivo* function (e.g. in the cartilaginous trachea (Macchiarini et al., 2008) or in myofibrous conduits (Dolgin, 2011)). However, these same cells fail to achieve functional parity with native tissue cells when more considerable functional demands are placed on the regenerate structure. For example, we and others have noted a striking deficiency in tissue engineered cartilage produced from MSCs relative to that produced by chondrocytes (Erickson et al., 2009a; Huang et al., 2010a; Mauck et al., 2006), where the bulk mechanical properties of MSC-based constructs are ~50% lower than that of chondrocyte-based constructs cultured

identically. Moreover, on a molecular level (assessed across an entire construct), MSCs in 3D culture fail to fully establish the chondrogenic phenotype (Huang et al., 2010c), with the timing and magnitude of several hundred genes differentially regulated even after long periods of chondrogenic induction. This marked disparity in bulk expression likely contributes to the failure of these cells to produce a functional extracellular matrix.

A further complexity of these 3D culture systems is the spatially varying nutrient gradients that arise as a result of diffusional constraints and nutrient utilization at the construct boundaries. Such gradients in nutrient supply likely result in spatially and temporally varying levels of both nutrients and chondrogenic induction factors, and so, differences in local matrix formation. If chondrogenic MSCs are less able than chondrocytes to function under nutritional constraints, then gradients would tend to exacerbate differences between constructs formed from these two cell types. To investigate this possibility, the goal of this study was to quantify and compare the local properties of chondrocyte- and MSC-laden agarose constructs so as to better understand the underlying mechanisms that currently limit the clinical application of MSC-based engineered cartilage.

To carry out this study, we evaluated spatial and temporal production of extracellular matrix, and measured the local (depth dependent) properties of constructs via microscopic mechanical analysis. Here we show that, consistent with previous findings, the bulk properties of free-swelling MSC-laden constructs (cultured with TGF- β 3) increase with time, but plateau at a level significantly lower than chondrocytes.

Microscopic analysis of local properties illustrated several important points that were not fully appreciated with macroscopic testing. First, the properties of all free-swelling constructs (both MSC- and chondrocyte-based) were depth-dependent, with the highest properties measured at the top surface of the construct (where maximal nutrient exchange would be expected). Most interestingly, comparing properties within this superficial region, we found that MSC-based constructs matched or exceeded that of chondrocyte-based constructs. These data indicate that MSCs are in fact capable of producing mechanically robust tissue, but can do so only under these optimal conditions. A second important finding emerged when we reduced diffusional constraints (by limiting unstirred layers with orbital shaking). Under these dynamic conditions, bulk properties of MSC-laden construct increased substantially, with local analysis showing equivalent properties between both chondrocytes and MSCs in both the superficial and deep zones. However, within the central region of MSC-based constructs, properties remained significantly lower than that of chondrocyte-based constructs cultured identically. When cultured under dynamic conditions, chondrocyte-based constructs achieved a high and nearly linear profile in mechanical properties through the depth, while markedly lower properties persisted in the center of MSC-based constructs. This observation was supported by both semi-quantitative analysis of proteoglycan deposition through the depth, as well as regional analysis of biochemical constituents. Despite the measured depth-dependent mechanical profiles of chondrocyte-laden FS(+TGF- β 3) constructs, proteoglycan deposition assessed by Alcian Blue staining appeared relatively uniform. It is not clear whether this represents limitations in the sensitivity of this assay (i.e. inability to discriminate between higher concentrations of proteoglycan), or whether it suggests

the presence of additional matrix components or structural organization that is critical for mechanical function. Furthermore, low proteoglycan staining intensity was observed at the very periphery of both dynamically cultured MSC and chondrocyte-laden constructs. One possible explanation for this may be loss of proteoglycans due to agitation of the constructs. However, as GAG content in the media was not measured, additional factors such as altered regional GAG production due to shear fluid forces at the periphery cannot be ruled out, and future studies on this topic are warranted.

From the MSC data, it was clear that the distance from the free edge is a critical determinant of matrix formation (and hence functional properties), and that these gradients were at least in part governed by diffusion limits in this 3D system. Cells far from a nutrient supply may either fail to fully differentiate (lacking a sufficient supply of pro-chondrogenic factors), or be so starved for nutrients that they fail to form matrix even after the differentiation event has occurred. This is an important and not often discussed feature of MSC chondrogenesis. That is, not only must MSCs differentiate to achieve anabolic functionality (i.e. matrix production) matching chondrocytes, but they also must function in a constrained and nutrient poor environment; this being a hallmark of how a chondrocyte operates in native cartilage tissue (Mobasheri et al., 2005; Schipani et al., 2001). In one recent study, it was reported that nutrient availability can impact the growth of even chondrocyte-based constructs, where, below a certain nutrient threshold, viability was markedly compromised within the center of constructs (Heywood et al., 2006; Heywood et al., 2004). Based on this, we quantified MSC viability throughout the construct depth, as a function of time, presence of TGF- β 3, and culture condition (static

versus dynamic). Remarkably, while chondrocytes had a relatively stable level of viability overall and in each region of the construct, MSC-based constructs showed dramatic decreases in viability from Day 1 levels for all culture conditions and within all regions. While viability was poor overall without chondrogenic induction (i.e. without TGF- β 3), striking declines in viability were noted within the central regions of free-swelling constructs, even when cultured with TGF- β 3. Of further note, these decreases in viability and positive TUNEL staining were present as early as 21 days into culture, at a time where depth dependent strain profiles were already established. Follow up studies (not shown), demonstrated that these declines in viability, and initiation of apoptotic cascades, begin as early as one week into culture, well before appreciable matrix has been deposited.

One further interesting observation of this study was that not every MSC within the central regions of constructs underwent cell death. Even under the most demanding conditions (central and bottom regions of free swelling constructs), a minor population survived, underwent chondrogenesis and produced matrix that was increasingly functional with time. It is well-appreciated that marked heterogeneity in differentiation potential exists in adult stem cell populations (Halleux et al., 2001; Mareddy et al., 2007; Okamoto et al., 2002; Pittenger et al., 1999; Russell et al., 2010). This heterogeneity in differentiation potential may have translated to heterogeneity in survival under these challenging microenvironmental conditions. The MSC sub-population that remained viable in the center of the constructs may represent a fraction of cells uniquely suited to take on the chondrogenic phenotype, addressing both anabolic and metabolic demands of

tissue formation and *in vivo* function. For effective clinical repair or replacement of cartilage, a tissue analog must maintain its homeostatic state and appropriately remodel within the implant site. Cartilage is avascular and relies on diffusion for all nutrient exchange. If a portion of the MSC population is unable to survive *in vitro* in these constructs, where the nutritional gradients produced are created solely from cell utilization, the effects will likely be exacerbated when exposed to the low nutrient, low oxygen conditions of the synovial joint. Thus, identification of this subpopulation may be a critical step in furthering our goal of achieving a viable cell population throughout the construct, and improving chondrogenesis for *in vitro* and *in vivo* application.

Overall, this work demonstrates that MSCs are capable of creating robust and mechanically functional extracellular matrix that is comparable to chondrocytes in 3D culture. However, our findings also show that MSCs can only function in this manner in regions with ample nutrient supply. Although dynamic culture increased the mechanical properties of MSC-laden constructs on a macroscopic level, the marked decrease in mechanical properties through the depth revealed that persistent differences remain between the two cell types. The observed decreases in cell viability provide some explanation for the mechanical deficits we measured, and point to a new frame of reference by which to judge the efficiency of chondrogenic induction. On a molecular level, anabolic function by MSCs is robust, while their ability to function and persevere in a constrained environment appears to be lacking. As nutrients are consumed from the edge of the construct to the center, a condition of low glucose, low oxygen, and absence of chondrogenic factors would likely be present. Chondrocytes are well suited to operate

in this context, with robust pathways (including hypoxia inducible factor-1alpha (Schipani et al., 2001) and glucose transporters (Mobasheri et al., 2005) that are tuned for operation in this native state of duress. While the prochondrogenic effects of low oxygen tension have been noted (Adesida et al., 2012), MSCs within the center of the constructs would likely experience both low oxygen and low nutrient conditions, the combinatorial effect of which has been shown to cause marked cell death in this cell type (Potier et al., 2007).

Differences in nutrient consumption and waste production rates between chondrocytes and MSCs may in fact be creating such gradients, providing drastically different microenvironments within individual constructs. If MSCs utilize vital resources in a differential manner compared to chondrocytes, particularly if they have higher anabolic activity as it appears they may at the periphery, conditions in the center of constructs would be further exacerbated. If nutrient consumption at the periphery could be attenuated slightly, or physical conduits (channels) were provided to improve media access to the center (Bian et al., 2009; Buckley et al., 2009), the health of the MSC population in the center of the constructs might be preserved at early time points. That some MSCs do survive and thrive under these conditions, however, speaks to the overall heterogeneity of these stem cell populations, and suggests that proper sorting of cells, based on anabolic and metabolic chondrogenic efficiency, may yield improved *in vivo* tissue regeneration through an optimized cell population. Taken together, these data better identify crucial underlying mechanisms that have limited the clinical potential of

chondrogenic MSCs, and provide new strategies for bringing stem cell-based cartilage tissue replacements to the clinic.

CHAPTER 4: FUNCTIONAL PROPERTIES OF MSC-BASED ENGINEERED CARTILAGE ARE UNSTABLE WITH VERY LONG TERM IN VITRO CULTURE

4.1 Introduction

Differences between MSC- and chondrocyte-based engineered constructs have been investigated on the molecular, microscopic tissue, and macroscopic tissue level (Boeuf et al., 2008; Erickson et al., 2012; Farrell et al., 2012; Huang et al., 2010c). Multiple studies have noted that MSC-based constructs increase in content and properties for a period of time, before reaching a plateau in cartilage-like ECM content and macroscopic (whole tissue level) equilibrium mechanical properties (Huang et al., 2010a; Mauck et al., 2006; Vinardell et al., 2012). Our previous studies showed that this plateau and the resultant lower properties in MSC-laden construct properties (in comparison to chondrocyte-laden constructs) was due in part to the lack of tissue elaboration and compromised stem cell health in central regions of constructs that were deprived of nutrients (Chapter 3). This deficit could be partially rescued by increasing nutrient supply via exposure to dynamic culture systems (i.e. orbital shaking) that improved nutrient access. However, even with this modification, the mechanical properties of MSC-laden constructs remained significantly lower than chondrocyte-laden constructs cultured similarly.

One potential reason for the lack of mechanical equivalence between engineered cartilage constructs formed from MSCs and chondrocytes may simply be that a lag exists during

which MSCs differentiate to the chondrogenic state. Chondrocytes, and the tissue they produce, are exposed to a number of soluble and mechanical factors through development, which culminates over a period of years in a tissue with refined properties (Koyama et al., 2008; Williamson et al., 2001). Conversely, engineered tissues based on MSCs are forced to undergo both differentiation and maturation within an abbreviated time scale. Notably, MSC-based constructs appear to respond negatively to dynamic loading early in culture (Thorpe et al., 2008), but respond in a positive fashion after a brief period (1-3 weeks) of differentiation (Huang et al., 2010a; Mouw et al., 2007). Supporting this notion, whole genome profiling revealed that many genes remain differentially regulated between MSCs and chondrocytes cultured in agarose after 28 days (Huang et al., 2010c). However, gene expression remained dynamic through day 56, suggesting that MSCs may have the capacity to continue towards a more chondrogenic state with prolonged culture. Thus the disparity in mechanical properties might be a function of insufficient time to achieve the chondrogenic state, rather than an innate limitation in cartilage-forming potential by MSCs. An alternative explanation for the disjunction between chondrocyte and MSC-based engineered cartilage may lie in the completeness of phenotypic conversion as discussed in Chapter 2.

Collectively, these data suggest that assessment of cartilage tissue development over a longer period, within a highly controlled chemical environment, will be required to fully appreciate both the potential of these engineered tissues, and to further their *in vivo* efficacy. The purpose of this study was therefore to evaluate the long-term time course of cartilage development and phenotypic stability in MSC- and chondrocyte-laden three-

dimensional agarose hydrogel constructs. We evaluated the cartilage-like properties of these constructs in both free-swelling and dynamic culture (to increase nutrient supply) over a long *in vitro* culture period (4 months). Furthermore, to investigate material dependency, we assessed whether the long-term chondrogenic tissue development and phenotypic stability differed in an alternative 3D hydrogel system (photocrosslinkable hyaluronic acid (HA) (Burdick et al., 2005; Chung et al., 2008; Erickson et al., 2009b). We hypothesized that a lack of inherent potential, rather than simply a lag phase in tissue production, governs the long term maturation of MSC-laden constructs. We further hypothesized that MSC-based constructs would achieve a stable equilibrium state (in terms of mechanics and biochemical content) that was lower than chondrocyte-based constructs similarly maintained.

4.2 Materials and Methods

4.2.1 Study 1: Long-Term Culture of Cell-Seeded Agarose Hydrogels

Juvenile bovine bone marrow derived MSCs were isolated from the femurs of three donor calves (3-6 months old; Research 87, Boylston, MA) (Mauck et al., 2006) and expanded through passage 2 in medium consisting of high glucose Dulbecco's modified Eagle medium (DMEM; Gibco, Invitrogen Life Sciences, Carlsbad, CA), 10% fetal bovine serum (FBS, Gibco), and 1% penicillin-streptomycin-fungizone (PSF; Gibco). Primary chondrocytes were isolated from the carpometacarpal joint of the three donors. Briefly, cartilage was diced and subjected to pronase digestion (2.5 mg/mL, 1 hr @ 37°C, Calbiochem/EMD Chemicals, Gibbstown, NJ) followed by collagenase digestion (0.5 mg/mL, 6 hrs @ 37°C, Sigma-Aldrich, St. Louis, MO) (Mauck et al., 2003b). Expanded

MSCs and freshly isolated chondrocytes were independently encapsulated in 2% agarose at a density of 20 million cells/mL. Specifically, a cell suspension (40 million cells/mL in a chemically defined media) was homogenously mixed with molten 4% w/v agarose (type VII (Sigma), 49°C) at a 1:1 ratio and cast between two parallel plates (Mauck et al., 2003b; Mauck et al., 2006). Constructs 4 mm in diameter and 2.25 mm in depth were extracted from the hydrogel slab using a biopsy punch. Constructs were fed twice weekly with chemically defined media with (+) or without (-) supplementation of 10 ng/mL transforming growth factor-beta 3 (TGF- β 3; R&D Systems, Minneapolis, MN). Chemically defined media consisted of high glucose DMEM, PSF, dexamethasone, ascorbate 2-phosphate, insulin, transferrin, selenous acid, bovine serum albumin, and linoleic acid as in Chapter 3. Constructs were cultured in free swelling (FS) or dynamic conditions (Dyn) through 112 days. For dynamic culture, constructs were exposed to continuous orbital shaking at 1.2 Hz (Bellco 115V Orbital Shaker, Bellco Glass, Inc., Vineland, NJ). Throughout the remainder of this chapter, FS(+) or Dyn(+) refers to constructs in free swelling or dynamic conditions with TGF- β , while FS(-) and Dyn(-) refers to constructs under those same conditions without TGF- β . CM(-) and CM(+) denote groups cultured without or with TGF- β , regardless of free swelling or dynamic conditions.

4.2.2 Study 1: Mechanical Analysis of Bulk Properties

Mechanical properties of constructs (n=5) were assessed via uniaxial unconfined compression (Mauck et al., 2000). First, constructs were equilibrated under creep (tare load for Days 1-28=2 g; Day 56=5 g; Day 112=10 g) for 300 sec. Stress relaxation tests

were carried out by applying 10% strain at a strain rate of 0.05%/sec followed by a 1000 sec relaxation phase. Stress relaxation data was curve fit with a double exponential decay function using a custom MATLAB script (**Appendix 2**). Equilibrium modulus was calculated from equilibrium load and sample geometry. After stress relaxation, a 1% sinusoidal strain was applied at 1 Hz, and the dynamic modulus was calculated from the dynamic stress-strain response. Tested samples were frozen at -20°C for subsequent biochemical assessment.

4.2.3 Study 1: Histological Analysis

Construct halves (n=2) were fixed in 4% paraformaldehyde (FD NeuroTechnologies, Inc, Ellicott City, MD), paraffin processed following dehydration with a series of ethanol solutions, and sectioned (8 μm). After rehydration, sections were stained for proteoglycans (Alcian Blue, Rowley Biochemical, Inc, Danvers, MA) or collagens (stained after 1 hr hyaluronidase incubation [1 mg/ml] at 37°C (Melrose et al., 2004); Picrosirius Red [Sirius Red (Sigma), Picric Acid (Fisher Scientific)]). Alizarin Red (Rowley Biochemical) staining was performed to identify calcium deposits. Finally, immunohistochemistry was performed to discriminate between type I and type II collagen deposition. Specifically, deparaffinized sections were rehydrated and subjected to proteinase K antigen retrieval for 15 min at 37°C . Sections were then incubated with either a type II collagen antibody (5 $\mu\text{g}/\text{mL}$; Developmental Studies Hybridoma Bank, University of Iowa, Iowa City, IA) or a type I collagen antibody (10 $\mu\text{g}/\text{mL}$; anti-collagen type I Antibody, clone 5D8-G9, Millipore) for 1 hr. After washing, signal was detected

using the Millipore Immunoperoxidase Secondary Detection System (EMD Millipore Corporation, Billerica, MA) per the manufacturer's protocol.

4.2.4 Study 1: Biochemical Analysis

Matrix components were solubilized via papain digestion at 60°C for 24 hours (20 µl papain per 1 mL buffer [0.1 M sodium acetate, 10 M cysteine HCl, 0.05 M ethylenediaminetetraacetic acid, pH 6.0]). Glycosaminoglycan (GAG) content was quantified using the 1,9-dimethylmethylene blue dye-binding assay (Farndale et al., 1986), and collagen content quantified using the orthohydroxyproline assay (Stegemann and Stalder, 1967). An OHP:collagen correction factor of 7.14 was used to convert µg of OHP to µg of collagen (Neuman and Logan, 1950).

4.2.5 Study 1: Quantification of Viability

Using the LIVE/DEAD Cell Viability Assay Kit for mammalian cells (Molecular Probes, Invitrogen, Life Sciences), construct halves (n=3) were stained for 30 min in PBS. Calcein-AM and ethidium-homodimer-1 signal were acquired in the central region of the construct under 10X magnification. A custom MATLAB script (The MathWorks Inc, Natick, MA) was used to count the number of cells within each channel, from which percent viability was calculated (Chapter 3).

4.2.6 Study 2: Long-Term Culture of Cell-Seeded Hyaluronic Acid Hydrogels: Hyaluronic Acid Hydrogel Formation and Cell Encapsulation

MSCs (2 donors) were isolated and expanded through passage 2 as in Study 1. Cells were suspended at a density of 60 million cells/mL in a 1% (w/v) methacrylated hyaluronic acid (HA) solution that was subsequently crosslinked into a hydrogel via a UV light initiated addition reaction. The HA hydrogel methacrylation process and UV cell encapsulation process were previously described in (Burdick et al., 2005; Chung et al., 2008; Erickson et al., 2009b). Constructs were fed thrice weekly with 1 mL/construct of CM+ through 126 days of culture in free swelling conditions.

4.2.7 Study 2: Mechanical, Biochemical, and Histological Analyses

Using a cryotome, the top and bottom of each construct was leveled. Compressive equilibrium modulus was evaluated (n=4) via unconfined compression as described in Study 1 (creep tare load = 2 g for all time points assessed). Following testing, samples were papain digested and assessed for glycosaminoglycan and collagen content as described in Study 1. Paraffin processed sections were stained for collagens (Picrosirius Red) and proteoglycans (Alican Blue) and imaged under 10x magnification.

4.2.8 Statistical Analysis

The statistical software SYSTAT (Systat Software, Inc., Chicago, IL) was used to conduct pair-wise comparisons between groups. For Study 1 (agarose hydrogel), significance ($p < 0.05$) was established with 1-way or 2-way ANOVA and Tukey's post-hoc correction (the independent variable for viability was day; independent variables for

equilibrium modulus, dynamic modulus, GAG content, and collagen content were day and culture condition). For Study 2 (HA hydrogel), significance ($p < 0.05$) was established with 1-way ANOVA and Tukey's post-hoc correction with day as the independent variable for equilibrium modulus, dynamic modulus, GAG content, and collagen content.

4.3 Results

4.3.1 Study 1: Long-Term Agarose Biomechanical and Biochemical Analyses

In order to determine the stability of cell-seeded agarose constructs over long term culture, we evaluated functional outcomes at defined time points through 112 days of culture. Consistent with previous findings, the equilibrium modulus of constructs increased with time (D14 to D112; $p < 0.001$) for chondrocyte-laden constructs in CM(+) conditions (**Figure 4-1A**). Peak modulus was achieved on Day 112, and was either stable from Day 56 to Day 112 in free swelling conditions (FS+; 341 to 434 kPa) or increased in dynamic conditions (Dyn+); 538 kPa to 707kPa). Dyn(+) construct modulus was markedly higher than FS(+) constructs at both time points. Dynamic modulus increased with time (D14 to D112; $p < 0.001$) in all culture conditions for chondrocyte-laden constructs, and either increased from Day 56 to Day 112 for FS(-) (2.01 to 4.90 MPa), Dyn(-) (2.00 to 3.21 MPa), and FS(+) (7.75 to 11.1 MPa) conditions or was stable for Dyn(+) (8.61 to 8.98 MPa) conditions (**Figure 4-1B**).

Contrary to these generally stable or increasing properties in chondrocyte-based constructs, mechanical properties of MSC-laden constructs were unstable over long term

culture in all conditions. In the absence of TGF- β [FS(-) and Dyn(-)], MSC-laden constructs failed to develop tissue with appreciable equilibrium modulus by Day 56; however, there was an increase in dynamic modulus at Day 112 for both FS(-) and Dyn(-) constructs (**Figure 4-1A**). When cultured in the presence of TGF- β [FS(+) and Dyn(+)], equilibrium modulus increased for MSC-laden constructs through Day 28, with Dyn(+) constructs reaching a higher equilibrium modulus compared to FS(+) conditions (124 and 220 kPa, respectively). Dynamic modulus followed similar trends, reaching 1.09 MPa in FS(+) conditions and 1.74 MPa in Dyn(+) conditions at Day 28. At Day 112, there was a decline in equilibrium modulus from Day 56 values. While this decline was substantial in FS(+) conditions (138 to 82 kPa), it was even more marked in Dyn(+) conditions (217 to 2 kPa). Similarly, there was a decline in dynamic modulus at Day 112 in Dyn(+) conditions; however, this decline was less dramatic (1.95 to 0.89 MPa).

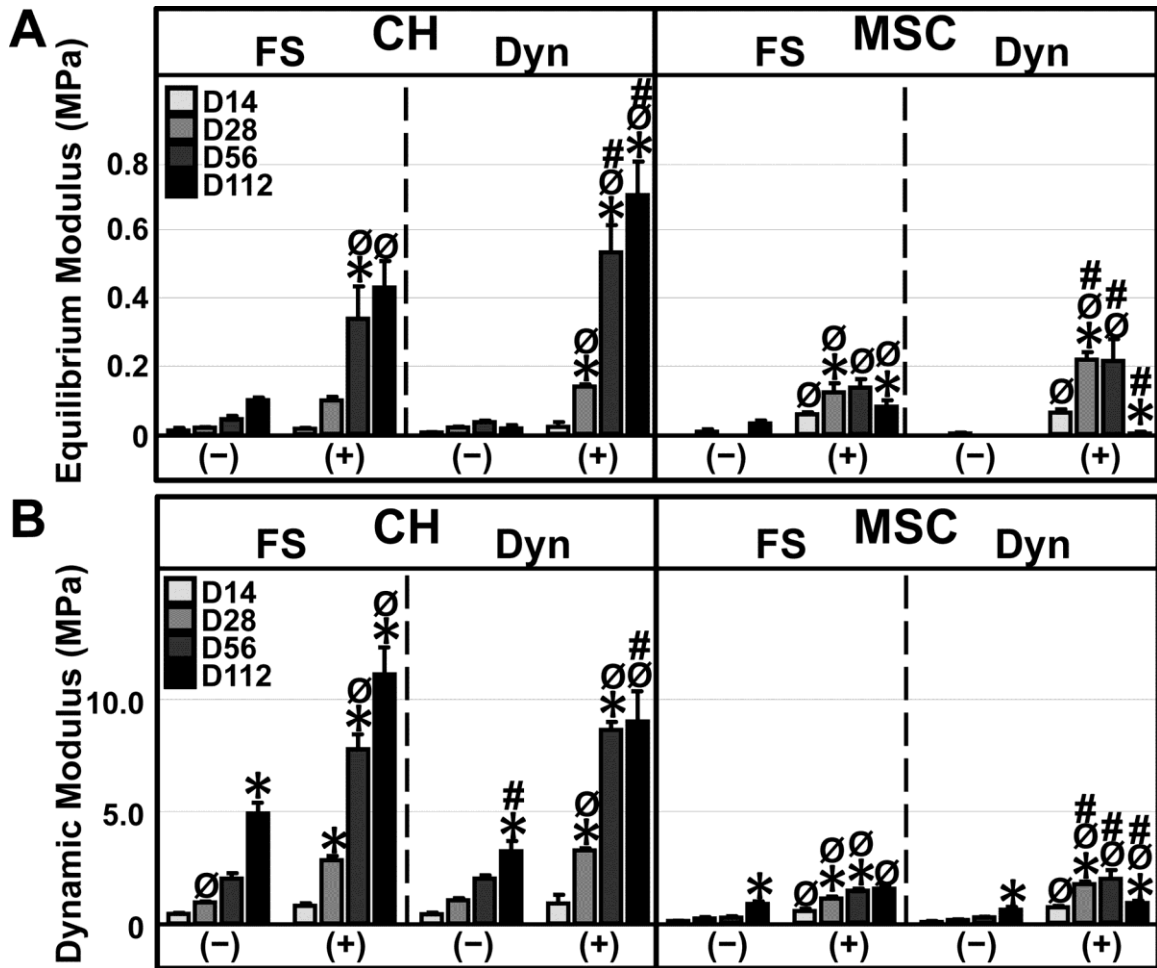


Figure 4-1: Mechanical properties of chondrocyte (CH) and mesenchymal stem cell (MSC)-laden agarose hydrogels cultured under free swelling (FS) or dynamic (Dyn) conditions in the absence or presence of TGF-β (-/+). (A) Equilibrium modulus through 112 days (D112) demonstrating a progressive increase and/or stability in properties in CH-laden constructs, and an overall lower and unstable mechanical growth trajectory for MSC-laden constructs in CM(+) conditions. (B) Dynamic modulus of constructs showing a similar growth trajectory (with a particular instability in this measure for MSC-laden Dyn(+) constructs). Significance established with $p < 0.05$. (*) vs. previous time point of same group; (#) Dyn(-) vs. FS(-) or Dyn(+) vs. FS(+) within cell type and time point. (Ø) FS(-) vs. FS(+) and Dyn(-) vs. Dyn(+) within cell type and time point.

Analysis of glycosaminoglycan (GAG) and collagen content illustrated that the loss of construct mechanical properties was due to a loss of tissue constituents in MSC-laden constructs. For chondrocyte-laden constructs cultured in the presence of TGF-β, GAG content increased from D56 to D112 in both FS(+) (1.20 to 2.34 mg/construct) and Dyn(+) (1.73 to 4.31 mg/construct) constructs (**Figure 4-2A**). Conversely, for MSC-

laden constructs, GAG levels dropped from 1.30 to 1.03 mg/construct in FS(+) conditions and 1.22 to 0.28 mg/construct in Dyn(+) conditions. Collagen content increased for chondrocyte-laden constructs from Day 56 to Day 112 in FS(+) (~0.08 to 0.15 mg/construct) and Dyn(+) (0.16 to 0.18 mg/construct) conditions (Figure 4-2B). Similarly, collagen content of MSC-laden FS(+) constructs increased from Day 56 to Day 112 (0.06 to 0.09 mg/construct). However, there was a decline in MSC-laden Dyn(+) constructs (0.07 to 0.04 mg/construct) over this same time period.

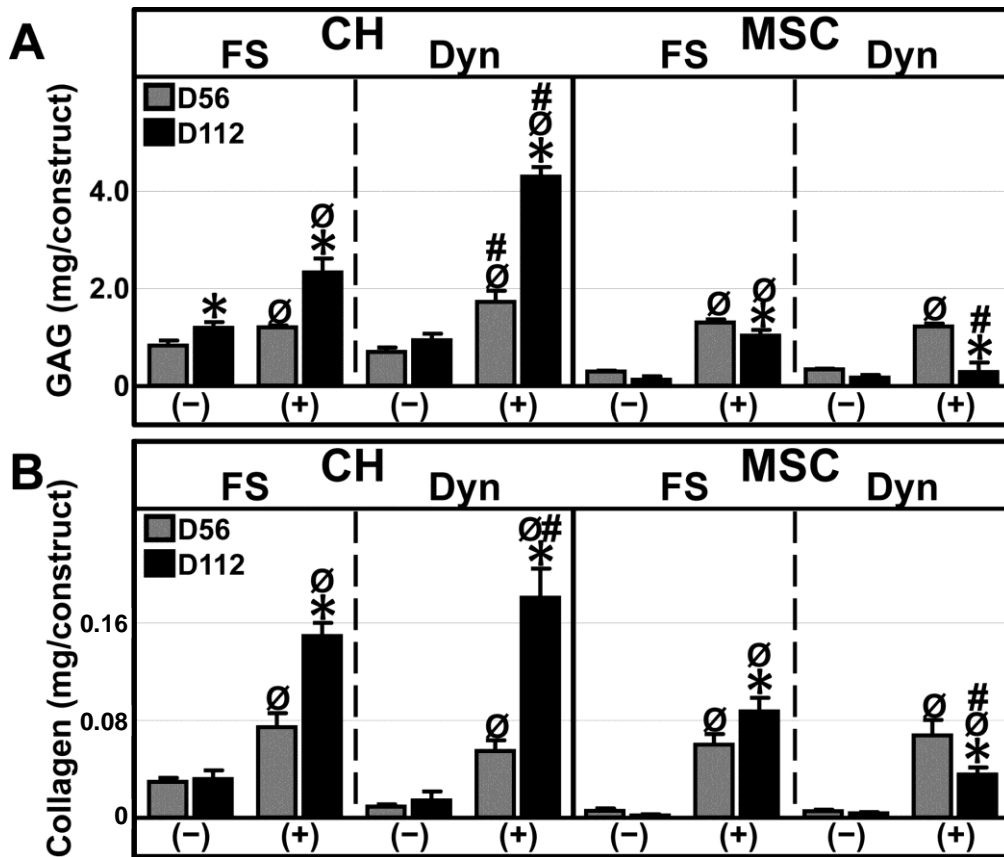


Figure 4-2: Biochemical content of CH and MSC-laden agarose constructs on Day 56 (D56) and Day 112 (D112). (A) Glycosaminoglycan (GAG) content from D56 to D112 differs with cell type and culture condition, with increases in GAG content apparent in CH-based constructs and loss of GAG content in MSC-based constructs. (B) Collagen content per construct similarly differs with cell type and culture condition. Significance established with $p < 0.05$. (*) vs. previous time point of same group; (#) Dyn(-) vs. FS(-) or Dyn(+) vs. FS(+) within cell type and time point. (Ø) FS(-) vs. FS(+) and Dyn(-) vs. Dyn(+) within cell type and time point.

4.3.2 Study 1: Histology and Immunohistochemistry

Staining for proteoglycans showed no evidence of tissue instability from Day 56 to Day 112 for chondrocyte-laden constructs (**Figure 4-3A**). Conversely, lighter and more diffuse staining of proteoglycans was apparent in MSC-laden FS(+) and Dyn(+) constructs when comparing Day 112 to Day 56. There were no apparent changes in collagen staining at these same time points (**Figure 4-3B**).

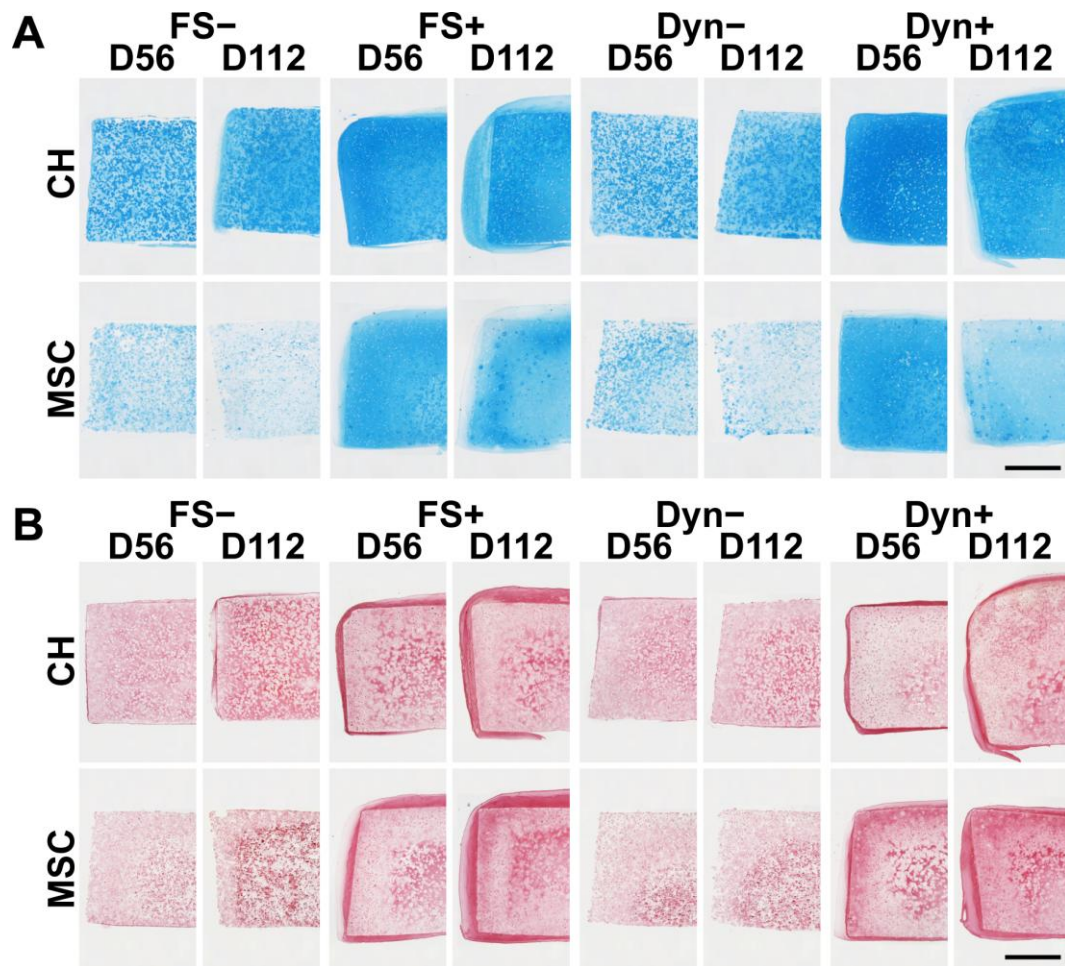


Figure 4-3: Histological analysis reveals differences in matrix formation and retention between groups on D56 and D112. (A) Alcian Blue staining showing differences in proteoglycan accumulation and distribution; most notably a lighter, more diffuse staining in MSC FS(+) and Dyn(+) groups in D112 compared to D56 constructs. Scale = 1mm. (B) No marked differences in collagen staining are apparent via Picrosirius Red staining. Scale = 1mm

To determine whether the loss in mechanics represented a shift in phenotype, we next stained for collagen type on Days 56 and 112. The presence of type II collagen would be indicative of positive and sustained chondrogenesis, while the presence of type I collagen would be indicative of a shift towards a fibrocartilage phenotype or potential hypertrophic differentiation. All groups stained heavily for type II collagen throughout the construct, and this was consistent over time (**Figure 4-4A**). Positive type I collagen staining was only apparent in the central regions of MSC-laden constructs cultured in the absence of TGF- β (**Figure 4-4B**). This staining was particularly evident in higher magnification images of MSC FS(-) constructs, with pockets of intense type I collagen staining along with more dispersed staining in inter-territorial regions (**Figure 4-5A**).

The presence of type I collagen and sudden increase in mechanical properties of MSC FS(-) and Dyn(-) constructs at the final time point suggested the emergence of a hypertrophic phenotype. To test for overt hypertrophy, Alizarin Red staining for calcium deposits was performed (**Figure 4-5B**). In both FS(-) and Dyn(-) MSC-laden constructs, there was a large amount of positive mineral staining in the center of constructs, whereas the remaining groups were negative for mineral deposition.

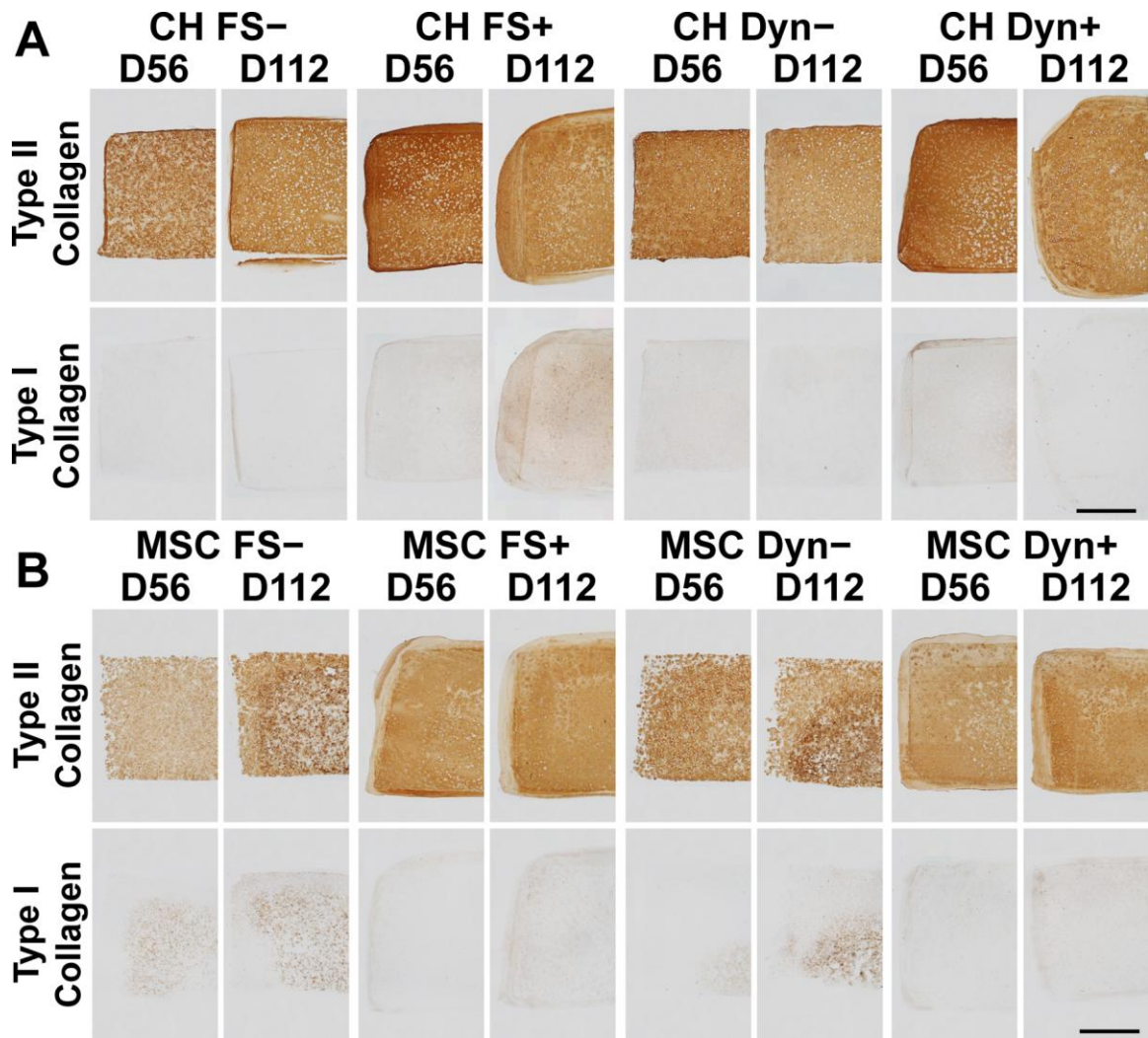


Figure 4-4: Immunohistochemical analysis on D56 and D112. (A) CH-laden hydrogels stain intensely for type II collagen, with little or no staining of type I collagen, indicative of a stable chondrogenic phenotype. Scale = 1mm. (B) Although MSC-laden hydrogels stain less intensely for type II than their CH counterparts, staining is relatively stable from D56 and D112. Positive type I collagen staining is apparent only in MSC FS(-) and Dyn(-) conditions, and increases from D56 to D112. Scale = 1 mm

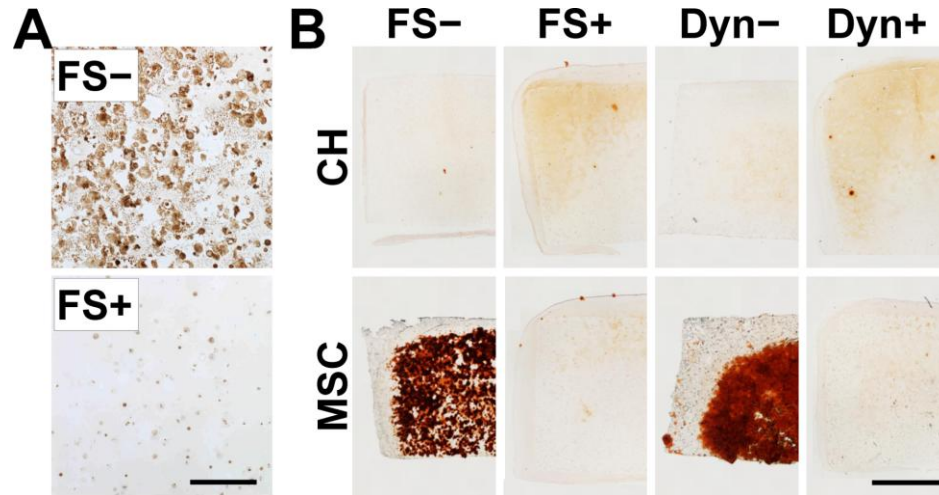


Figure 4-5: (A) Higher magnification of type I collagen staining illustrates pockets of intense deposition in MSC FS(-) conditions at D112. Scale = 200 μm . (B) Positive Alizarin Red staining for MSC FS(-) and Dyn(-) conditions at D112 indicates that these constructs are heavily calcified, despite the absence of specific pro-hypertrophic signals. Scale = 1mm

4.3.3 Study 1: Cell Viability

Instability of MSC-laden constructs in long-term culture could potentially be precipitated by deficits in cell health and viability. To that end, we quantified cell viability over time in culture (**Figure 4-6A**). While there was some initial decline in viability in the center of chondrocyte-laden constructs in CM(-) conditions by Day 14 (an ~10% decline), there was little further deviation through Day 56, with values ranging from 75-85% for all conditions at Days 28 and 56. At Day 112, there was a small additional decline in FS(+) and Dyn(+) with viability reaching 65% and 70%, respectively.

In a stark contrast, there was an immediate decline in viability in FS(-) and FS(+) MSC-laden constructs (~15-20% decline by Day 4). This decline in viability was slightly delayed with dynamic culture. In FS(+), viability stabilized at ~40-45% between Days 14 and 56. Differences in viability over the peak growth period (D28) for MSC-laden

constructs are shown in **Figure 4-6B**. By Day 112, MSC viability had fallen further to very low levels in all conditions: 6% in FS(-), 25% in FS(+), 18% in Dyn(-), and 8% in Dyn(+).

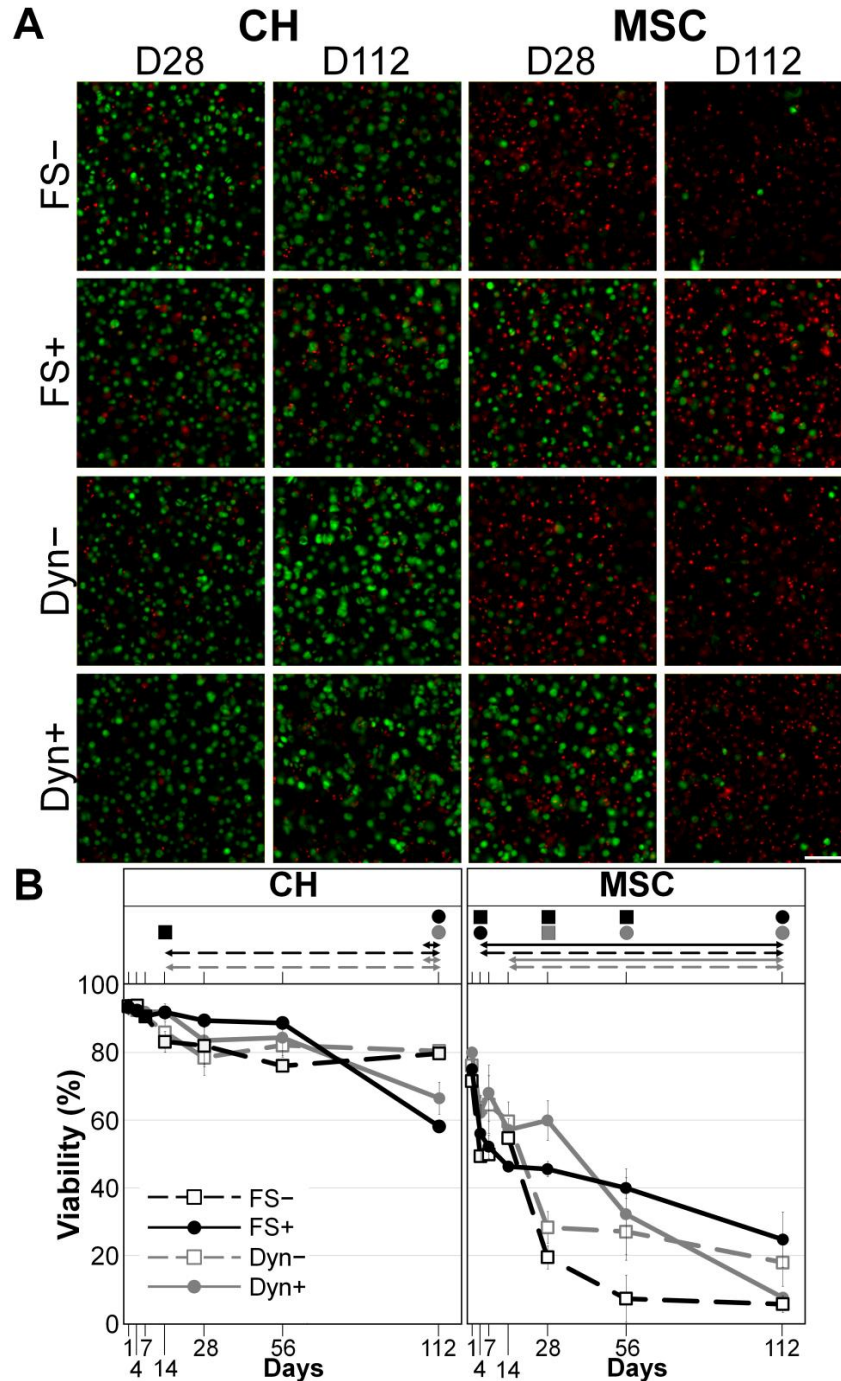


Figure 4-6: Short and long-term viability in CH and MSC-laden constructs. (A) Marked differences in viability between groups are observed as early as D28. MSC-based cultures continue to decline through D112. Nuclei of dead cells are labeled in red, cytoplasm of live cells are labeled in green. Scale = 100 μ m. **(B)** Quantification of percent viability in the center of constructs shows a marked decline in MSC viability at early time points, reaching an extremely low level by D112, compared with much smaller changes in CH-based construct viability over the same time course. Significance established with $p < 0.05$. Markers indicating significance included in box above plots. (Line) vs. Day 1 with line style and color corresponding to respective group. (Circle and square) vs. previous time point with marker style and color corresponding to respective group.

4.3.4 Study 2: Long-Term Culture of MSC-Seeded Hyaluronic Acid Hydrogels: Biomechanical, Biochemical, and Histological Analyses

To determine if the instability in MSC-laden constructs was a function of the hydrogel culture system employed, we next carried out a similar long-term study investigating MSCs in FS(+) conditions through 126 days in a photocrosslinked HA hydrogel. Equilibrium modulus (**Figure 4-7A**), dynamic modulus (**Figure 4-7B**), and glycosaminoglycan content (**Figure 4-7C**) increased from Day 14 values ($p < 0.001$), peaking at Day 56 at 203 kPa, 2.19 MPa, and 1.28 mg/construct, respectively. Following these peaks, all three metrics declined substantially at 126 days to 4 kPa, 0.51 MPa, and 0.27 mg/construct, respectively. Collagen content continued to increase through Day 84 to 0.11 mg/construct with no decline at Day 126 (**Figure 4-7D**). Histological staining confirmed a dramatic loss in proteoglycans and an increase in collagen at Day 126 (**Figure 4-7E**).

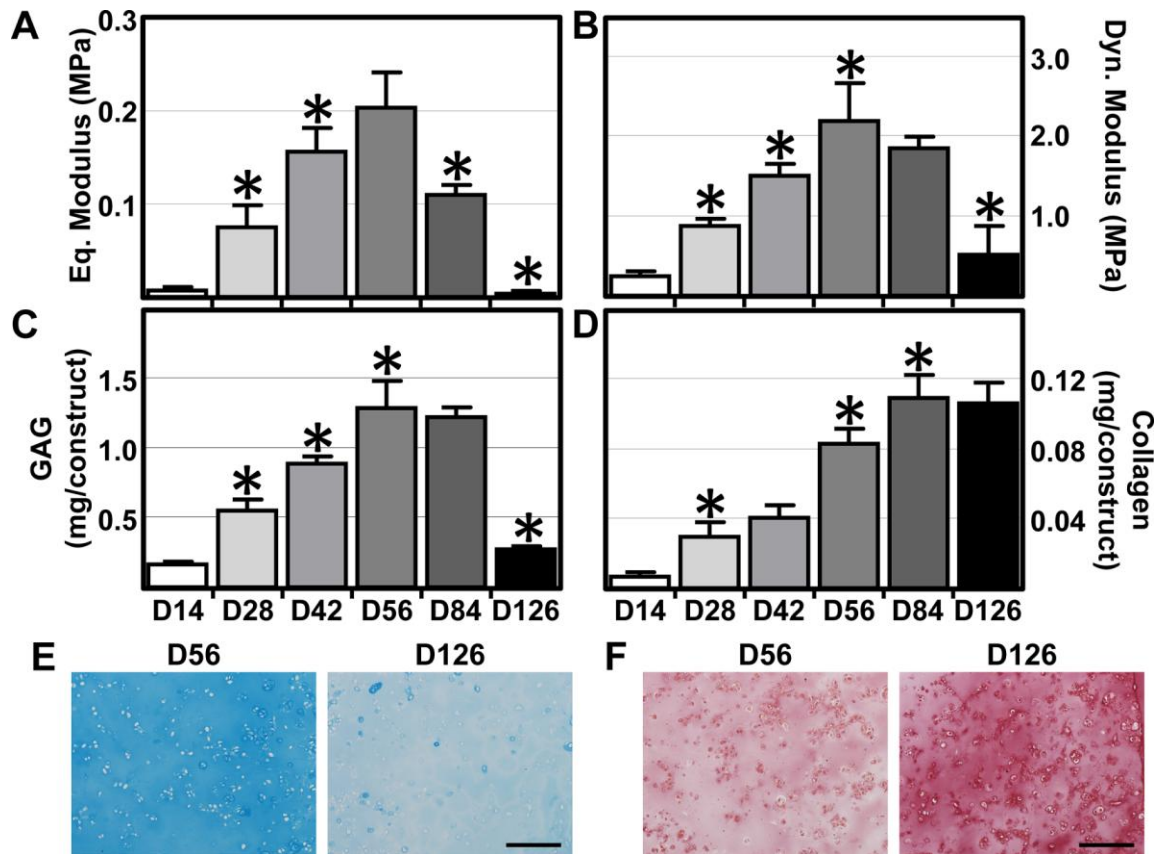


Figure 4-7: Mechanical, biochemical, and histological assessment of MSCs cultured in a hyaluronic acid (HA) hydrogel over long-term *in vitro* culture. (A) Equilibrium modulus and (B) dynamic modulus show instability in construct properties similar to that of agarose constructs, with marked declines occurring by D126. (C) Glycosaminoglycan (GAG) content per construct declines similarly while (D) collagen per construct is stable. Significance established with $p < 0.05$. (*) vs. previous time point. Histological staining of (E) proteoglycans (Alcian Blue) and (F) collagens (Picrosirius Red) confirm biochemical assays. Scale = 200 μm .

4.4 Discussion

For a cell-based biologic cartilage repair method to be successful, the neo-tissue formed must reach a stable equilibrium state with sufficient mechanical function. Ideally, this function would match that of native tissue and persist over the lifetime of the patient. Previous reports have noted that at time scales of approximately 8 weeks, MSC-laden hydrogels cultured *in vitro* under pro-chondrogenic conditions plateau in their functional maturation, with a lower equilibrium modulus compared to chondrocyte-based constructs

cultured identically (Erickson et al., 2009a; Erickson et al., 2012; Huang et al., 2009; Mauck et al., 2006). Furthermore, while adult derived stem cell-based treatments are alluring, their phenotypic instability upon implantation remains a perplexing issue (Pelttari et al., 2006; Studer et al., 2012). Although there has been much progress in engineering a mechanically robust cartilage tissue with these cells, stem cell-based cartilage properties can deteriorate as the tissue undergoes mineralization when presented with an *in vivo* subcutaneous environment (Pelttari et al., 2006), or when challenged with hypertrophic factors *in vitro* (Mueller and Tuan, 2008). These findings, coupled with the recognized limitations of microfracture, which produces a repair tissue that is unstable (Mithoefer et al., 2009), might suggest that bone marrow derived stem cells simply lack the capacity to produce a stable cartilaginous tissue.

To address this issue, this study evaluated the potential of MSC-based cartilage constructs (relative to chondrocyte-based constructs) over long term culture in a well defined, stable *in vitro* environment. In doing so, we attempted to ask and answer two questions. First, we sought to determine whether the plateau in mechanical properties with time (through 56 days) simply represents a lag phase (during which MCS undergo an initial round of chondrogenesis), and from which they might continue to produce matrix and increase in mechanical properties to match cartilage. Second, we attempted to clarify whether MSC-laden tissue engineered constructs remain stable in their chondrogenic phenotype over the long term, or whether they deteriorate towards a hypertrophic state with prolonged cultivation. To answer these questions, we investigated the development of mechanically viable chondrocyte- and MSC-laden tissue

engineered constructs in a popular three-dimensional agarose hydrogel system with long term culture (112 days). To assess cell health and stability, we analyzed the time progression of cell viability. Additionally, we evaluated the presence of cartilaginous (proteoglycans and type II collagen) and hypertrophic (type I collagen and calcium) matrix constituents via histological and immunohistochemical staining.

Through 56 days of culture, our results were consistent with previous reports (Erickson et al., 2009a; Erickson et al., 2012; Mauck et al., 2006). Namely, provision of TGF- β in chondrogenic culture medium resulted in an increase in GAG and collagen content and equilibrium modulus with time for both MSC- and chondrocyte-based constructs. Likewise, the absence of TGF- β resulted in less maturation in chondrocyte-based constructs and very little maturation of MSC-based constructs. Dynamic culture improved equilibrium modulus over free swelling controls for both cell types; however, chondrocytes continued to outperform MSCs. When we cultured these constructs for an additional 56 days (through Day 112), however, MSC-based constructs not only failed to match properties of chondrocyte-based constructs, but rather evinced a marked decline in mechanics from Day 56 to Day 112. This decline in properties was exacerbated with dynamic culture.

The basis for the mechanical instability observed in MSC-laden constructs was further investigated at the cellular level. We found that while chondrocyte viability was relatively high and stable through long term culture, MSC viability progressively declined for all conditions. In free swelling conditions in the presence of TGF- β , there

were two phases of decline. The first decline occurred very soon after encapsulation, with viability stabilizing at ~40% between Days 14 and 56. The second reduction in viability, to lows around ~25%, occurred between Days 56 and 112. We hypothesize that the immediate decline in viability may be a consequence of metabolic stress, as dynamic culture mildly delayed the decline from Day 1 levels. However, the low MSC viability in all conditions at Day 112 suggested that the *in vitro* culture conditions, even with optimal nutrient supply, are not suitable for long term MSC stability.

One interesting caveat to these findings was that although there was a decline in mechanics and viability of MSC-laden constructs in the CM(+) conditions, these constructs remained negative for indicators of hypertrophic differentiation (including type I collagen and calcium). However, the progressive loss of Alcian Blue staining and GAG content suggested these constructs were in a catabolic state, losing key matrix constituents over this time period. It is not yet clear whether this response is a natural consequence of the time course of chondrogenesis, or whether this represents a catabolic response on the part of the MSCs in response to nutrient deprivation; this mechanism is currently being explored. In the absence of TGF- β , not only was there a dramatic decline in MSC viability, but constructs also stained heavily for calcium deposits and moderately for type I collagen. Along with this observation, we noted a moderate increase in dynamic modulus in free swelling conditions, which might be attributed to calcification of the tissue. In additional replicates (not shown), we found that once this calcification traversed the entire thickness of the construct, there was a significant spike in equilibrium modulus as well. Spontaneous calcification without the addition of hypertrophic medium

supplements, including a phosphate source, is alarming and suggests that the continued presence of TGF- β may be required to prevent this unwanted phenotypic transition. Such a finding would suggest that *in vivo* application of MSCs for cartilage repair will require prolonged provision of TGF- β to prevent unwanted phenotypic transitions.

In our original studies, we employed a simple agarose hydrogel to encapsulate cells. Agarose is a relatively inert biomaterial, offering no cell adhesion or other interactions (Buschmann et al., 1992). To determine if the instability in our MSC cultures was a function of the hydrogel used, a hyaluronic acid hydrogel supportive of MSC chondrogenesis was utilized in a follow-up study. This material provides cell-material interactions via both CD44 and CD168 surface receptors (Bian et al., 2013) and is more supportive of the chondrogenic phenotype than inert gels such as unmodified polyethylene glycol and agarose (Chung and Burdick, 2009). This hydrogel is also clinically relevant because it can be crosslinked *in situ* and can be readily remodeled as the tissue matures. Supporting our findings in agarose hydrogels, a similar time scale of matrix elaboration and mechanical property increases, peaking at Day 56, was followed by catabolic declines by Day 126 in this HA hydrogel. These findings suggest that the natural time course of MSC chondrogenesis and subsequent functional declines are not dependent on the material employed.

Taken together, our results show that, in a defined *in vitro* culture system where conditions are regulated to promote and preserve the chondrogenic state, MSC instability may be an innate characteristic of the cell type, involving both loss of viability and

phenotypic conversion. These data have significant implications for *in vivo* application of MSC-based engineered constructs. Our data suggest that if such constructs are implanted at a point of peak mechanics, and ultimately fail *in vivo* long term, this failure may be the natural progression of the cell phenotype rather than a reaction to the *in vivo* environment. The expansion and chondrogenic culture conditions used for these studies are amongst the most popular for MSC based cartilage tissue engineering; however, methods to prevent MSC hypertrophy, including mechanical loading (Bian et al., 2012), application of soluble factors such as parathyroid hormone-related protein (Bian et al., 2011b; Kim et al., 2008; Mueller et al., 2013; Mwale et al., 2010), or co-culture with chondrocytes (Bian et al., 2011a; Cooke et al., 2011; Fischer et al., 2010) should be further explored. Further, efforts should be focused on maintaining MSC viability after encapsulation by limiting metabolic stress, either through the provision of anabolic factors with sustained release from the material, by pre-conditioning MSCs to this environment before implantation, or by pre-selecting MSC subpopulations that are particularly resistant to loss of viability under the taxing *in vivo* conditions. Such steps are critical, as clinical success of stem cell based cartilage tissue will require not only that these cells achieve a high anabolic state, but more importantly, that cell health, phenotypic stability, and functional properties are retained over the long term and post-implantation.

CHAPTER 5: FUNCTIONAL CONSEQUENCES OF GLUCOSE AND OXYGEN DEPRIVATION ON ENGINEERED MESENCHYMAL STEM CELL-BASED CARTILAGE CONSTRUCTS

5.1 Introduction

In the presence of chondrogenic soluble factors (including transforming growth factor-beta), MSCs are capable of producing a cartilage-like matrix high in glycosaminoglycan content and with increasing mechanical properties (Johnstone et al., 1998; Kavalkovich et al., 2002; Mauck et al., 2006; Pittenger et al., 1999). However, as mentioned in Chapters 3 and 4, when cultured in the same 3D environment and under the same soluble factor conditions, chondrocytes outperform MSCs. Specifically, MSC-laden constructs increase in functional properties early in culture, but plateau in their development between 28-56 days of culture, while chondrocyte-laden constructs continue to increase in mechanical function (Huang et al., 2010a; Mauck et al., 2006). In Chapter 3, using a three-dimensional agarose hydrogel culture model and local analysis of mechanical properties, we showed that the properties of MSC-based constructs are higher at the construct periphery compared to the same region of constructs based on chondrocytes that were cultured identically. The marked disparity in overall (bulk) construct properties arose from deficiencies in the central regions of constructs, where MSC-based construct properties were significantly lower than that of chondrocyte-based constructs. This deficit in mechanical properties in the central core was associated with a loss of cell viability and lower GAG content in this region, relative to chondrocyte-based constructs. Since MSCs perform well in areas of maximal nutrient supply (at the construct

periphery), but very poorly within central regions (where nutrient supply is lower), these data suggest that MSCs might be more sensitive than chondrocytes to deprivation of nutrients and other metabolic factors. Such differences may have an impact on translation of MSC-based engineered cartilage.

In vivo, cartilage thickness can range from 1-7 mm, and since the tissue lacks a blood supply (and so all nutrients are derived from diffusion), chondrocytes naturally function in both a nutrient-poor and hypoxic environment (with oxygen levels of ~1-7%) (Silver, 1975; Zhou et al., 2004). Once implanted into the joint space, cells within an engineered cartilage tissue must be able to withstand the *in vivo* environment in addition to the self imposed microenvironments developed through nutrition utilization and diffusion constraints (Buckley et al., 2012; Zhou et al., 2008). As a number of factors may contribute to the performance and health of MSCs (Deschepper et al., 2011; Potier et al., 2007), we investigated the consequence of decreased nutrient and metabolite availability (glucose and oxygen) on the functional properties of MSC-laden constructs as a function of time in culture. These studies were carried out in both thick (2.25 mm) as well as in thin constructs (0.75 mm) to minimize diffusional limitations. Our findings illustrate that, under chondrogenic conditions (with TGF- β), MSC-based engineered constructs are exquisitely sensitive to nutrient deprivation (low glucose), but are generally less sensitive to hypoxic challenge.

5.2 Materials and Methods

5.2.1 MSC Isolation and Hydrogel Culture

Bone marrow derived mesenchymal stem cells (MSCs) were isolated from the femur of two donor calves (3-6 months old; Research 87, Boylston, MA, USA) as in previous chapters. Cells were expanded through passage 2 in a high glucose basal medium (BM) [Dulbecco's Modified Eagles Medium (DMEM; Gibco, Invitrogen Life Technologies, Carlsbad, CA), 10% fetal bovine serum (FBS, Gibco), and 1% penicillin, streptomycin, and fungizone (PSF; Gibco)]. Upon reaching confluency, passage 2 cells were trypsinized and resuspended in chemically defined media at a density of 40 million cells/mL. The cell suspension was mixed with 4% w/v molten Type VII agarose (49°C; Sigma-Aldrich, St. Louis, MO, in PBS) at a 1:1 ratio, resulting in a homogenized 2% agarose solution with a cell density of 20 million cells/mL. The agarose/cell solution was cast between two parallel glass plates separated by either a 0.75 mm spacer or 2.25 mm spacer. A 4 mm biopsy punch was used to extract gels, resulting in cylindrical gels 4 mm in diameter with a thickness of 0.75 mm ('thin') or 2.25 mm ('thick').

Constructs were cultured in conditions of varying glucose, oxygen, and transforming growth factor-beta 3 (TGF- β 3) concentrations through 28 days (**Figure 5-1**). Chemically defined media consisted of DMEM, PSF, dexamethasone, ascorbate 2-phosphate, insulin, transferrin, selenous acid, bovine serum albumin, and linoleic acid. Low glucose DMEM contained 1 g/L glucose (Gibco), whereas high glucose DMEM contained 4.5 g/L glucose (Gibco), with the latter being the concentration of glucose used in previous chapters. Media was supplemented with either 0 ng/mL (-) or 10 ng/mL (+) transforming growth

factor-beta 3 (TGF- β 3; R&D Systems, Minneapolis, MN). Constructs were cultured in a humidified incubator at 37°C with 5% CO₂ in ambient air (oxygen concentration of ~21% (normoxic)), or within a humidified hypoxic culture glove box chamber (HypOxystation; HypOxygen, Frederick, MD) providing continual hypoxic culture conditions at 37°C, 5% CO₂, and 2% oxygen (hypoxic). Breathe-Easy semipermeable membranes were used to prevent media evaporation. A summary of culture conditions and text abbreviations are provided in **Table 5-1**. Media was changed twice weekly, with the volume scaled to construct size; 1 mL/construct for 2.25 mm ‘thick’ constructs and 0.333 mL/construct for 0.75 mm ‘thin’ constructs. Used media was sampled weekly, 3 days after the previous feeding, and glucose concentration measured using the Amplex Red Glucose Assay (Molecular Probes, Invitrogen Life Technologies, Carlsbad, CA).

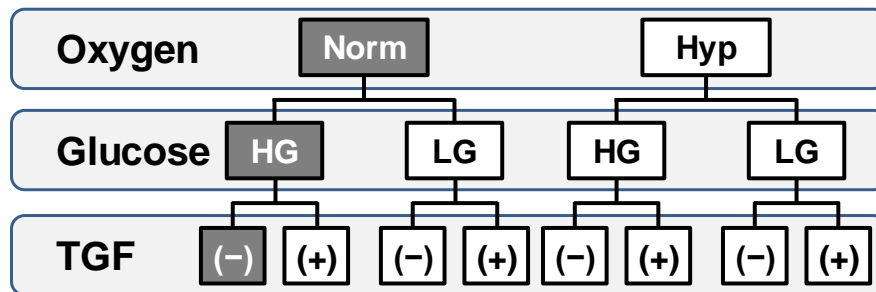


Figure 5-1: Schematic illustration of culture conditions and their combinations. Gray boxes indicate control conditions.

Table 5-1: Culture conditions and abbreviations.

Factor	Condition	Quantity	Abbreviation
Oxygen	Normoxia	~21% O ₂	Norm
	Hypoxia	2% O ₂	Hyp
Glucose	High Glucose	4.5 g/L	HG
	Low Glucose	1.0 g/L	LG
TGF- β	No TGF	0 ng/mL	(-)
	With TGF	10 ng/mL	(+)

5.2.2 Quantification of Cell Viability

‘Thick’ and ‘thin’ constructs were stained with the Live/Dead cell viability kit (Molecular Probes, Life Technologies) at various points in culture. ‘Thick’ constructs were halved through the median plane and imaged at 2X magnification on Day 28. For ‘thin’ constructs, images of both axial surfaces (construct top and bottom) were acquired with 2X and 10X magnification. Samples were imaged on Days 7, 14, 21, and 28. Percent viability of thin constructs was calculated by counting the number of objects in the dead cell channel (ethidium homodimer-1) and live cell channel (calcein) in the 10X images using a custom Matlab program. Since viability percentage differed greatly between the two surfaces, the sides of minimum and maximum viability were grouped for each condition.

5.2.3 Construct Mechanical Properties and Biochemical Content

Thick constructs were tested via unconfined uniaxial compression with a custom testing apparatus. Constructs (n=4) were equilibrated under a 2 g creep test for 300 sec before

stress relaxation testing (10% strain applied at 0.05% per second followed by a 1000 sec relaxation phase). Load at equilibrium and sample geometry were used to calculate the equilibrium modulus. After stress relaxation testing, a 1% sinusoidal dynamic strain was applied at 1 Hz, with dynamic stress and strain used to calculate the dynamic modulus. Mechanically tested constructs (n=4) were digested with papain for 24 hrs at 60°C as previously described. Sulfated glycosaminoglycan (GAG) and collagen content were measured via the 1,9-dimethylmethylene blue dye-binding assay and the orthohydroxyproline assay, respectively, as in Chapters 3 and 4. DNA content was measured via the Quant-iT PicoGreen dsDNA Kit (Invitrogen Life Technologies) according to manufacturer's protocol. GAG, collagen, and DNA content is presented as percent of construct wet weight (% ww).

5.2.4 Histology and Immunohistochemistry

Constructs (n=3) were fixed with 4% paraformaldehyde, dehydrated, and paraffin embedded. Paraffin embedded constructs were sectioned to 8 µm thickness onto glass slides. Sections were stained for proteoglycans with Alcian Blue (pH 1.0; Rowley Biochemical Inc, Danvers, MA, USA). Additional sections underwent immunohistochemical detection of type II collagen (5 µg/mL; Developmental Studies Hybridoma Bank, University of Iowa, Iowa City, IA) as in Chapter 5, after proteinase K mediated antigen retrieval (37°C for 15 min) and following the manufacturer's instructions for the Millipore Immunoperoxidase Secondary Detection System (EMD Millipore Corporation, Billerica, MA).

5.2.5 Statistics

Statistical analysis was carried out with the software package SYSTAT (Systat Software, Inc., Chicago, IL, USA) to determine significance ($p < 0.05$) between groups, with Tukey's post-hoc tests used for pairwise comparisons. For hydrogel equilibrium modulus, dynamic modulus, GAG content, collagen content, and DNA content, a 2-way ANOVA was conducted with media type (HG+, HG-, LG+, LG-) and oxygen (normoxic, hypoxic) as the independent variables. For viability and glucose concentration of thin constructs, a 3-way ANOVA was conducted with the independent variables of oxygen, glucose, and TGF- β supplementation.

5.3 **Results**

5.3.1 Impact of Oxygen and Glucose on Construct Mechanics and Matrix Content

Standard conditions for construct culture consisted of ~20% oxygen (Norm) and 4.5 g/L glucose (high glucose; HG). Under these control conditions, and with the addition of TGF- β (+) (versus no TGF- β (-)), construct equilibrium (142 vs. 20 kPa) and dynamic modulus (1.0 vs. 0.2 MPa) increased markedly by Day 28 (**Figure 5-2A, B**; $p < 0.05$). Culture in low oxygen (Hyp; 2%) in HG+ conditions reduced the equilibrium and dynamic moduli at this time point to 77 kPa and 0.5 MPa, respectively. Hyp HG- did not differ from Norm HG- conditions, with constructs reaching an equilibrium modulus of 19 kPa and a dynamic modulus of 0.2 MPa. While modest decreases were observed under hypoxic conditions, more marked declines were found in (+) constructs cultured in 1 g/L DMEM (low glucose; LG) compared to HG of the same oxygen tension. Equilibrium moduli dropped to 8 kPa in Norm conditions and to <1 kPa in Hyp

conditions, with dynamic modulus following a similar pattern, reaching ~0.2 and <0.1 MPa, respectively.

Glycosaminoglycan (GAG) content of Norm HG control constructs increased in (+) conditions, reaching ~2.7 %ww; higher than that of the Norm HG⁻ conditions (1.2 %ww, **Figure 5-2D**). Similar to trends in mechanical properties, hypoxic culture decreased GAG content by ~30% (to 1.9 %ww) in Hyp HG⁺ conditions. Under LG conditions, GAG content decreased by 67% and 63%, reaching 0.9 %ww in Norm LG⁺ conditions and 0.7 %ww in Hyp LG⁺ conditions. A similar result was apparent in terms of collagen content, where Norm HG⁺ conditions had the greatest collagen content at 0.7 %ww, Hyp HG⁺ conditions resulted in a 44% decrease, and LG⁺ conditions resulted in a 61% (Norm) and 57% (Hyp) decrease compared to their respective HG⁺ controls of similar oxygen tension (**Figure 5-2E**). The higher GAG and collagen content in HG⁺ conditions was not due to increased cell content (**Figure 5-2C**).

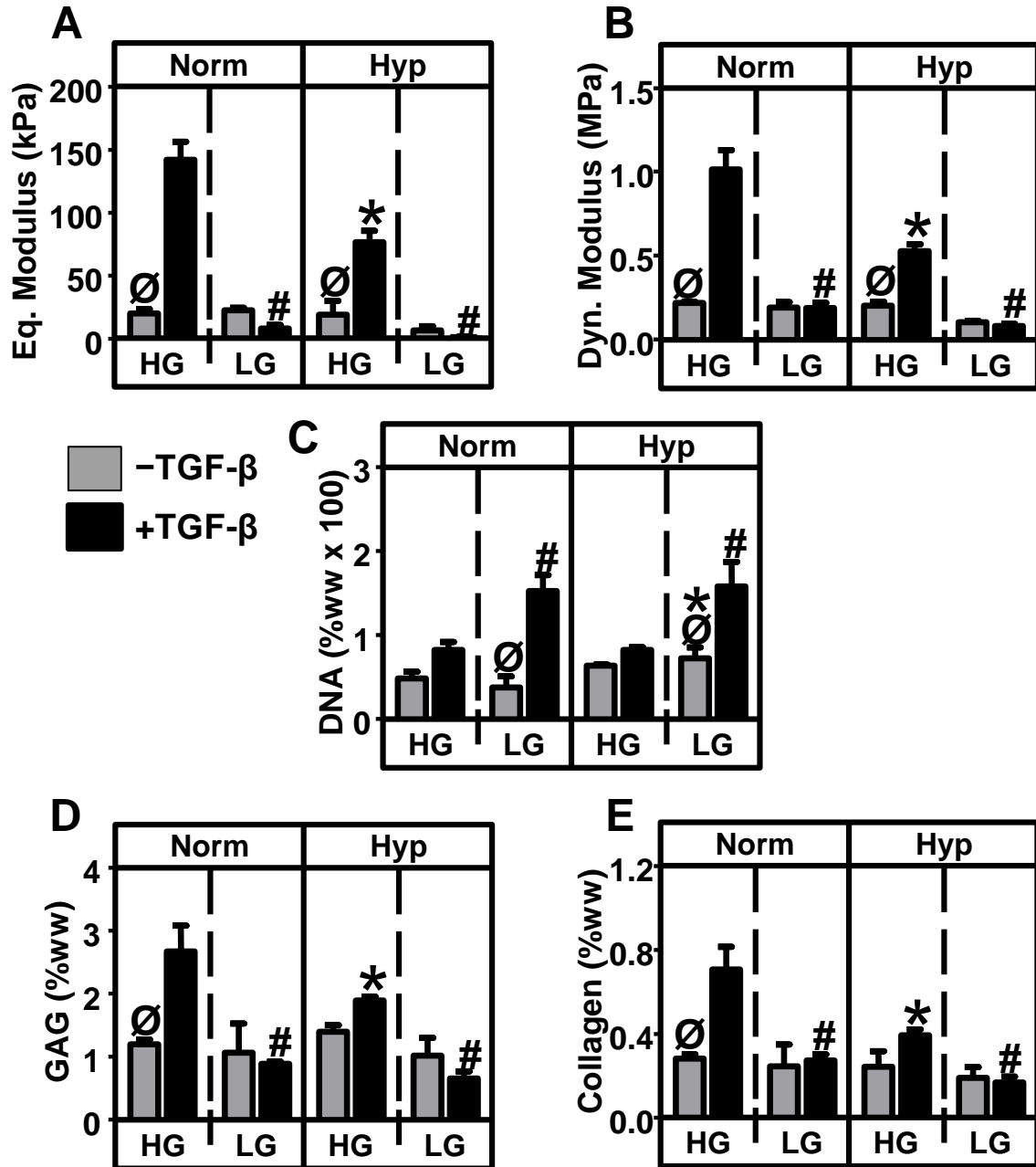


Figure 5-2: Biomechanical and biochemical findings illustrate that low glucose conditions have a greater impact than low oxygen on limiting functional maturation. Biomechanical properties: (A) equilibrium modulus and (B) dynamic modulus. Biochemical constituents: (C) DNA content, (D) glycosaminoglycan content, and (E) collagen content all reported as a percent wet weight (% ww). * indicates significant difference of Norm vs. Hyp ($p < 0.05$) in same TGF and glucose condition. # indicates significant difference of LG vs. HG ($p < 0.05$) in same TGF and oxygen condition. ∅ indicates significant difference of (-) vs. (+) ($p < 0.05$) in same glucose and oxygen condition.

5.3.2 Matrix Distribution and Cell Viability in Thick Constructs

Staining for proteoglycans and type II collagen in Norm HG conditions resembled patterns previously described for this culture system, with lighter, punctate staining homogenously distributed in (-) conditions and more intense staining in (+) conditions, with the greatest intensity towards the construct periphery (**Figure 5-3A, B**). In LG+ conditions, matrix staining was almost completely restricted to the periphery of the constructs. Little difference was apparent when comparing Norm to Hyp constructs. Imaging of viability in construct cross sections for thick constructs showed similar patterns, where viable cells were restricted to only the periphery of LG+ constructs with little difference between the Norm HG+ and Hyp HG+ conditions (**Figure 5-4A**).

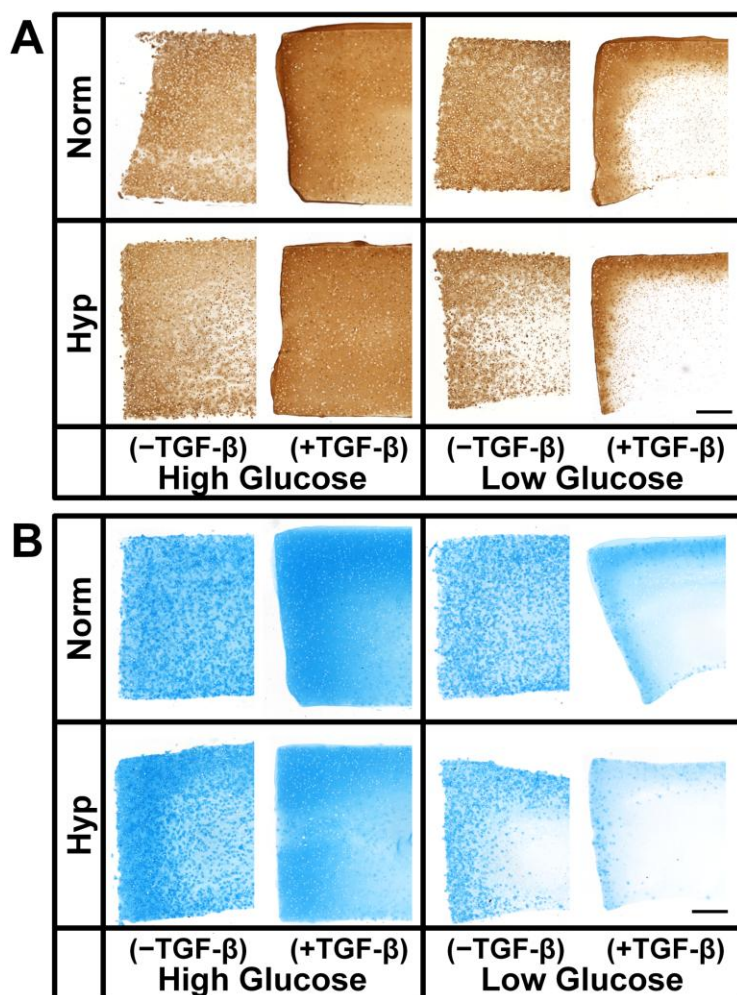


Figure 5-3: Matrix distribution in engineered constructs as a function of low-glucose and hypoxic culture conditions. (A) Immunohistochemical staining for type II collagen reveals punctuate homogeneous staining in both LG and HG CM(-) conditions, with relatively homogenous staining in HG(+) conditions. Regional differences are marked with transition to LG+ conditions, where matrix deposition is limited to the construct boundary. No obvious differences were noted between Norm and Hyp conditions. (B) Alcian Blue staining showed similar proteoglycan deposition, with the exception of slightly lighter staining apparent in Hyp HG+ conditions compared to Norm HG+. Scale = 500 μ m

5.3.3 Evaluation of Viability and Glucose Utilization in Thin Constructs

Given the clear differences between the construct edge and center, we next fabricated ‘thin’ constructs (0.75 mm thick) in order to limit the distance over which nutrients need travel. Since cross sections of these thin constructs were difficult to image, viability was

calculated for both the top and bottom surface of each construct, from which the maximum viability and minimum viability were determined (**Figure 5-4C, D**). For Norm HG+ thin constructs on Day 28, viability was high on both surfaces, with minimum and maximum viability of ~90%. This finding indicates a stable and viable cell population in these thin constructs through the depth. At this same time point, in Norm LG- and Hyp LG+ conditions, the maximum viability was significantly lower than Norm HG+. The lowest maximum viability was observed in the Hyp LG+ group, which reached 45% (a 52% decline compared to Norm HG+ levels). Minimum viability was significantly lower for all Hyp conditions and for both Norm LG conditions. The lowest minimum viability was observed in LG+ constructs cultured under Norm and Hyp conditions, 37% and 3%, respectively.

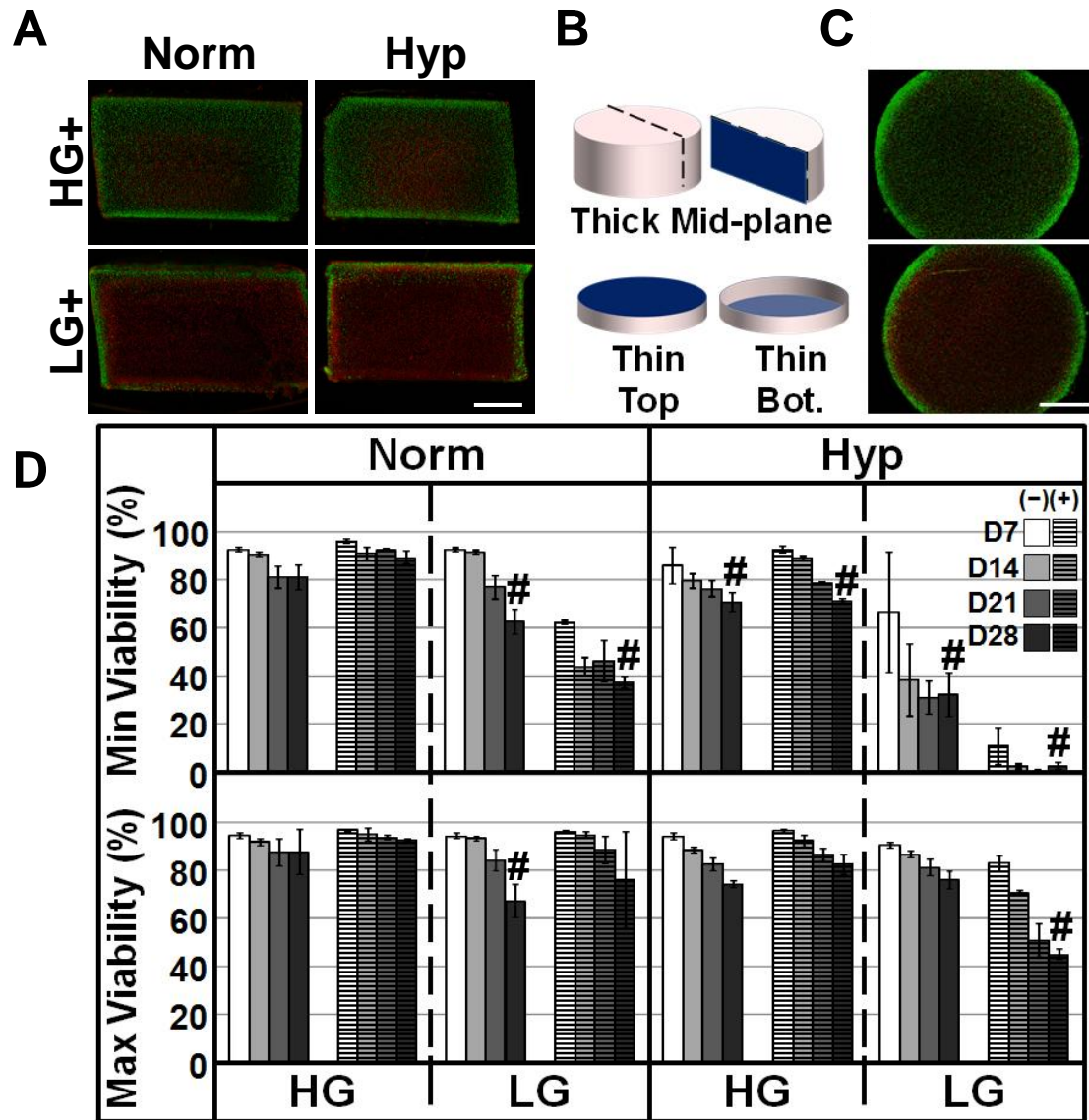


Figure 5-4: Distribution of viability in engineered constructs as a function of low-glucose and hypoxic culture conditions. (A) Live/dead staining of thick constructs (mid-plane, B) shows viable cells restricted to the periphery in LG+ conditions, with few differences between Hyp and Norm conditions. Scale = 500 μ m. (B, bottom, and C) Example image of thin Norm LG+ construct showing marked differences in viability on the top and bottom of the same construct. (D) Percent viability calculated from the top and bottom of thin constructs (where maximum viability occurs at the top of the construct with maximal nutrient exchange). Normoxic, high glucose conditions maintain a high level of viability, while low glucose conditions promote loss of viability, especially in the context of TGF- β and hypoxia. # indicates significant difference from Norm HG+ ($p < 0.05$) on Day 28.

Since it was apparent from the above that LG conditions evoked the most severe loss in viability and matrix deposition, we next measured glucose levels in media. These samples were taken at weekly intervals, with media sampling done 3 days after the addition of media. Fresh media glucose levels were ~25mM for high glucose DMEM and ~5mM for low glucose DMEM. Results from this analysis showed that glucose levels in ‘used’ media were lower when constructs were cultured in the presence of TGF- β (**Figure 5-5A, B**), indicative of their higher level of metabolic activity. In both Norm and Hyp HG+ cultures, glucose concentrations fell to ~5 mM after 3 days, with no difference between the two groups at Day 28. While a small fraction of the starting glucose remained in Norm and Hyp LG- cultures (0.5-1.5 mM), glucose concentration in LG+ cultures fell to very low levels (~0.05 mM) after three days of culture, with no difference between the Norm and Hyp groups.

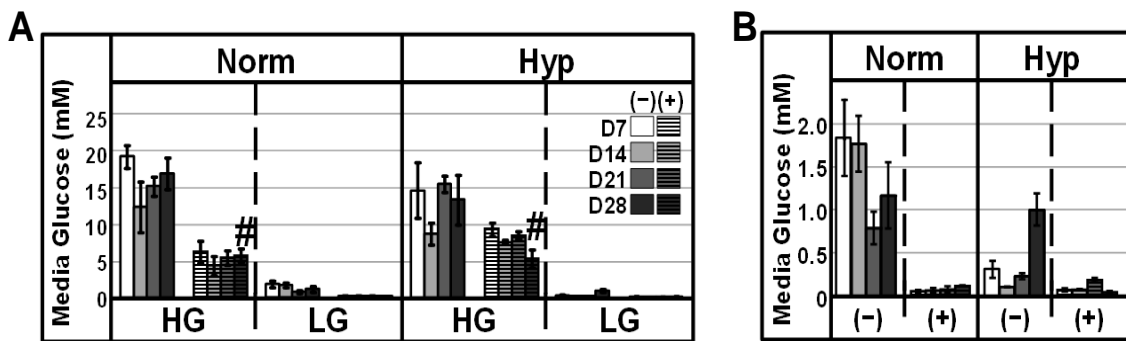


Figure 5-5: Glucose concentration in media as a function of low-glucose and hypoxic culture conditions. (A) Measured media glucose levels 3 days after feeding. The initial high glucose media concentration was ~25 mM whereas the initial low glucose media concentration was ~5 mM. (B) Media glucose values for the LG groups only (note change in scale). # indicates significant difference for CM- vs. CM+ of same oxygen level and starting glucose concentration on Day 28 (p<0.05).

5.4 Discussion

Given the limited supply of healthy autologous chondrocytes, strategies to further tissue engineering and regenerative medicine approaches for cartilage repair have focused on the application of stem cells. For clinical success, these cells must not only survive and produce extracellular matrix in the context of the microenvironmental conditions engendered by nutrient utilization and waste production, but once implanted, must do the same in the hypoxic and nutritionally limited conditions of the anatomic space in which cartilage resides. We have previously reported regional differences in cell health, matrix production, and mechanical properties in MSC-laden tissue engineered cartilage, where the highest properties were found at the construct periphery (Chapter 3). We hypothesized that when MSCs are induced to undergo chondrogenesis, they achieve a high anabolic state, but as a consequence, generate self-imposed gradients in nutrient supply that compromise cell viability and matrix deposition in the central and bottom portions of the constructs. Given these gradients of nutrients and other metabolic factors due to utilization at the periphery (Buckley et al., 2012; Heywood et al., 2006; Heywood et al., 2004; Zhou et al., 2008), we first investigated how decreasing the available glucose and oxygen impacted the overall functional properties of three-dimensional MSC-laden agarose constructs.

Although MSC viability and function were each compromised by glucose and oxygen deprivation in the presence of TGF- β , our data showed that glucose is the driving factor in limiting construct maturation. With chondrogenesis, glucose is consumed by MSCs at a greater rate (Pattappa et al., 2011), and within a three-dimensional context, is consumed

by cells located at the construct periphery. As a consequence, glucose becomes a limiting factor in the health and long-term matrix production by MSCs at the center of these engineered tissues. Conversely, and consistent with published data on chondrocytes cultured similarly (Yodmuang et al., 2013), hypoxic culture had a lesser effect on functional outcomes. On its own, hypoxic culture (in the presence of high glucose) resulted in constructs with slightly lower glycosaminoglycan content and mechanical properties. Of note, however, there was no discernable difference in cell viability in thick constructs when comparing hypoxic to normoxic culture, suggesting that this factor does not compromise cell vitality, but rather impacts matrix production. In low glucose conditions, constructs cultured in the presence of TGF- β had the lowest mechanical function, with viable cells and matrix deposition restricted to the periphery of the construct. In the absence of TGF- β , constructs had generally low mechanical function regardless of culture condition, with cells depositing less contiguous matrix compared to their TGF- β treated counterparts.

To reduce the extent of diffusion gradients within constructs and gain a better understanding of how limiting nutrient availability impacts MSC health, we decreased construct thickness by one-third and scaled media volume accordingly. Although decreasing thickness decreased the effects of nutrient gradients in high glucose conditions (there was no statistical difference in cell viability between the top and bottom of Norm HG+ constructs), gradients were still apparent when these thin constructs were cultured under conditions of nutrient deprivation. Specifically, we found it necessary to image both sides of the construct and group viability percentages into categories of side of

maximum or minimum viability, as stark differences developed in low glucose conditions. In these constructs, maximal viability occurred at the construct surface exposed to the defined oxygen level (2%) and the ambient media glucose concentration. Despite the fact that glucose levels reached lows of 0.05mM at this boundary over a three day culture period in Hyp LG+ conditions, a considerable fraction (52%) of the MSC population survived, even when further stressed to differentiate via the inclusion of TGF- β in the medium.

The data presented here on the impact of hypoxia on MSC chondrogenesis is somewhat conflicting with respect to previous literature. For instance, it has been reported that at early time points (~14 days), hypoxic culture can have a positive impact on glycosaminoglycan production in TGF- β containing conditions in both pellet culture systems and in electrospun scaffolds (Markway et al., 2010; Meretoja et al., 2013). One possible explanation for the negative response we see at later culture times could be the interplay between the secretome of the cells cultured in this hypoxic environment and the addition of TGF- β . Differentiation with TGF may in fact be ‘over-stimulating’ cells, forcing them to adopt a highly anabolic state despite not having the nutrients to sustain this high level of activity. It is also noteworthy that the MSC populations utilized in these studies were expanded in standard conditions (21% O₂ in high glucose DMEM containing serum). Others have suggested that alternative expansion techniques, for example expansion in low oxygen or low glucose conditions, may impact the properties of these populations and their resultant chondrogenic potential (Muller et al., 2011; Ranera et al., 2013). Whether such expansion methods select for subpopulations that are

suited for activity under nutrient constrained conditions (by forcing the expansion of only vital subpopulations), or whether it habituates all MSCs towards this status, bears further exploration. The impact of these modified expansion techniques could translate to improvements in the population response to stressors in larger scale three-dimensional hydrogels with clinical application.

Taken together, our data indicate that the functionality of MSC-laden constructs is dependent on both oxygen and glucose availability, with glucose availability having the greatest impact on functional maturation. While the minimum concentration of glucose that could sustain functional growth was not identified in this study, we did observe that greater than 40% of the population survived with glucose levels that reached one-one hundredth of blood plasma in 2% oxygen tension. Future work will focus on identifying the molecular signatures that identify those MSC sub-populations that are capable of both robust chondrogenesis and maintenance of viability under challenging metabolic conditions. Such markers may enable the isolation of a more robust and homogenous stem cell population for improved *in vivo* cartilage repair.

CHAPTER 6: VARIATION IN FUNCTIONAL CHONDROGENESIS AND RESPONSE TO ENVIRONMENTAL STRESSORS IN CLONAL MESENCHYMAL STEM CELL POPULATIONS

6.1 Introduction

In our assessment of how MSCs and chondrocytes differ from one another thus far, we found that, in the short term (<56 days), MSCs are sensitive to environmental stressors (Chapters 5), and in the long term (>56 days), the MSC phenotype is unstable (Chapter 4). However, the heterogeneous nature of bone marrow derived MSC populations may complicate the interpretation of such findings. In conditions of low oxygen and low glucose, for example, we noted that a portion of the stem cell population remained viable and could produce matrix. The question then arises as to which part of the population resulted in non-viable cells that were incapable of achieving a stable chondrogenic state, and what fraction of the population could successfully differentiate and thrive under chondrogenic conditions.

Since their identification in the 1970s (Friedenstein et al., 1970), it has been noted that MSC populations are heterogeneous, with populations isolated via plastic adherence containing colonies of varying sizes and densities (**Figure 6-1**). In 1999, it was demonstrated that individual colonies from human MSC bone marrow isolates had differential differentiation capacities, with some colonies incapable of undergo chondrogenesis (Pittenger et al., 1999). Since then, multiple studies from independent groups have confirmed varying differentiation capacity of clonal colonies derived from a single parent population (Halleux et al., 2001; Mareddy et al., 2007; Okamoto et al.,

2002; Pevsner-Fischer et al., 2011; Russell et al., 2010). However, a precise definition of a tri-potent MSC based on surface markers is not possible, as no surface marker exists that is exclusive to the MSC (Sivasubramaniyan et al., 2012). Furthermore, colonies with variable differentiation potential express a similar surface marker profile, including CD29, CD44, CD73, CD90, CD105, and CD166 (Mareddy et al., 2007). Finally, it has been shown that colonies capable of tripotential differentiation can vary in the degree of the amount of matrix they produce when they undergo chondrogenesis (Russell et al., 2010). Since there are no surface markers that predict efficacy, and there exists marked differences in chondrogenic matrix production within the most versatile MSC colonies, functional assays remain the only metric by which to determine colony (or clone) dependent differences in chondrogenic functionality.

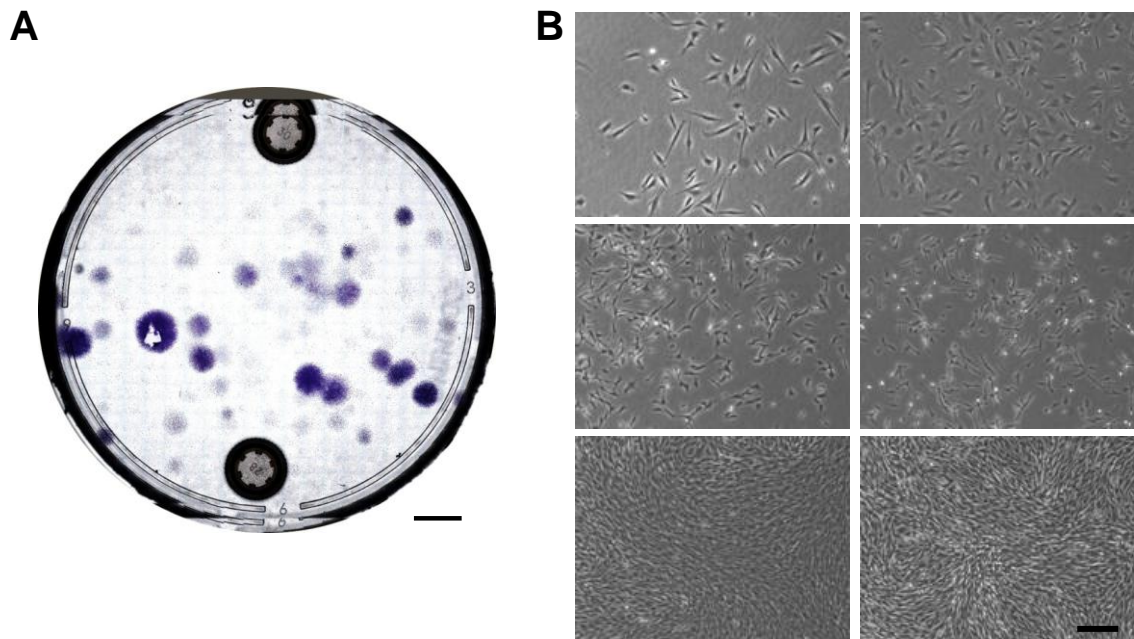


Figure 6-2: Gross assessment of colony heterogeneity. (A) Crystal violet staining of an MSC marrow isolate after 14 days in culture showing colonies of varying sizes and densities. Scale = 10 mm. (B) Phase contrast images of cell colonies after 11 days of culture show varying cell densities and cell morphologies. Scale = 500 μ m

To gain a better understanding of both intra-colony (or clone) heterogeneity and inter-colony heterogeneity in a mixed parent population, we conducted a series of experiments using various donor matched mixed parent populations and colony (clonal) subpopulations. Using an array of multi-scale measurement techniques, we investigated the differences in the ability of these different populations to produce mechanically functional matrix, upregulate chondrogenic genes at a single cell level, and withstand low oxygen and low glucose conditions while maintaining the capacity to produce cartilage matrix molecules.

6.2 Materials and Methods

6.2.1 Micromechanics

6.2.1.1 Study 1: Agarose Culture of Chondrocytes and MSCs

To begin to assess the differences in single cell response in MSC and chondrocyte populations, micromechanical techniques were used to investigate the capability of these cells to produce a functional pericellular matrix, thus shielding them from mechanical deformation when strain is applied to the hydrogel construct (Knight et al., 1998; Lee et al., 2000; Vigfusdottir et al., 2010). As described in Chapters 3 and 4, primary chondrocytes were isolated from diced cartilage of the tibial plateau of three juvenile bovine calves (Research 87, Boylston, MA) through a series of pronase and collagenase digestions. Donor match MSCs were harvested from the femoral and tibial cancellous bone marrow of the same calf joints and expanded through passage 2 (P2) in serum containing media (basal media; BM). Primary (passage 0) chondrocytes and P2 MSCs were encapsulated in 2% agarose at a density of 3 million cells/mL to limit the

mechanical interactions of the pericellular environment when the construct was compressed. Constructs (4 mm diameter, 2.25 mm thick) were cultured for 8 days in chemically defined media (CM) in the presence of 10 ng/mL TGF- β 3, with Day 1 gels maintained in CM without TGF- β 3 (CM-) to obtain a baseline measurement of cell deformation without the contribution of the pericellular matrix. At each time point, constructs were halved through the mid-sagittal plane, with one half undergoing micromechanical testing and the remaining half fixed in 4% paraformaldehyde for histological assessment of matrix accumulation.

6.2.1.2 Study 2: Agarose Culture of Mixed Parent and Clonal MSC Populations

Clonal MSC subpopulations from a single donor were isolated using the trypsin droplet technique (adapted from (Bartov et al., 1988)). Briefly, two marrow isolates from the same donor were plated and cultured for 10-11 days, until such time as clearly demarcated colonies were present. One plate was maintained as a heterogeneous parent population. In the second plate, colonies were identified at 4X magnification (under bright field microscopy), and the position of each colony was marked by pressing a piece of tape (with an ~7.5 mm hole punched in the center) against the bottom of the plate and outlining the edge of the colony (**Figure 6-2A**). The plate was then washed with phosphate buffered saline (PBS) and a cell scraper was used to remove cells in regions outside of the identified colonies. After aspirating the PBS, a surgical spear was used to outline the outer rim of each colony, drying the plate to allow for sufficient surface tension to hold a droplet of trypsin in place. This procedure was performed quickly to ensure the colony did not dry out. A droplet of trypsin was added to each colony (**Figure**

6-2B) and cells were incubated at 37°C for 2-5 min, after which a 100 µl pipette was used to gently agitate the droplet and transfer the colony to either a 6-well or 24-well (depending on colony size) tissue culture treated plate containing basal medium (DMEM with 10% FBS and 1%PSF). Colonies were cultured through passage 2, replating at a density of ~5,000 cells/cm² at each passage.

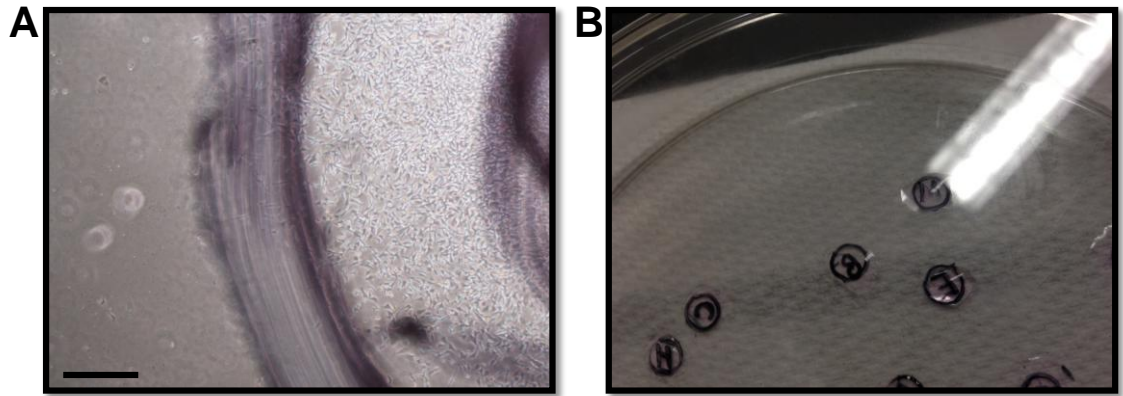


Figure 6-3: Isolation of colonies. (A) Edge of colony outlined under 4X magnification. Cell colony is apparent on the right side of marker line with relatively few cells located on the left side of the line. Scale = 500 µm. (B) Image of plate with trypsin droplets over identified colonies. Representative of typical spacing between colonies.

These isolated clonal subpopulations and the matched heterogeneous parent population, in addition to a second non-donor matched heterogeneous population, were encapsulated in 2% agarose at a density of 3 M cells/mL (slightly lower for some populations due to low cell yield) and cultured through 8 days in CM+, with a subset maintained in CM- for Day 1 assessment of baseline deformation values.

6.2.1.3 Study 3: HA Culture of Mixed Parent and Clonal MSC Populations – 2 and 3-Dimensional

As in Study 2, MSC clonal populations and a donor matched heterogeneous parent population were expanded through passage 2 in BM. Cells were encapsulated (3 M cells/mL) in a UV photocrosslinkable 1% hyaluronic acid hydrogel solution described in Chapter 4 (Burdick et al., 2005; Chung et al., 2008; Erickson et al., 2009b). As in Studies 1 and 2, constructs 4 mm in diameter and 2.25 mm thick were cultured for 1 day in CM– or 7 days in CM+. On Day 1 and Day 7, constructs were halved and tested for micromechanical response.

6.2.1.4 Micromechanical Testing

Construct halves (n=3 per group) were stained with 4 μ M calcein-AM in PBS for 30 min. Micromechanical testing was conducted using a custom unconfined compression testing device based on (Knight et al., 1998). The device was constructed to fit the stage of an inverted Olympus Fluoview FV1000 confocal microscope (Olympus America Inc, Center Valley, PA), with the coverglass bottomed PBS bath and platens recessed into the stage to achieve the necessary focal plane (**Figure 6-3**). The device was equipped with a linear stage and micrometer with digital readout in series with one platen, and a load cell connected in series with the opposing platen. Constructs were placed in the PBS bath with the mid-sagittal plane downward and imaged at 0% or 30% (40% for Study 3) compressive grip-to-grip stain with a 20X UPlanFL objective (optical zoom 1.5X for MSCs and 2.5X for chondrocytes). Images were acquired through approximately 60 μ m of the construct depth with a step interval of 2.34 μ m per slice.

In Studies 1-3, image stacks were compressed through the z-direction using a maximum intensity command, and the 2D images were processed with the binary object identification and characterization commands in MATLAB, thus allowing for the calculation of object area and the length of the bounding box surrounding an object (**Appendix 3**). Bounding box aspect ratio was calculated as the ratio of the Y bounding box length over the X bounding box length. In Study 3, using additional custom MATLAB script enabling the identification of the same object through an image stack, object volume and three-dimensional object bounding box parameters were quantified (**Appendix 4**). For each image stack, a mean parameter value was obtained from the average of the response of all cells within the image. Additionally, the standard deviation of each parameter value was calculated to determine how variable the response was in a single image. This resulted in three image means and three image standard deviations for each group and condition from which an average of the mean response and an average of the standard deviation of the mean response could be calculated.

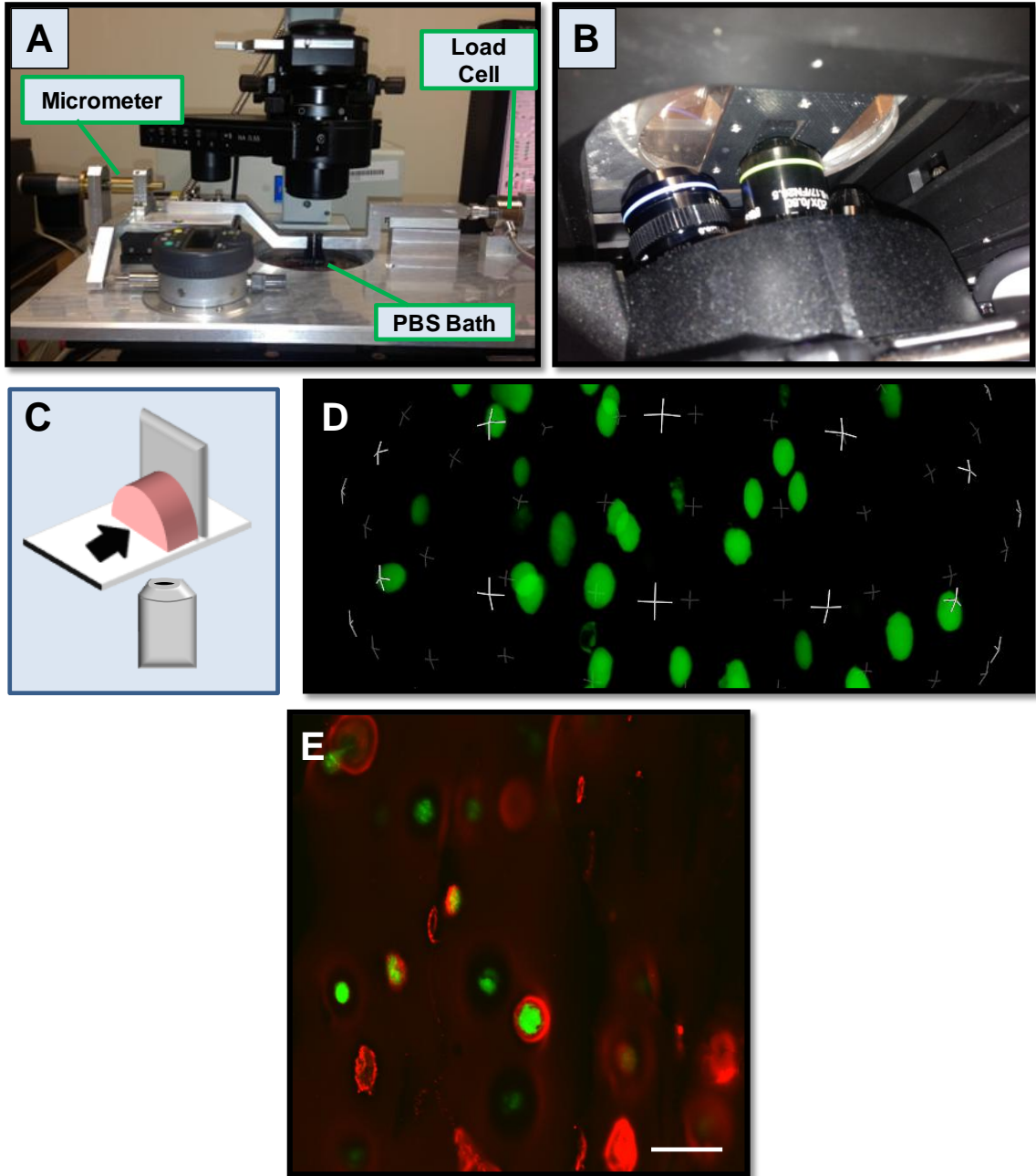


Figure 6-4: Micromechanical testing apparatus and protocol. (A) Custom device equipped with linear stage, micrometer, and load cell for uniaxial compression testing during confocal imaging. (B) Underside of device showing capacity for imaging via inverted microscope through a coverglass bottomed PBS bath. (C) Schematic showing geometry of halved constructs and direction of uniaxial compression. (D) Representative three-dimensional reconstruction of MSCs (green) compressed to 40% grip-to-grip applied strain on Day 1. (E) Two-dimensional image slice of MSC-laden (MSC=green) construct, under 40% axial strain, stained for matrix components (unfixed; anti-chondroitin sulfate; red), demonstrates compression of both dense pericellular matrix (negative space) and cell. Scale = 50 μ m

6.2.1.5 Histological Assessment of Pericellular Matrix Accumulation

Fixed constructs were dehydrated in a series of alcohol dilutions and paraffin embedded. Sections (8 μm) were stained with Alcian Blue for the identification of proteoglycans.

6.2.1.6 Statistics

For all studies, significance was established by ANOVA with Fisher's LSD post-hoc analyses, with significant differences determined by a p-value of $p < 0.05$ and trending differences at $p < 0.10$. Two-way ANOVA comparisons of Y/X bounding box aspect ratio (Studies 1-3; 2D and 3D) and cell area (Studies 1 and 3) were conducted with grouped day and cell population and applied strain as the independent factors. For Studies 1 and 3, one-way ANOVA comparisons were conducted for the image standard deviation of the bounding box area at Day 8 and 30% strain (40% in Study 2) with cell population as the independent variable. Three-dimensional analyses were carried out with a one-way ANOVA comparison of bounding box ratio at 40% strain with day grouped with cell population. An additional one-way ANOVA was conducted to compare cell volume on Day 1 at 0% and 40% applied strain.

6.2.2 Analysis of Single Cell Gene Expression - Fluorescence In-Situ Hybridization (FISH)

While heterogeneity in matrix production and micromechanical properties is an important outcome to assess when attempting to isolate a more robust chondrogenic subpopulation, assessment on a molecular level provides the opportunity to better understand this heterogeneity and develop screening tools. We therefore employed fluorescence *in-situ*

hybridization techniques (Raj et al., 2008) to determine how variable gene expression is in single colony populations and to determine if there are populations with a greater propensity for chondrogenic induction. Heterogeneous and clonal MSC subpopulations were expanded through passage 3 in basal media (BM; DMEM with 10% FBS). Cells were replated in a eight well coverglass chamber (#1 coverglass) at a density of $\sim 2,500$ cells/cm² and allowed to adhere overnight, after which media was replaced with chemically defined media without (CM⁻) or with (CM⁺) 10 ng/mL TGF- β for 7 days, with one media change through the culture period. Cells were washed with phosphate-buffered saline (PBS) and fixed with 4% paraformaldehyde (PFA) for 10 min. Following additional PBS washes, cells were permeabilized with 70% ethanol diluted in RNase-free DEPC-treated water. Probe hybridization was conducted as in (Raj et al., 2008). Multiple, singly labeled, oligonucleotide probes were developed against the bovine aggrecan (AGG) and cartilage oligomeric matrix protein (COMP) sequences (Biosearch Technologies). Cells were counterstained with DAPI, and imaged at 60X or 100X with an inverted Nikon Eclipse Ti Fluorescence Microscope. Single mRNA molecules (identified as bright, punctate dots, **Figure 6-4**) were quantified using a custom MATLAB script (Raj et al., 2008). To confirm the presence of heterogeneity in a single MSC colony, a follow-up study was conducted with a newly formed unpassaged P0 colony. Briefly, an MSC colony isolated through plastic adherence was allowed to culture in basal media without passage for 11 days following the initial marrow isolation. The colony was subsequently cultured in CM⁺ for four days with one media change occurring after 2 days of culture. The colony was then washed, fixed, and permeabilized as described above and labeled with probes for AGG, COMP, and GAPDH.

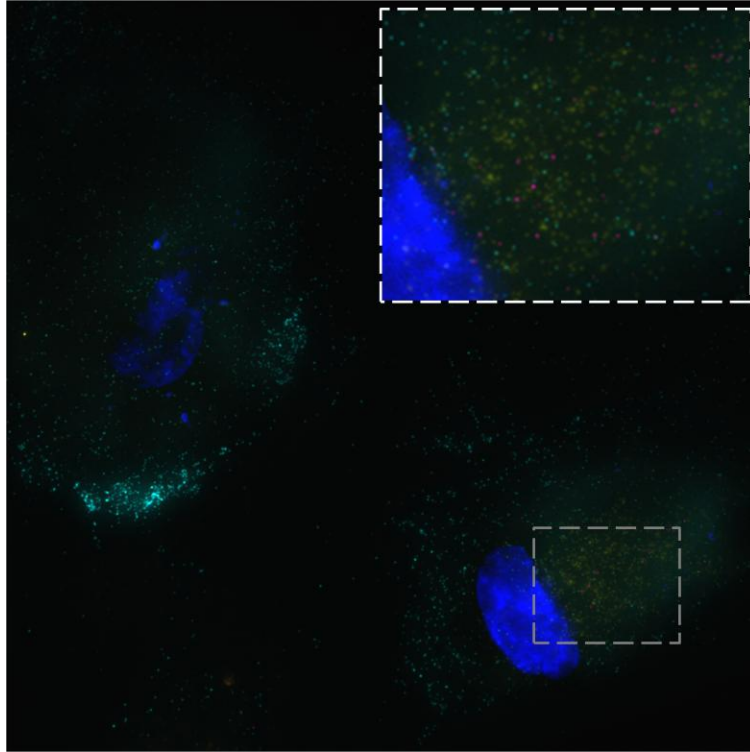


Figure 6-5: Identification of single mRNA molecules (small dots) labeled with a series of oligonucleotide sequences for three distinct genes (COMP=Pink; Aggrecan=Yellow; GAPDH=Cyan) using fluorescence *in-situ* hybridization.

6.2.3 Pellet Culture, Viability, and Biochemical Analysis of Clonal MSC Subpopulations

Cells from each clonal subpopulation were pelleted (20,000 cells per pellet) in a 96-conical well plate and cultured in low glucose/high glucose DMEM under normoxic/hypoxic conditions as described previously in Chapter 5, with all medium containing 10 ng/mL TGF- β 3. Pellets were cultured with 100 μ l media per pellet under Breathe-Easy semi-permeable membranes to prevent media evaporation. Pellets were fed twice weekly for 14 days. Sample number varied for each subsequent assay (n=1-3), dependent on cell yield from each colony. On day 14, pellets were stained using the Live/Dead assay kit as previously described. Confocal stacks were acquired from the

edge of the pellet to a depth of 100 μm using an Olympus Fluoview FV1000 confocal microscope with a 10X UPlanFL objective and 2X optical zoom. Volocity 3D Image Analysis Software (PerkinElmer, Waltham, MA) was used to reconstruct pellet volume (green/live channel) and count objects (nuclei of dead cells; red/dead channel) within that volume. Data are presented as number of dead cells counted/pellet volume. Additional pellets were digested with papain as described previously. Glycosaminoglycan content was measured via the DMMB assay and DNA content quantified with the Quant-iT PicoGreen dsDNA Kit. Matrix production is presented as μg GAG per pellet and μg GAG per μg DNA. Since sample numbers for each group in each assay were dependent on colony yield (n=1-3), statistical comparisons were not performed.

6.3 Results

6.3.1 Micromechanics

Micromechanical assessment of pericellular matrix properties was conducted through the quantification of the deformation parameter ‘aspect ratio.’ The bounding box aspect ratio is defined as the ratio of the length of the bounding box in the Y direction to the length in the X direction (the axis of applied uniaxial compression; note axes inverted in **Figure 6-5** compared to experimental protocol). If spherical, the Y and X length will be equivalent, and therefore, the aspect ratio will be 1. Deviation from 1 indicates a non-uniform shape. An aspect ratio >1 is expected with applied strain to the bulk construct. If the matrix surrounding the cell is of a sufficiently higher modulus than the construct biomaterial, stress shielding will ensue and the aspect ratio will remain near 1. This is demonstrated in **Figure 6-5**.

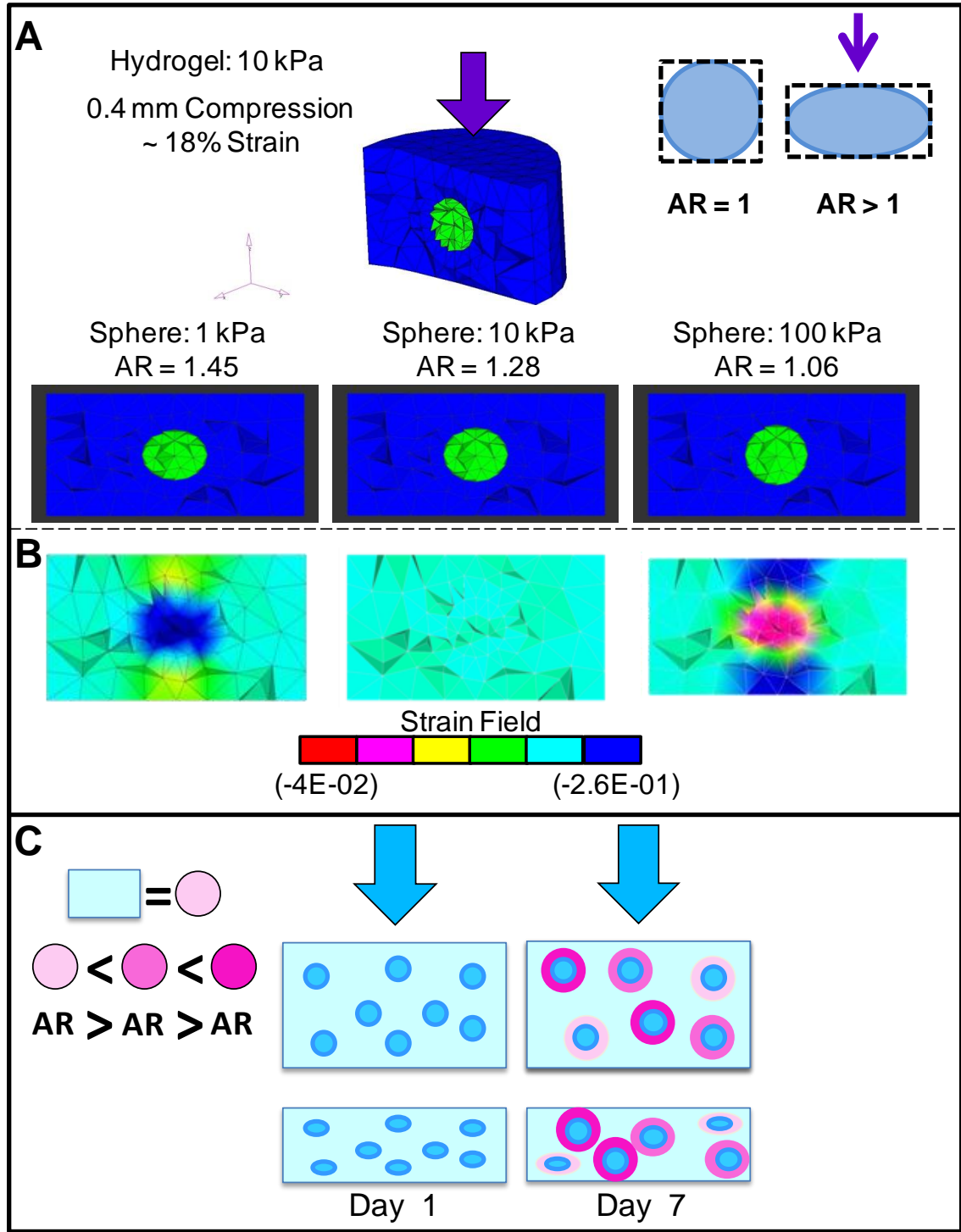


Figure 6-6: FE analysis of a deformable spherical inclusion within a deformable cylindrical construct subjected to axial compression (purple arrow). By varying the modulus of the spherical inclusion, compression applied to the cylindrical construct (which has a constant modulus) results in differing (A) levels of deformation of the inclusion (aspect ratio; AR) and (B) strain fields in and around the inclusion, depending on the properties of the inclusion. (C) Schematic representation of expected results of cell deformation for a heterogeneous population that has deposited matrix of varying stiffness.

6.3.1.1 Study 1: CH vs. MSC – 2-Dimensional

Micromechanical assessment began with a comparison of chondrocyte and MSC population response. On Day 1, there was an increase in mean image bounding box aspect ratio for all groups with the application of 30% strain (**Figure 6-6A, B**). Although all groups continued to deform on Day 8 ($p < 0.05$ 30% vs. 0%, with a trend for CH2, $p < 0.10$), there was a decrease in the aspect ratio at Day 1 compared to Day 8 at 30% strain. Comparing donor matched CH and MSC populations, there were no differences in bounding box aspect ratio at 0% strain (Day 1 and Day 8) or at 30% strain on Day 1. However, a comparison of aspect ratios on Day 8 with 30% applied strain revealed that Donor 3 MSCs deformed significantly more ($p < 0.05$) than CHs, with Donor 2 having a similar trending response ($p < 0.10$). To determine how variable the response was within a population, the standard deviation of the cell bounding box aspect ratio was calculated from single image frames. On Day 8 at 30% applied strain, MSCs had a higher image standard deviation than chondrocytes for all donors (**Figure 6-6C**). Histological assessment of proteoglycan deposition (Donor 3), illustrates an overall more intense, less diffuse staining of proteoglycans surrounding chondrocytes (**Figure 6-6D**). Quantification of 2D projected cell area illustrates a conservation of cell area with compression, with MSCs increasing in cell area with time (**Figure 6-7**).

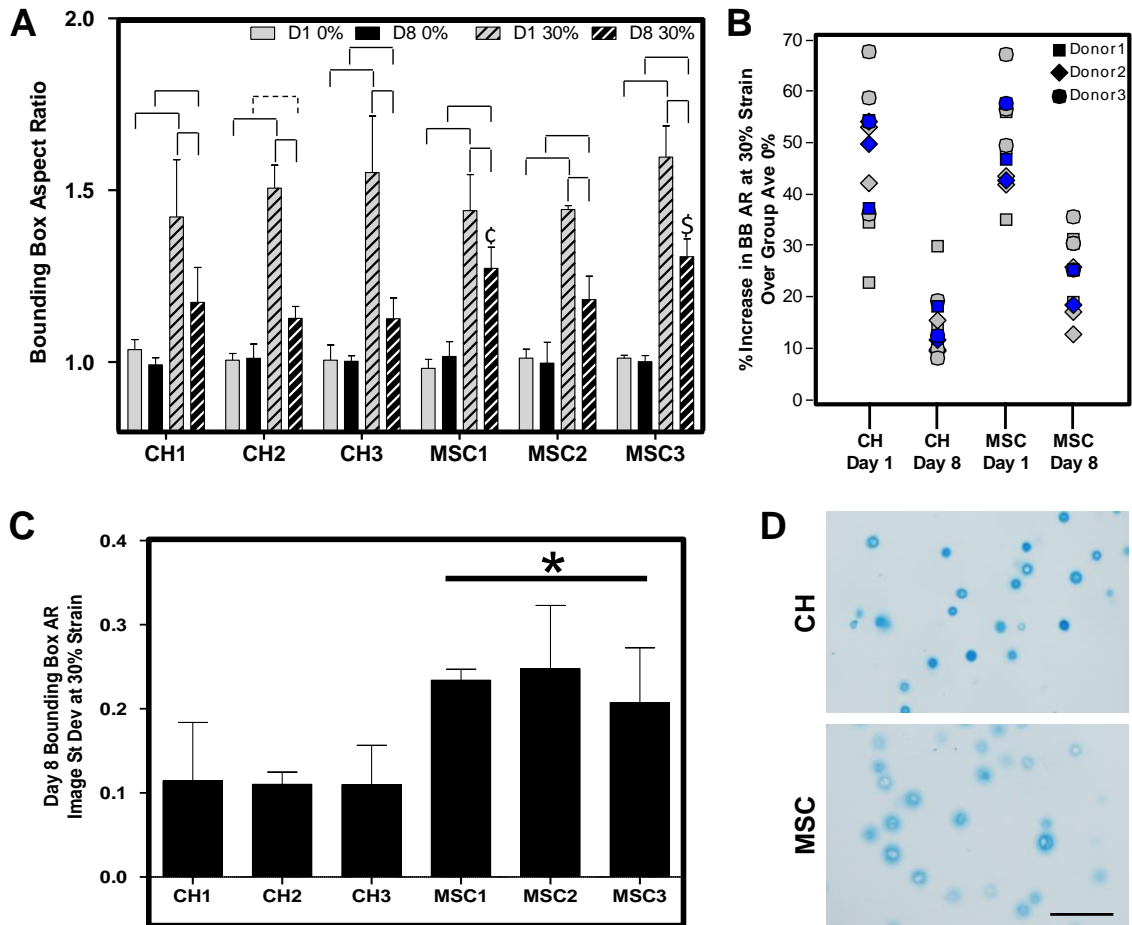


Figure 6-7: Two-dimensional assessment of bounding box ratio in 2% agarose at 0% and 30% applied strain for donor matched chondrocytes (CH) and mesenchymal stem cells (MSCs) after 1 day of culture in CM⁻ or 8 days of culture in CM⁺. (A) Average of image mean bounding box aspect ratio (Y/X) from a 2D z-projection of a single construct (n=3 constructs). \$ indicates significance at p<0.05, ϵ indicates trend at p<0.10 for MSC vs. donor matched CH at same day and same applied strain. Solid line indicates significance within group; dotted line indicates trend. (B) Percent increase in mean bounding box aspect ratio from 0% to 30% strain of 3 images from each donor (gray) with average of n=3 images from each donor indicated with blue dot. (C) Standard deviation of bounding box aspect ratio calculated from each image processed (n=3 images from each donor). * indicates significance at p<0.05 MSC vs. donor matched CH. (D) Alcian Blue staining of proteoglycans in the pericellular regions of Donor 3 constructs, showing more consistent matrix formation around chondrocytes. Scale = 100 μ m

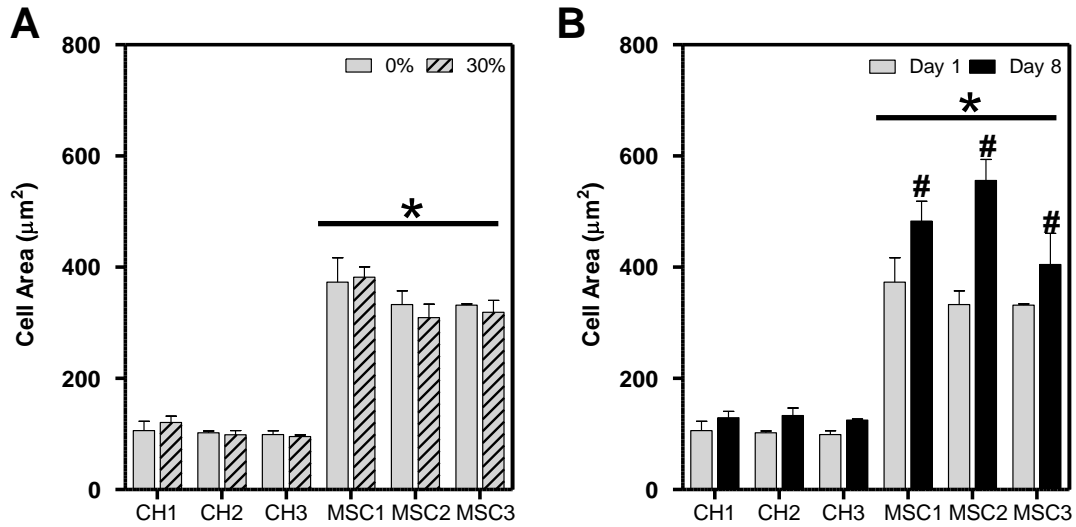


Figure 6-8: Conservation of cell area in the X-Y direction of 2D projected stacks with the application of 30% strain (A) and changes in area for MSCs with time in culture (B). * indicates significance for MSC vs. donor matched CH ($p < 0.05$). # indicates significance for MSC Day 1 vs. Day 8 ($p < 0.05$).

6.3.1.2 Study 2: Agarose – MSC Mixed Parent Populations vs. Colony Subpopulations – 2-Dimensional

Due to the high standard deviation of the response in MSC deformation compared to chondrocytes, we investigated if there were colony dependent differences in mechanically functional matrix deposition. By comparing the differences in bounding box aspect ratio at 30% strain from Day 1 and Day 8, with a more negative number indicative of a greater decline in deformation, we found variable responses between colonies (**Figure 6-8B**). Specifically, while there was only a trending decline for both mixed parent populations (Het1 and Het2, $p < 0.01$), there were many individual clonal subpopulations that showed significant declines (30% at Day 1 vs. 30% at Day 8, $p < 0.05$). However, some clonal populations continued to deform at a level close to or matching their Day 1 baseline deformation values (C1, C8, and C9). Histological

staining of select colonies Het1, C1, and C5 support the notion that colonies with less matrix staining (C1) maintain high levels of deformation compared to colonies with increased matrix staining (C5).

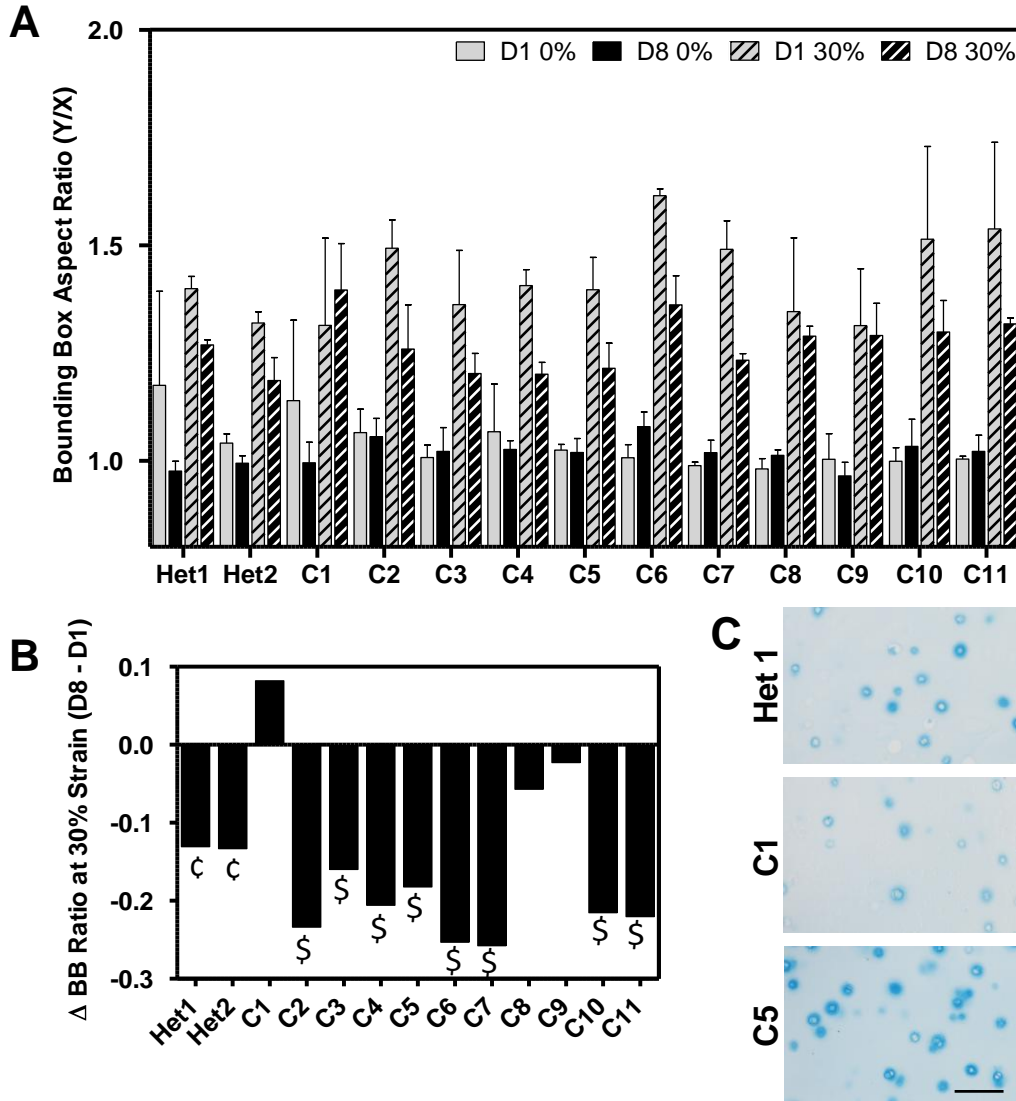


Figure 6-9: Two-dimensional assessment of bounding box ratio in 2% agarose at 0% and 30% applied strain for donor matched MSC parent population (Het1) and MSC colony subpopulations (C1-C11) and an additional non-donor matched parent population (Het2) after 1 day of culture in CM⁻ or 8 days of culture in CM⁺. (A) Average of mean bounding box aspect ratio (Y/X) from a 2D z-projection of a single construct (n=3 constructs). (B) Difference in bounding box aspect ratio at 30% applied strain from Day 8 to Day 1, with the more negative number indicating less deformation on Day 8. Significance was calculated from comparisons of Day 1 vs. Day 8 (see A for raw values and error bars) with \$ indicating significance at p<0.05 and ϵ indicating trend at p<0.10. (C) Alcian Blue staining of proteoglycans in pericellular region of select groups. Scale = 100 μm

6.3.1.3 Study 3: HA – MSC Mixed Parent Populations vs. Colony Subpopulations – 2 and 3-Dimensional

A more complete assessment of differential micromechanical responses of MSC parent populations and colony subpopulations in two dimensions and three dimensions was conducted with cells encapsulated in a hyaluronic acid hydrogel, a photocrosslinkable gel supportive of chondrogenesis with the capacity to withstand higher compressive strains than agarose before failure. From a 2-dimensional projection of the stacks along the z-direction, we once again found that there are different responses in the deformation of colony subpopulations with time (**Figure 6-9**). Some colonies, such as Colony 3, had a drastic reduction in cell deformation by Day 7, whereas Colony 8 showed no difference in bounding box aspect ratio by Day 7. However, while there were colonies that spanned the response of the mixed parent population, the standard deviations within a single population response remained high. Once again, 2-dimensional cell projected area was conserved with deformation as in Study 1 (**Figure 6-10**).

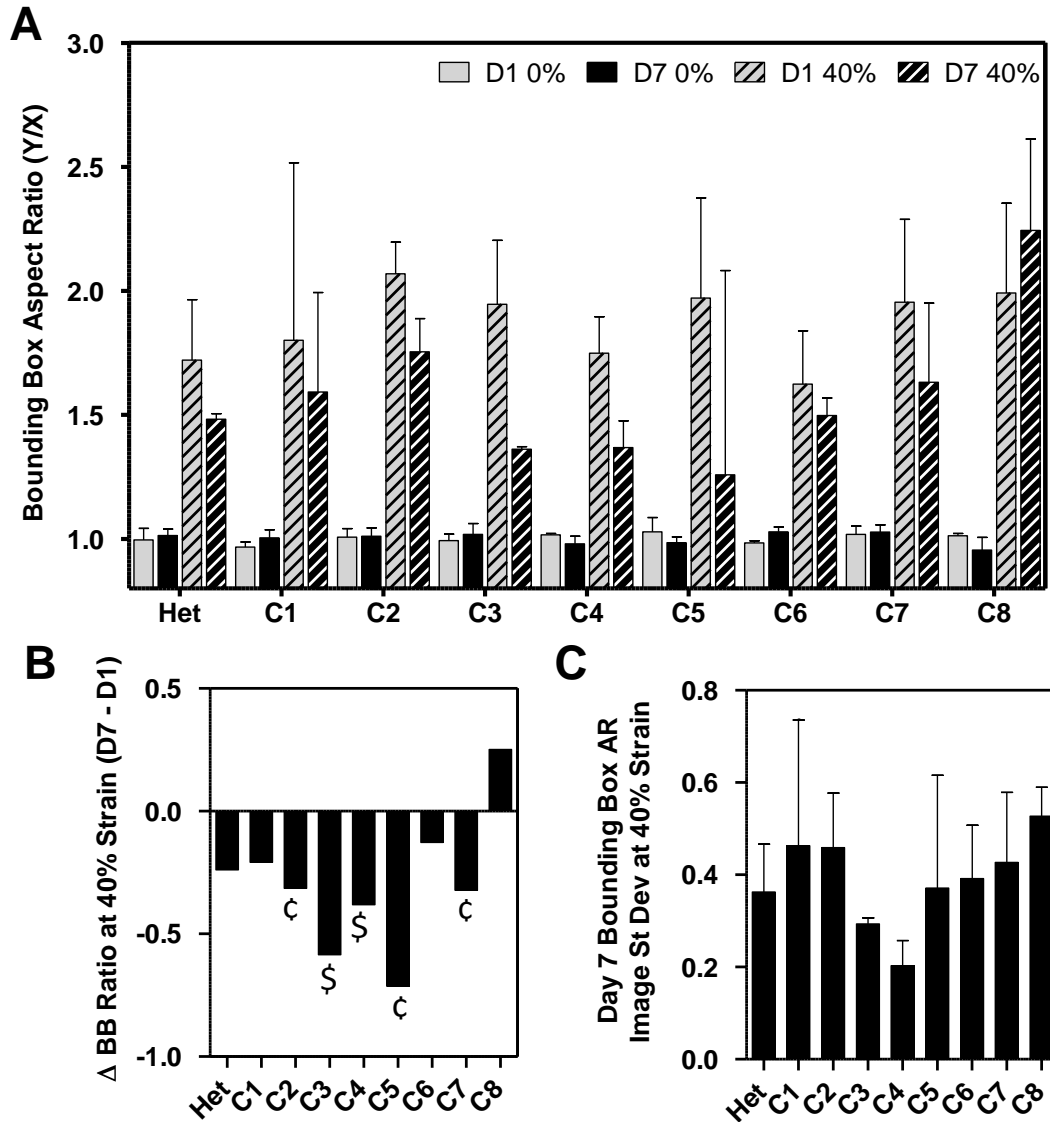


Figure 6-10: Two-dimensional assessment of bounding box ratio in 1% HA at 0% and 40% applied strain for a donor matched MSC parent population (Het1) and MSC colony subpopulations (C1-C8) after 1 day of culture in CM- or 7 days of culture in CM+. (A) Average of mean bounding box aspect ratio (Y/X) from a 2D z-projection of a single construct (n=3 constructs). (B) Difference in bounding box aspect ratio at 40% applied strain from Day 7 to Day 1 with a more negative number indicating less deformation at Day 7. Significance was calculated from comparison of Day 1 vs. Day 7 (see A for raw values and error bars) with \$ indicating significance at p<0.05 and € indicating trend at p<0.10. (C) Standard deviation of bounding box aspect ratio calculated from each image processed (n=3 images from each donor).

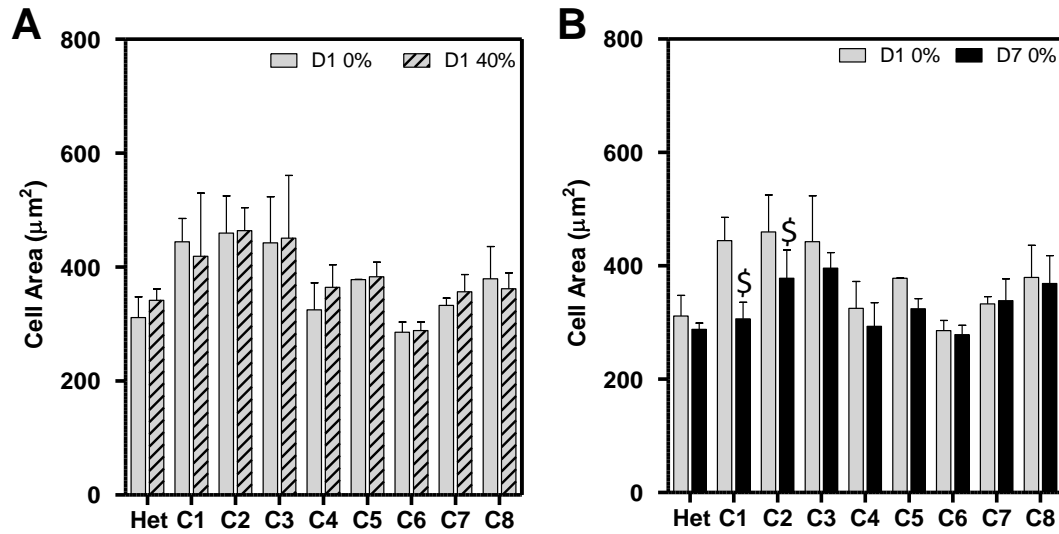


Figure 6-11: Quantification of cell area illustrates conservation of area in the X-Y direction of 2D projected stacks with the application of 40% strain (A) and moderate changes in area for some colony subpopulations with time (B). \$ indicates significance Day 1 vs. Day 7 ($p < 0.05$).

The same image stacks that underwent z-direction compression and two-dimensional analysis were analyzed again with custom MATLAB code identifying objects in three-dimensional image stacks, eliminating any cell that did not reside completely within the image stack boundaries. Bounding box ratio in the X-Y plane (equivalent to 2D plane) once again revealed that Colony 3 had the greatest decrease in bounding box deformation aspect ratio with time in culture at 40% applied strain (**Figure 6-11A**). Z-length was not significantly increased with applied deformation, even at Day 1, indicating that cell deformation occurred primarily in the direction of uniaxial compression (**Figure 6-11B**). Quantification of volume confirmed 2-dimensional cell area calculations in that there was a conservation of volume with applied strain (**Figure 6-11C**).

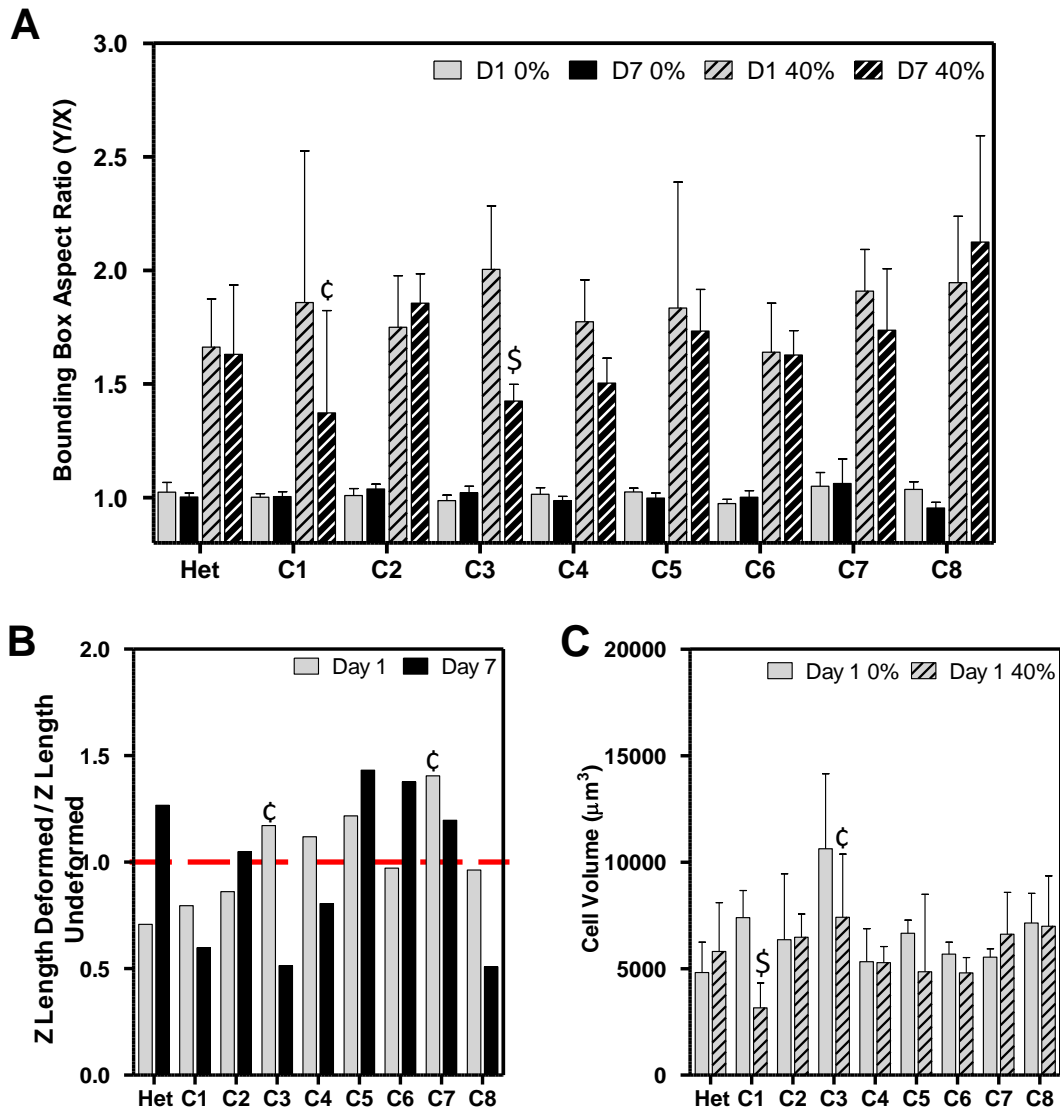


Figure 6-12: (A) Three-dimensional assessment of cell deformation in 1% HA at 0% and 40% applied strain for donor matched MSC parent population (Het1) and MSC colony subpopulations (C1-C8) after 1 day of culture in CM⁻ or 7 days of culture in CM⁺. Significance of D1 40% vs. D7 40% indicated with \$ ($p < 0.05$) with trend indicated with ϵ ($p < 0.10$). (B) Ratio of z-bounding box length (object length through the depth in the z-stack) at 40% deformation to 0% deformation shows no overall trend of z-elongation with compression (ratio > 1 with 1 indicated by red line). ϵ indicates trend z-length at 0% strain vs. z-length at 40% strain with $p < 0.10$. (C) 3D quantification of cell volume follows 2D quantification of cell area, with overall conservation of volume with compression. ϵ indicates trend at 0% strain vs 40% strain with $p < 0.10$.

6.3.2 Single Cell Gene Expression in Clonal Colonies

To investigate the potential for molecular heterogeneity at the single colony and single cell level, two independent studies (2 donors) were conducted with mixed parent populations and donor matched colony subpopulations. Quantification of population mean and median of mRNA counts per cell showed an increase in COMP and AGG expression in the presence of TGF- β for all groups (Studies 1 and 2). A summary of descriptive statistics can be found in **Tables 6-1 and 6-2**. For example, in Study 1, mean COMP expression levels across groups ranged from 7 to 214 in cells cultured in CM⁻ and 62 to 2306 counts per cell in CM⁺. Population standard deviation ranged from 3 to 258 counts per cell in CM⁻ and 26 to 1904 counts per cell in CM⁺. This increase in standard deviation indicates that there was not simply a shift in the mean of the data, but rather an increase in the spread of the data with TGF- β induction. This intra-population spread was apparent in both studies for both matrix molecules assessed (**Figures 6-12A and Figures 6-13A**). Boxplots and interquartile range values support the notion of a large spread in the data for colonies, along with an increased mean expression with chondrogenic induction. Colony dependent responses were also apparent. For example, in Study 1, the mean fold expression increase in Colony 4 mean (**Figure 6-12B**) was high for both COMP and AGG, with interquartile ranges and standard deviations lower than colonies with similar mean values (C3 and C7, Study 1), where as Colony 2 (Study 1) had a lesser response to TGF- β . Study 2 yielded similar findings, with a larger spread in data with TGF- β induction in the colony subpopulations compared to the mixed parent population, with some colonies (C3) having a large increase in COMP and AGG expression with the addition of TGF- β (**Figure 6-13**).

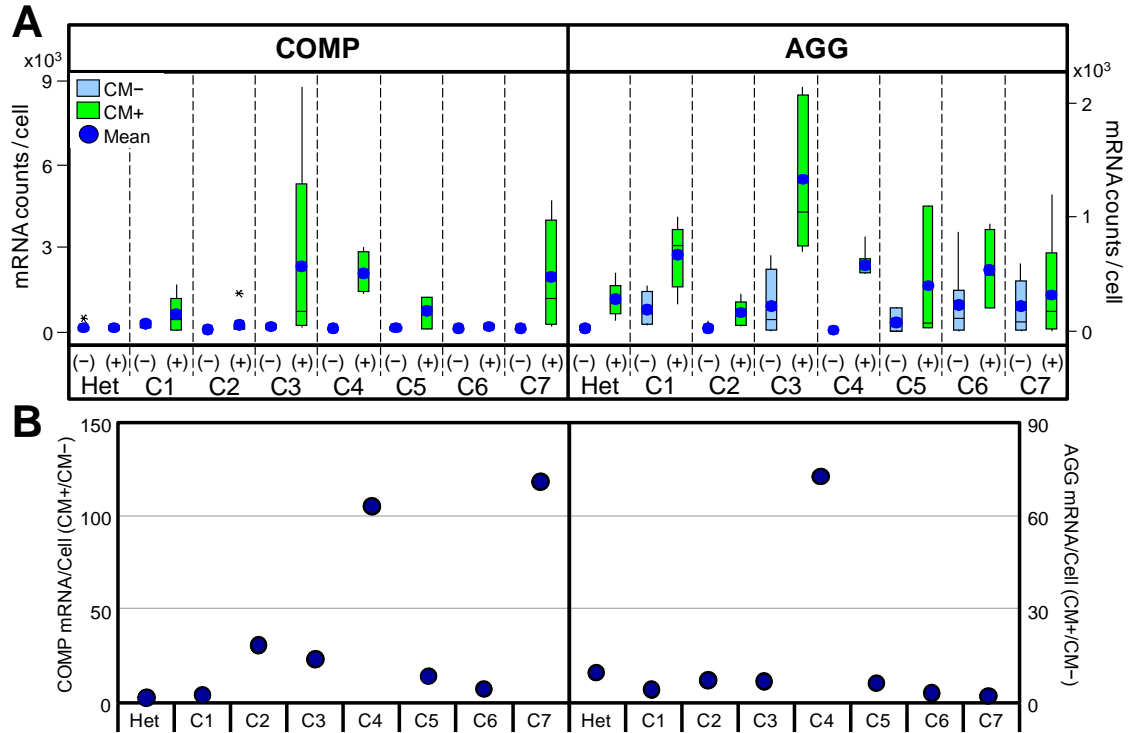


Figure 6-13: Single cell RNA quantification. (A) Boxplots of single cell mRNA counts of cartilage oligomeric matrix protein (COMP) and aggrecan (AGG) showing median, quartiles, and outliers (asterisks) for a heterogeneous MSC population and colony derived subpopulations from the same donor. Blue dot indicates mean mRNA count within the population. Cells were cultured in monolayer in chemically defined media without TGF- β (CM⁻) or chemically defined media with TGF- β (CM⁺) for 7 days. **(B)** Fold increase of mean mRNA values (CM⁺/CM⁻) for each population.

Table 6-1: Descriptive statistics of mRNA counts in populations shown in Figure 6-12.

	Het		C1		C2		C3		C4		C5		C6		C7	
	(-)	(+)	(-)	(+)	(-)	(+)	(-)	(+)	(-)	(+)	(-)	(+)	(-)	(+)	(-)	(+)
COMP																
Mean	75.50	61.56	213.75	556.17	6.70	195.50	105.75	2305.80	19.50	2036.33	53.67	663.33	21.00	114.25	16	1881.2
Median	9.50	27.00	257.50	376.00	5.00	26.00	108.00	679.00	21.50	1903.50	61.00	825.00	3.00	106.00	14	1100
StDev	163.56	85.38	142.02	622.20	5.46	442.41	76.82	3668.60	8.35	715.55	48.42	576.75	37.90	82.05	11.74734	2013.329
Var	2.68E+04	7.29E+03	2.02E+04	3.87E+05	2.98E+01	1.96E+05	5.90E+03	1.35E+07	6.97E+01	5.12E+05	2.34E+03	3.33E+05	1.44E+03	6.73E+03	1.38E+02	4.05E+06
Range	4.08E+02	2.10E+02	3.22E+02	1.61E+03	1.40E+01	1.28E+03	1.87E+02	8.68E+03	1.90E+01	1.69E+03	9.60E+01	1.12E+03	1.05E+02	1.91E+02	3.60E+01	4.57E+03
IQ Range	15.75	48.00	114.25	698.75	8.25	45.25	61.75	1557.00	8.50	1162.00	48.00	559.50	13.25	91.25	10	3026
Skew	2.44	1.48	-1.55	1.15	0.67	2.78	-0.17	2.06	-1.16	0.38	-0.67	-1.16	2.08	0.49	1.347206	0.731296
Kurt	5.95	0.47	2.61	0.64	-1.15	7.76	1.18	4.31	0.97	-2.04	N/A	N/A	3.99	-0.56	2.305146	-1.68415
AGG																
Mean	29.67	275.11	193.50	670.50	25.10	162.63	216.75	1330.80	8.00	580.17	71.33	396.00	223.75	528.25	219.2857	316.8
Median	27.00	250.00	169.50	750.50	14.00	167.50	101.00	1038.00	9.00	544.00	2.00	69.00	105.00	490.00	80	174
StDev	23.31	142.05	148.11	286.18	27.18	106.09	308.55	688.99	3.46	120.63	120.09	604.00	297.87	360.60	247.3087	493.8843
Var	5.43E+02	2.02E+04	2.19E+04	8.19E+04	7.39E+02	1.13E+04	9.52E+04	4.75E+05	1.20E+01	1.46E+04	1.44E+04	3.65E+05	8.87E+04	1.30E+05	6.12E+04	2.44E+05
Range	6.30E+01	4.17E+02	3.53E+02	7.62E+02	8.90E+01	2.86E+02	6.57E+02	1.43E+03	8.00E+00	3.25E+02	2.08E+02	1.07E+03	8.61E+02	7.45E+02	5.84E+02	1.19E+03
IQ Range	28.25	141.00	125.00	350.75	30.50	162.50	299.25	1240.00	2.00	54.00	104.00	533.50	325.75	532.75	406.5	141
Skew	0.48	0.47	0.90	-0.62	1.81	0.27	1.57	0.48	-1.54	2.13	1.73	1.72	1.62	0.28	0.548157	2.094956
Kurt	-0.60	-0.70	1.48	-0.85	3.52	-1.40	2.24	-3.08	2.89	4.80	N/A	N/A	2.71	-4.12	-1.93753	4.502693
n	6	9	4	6	10	8	4	5	4	6	3	3	8	4	7	5

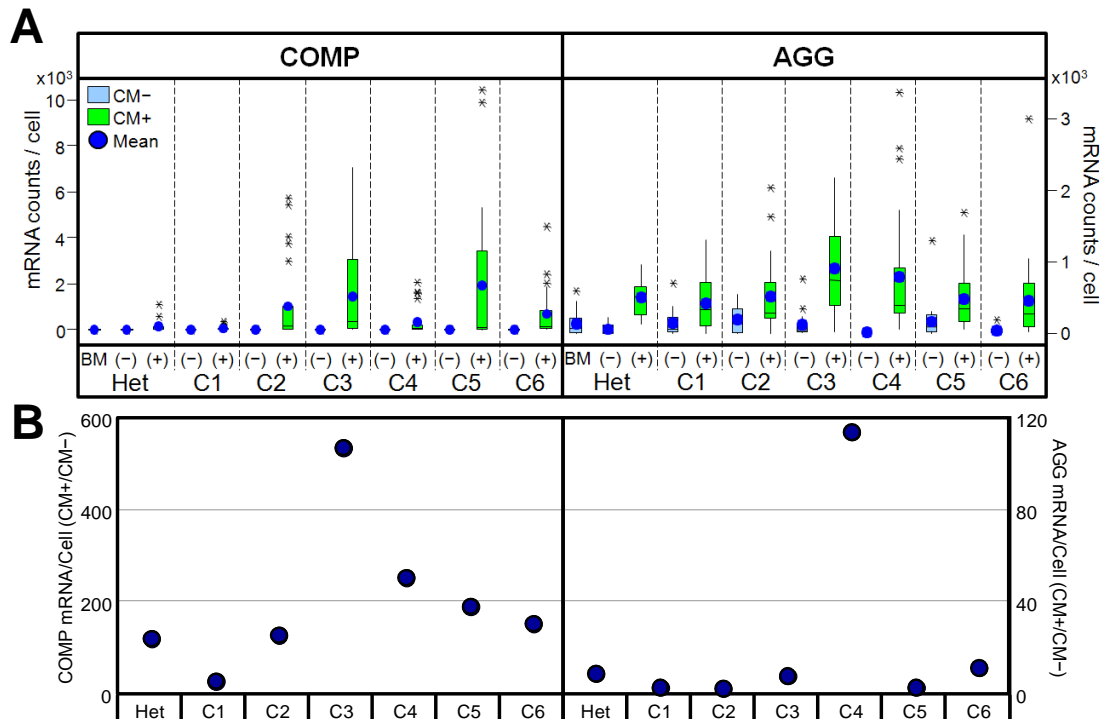


Figure 6-14: Repeated study of single cell RNA quantification shown in Figure 6-12 with different mixed parent and clonal populations. (A) Boxplots. Blue dot indicates mean mRNA count within the population. Cells were cultured in monolayer in basal media (BM), chemically defined media without TGF- β (CM-), or chemically defined media with TGF- β (CM+) for 7 days. (B) Fold increase of mean mRNA values (CM+/CM-) for each population.

Table 6-2: Descriptive statistics of mRNA counts in populations shown in Figure 6-13.

	Het		C1		C2		C3		C4		C5		C6		
COMP	Basal	(-)	(+)	(-)	(+)	(-)	(+)	(-)	(+)	(-)	(+)	(-)	(+)	(-)	(+)
Mean	0.69	1.17	141.44	1.39	41.81	7.82	1013.41	2.67	1434.00	1.25	317.44	10.04	1917.74	4.30	663.52
Median	0.00	1.00	21.50	1.00	3.00	6.00	123.00	1.00	321.00	0.50	27.00	1.00	75.00	1.00	143.00
StDev	1.16	2.53	289.75	1.79	84.07	8.88	1734.09	4.79	1956.05	1.80	612.36	17.79	3168.71	12.76	1019.18
Var	1.34E+00	6.38E+00	8.40E+04	3.19E+00	7.07E+03	7.89E+01	3.01E+06	2.29E+01	3.83E+06	3.25E+00	3.75E+05	3.17E+02	1.00E+07	1.63E+02	1.04E+06
Range	4.00E+00	1.10E+01	1.09E+03	7.00E+00	3.37E+02	3.20E+01	5.73E+03	2.40E+01	7.03E+03	7.00E+00	2.07E+03	6.10E+01	1.04E+04	6.70E+01	4.51E+03
IQ Range	1.00	1.00	121.50	1.75	27.50	8.00	915.00	1.00	2786.75	2.25	194.00	9.75	3008.00	1.50	756.00
Skew	2.00	3.85	2.83	2.12	2.53	1.98	1.85	3.85	1.45	1.92	2.04	2.07	1.76	4.91	2.49
Kurt	3.64	15.66	8.22	5.16	6.23	3.48	2.22	16.20	1.43	4.36	2.77	3.36	2.34	24.86	7.21
AGG															
Mean	141.00	57.06	501.19	147.50	421.41	194.88	509.52	112.70	914.67	6.95	791.00	163.81	488.83	40.96	458.52
Median	78.50	34.00	513.00	58.50	329.00	173.00	293.00	48.00	742.00	1.00	395.00	86.00	341.00	23.00	271.00
StDev	158.93	69.25	244.90	183.16	363.60	187.04	500.58	162.80	623.29	10.02	859.52	254.79	424.09	45.31	593.41
Var	2.53E+04	4.80E+03	6.00E+04	3.35E+04	1.32E+05	3.50E+04	2.51E+05	2.65E+04	3.88E+05	1.00E+02	7.39E+05	6.49E+04	1.80E+05	2.05E+03	3.52E+05
Range	5.89E+02	2.28E+02	8.26E+02	7.05E+02	1.31E+03	5.49E+02	2.04E+03	7.63E+02	2.16E+03	2.90E+01	3.32E+03	1.30E+03	1.63E+03	1.91E+02	2.97E+03
IQ Range	180.50	89.00	308.50	184.50	583.00	318.00	464.50	104.00	810.25	13.25	450.00	224.75	533.50	48.00	585.50
Skew	1.36	1.29	0.20	1.94	0.99	0.57	1.69	2.89	0.74	1.21	1.88	3.75	1.43	1.86	3.26
Kurt	1.29	0.70	-0.58	4.19	0.30	-0.87	2.59	9.87	-0.29	-0.05	2.90	16.65	1.99	3.77	13.30
n	26	18	16	18	27	17	27	27	24	20	25	26	23	27	27

To determine if the large spread in inter-colony data was due to the devolution of the population with time in culture and passage, a single un-passaged MSC colony was cultured in the presence of TGF- β during a shortened culture time (10 days in basal media and 4 days in CM+) without passage. Although expression in GAPDH appeared relatively uniform across the colony, spots of high COMP and AGG expression were apparent, indicating inhomogeneous chondrogenic induction in a single colony population that has not been passaged (**Figure 6-14**).

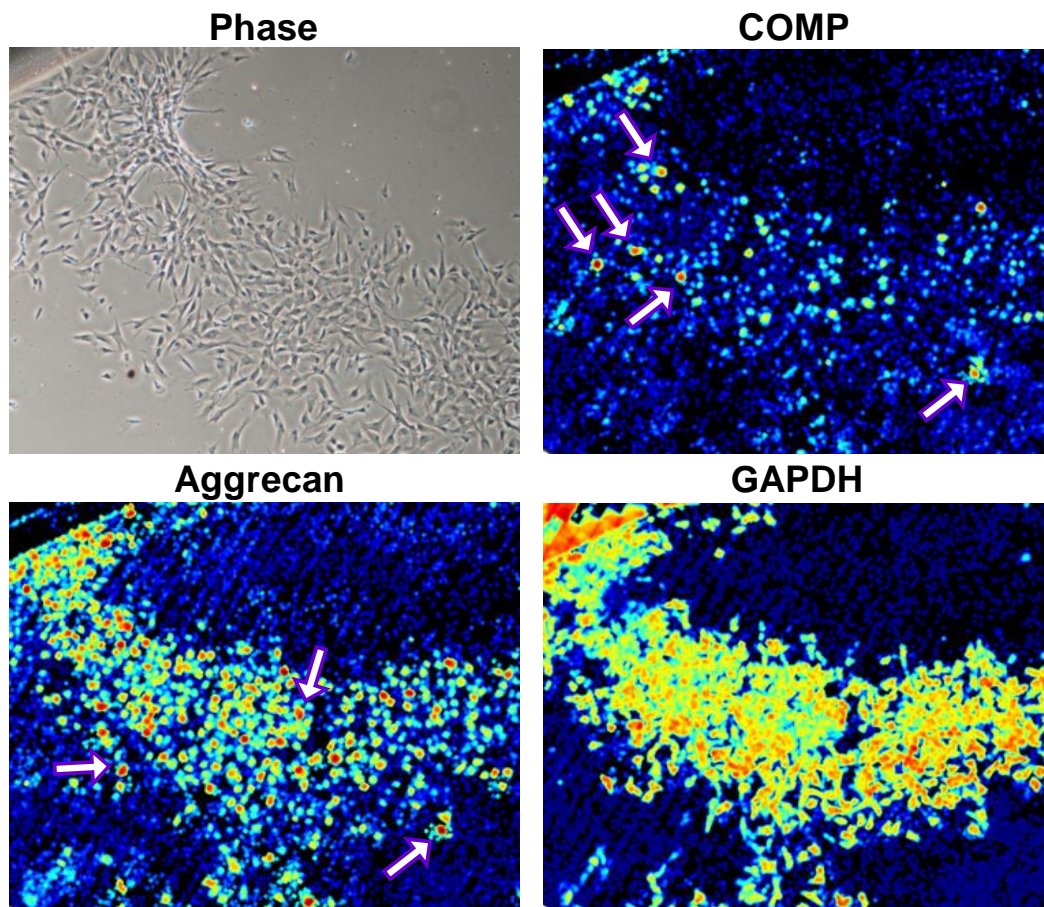


Figure 6-15: Heat maps of single cell mRNA counts in an un-passaged MSC bone marrow colony in monolayer culture (11 days in basal media followed by CM+ for 4 days). Phase contrast image (A), note slightly different image frame and scale. Variable induction is present in this single, unpassaged colony. Signal intensity for COMP (B) and Aggrecan (C), showing isolated regions of high expression (red), with a few (but not all) of these hot spots highlighted with arrows. Conversely, more consistent levels of GAPDH expression (D) are observed across the colony.

6.3.3 Clone Dependent Response to Stressors

Results in Chapter 5 illustrated that MSCs are sensitive to metabolic stressors, including low oxygen and low glucose conditions. However, because not every cell under the most taxing situation (Hyp LG+) lost viability, and because the heterogeneous MSC population is comprised of cells of different clonal origin, we evaluated the impact of these stressors on a clone-by-clone basis using micro-pellets. For this study, we isolated a total of 15 clonal colonies and 2 heterogeneous parent populations from 2 different donors, and evaluated viability and GAG content over a 14 day period. Consistent with the hydrogel studies in Chapter 5, the poorest performing groups were those cultured under Hyp LG+ conditions. However, within a single donor, there was marked variability in the response between individual clonal populations. Notably, for the first donor (**Figure 6-15B**), some clonal colonies (C3 and C6) performed poorly, with little matrix production in all culture conditions and a marked increase in the number of dead cells in Hyp LG+ compared to all other conditions. However, other poor performing clonal colonies such as C2 and C5 had a more consistent and slightly higher baseline in the number of dead cells per volume. Clonal colonies (C1 and C4) and the heterogeneous parent population, each with high GAG per pellet, were still susceptible to low glucose culture, resulting in lower GAG/pellet and GAG/DNA compared to their Norm HG+ counterparts. Data from the second donor (**Figure 6-15C**) revealed a slightly different response. Although once again the response was variable between clonal colonies, some (C2 and C7) responded favorably to Hyp HG+ conditions in terms of GAG/pellet, a finding that generally does not match the hydrogel results (**Figure 6-15B**), where the highest performing groups were consistently Norm HG+.

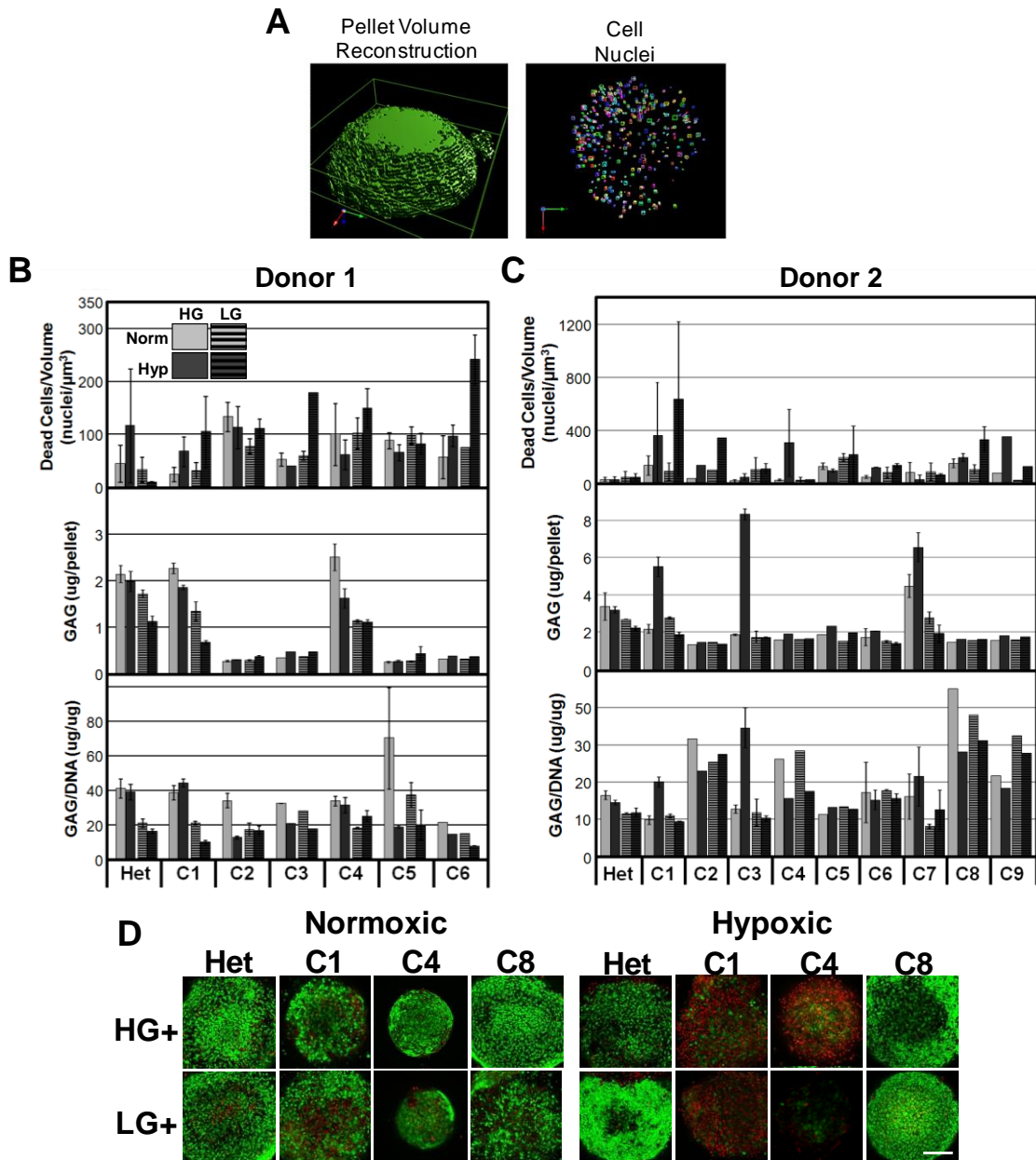


Figure 6-16: Impact of low glucose and hypoxic culture conditions on differentiation and viability of MSC clonal populations cultured as micro-pellets. (A) 3D reconstruction of partial pellet volume (Left) with visualization of cell nuclei (Right) identified as non-viable by ethidium homodimer staining. (B and C) Quantification of cell death (Top), glycosaminoglycan content per pellet (Middle), and glycosaminoglycan content per DNA (Bottom) showing variable responses of clonal subpopulations (C1-C6 from Donor 1; C1-C9 from Donor 2) compared to the heterogeneous parent population (Het) after 14 days of culture. n=1-3 per clonal population. (D) Select z-projections of Live/Dead stacks from Donor 2. Scale = 200 μ m

6.4 Discussion

Standard isolation protocols result in MSC populations that are heterogeneous in their chondrogenic potential (Pittenger et al., 1999). Current cell sorting techniques, such as cell surface markers (Sivasubramaniyan et al., 2012), lack the capacity to select individual cells in terms of differentiation capacity (Mareddy et al., 2007). Additionally, previous reports of chondrogenic heterogeneity of stem cells have shown functional differences of subpopulations solely based on matrix production capacity (Russell et al., 2010). However, these studies were performed in pellet culture and under high nutrient conditions, and so failed to assess differences at the single cell level. Furthermore, there is currently a lack of information regarding the differences in the mechanical function of the matrix produced by single cells, and on their ability to remain stable and produce such matrix in the stressful environments that they will ultimately see *in vivo*. As such, a series of experiments were conducted to gain a better understanding of colony dependent heterogeneity in mixed parent and colony derived populations when cultured under chondrogenic conditions.

In cartilage, chondrocytes surround themselves with a pericellular matrix, the matrix in the direct vicinity of the cell, that mediates mechanical strain transfer from the tissue to the cell (Guilak et al., 2006). Previous studies have noted that within sparsely seeded agarose hydrogels, both chondrocytes (Knight et al., 1998) and MSCs (Vigfusdottir et al., 2010) produce dense matrix with time in culture, which at early times, is located pericellularly. Accumulation of this pericellular matrix shields the cells from applied strain when that matrix becomes stiffer than the surrounding hydrogel material. While

interesting, these studies did not directly compare cell types (chondrocytes vs. MSCs), and further, did not investigate population dynamics or heterogeneity. In this chapter, we employed similar micromechanical techniques to compare the response of donor matched chondrocyte and MSC (mixed parent) populations to applied strain in an agarose hydrogel. Quantification of the deformation parameter ‘bounding box aspect ratio’ revealed that chondrocyte populations not only produced matrix of higher mechanical function by Day 8, but did so in a more homogenous manner (lower standard deviation within a single image frame). Proteoglycan staining revealed intense staining localized in a compact manner around chondrocytes. Conversely, MSC populations had lighter, more diffuse pericellular staining, indicating they had produced less matrix or ECM molecules of different molecular weights, sulfation levels (charges), and diffusivity when compared to chondrocytes. It should be noted that, due to restrictions on the range of mechanical properties we can assess with these hydrogel micromechanical experiments (i.e. we cannot discriminate between two objects that may have different moduli after they become significantly stiffer than the surrounding material), we may be underestimating the heterogeneity of chondrocyte populations. Additional methods to further these experiments are discussed in the following chapter.

We next investigated whether differences exist between colony subpopulations compared to parent populations in agarose and hyaluronic acid hydrogels. In both studies, we found colony subpopulations typified by responses on both sides of the deformation spectrum compared to the parent population. For example, while Colony 1 (Study 2) produced low amounts of matrix and continued to deform at Day 8, more so than the heterogeneous

population, Colony 5 (Study 2) had more pericellular matrix accumulation and a greater attenuation of deformation with applied strain by Day 8 compared to Day 1 relative to the parent population. Notably, however, image standard deviation of aspect ratio of colony subpopulations remained comparable to the heterogeneous parent population. This indicates that, within a single image frame, these clonal MSC populations that experience the same growth conditions and the same applied bulk strain, still possess marked variability in their ability to produce mechanically robust matrix within a single colony population. Therefore, we concluded that we were able to isolate colonies that had differential mean responses compared to the mixed parent population, but that these mean responses maintained a high degree of variability. This may suggest that as a single colony expands from a single cell, heterogeneity may be regenerated within the population.

To investigate this further, we used a novel single cell gene expression technique (Raj et al., 2008) to determine if intra- and inter-colony population heterogeneity existed on a molecular level. Using quantitative fluorescence *in-situ* hybridization (FISH), counts of individual mRNA molecules of chondrogenic genes were acquired within single MSCs undergoing chondrogenesis. While the data did follow the expected trend of increased population mean expression of chondrogenic genes with the provision of TGF- β , there was a surprising increase in the spread of the data. That is, within a single clonal colony, cell-by-cell analysis of mRNA copy number showed a wide range of responses. Although there was a large increase in data variability with an increase in mean expression for most colonies, some colonies did experience a shift in mean expression

while maintaining lower variability (such as Colony 4). This indicates that there may be colonies with high chondrogenic potential with a fairly homogenous response; however, most of the data suggests that, with TGF- β induction, there is large variation in individual cell gene expression, even within colony subpopulations. This was further confirmed with the chondrogenic induction of a passage 0 colony. Results of this assay showed that the heterogeneous response within a colony is not a consequence of passage and increased time in culture, but rather emerges very rapidly within the initial colony as it forms. Interestingly, the pattern of expression did not follow a particular spatial trend; high expressing and low expressing MSCs were present (and dispersed) throughout the colony.

In Chapter 5, the observation that not all MSCs died, despite low glucose levels, suggested that there may be heterogeneity in the response of MSC populations to metabolic stressors. To test whether subsets of a heterogeneous MSC population would respond differently to metabolic stressors, we evaluated clonal sub-population responses to these stressors (low glucose and low oxygen) using a chondrogenic micro-pellet assay. Results from this analysis showed that some clonal populations were more susceptible to low glucose and/or hypoxic conditions than others. Specifically, while most performed poorly in Hyp LG+ conditions (similar to that observed in the parent population in hydrogels), a number of colonies did not produce appreciable matrix (GAG per pellet) at all. For most of these poorly performing subpopulations, we found either a higher basal level of dead cells in the micro-pellet regardless of condition, or a marked increase in cell death in Hyp LG+ conditions. One possible explanation is that some colonies (such as

C2 and C5, Donor 1) experienced an immediate insult from the stressors, resulting in cell death and lack of matrix production. Conversely, other colonies (such as C3 and C6) may have lacked the innate capacity to undergo chondrogenesis, and so were not metabolically adaptable to Hyp LG+ conditions, resulting in cell death. Furthermore, data from Donor 2 showed that hypoxia may be pro-chondrogenic in a colony dependent manner. This observation was not present in the results of Donor 1. These two sets of data therefore suggest that both donor and clonal variability may play a role in overall response of a heterogeneous cell population (a combination of multiple donors) to environmental stressors for cartilage tissue engineering studies.

Our data support the idea of prominent heterogeneity in MSC chondrogenic functionality. However, while there are shifts in the mean response when comparing subpopulations to each other, or to the mixed parent populations, intra-population heterogeneity and large variability in the data persisted, even in clonal populations. When initiating these studies, we expected that, for MSCs from a single colony exposed to TGF- β , a more consistent response would be observed, both in their resistance to deformation in 3D culture and expression profiles. Contrarily, standard deviations for colonies subjected to these assays remained just as high as the parent population. One possible explanation for the lack of difference in the standard deviations of the heterogeneous population compared to the colony subpopulations is the devolution of the colony populations with time in culture. Furthermore, differences observed may be a consequence of stem cell isolation and expansion techniques, as cell-cell contact and other biophysical factors may be contributing to population changes. For example, it has been shown that cells within

different regions of a colony (inner vs. outer) can vary in their morphology and commitment of differentiation; however, when replated at clonal densities, the differences are no longer apparent (Ylostalo et al., 2008). Contrary to this interpretation though, and quite interestingly, we showed by FISHing a single P0 colony that heterogeneity on the molecular level already exists, suggestive of a rapid devolution in a spatially independent fashion. Another alternative interpretation (and one that is quite possible) is that the mixed parent population may be relatively homogeneous with culture time, as rapidly dividing colonies take over.

Taken together, our data suggest that it may not be possible to generate large numbers of MSCs from a clonogenic cell line with every daughter cell having the exact capacity of the parent cell from which it was derived, particularly when expansion occurs after the cell has been removed from its *in vivo* environment. The bone marrow is a complex organ containing stem cells of multiple lineages (hematopoietic and non-hematopoietic) residing in different niches, with interplay between these populations (Mendez-Ferrer et al., 2010). Identification of single cell chondrogenic characteristics remains a challenge and is so far incomplete. Future successes in the isolation of a homogenous, highly chondrogenic stem cell population may require that first, epigenetic differences of these cells be identified and correlated with functional performance, and that second, new culture methods be developed to stabilize such epigenetic signatures through isolation and *in vitro* cell expansion. Creation of ‘niche-like’ environments (i.e. soft expansion materials) have shown some promise in muscle-derived stem cell propagation *in vitro*

(Gilbert et al., 2010), and this and other techniques may likewise attenuate the devolution towards heterogeneity that we see in our clonal MSC populations.

CHAPTER 7: TUNABLE AND DEPTH-DEPENDENT MECHANICS OF AGAROSE/POLY(ETHYLENE GLYCOL) DIACRYLATE INTERPENETRATING NETWORKS

7.1 Introduction

Chondrocytes encapsulated in hydrogels rapidly ensconce themselves in a dense pericellular matrix, which moderates transmission of strain from the surrounding material to the cell. Past studies, including those described in Chapter 6, have characterized the time scale at which chondrogenic cells produce this dense pericellular matrix and become shielded from applied strain when the pericellular matrix modulus exceeds that of the hydrogel they are encapsulated within. However, these studies tell us nothing of the mechanical properties of the pericellular matrix once the cells cease to deform, only that they have exceeded the threshold necessary for complete stress shielding, and further does not allow us to discriminate between two objects with significantly different moduli exceeding this threshold imparted by the properties of the starting biomaterial (**Figure 7-1**). Investigation into population heterogeneity of pericellular matrix mechanical properties using micromechanical techniques is therefore limited by the range of moduli we can achieve with the starting biomaterial. Furthermore, tuning mechanical properties of a hydrogel often involves increasing monomer or macromer density. However, if we were to increase the density of the starting biomaterial, say agarose, at the time of encapsulation, the diffusivity of both nutrients and matrix molecules would be altered, thus impacting growth characteristics (Mauck et al., 2003a; Sengers et al., 2004). Therefore, micromechanical studies investigating a range of pericellular matrix properties

require further protocol development. Most ideally, a hydrogel that could be variably ‘stiffened’ after the cell culture period is complete (**Figure 7-2**).

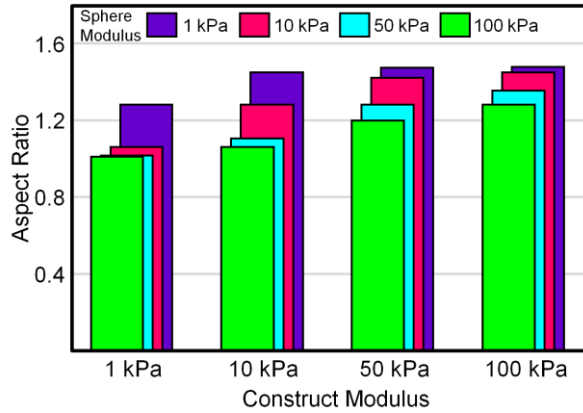


Figure 7-1: Aspect ratio quantification from a finite element model of spherical inclusions with varying moduli situated within cylindrical hydrogel constructs that also have varying moduli and are subjected to compression. These data demonstrate that one cannot discriminate between mechanical properties of spheres with high moduli (50 and 100 kPa) in hydrogels of a low modulus (1 kPa).

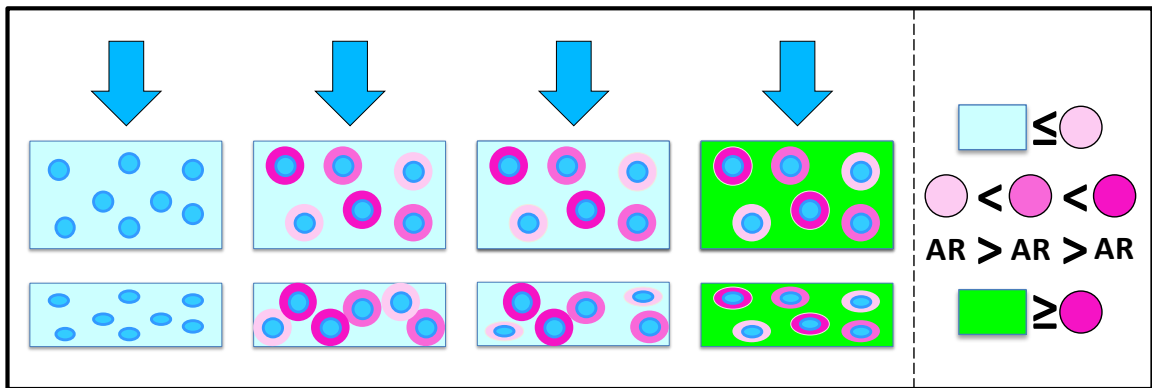


Figure 7-2: Schematic demonstrating the use of a secondary polymer network to increase the mechanical properties of the interstitial space after matrix has been deposited around cells.

Towards that end, hydrogel networks can be sequentially manipulated via the formation of interpenetrating networks (IPNs) or dual networks (DN), i.e. adding a secondary polymer network to a primary network thus resulting in two distinct interwoven polymer networks (Kris Kostanski et al., 2009). Reports on the fabrication of these networks have

shown that hydrogel characteristics can be drastically altered, reaching mechanical properties and durability greater than the sum of the individual networks (Gong et al., 2003; Yokota et al., 2011). These cell-free, water-swollen dual networks can achieve mechanical properties on the order of those of cartilage (Yokota et al., 2011). Recently, an agarose/poly(ethylene-glycol) diacrylate (PEG-DA) interpenetrating network (IPN) was described as a means to improve gel mechanical integrity for cartilage tissue engineering applications (Yokota et al., 2011). While this study confirmed that agarose/PEGDA IPNs are possible, it did not explore the tunable nature that is characteristic of these hydrogel networks. To further expand the range of these IPNs, the objective of this study was to fabricate agarose/PEG-DA IPNs with a range of mechanical properties. Furthermore, to more precisely define the local mechanical attributes of such networks, we assessed both bulk and local mechanical properties. This work provides insight into the synergistic relationship between individual IPN/DN constituents and validates a new tool for mechanobiology and micromechanical analysis.

7.2 Materials and Methods

7.2.1 PEG-DA Hydrogel Fabrication

Poly(ethylene glycol) diacrylate (PEG-DA; 400Da; Scientific Polymer, Ontario, NY) was diluted in a PBS/photoinitiator (PI; I2959; Ciba-Geigy, Tarrytown, NY) solution, resulting in PEG-DA solutions at 2.5, 5, 7.5, 10, 15, and 20% w/v with a PI concentration of 0.05% w/v. Using electrophoresis casting equipment and 2.25 mm spacers, pure PEG-DA gels were polymerized with long-wave ultraviolet radiation for 10 minutes. Cylindrical constructs 4 mm in diameter and 2.25 mm thick were cored from the gel

slabs.

7.2.2 Agarose Hydrogel Fabrication

In bulk mechanical testing studies, molten 2% agarose was cast between 2 parallel plates as above and constructs 4 mm in diameter and 2.25 mm thick were formed. For assessment of local mechanical properties, fluorescent microspheres were employed as fiducial markers. Briefly, molten 4% agarose (Type VII, Sigma) was mixed in a 1:1 ratio with PBS containing 15 μm fluorescent microspheres, resulting in a 2% agarose gel with 0.1% w/v microspheres.

7.2.3 Agarose/PEG-DA Interpenetrating Network Fabrication

Agarose constructs (2%, prefabricated as described above, 4 mm \varnothing , 2.25 mm thick) were allowed to soak in PEG-DA solutions (2.5, 5, 7.5, 10, 15, and 20% w/v; 0.05% PI w/v) for 24 hours on an orbital shaker (**Figure 7-3**). To verify PEG-DA penetration and polymerization, a subset of constructs was soaked in PEG-DA solutions containing 50 μM PolyFluor 570 (Methacryloxyethyl Thiocarbonyl Rhodamine B). IPNs were formed by polymerizing for 10 min through one face (Not Flipped), or for 5 min through each face (Flipped) with or without nitrogen gas flooding (all constructs polymerized in the presence of nitrogen following rhodamine incorporation studies).

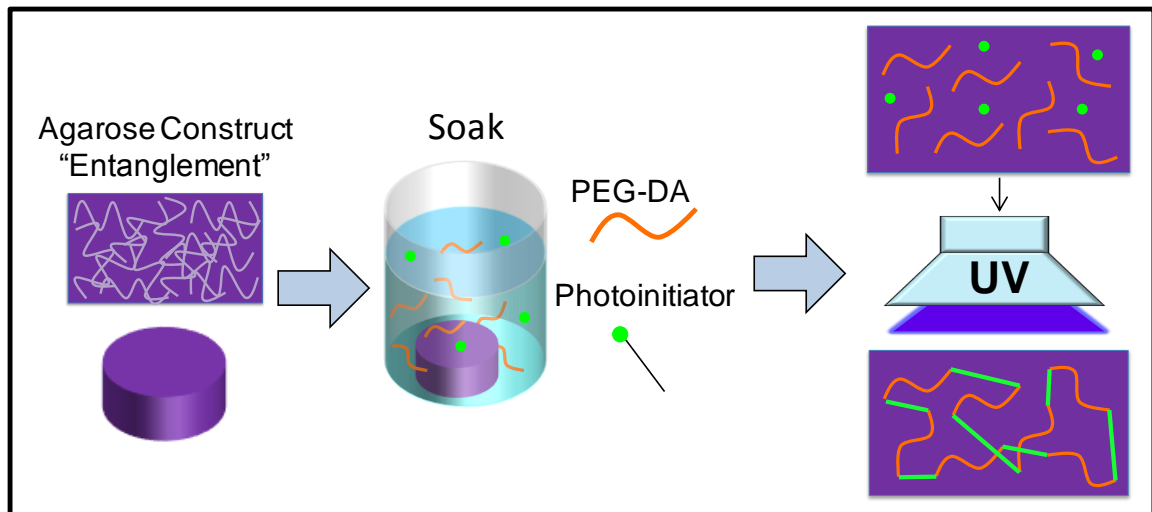


Figure 7-3: Schematic of IPN formation. Agarose constructs are soaked in a PEG-DA/photoinitiator solution for 24 hours, after which the secondary PEG-DA network is crosslinked with UV light.

7.2.4 Bulk Mechanical Testing

Constructs (n=5) were tested in uniaxial unconfined compression as described in previous chapters. Briefly, constructs were allowed to equilibrate under a 2 g tare load for 5 min, followed by a stress relaxation test. Ten percent strain was applied at a rate of 0.05% strain per second, followed by a 1000 sec relaxation phase. Equilibrium modulus was calculated from the sample geometry and load at equilibrium.

7.2.5 Local Mechanical Testing

Agarose and IPN constructs were halved through the mid-sagittal plane. Using a microscope-based device, construct halves were tested in uniaxial compression, with images taken and load recorded at 0%, 4%, and 8% platen-to-platen strain (n=3). Regional Lagrangian strain (E_{xx}) was calculated by texture tracking (microspheres) using the digital image correlation software, Vic2D (Correlated Solutions). Strain through the

depth of the construct was binned into 10% depth intervals. Regional strain and cross sectional area were used to compute local equilibrium modulus.

7.2.6 Statistics

Significance was assessed by ANOVA with Tukey's post-hoc test ($p < 0.05$).

7.2.7 Cell Viability

Monolayer cultures of MSCs were incubated in basal media (DMEM, 10% FBS, 1% PSF) containing 5% or 10% PEG-DA for 3 hours. Cell viability was qualitatively assessed with the Live/Dead Viability Kit for Mammalian Cells (Molecular Probes, Invitrogen). To determine the mode by which these solutions may be impacting viability, media/PEG-DA solution osmolality was measured with an osmometer.

7.3 Results

7.3.1 IPN Formation in the Presence and Absence of Nitrogen

Our data shows that polymerizing IPNs in the presence of nitrogen is a requirement. In the absence of nitrogen purge, polymerization was restricted to a small cylindrical region at the bottom center of the construct, towards the surface touching the tissue culture plate. In the nitrogen purged system, a more uniform polymerization profile was observed (**Figure 7-4A-D**). Intensity profiles of rhodamine incorporated into the hydrogel showed the need to flip the construct during the polymerization phase. A higher intensity of incorporated fluorescent rhodamine was found in the top half of non-flipped IPN

constructs whereas a more uniform distribution of fluorescent rhodamine incorporation was observed throughout the depth of flipped (**Figure 7-4E, F**).

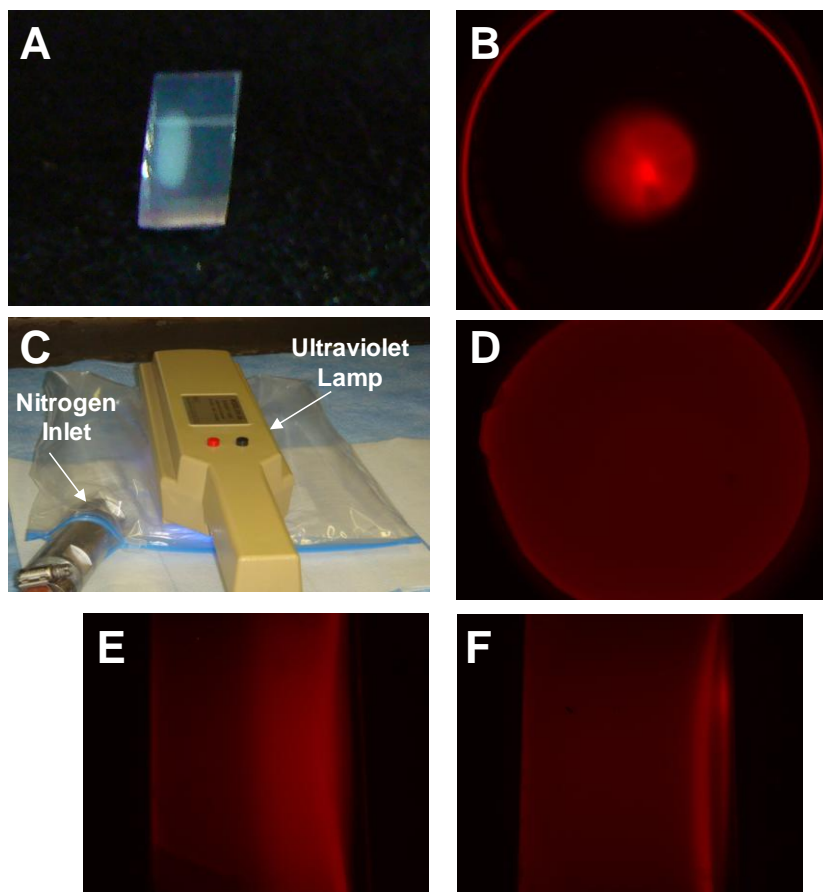


Figure 7-4: (A) Gross appearance of Agarose/IPN construct balanced on its side. Polymerization without the nitrogen gas flooding resulted in localized IPN formation in the bottom center of the construct. (B) Rhodamine incorporation confirmed region dependent polymerization without the use of nitrogen gas flooding (top view of construct). (C) Demonstration of UV polymerization under nitrogen gas flooding. (D) Rhodamine incorporation showing a more uniform polymerization of the secondary PEG-DA network in the presence of nitrogen. (E) Construct bisection showing non-uniform pattern of rhodamine incorporation when gels were not flipped. (F) More uniform intensity patterns were achieved by flipping constructs midway through polymerization duration.

7.3.2 Bulk and Local Mechanical Properties

Bulk equilibrium modulus of PEG-DA constructs increased with increasing concentration to approximately 600 kPa at a concentration of 20% PEG-DA. PEG-DA constructs with

concentrations of 7.5% and greater had a significantly higher modulus than pure agarose constructs (**Figure 7-5**). Hydrogels formed with PEG-DA concentrations of 2.5% and 5% lacked sufficient integrity for compression testing.

When formed into agarose/PEG-DA IPNs, a synergistic improvement in mechanical properties was observed ($p < 0.05$) with PEG-DA concentrations of 7.5% and greater. In the IPN ranges of 7.5-15%, a 2- to 9-fold increase in properties was observed compared to pure PEG-DA gels, with fold increase over pure PEG-DA gels decreasing with increased concentration (**Figure 7-5**). This synergistic stiffening was confirmed via testing of local modulus (**Figure 7-6**), where a stepwise increase in modulus was observed from pure agarose through agarose/20% PEG-DA IPNs ($p < 0.05$). Agarose gels had relatively homogenous properties through the depth. Conversely, IPNs had higher moduli at the gel periphery than in the central region (5% & 20%, $p < 0.05$). This inhomogeneity was most apparent in agarose/20% PEG-DA IPNs, where the central regions were 2-fold softer than the edges (1468 kPa vs. 2882 kPa, $p < 0.05$).

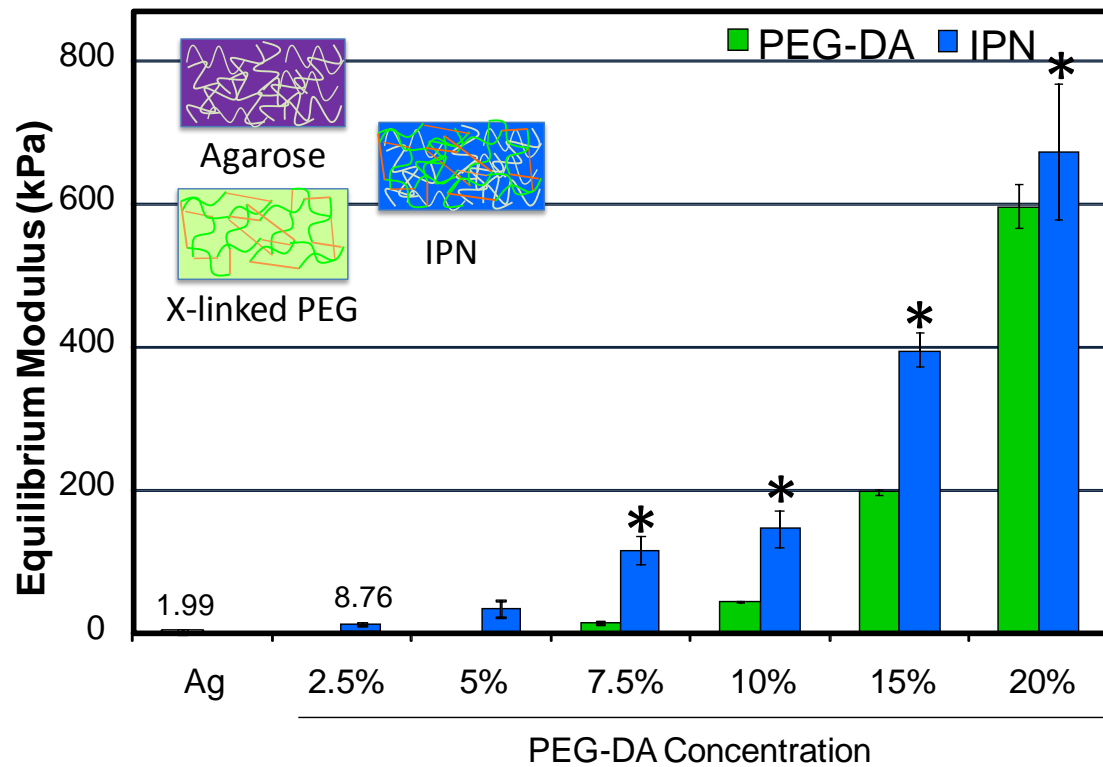


Figure 7-5: Bulk modulus of PEG-DA and IPN gels (all flipped). 2.5% and 5% PEG-DA failed to produce gels that could be mechanically assessed. * indicates $p < 0.05$ for PEG vs. IPN and PEG & IPN vs. Ag, $n=5/\text{group}$

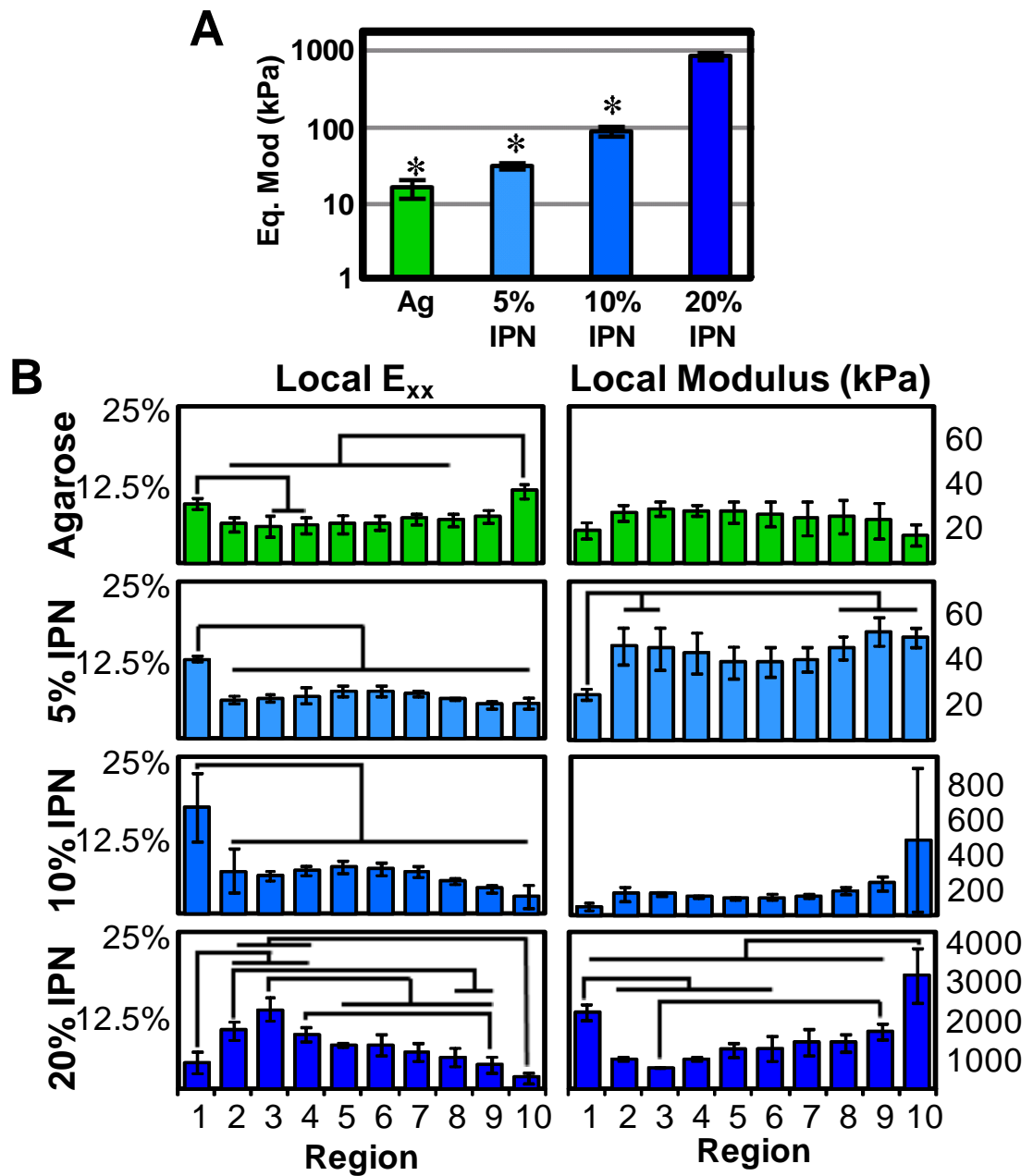


Figure 7-6: (A) Bulk modulus of gels tested via microscope testing device. * indicates $p < 0.05$ vs. 20% IPN. (B) Local strain (Left) per region and local modulus (Right) per region through the depth of agarose constructs and IPNs. Bar indicates significance ($p < 0.05$).

7.3.3 Cell Viability

To determine the feasibility of using such a technique with cell seeded hydrogels, a cell viability study was conducted in monolayer. Briefly, cells were incubated in solutions of basal media (BM; DMEM, 10% FBS, 1% PSF) with 5% or 10% PEG-DA for 3 hours. Drastic loss of cell viability was observed in both conditions (**Figure 7-7**). Assessment of osmolality of each solution revealed that high osmolalities may be contributing to the loss of viability (BM = 330 mOsm, BM +5% PEG-DA = 459 mOsm, BM+10% PEG-DA=617 mOsm).

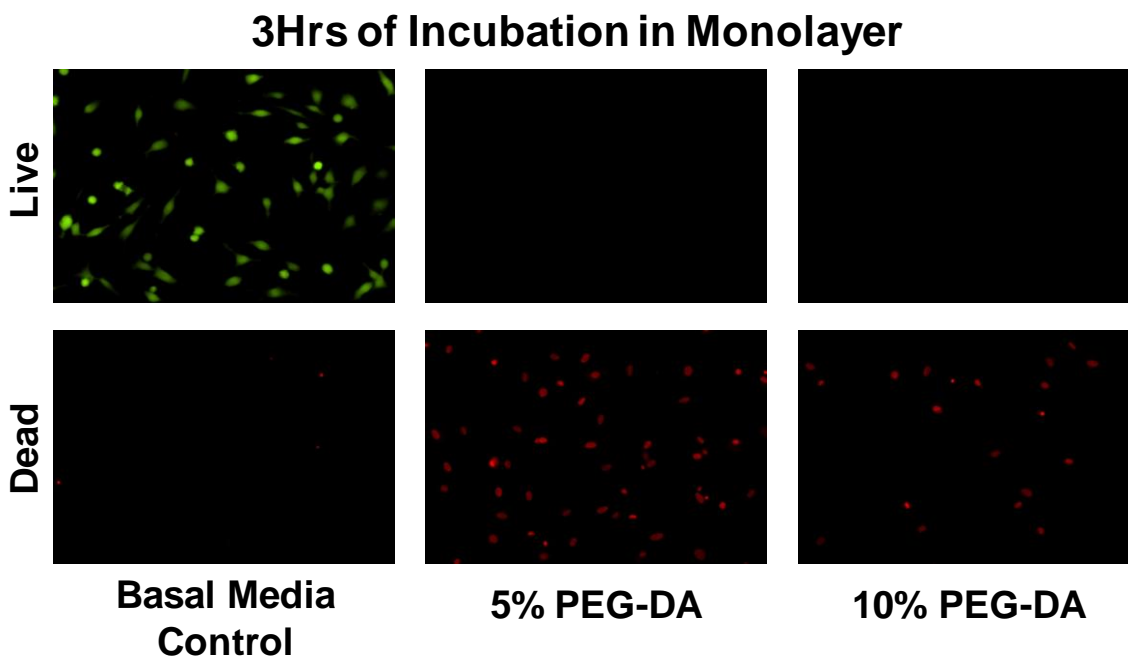


Figure 7-7: Dramatic loss of viability of cells cultured in basal media with PEG-DA for 3 hours compared to basal media alone.

7.4 Discussion

In this study, we fabricated and evaluated a range of agarose/PEG-DA IPNs. Increasing IPN concentration synergistically increased bulk mechanical properties. Local stiffening

was depth-dependent (most notably in higher concentrations), despite attempts to apply uniform UV coverage by flipping the gel during crosslinking. This finding suggests that care should be taken in the interpretation of cellular responses in these networks. Regardless of this depth-dependence, bulk and local modulus of IPNs was >100-fold higher than the agarose backbone. The tunability and spatial resolution of these networks, after formation of an initial cell-seeded construct, will enable a number of studies to be carried out that heretofore have not been possible. For example, several studies have shown that chondrocytes and stem cells in agarose do not deform in response to bulk gel deformation after production of a local pericellular matrix (PCM) that is stiffer than the surrounding hydrogel (Knight et al., 1998; Lee and Bader, 1995; Vigfusdottir et al., 2010), see Chapter 6. Moreover, mechanical loading of stem cell seeded agarose elicits negative responses early in culture, before the establishment of contiguous extracellular matrix, but positive responses at later time points (Huang et al., 2010a). Enhancing local matrix stiffness will allow for quantification of PCM mechanics (by recovering deformation capacity) and could help elucidate whether stem cell response to loading is dependent on differentiation state (time in culture) or microenvironmental stiffness and local deformation. Future studies will investigate if the system can be optimized, for example by using PEG-DA of higher molecular weight, to maintain higher levels of viability.

CHAPTER 8: RAR INVERSE ACTIVATION FOR STEM CELL BASED CARTILAGE ENGINEERING

8.1 Introduction

Although mesenchymal stem cells (MSCs) have emerged as a viable alternative for cartilage repair strategies (Johnstone et al., 1998; Mauck et al., 2006), stem cell based cartilage repair has yet to reach clinical efficacy due to incomplete chondrogenic differentiation (Huang et al., 2010b) and the progression to an unstable hypertrophic phenotype (Johnstone et al., 1998; Mackay et al., 1998; Mueller et al., 2010; Peltari et al., 2006; Vinardell et al., 2012) when these cells are chondrogenically induced with TGF- β 3 alone. Retinoids play central roles in skeletogenesis, and temporal and spatial control of the three retinoic acid receptors (RARs; α , β , γ) are critical for cartilage development (Cash et al., 1997; Hoffman et al., 2003; Koyama et al., 1999). Furthermore, there are elevated levels of retinoic acid in the synovial fluid of OA patients, indicating that retinoic acid is possibly involved in osteoarthritis (Davies et al., 2009).

The retinoic acid receptor (RAR) is a type II nuclear receptor. RARs form heterodimeric complexes with retinoid X receptors (RXRs) which can then bind to the retinoic acid response element (RARE) on DNA. In the absence of a ligand, the RAR is bound in a complex with a corepressor; however, in the presence of an agonist, such as all-*trans*-retinoic acid, there is dissociation of the corepressor with recruitment of a coactivator. In the presence of an antagonist, there is dissociation of the corepressor without recruitment

of the coactivator, and in the presence of an inverse agonist, there is stabilization of the corepressor. RARs have been targeted for therapeutic use. For example, the use of an RAR- γ agonist has been shown to prevent heterotopic ossification, and therefore is a potential therapeutic for fibrodysplasia ossificans progressiva (Shimono et al., 2011). Furthermore, repression of RAR signaling has previously been associated with altered chondrogenesis. Specifically, RAR- α overexpression negatively impacts BMP mediated chondrogenesis, whereas RAR- α antagonism is prochondrogenic (Weston et al., 2002; Weston et al., 2000). However, only a few reports to date have targeted RARs for cartilage tissue engineering applications, with the most recent focusing on the RAR- β antagonist LE135. Though limited in number, these reports have yielded contradictory results (Henderson et al., 2011; Kafienah et al., 2007; Li et al., 2011). For instance, Kafienah (Kafienah et al., 2007) showed that LE135 was prochondrogenic, though not as potent as TGF- β in its action. Conversely, Li (Li et al., 2011) and Henderson (Henderson et al., 2011) showed that LE135 treatment was not prochondrogenic, with Li further showing that it negated the chondrogenic effects of TGF- β when the two factors were added together. Additionally, the functional consequence of these molecules has not been studied. Since antagonists should have limited direct effect on transcription, the objective of this study was to assess the molecular and functional effects of both antagonists as well as a pan-RAR inverse agonist on mesenchymal stem cell (MSC) chondrogenesis through biochemical, mechanical, and gene analyses.

8.2 Materials and Methods

8.2.1 Pellet Culture

Juvenile bone marrow derived MSCs were isolated as described in previous chapters and expanded through passage 2. MSCs were pelleted (250,000 cells) and cultured for 21 days in chemically defined media (CM) with or without (+/-) 10 ng/mL TGF- β 3. Media was supplemented with four doses (spanning 0.5-5 μ M) of all-*trans*-retinoic acid (RA, Sigma), antagonists specific to each RAR (α [BMS195614], β [LE135], γ [MM11253]; Tocris Biosciences, Bristol, UK), a combination of $\alpha\beta\gamma$ (added to result in a total antagonist concentration of 0.5-5 μ M), or a pan-RAR inverse agonist (IA, BMS 493, Tocris Bioscience). GAG content was measured via the DMMB assay, and proteoglycans stained with Alcian Blue as described previously.

8.2.2 Hydrogel Culture

MSCs were encapsulated in 2% agarose at a density of 20 million cells/mL as described in previous chapters. Constructs (4 mm in diameter, 2.25 mm in depth) were cultured in CM⁻, CM⁺, or in CM⁺ supplemented with three doses of the pan-RAR inverse agonist (0.1 μ M, 0.5 μ M, or 1 μ M) for 21 days. Construct compressive equilibrium modulus and glycosaminoglycan content were quantified using methods previously described.

Additional constructs were cultured for 7 days in CM⁻, CM⁺, CM⁻/2 μ M IA, and CM⁺/2 μ M IA for histological assessment of proteoglycans via Alcian Blue staining of paraffin processed constructs. Gene expression analyses of 96 genes was conducted using Signal Transduction PathwayFinder™ PCR Array plates (SABiosciences, QIAGEN, Valencia,

CA) on Day 7 in CM+ and CM+/2 μ M IA (n=3 combined) using the $\Delta\Delta$ Ct method (where MSC monolayers in basal media served as controls). Data from this study is presented as fold change of CM+/2 μ M IA relative to CM+ alone.

8.2.3 Statistics

Significance ($p < 0.05$) was established with 1-way ANOVA and Tukey's post-hoc correction.

8.3 **Results**

8.3.1 Pellets

Consistent with previous reports, inclusion of TGF- β resulted in a marked increase in GAG content for control pellets (CM- vs. CM+). Assessment of the chondrogenic induction potential of the RAR-agonist and antagonists in the absence of TGF- β revealed no increase in GAG content over CM- controls. In the presence of TGF- β , and consistent with previous reports, there was significantly less GAG in the RAR- β antagonist group and significantly higher (57%) GAG in the high dose (5 μ M) of the RAR- α group compared to the CM+ control. Combining RAR- α , β , and γ antagonists negated the positive effects α had in CM+ conditions, decreasing GAG levels by 62% (5 μ M) compared to CM+, and resulting in very light proteoglycan staining. The inverse agonist had significant pro-chondrogenic effects, with marked increases in GAG content (>200%, 5 μ M, **Figure 8-1**) and intense proteoglycan staining evident in both CM- and CM+ conditions.

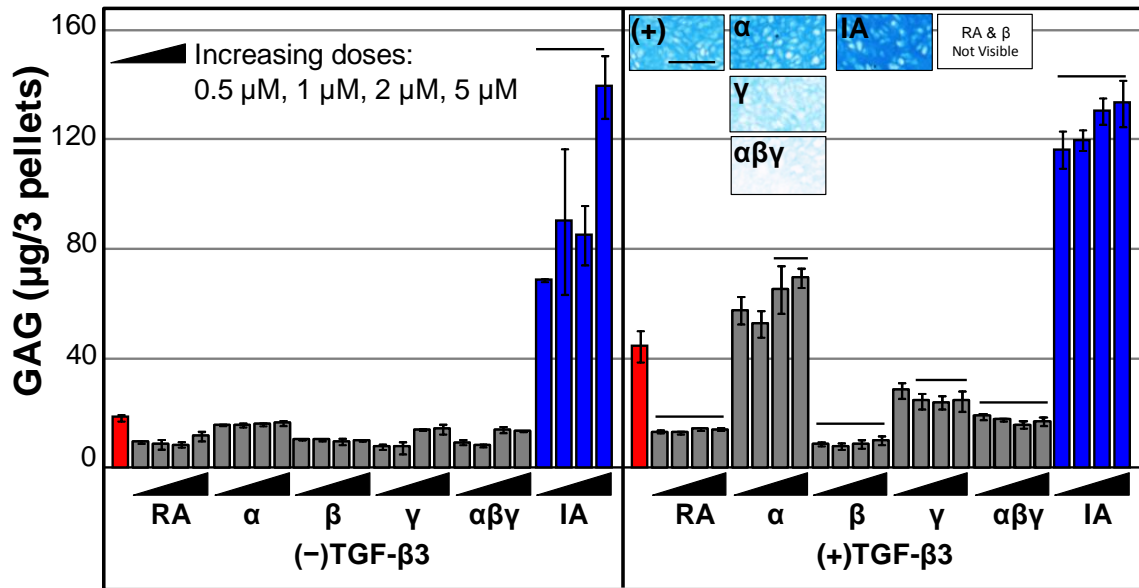


Figure 8-1: Dose response of MSC pellets with addition of RA, α , β , and γ antagonists, and IA relative to CM⁻ and CM⁺ with controls (in red). Bar indicates significance vs. CM⁻ or CM⁺ control ($p < 0.05$). (Inset) Staining of D21 pellets with 5 μ M treatment. Scale=100 μ m

8.3.2 Hydrogels

Functional improvements resulting from the application of the inverse agonist were evaluated in 3D hydrogel culture. After 21 days of culture, addition of BMS (1 μ M; highest concentration assessed) to CM⁺ media had a striking effect on both GAG and equilibrium modulus (**Figure 8-2**) with a 59% increase in GAG and an 87% increase in equilibrium modulus. Histological staining revealed an increase in intensity of pericellular staining of proteoglycans in both CM⁻/IA and CM⁺/IA conditions by Day 7 with IA supplementation at 2 μ M (**Figure 8-3**).

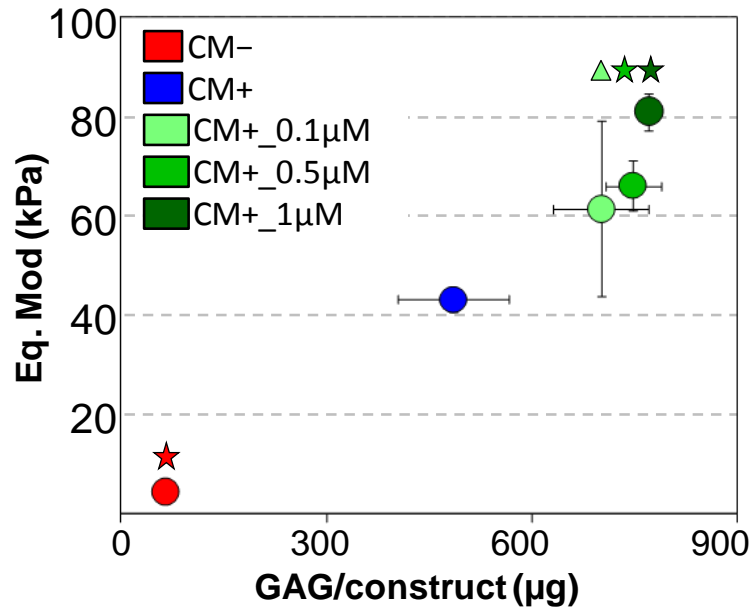


Figure 8-2: GAG content and equilibrium modulus of MSC-seeded hydrogels after 21 days of culture in CM+ without or with IA exposure. Significance established at $p < 0.05$, star = GAG and eq. mod vs. CM+; triangle = GAG only vs. CM+

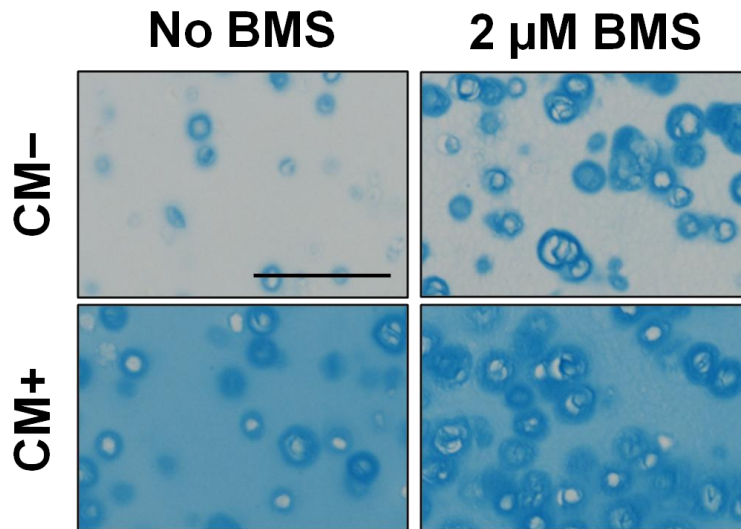


Figure 8-3: Pericellular proteoglycan deposition increased in both CM- and CM+ conditions with IA supplementation. Scale = 100 µm

PCR revealed the down-regulation of several genes (CM+/2 μ M IA vs. CM+), including metabolic (NQO1, LDHA) and anti-apoptotic (BCL2, BIRC3) genes, and the up-regulation of one gene involved in chondrogenesis (WNT5A) and down-regulation of one gene implicated in stress response and cell survival during terminal differentiation of chondrocytes (GADD45 β) (Figure 8-4).

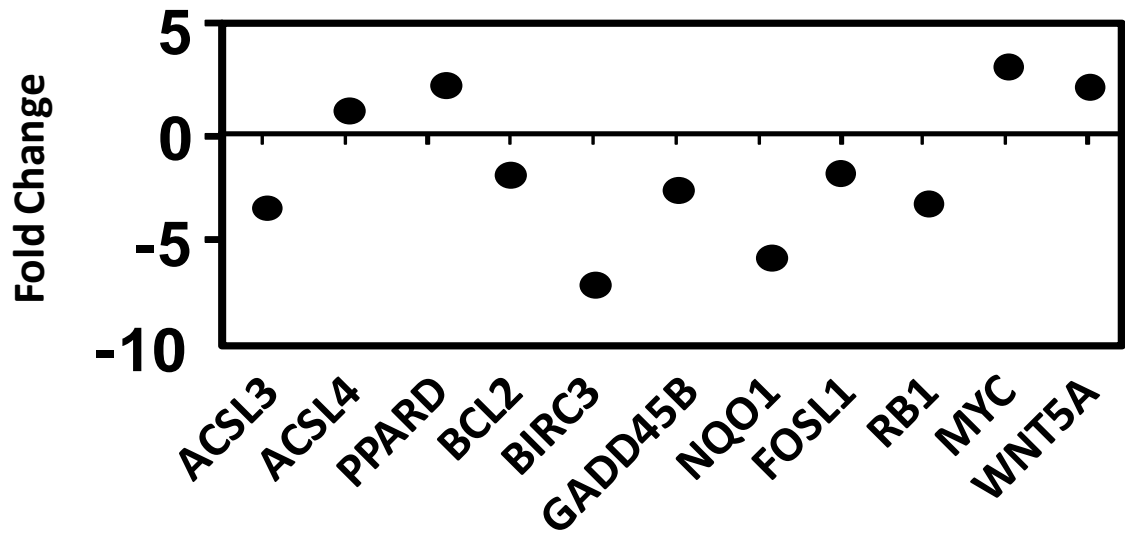


Figure 8-4: RT-PCR plate array findings depicting highest fold changes of CM+/2 μ M IA compared to CM+ after 7 days of culture.

8.4 Discussion

Previous chapters have noted that differences in the performance of chondrocytes and MSCs may be linked to MSC metabolism, cell health, and response to environmental stressors when undergoing TGF- β mediated chondrogenesis. We hypothesize that it will be necessary to target additional pathways to achieve a stable chondrogenic phenotype, with the retinoic acid pathway being one such target. We have identified an inverse agonist of the RAR that is prochondrogenic (both in the absence and presence of TGF-

β3) and capable of increasing the functional properties of MSC-laden cartilage tissue engineered constructs. Through the use of a pathway finder array, we found that the inverse agonist up-regulated several anabolic genes (such as WNT5A, which promotes chondrogenesis via inhibition of canonical WNT signaling) and down-regulated several anti-apoptotic genes, suggesting that IA treated cells are more chondrogenic and under less stress. However, a more complete picture of the complex regulation of MSC chondrogenesis by IA on a molecular level will require additional analysis; microarray screening of MSC-seeded constructs after treatment with IA is now underway. Due the nature of molecules targeting RARs, directly impacting chromatin structure and differentially regulating multiple downstream pathways, these ongoing and future studies will evaluate the genome-wide impact that the inclusion of the inverse agonist has on MSC chondrogenesis.

CHAPTER 9: SUMMARY AND FUTURE DIRECTIONS

9.1 Summary

Osteoarthritis is a disease of high incidence with significant clinical impact. Unfortunately, joint arthroplasty remains the gold standard repair strategy as there has been limited success in long-term repair with biological treatments. Research in cartilage repair strategies over the past two decades has focused on making biological repair a viable clinical option using tissue engineering strategies, and substantial progress has been made. However, much of this success has relied on the use of chondrocytes, the cell type found within cartilage tissue, which can be limited in number or can have altered performance due to the diseased state of the joint. Mesenchymal stem cells are one possible alternative to chondrocytes as they can undergo chondrogenesis in three-dimensional culture; however, these cells have yet to demonstrate the production of a stable, mechanically sound tissue equivalent to that produced by chondrocytes cultured identically. Thus, the objectives of this thesis were to use multi-scale approaches to better characterize where differences in matrix production and construct mechanics arise, to identify the time scales in culture over which chondrocytes and MSCs diverge in their production of a mechanically stable tissue, and to determine what specific environmental components (oxygen and glucose) are most responsible for poor outcomes in MSC-based constructs. Furthermore, we used colony isolation techniques to determine whether there are clonal subpopulations with a greater propensity for chondrogenic differentiation compared to the heterogeneous parent population.

In Chapter 3, we investigated where and why deficits in mechanical functionality arise through the assessment of local (microscopic) properties of cell-laden hydrogel constructs. We found that both chondrocyte- and MSC-laden constructs showed pronounced depth dependency, with ~3.5 and ~11.5 fold decreases in modulus from the surface to central regions, respectively. Importantly, in the surface region, properties were similar, suggesting that MSCs can produce matrix of mechanical equivalence to chondrocytes, but only in conditions of maximal nutrient support. Dynamic culture on an orbital shaker (which enhances diffusion) attenuated depth-dependent disparities in mechanics and improved the bulk properties compared to free swelling conditions. However, properties in MSC-based constructs remained significantly lower due to persistent mechanical deficits in central regions. MSC viability in these central regions decreased markedly, with these changes apparent as early as Day 21, while chondrocyte viability remained high. These findings suggest that, under optimal nutrient conditions, MSCs can undergo chondrogenesis and form functional tissue on par with that of the native tissue cell type. However, the lack of viability and matrix production in central regions suggests that chondrogenic MSCs do not yet fully recapitulate the advanced phenotype of the chondrocyte.

The success of stem cell-based cartilage repair requires not only that the regenerate tissue reach a native tissue-like state, but further that this state be stable over the lifetime of the patient. In Chapter 4, the long term stability of tissue engineered cartilage constructs was characterized through the assessment of compressive mechanical properties of chondrocyte and mesenchymal stem cell (MSC)-laden three dimensional agarose

constructs cultured in a well defined chondrogenic *in vitro* environment through 112 days. Consistent with previous reports, in the presence of TGF- β , chondrocytes outperformed MSCs through Day 56, under both free swelling and dynamic culture conditions, with MSC-laden constructs reaching a plateau in mechanical properties between Days 28 and 56. Extending cultures through Day 112 revealed that MSCs did not simply experience a lag in chondrogenesis, but rather that construct mechanical properties never matched those of chondrocyte-laden constructs. At time periods greater than 56 days, MSC-laden constructs underwent a marked reversal in their growth trajectory, with significant declines in glycosaminoglycan content and mechanical properties. Quantification of viability showed marked differences in cell health between chondrocytes and MSCs throughout the culture period, with MSC-laden construct cell viability falling to very low levels at these extended time points. These results were not dependent on the material environment, as similar findings were observed in a photocrosslinkable hyaluronic acid (HA) hydrogel system that is highly supportive of MSC chondrogenesis. These data suggest that, even within a controlled *in vitro* environment that is conducive to chondrogenesis, there may be an innate instability in the MSC phenotype that is independent of scaffold composition, and may ultimately limit their application in functional cartilage repair.

Based on the depth dependent results in Chapter 3, and the potential implication of nutrients in MSC health and matrix production, MSC-laden constructs were next cultured in decreased oxygen and glucose conditions to determine which is the limiting factor for MSC health and matrix production. Although MSC viability and matrix production were

both compromised by glucose and oxygen deprivation in the presence of TGF- β , our data showed that glucose deprivation is more significant in limiting construct maturation. Furthermore, while drastic declines in cell viability were apparent in low glucose conditions, there were only small changes observed in hypoxic conditions, indicating that decreased mechanical function in hypoxic conditions may be a consequence of cell activity rather than viability. Limiting diffusion gradients by decreasing scale, we were able to more fully characterize spent glucose concentration and stem cell viability. Interestingly, a considerable fraction of the population (52%) remained viable in hypoxic conditions with media glucose values reaching lows of 0.05 mM. This indicated that (1) metabolic activity of these MSCs may be driving glucose concentrations to levels well below the 0.05 mM measured in the media in the regions of decreased death (when provided with high glucose media), and (2) that the capacity of MSCs to undergo chondrogenesis and withstand these environments may differ within a population.

In completing the work that comprised Chapters 3-5, it became apparent that there is population variability in MSC matrix production and viability (when exposed to taxing conditions). In Chapter 6, colony isolation techniques were utilized to determine if there is colony dependent chondrogenic capacity and if isolated colony (or clonal) populations would be more homogeneous than their matched mixed parent counterpart. Surprisingly, through micromechanical and single cell gene expression analyses, we found that while there exist colony dependent shifts in the data, with some colonies proving more “chondrogenic” according to the defined metrics, there remained a consistently high variability (heterogeneity) within even single colony subpopulations. Regardless, shifts

in mean population response demonstrated that as a whole, some colony subpopulations exhibited increased functional chondrogenic potential over the mixed parent population. We therefore exposed colony subpopulations to conditions of decreased glucose and oxygen availability (as in Chapter 5) in order to determine if colony differences in matrix production and cell health would present when these subpopulations were cultured in taxing conditions. We found there were differences in the performance amongst colony subpopulations, suggesting that both donor and clonal variability may play a role in the overall response of a heterogeneous cell population to environmental stressors in the context of cartilage tissue engineering studies.

Given the findings of Chapter 6, in Chapter 7, we developed additional novel methods for the micromechanical evaluation of pericellular matrix mechanical properties, allowing us to discriminate between populations of cells that have produced enough matrix to achieve complete stress shielding. Through the use of photopolymerizable PEG-DA interpenetrating networks, we developed a method to increase the mechanical properties of hydrogel (agarose) constructs after the culture period has terminated, through a range of tuned mechanical properties. Before this technique can be implemented, however, further optimization is required to better maintain cell health and decrease the variation in local mechanical properties to achieve more homogenous strain transfer to the cells through the this PEG/agarose IPN. Once accomplished, this new method should allow for the identification of the most robust MSC subpopulations.

Finally, in Chapter 8 we considered the fact that chondrogenic induction of mesenchymal stem cells (MSCs) in tissue engineering and regenerative medicine applications is typically driven exclusively by transforming growth factor (TGF) and dexamethasone supplementation. While successful at initiating this lineage specification, this cocktail is limited by the fact that it can instigate progression to a catabolic and hypertrophic phenotype. Therefore, the results in the previous chapters regarding stem cell health, metabolism, and stability may be attributed to simply not reaching a complete chondrogenic state by restricting the pathways that are targeted. Proper retinoic acid receptor (RAR) signaling, directly targeting chromatin organization, is imperative for skeletogenesis, thus providing an independent pathway by which to drive stem cell chondrogenic induction. In Chapter 8, we identified an inverse agonist of RAR signaling that is prochondrogenic (both in the absence and presence of TGF- β 3) and capable of increasing the functional properties of MSC-laden cartilage tissue engineered constructs. Additionally, PCR analysis from this study revealed the down-regulation of several genes, including metabolic (NQO1, LDHA) and anti-apoptotic (BCL2, BIRC3) genes, the up-regulation of a gene involved in chondrogenesis (WNT5A), and the down regulation GADD45 β , a factor implicated in stress response and cell survival during terminal differentiation of chondrocytes. These data indicate that targeting the retinoic acid pathway may be one way to moderate stem cell metabolism, health, and phenotypic stability, and may therefore prove useful in addressing many of the shortcomings in the performance of MSCs previously discussed.

9.2 Limitations

9.2.1 Bovine vs. Human Cell Populations

Throughout this dissertation, juvenile bovine cells were utilized. This tissue source is popular in the cartilage tissue engineering literature as it is readily available, yields young/healthy cells in high numbers, and results in fairly consistent data. We must note however, that the performance of these cells often differs, and typically exceeds, that of adult human cells. We are therefore making assessments based on a highly anabolic and active cell source, and as such, concentrations of provisional nutrients at which these cells become stressed may not be directly applicable to adult human MSC studies. However, we do believe that the concepts of stem cell health, stability, and heterogeneity remain relevant to cartilage tissue engineering with adult human stem cell sources.

9.2.2 Micromechanical Assessments of Matrix Properties

One benefit to the use of the micromechanical techniques employed in this dissertation is the ability to assess mechanical differences of matrix produced by MSCs in the 3D environment (hydrogel) they are typically cultured in. However, as mentioned previously in Chapters 6 and 7, we can only infer whether a cell is producing matrix of better quality compared to its neighbor to a certain threshold, limited by the mechanical properties of the starting and surrounding biomaterial. Additional techniques such as atomic force microscopy are needed to obtain an absolute quantification of pericellular mechanical properties to validate these experiments.

9.2.3 Stem Cell Stability and Hypertrophy

In Chapter 4, we identify two phases of declines in stem cell viability. The first occurring immediately after encapsulation and the second occurring after extended time in culture (~112 days). While we believe the first decline to be linked to metabolism and decreased nutrient availability, the second decline occurs over the same time scale as decreases in construct mechanical properties, and we therefore believe it to be linked to instability of stem cell phenotype and hypertrophic events. However, all studies regarding colony dependent chondrogenic differences were conducted within a shortened time frame (<14 days). Therefore, while colony dependent differences may exist in the initial chondrogenic event, it does not exclude the possibility that all may reach a point of phenotypic instability with further culture time. If all mesenchymal stem cell populations ultimately prove to be unstable in the chondrogenic phenotype, then the results obtained on colony dependence may not be of clinical importance, and another cell type, or altered differentiation protocols, will be required to achieve successful cartilage repair over the long term.

9.3 Conclusions

Achievement of a stable engineered cartilage tissue using chondrogenic mesenchymal stem cells remains a significant challenge. The work encompassed by this thesis proved that MSCs are in fact capable of producing mechanically functional matrix equivalent to chondrocytes. However, due to nutritional stress, the health and viability of these cells (and therefore matrix production) is severely impacted within central regions of the construct. Furthermore, with increased culture time, mechanical failure (with loss of

GAG content) occurs, and this parallels another phase of decreased cell viability. In the search for a stem cell population capable of robust chondrogenesis, we have shown that both inter- and intra- colony heterogeneity exists, and that shifts in mean population response support the concept that more chondrogenic, but not necessarily less heterogeneous, subpopulations are present within a mixed parent MSC population. Future studies will focus on further assessing these select stem cell populations that are capable of robust chondrogenesis, and in defining characteristics that would allow for 'pre-selection' of this progenitor subpopulation. Additionally, differentiation pathways, such as those involving the retinoic acid receptor, will be targeted in an attempt to control stem cell metabolism, chondrogenesis, and phenotypic stability. Taken together, this thesis highlights the many potential pitfalls and challenges that are inherent to developing stem cell based cartilage *in vitro* (challenges that will likely be further exacerbated with *in vivo* translation), but also outlines future directions and approaches that may yet culminate in a clinically successful stem cell based cartilage replacement. Progress in this arena may one day provide a functional, cell-based solution for the millions of people worldwide that are currently suffering from osteoarthritis and other debilitating diseases of articular cartilage degeneration.

APPENDIX 1: CELL VIABILITY QUANTIFICATION MATLAB CODE

```
% Cell/Object Count Program - High Throughput
% Megan Farrell
% For inclusion in dissertation, September 2013

% Code based off examples by Steve Eddins, MathWorks.

% Purpose: For viability calculations; Count objects (cells or nuclei)
in
% each image and output with file name and edited images

% Runs automatically, reading in all subfolders in main directory.

% High throughput; goes through two sets of folders (Day and Gel). If
you
% do not have two layers of folders, code will error. M-file name will
% be included in file name directory; therefore, name appropriately so
it does not
% hit until last and result in an error

clear all
close all
warning off MATLAB:strrep:InvalidInputType
warning off Images:initSize:adjustingMag

way_large_directory=dir;
way_large_directory_length=length(way_large_directory);

% Call in directory folders

for z=3:way_large_directory_length

day=way_large_directory(z,1).name;

cd(day)

main_directory_names=dir;
main_directory_length=length(main_directory_names);

for i=3:main_directory_length

    sub_dir_name = main_directory_names(i,1).name;

    cd(sub_dir_name)

    file_names = dir('*.jpg');

    num_files=length(file_names);
```

```

    row_count = 1;

%-----

%Create empty matrices to hold output data and file names for all .jpg
files

data_out_matrix = [];
file_matrix = {};

%Loop through analysis for each image selected
for j = 1:num_files

    img_name = file_names(j,1).name;

    %-----Cell Count / Watershed_Filter_Analysis-----

    % Read in image and convert to black and white

img = imread(img_name);

I = rgb2gray(img);
I2 = imtophat(I, strel('disk', 10));

level = graythresh(I2);
BW = im2bw(I2,level);

    % Watershed function should separate touching objects; however, if
    % there is much noise, this function may result in more noise and
is
    % therefore eliminated in some instances when not needed.

D = -bwdist(~BW);
D(~BW) = -Inf;
L = watershed(D);
imshow(label2rgb(L,'jet','w', 'shuffle'))

% Label objects with bwlabel and count.

[labeled,numObjects] = bwlabel(L,4);
numObjects=numObjects-1;

figure, imshow(labeled);
impixelregion
%
img2=labeled;

% Eliminate objects that are very large (greater than 1000) pixels.

Area0=regionprops (img2, 'area');
indxb = find([Area0.Area] < 1000);
img3 = ismember(img2,indxb);

```

```

figure(2)
imshow(img3);

% Remove objects that are very small (less than 10 pixels) with
bwareaopen.

img4 = bwareaopen(img3, 10, 4);
figure(3)
imshow(img4);

% Relabel objects; save all modified figures; save data.

[labeled2,numObjects2]=bwlabel(img4);
pseudo_color = label2rgb(labeled2, @jet, 'w', 'shuffle');
figure(4), imshow(pseudo_color);

figure(5)
imshow(I);
hold on
h=imshow(pseudo_color);
hold off
set(h, 'AlphaData', 0.1);

fig2=figure(2);
fig3=figure(3);
fig4= figure(4);
fig5=figure(5);
imtool(labeled2);

str4 = ['.jpg'];
str5 = [];

img_out_name = strrep(img_name, '.jpg', '');

mkdir('Analyzed')

saveas(fig2, strcat(cd, '\Analyzed\', img_out_name, '_bw', '.jpg'));
saveas(fig3, strcat(cd, '\Analyzed\', img_out_name, '_bw_filtered', '.jpg'))
;
saveas(fig5, strcat(cd, '\Analyzed\', img_out_name, '_overlay', '.jpg'));
saveas(fig4, strcat(cd, '\Analyzed\', img_out_name,
'_watershed', '.jpg'));

file_matrix(row_count, 1) = cellstr(img_out_name); %Name of
image file analyzed
data_out_matrix(row_count, 1) = numObjects;
data_out_matrix2(row_count,1)=numObjects2;
row_count = row_count + 1;

```

```

    %Save BW modified image in same directory as .xls output file

    close all
    imtool close all
    clear BW D I I2 L ans fig2 fig3 filterindex h img labeled level
numObjects pseudo_color
end

headers = {'Originating File', 'Cell Count Watershed', 'Cell Count
Filter'};
headers = cellstr(headers);

xls_filename = strcat(sub_dir_name, '.xls');

xlswrite(xls_filename, headers, 'Sheet1', 'A1')
xlswrite(xls_filename, file_matrix, 'Sheet1', 'A2')
xlswrite(xls_filename, data_out_matrix, 'Sheet1', 'B2')
xlswrite(xls_filename, data_out_matrix2, 'Sheet1', 'C2')

close all
imtool close all

clear Area0 data_out_matrix data_out_matrix2 file_matrix file_names
headers i img_name img_out_name j labeled2 numObjects2 num_files
row_count xls_filename

    cd ..
end

cd ..
end

```

APPENDIX 2: STRESS RELAXATION CURVE FIT MATLAB CODE

```
% Stress Relaxation Fit Curve
% Megan Farrell
% For inclusion in dissertation, September 2013

% Purpose: to find initial, peak, and equilibrium load of stress
relaxation curve
% when construct do not fully relax

%-----

% First m-file = function
% Function based on GraphPad two phase decay function

function yhat=stress_relax_fun_fit(param, xdata)

yhat=param(1)+((param(5)-param(1))*param(2)*0.01)*exp(-
param(3)*xdata)+((param(5)-param(1))*(100-param(2))*0.01)*exp(-
param(4)*xdata);
end

%Parameters: param(1)=EquilibriumLoad; param(2)=PercentFast;
param(3)=KFast;
%param(4)=KSlow

%call in time; K fast and K slow are decay rates of the two different
decay
%phases and percent fast is the percent of decay that occurs in the
initial
%fast decay phase

%-----

% Second m-file = analysis code

% Loop through analysis for each file
% High throughput analysis code derived from initial code by Tiffany
Zachery (Mauck
% Lab)

clear all;
close all;
clc;

%Select multiple *.dat files%
```

```

prompt = {'Location to save your .xls output file...', 'Create a name
for your output file (or use the current date and time as your file
name):'};
dlg_title = 'Input for Individual File Analysis';
num_lines = 1;
def = {'D:\', datestr(now)};
ind_answer = inputdlg(prompt, dlg_title, num_lines, def);
if isempty(ind_answer) == 1
    h = msgbox('No files will be analyzed.', 'Action Canceled',
'error');
    uiwait(h)
    return
else
    add_extension = strfind(ind_answer(2), '.xls');
    xls_pathname = char(ind_answer(1));
end
if isempty(add_extension) == 0
    xls_filename = ind_answer(2);
    str1 = ['.xls'];
    str2 = [':'];
    str3 = ['.'];
    xls_filename = char(strrep(xls_filename, str2, str3));
    xls_filename = char(strcat(xls_filename, str1));
else
    str1 = ['.xls'];
    xls_filename = char(strcat(ind_answer(2), str1));
end
if isempty(xls_pathname) == 1
    xls_pathname = ['C:\Documents and Settings\All Users\Desktop\'];
end
window_title = ['Select one or more .dat files to analyze...'];
[filenames, pathname, filterindex] = uigetfile('*.*.dat', window_title,
'Multiselect', 'on');
if filterindex == 0
    h = msgbox('No files will be analyzed.', 'Action Canceled',
'error');
    uiwait(h)
    return
else
    if iscell(filenames) == 0
        num_files = 1;
    else
        num_files = numel(filenames);
    end
end

if num_files > 1
    filenames = sort(filenames);
end

xls_filename = strcat(xls_pathname, xls_filename);

%Loop through analysis for each file

```

```

out_row_count=1;

data_out_matrix = [];
file_matrix = {};
initial_load_matrix=[];
peak_load_matrix=[];

for i = 1:num_files
    if num_files == 1
        stress_relax_file = strcat(pathname, filenames);
    else
        stress_relax_file = char(strcat(pathname, filenames(i)));
    end
end
%-----

% Calculate Moving Average of Stress Relaxation Load; Read load in B,
write
% averaged load to column E

M=textread(stress_relax_file);

% Determine number of zero locations of stress relax test; i.e. if
errored
% and did not initially apply load with start of test (glitch in
program),
% there will be an additional 0 time point. If multiple 0's exists,
start
% analysis at second time 0 start.

starts=sum(M(:,1)==0.);

if starts==1
load=M(:,2);
time=M(:,1);
span = 10;
window = ones(span,1)/span;
smoothed_load = convn(load,window, 'same');

else

row_end=length(M(:,1));

zero_positions=find(M(:,1)==0);
new_start=max(zero_positions);
load=M(zero_positions:row_end, 2);
time=M(zero_positions:row_end, 1);
span = 10;
window = ones(span,1)/span;
smoothed_load = convn(load,window, 'same');

```

```

end

% Take 'filtered' data that was cleaned up with moving average and
% calculate following as initial measurements without fit:
% Peak load - exclude initial points because moving average can result
in
% high spike that is actually the peak load
% Equilibrium load - calculated from average of last 50 data points
% (excluding last 9 points because of increases in the data due to
moving
% average calculation)
% Initial load - taken as early point in load

row_count=length(smoothed_load);
lower_eq_ave=row_count-59;
higher_eq_ave=row_count-9;
eq_load=mean(smoothed_load(lower_eq_ave:higher_eq_ave));
peak_load=max(smoothed_load(100:3000));
initial_load=smoothed_load(5);

% Subset of Relaxation Data Only
last_time=length(smoothed_load)-50;
[peak_smooth, array_position_peak]=max(smoothed_load);
[min_time_difference, array_position_200sec]=min(abs(M(:,1)-200));

if array_position_peak>3000
    array_position_peak=array_position_200sec;
end

relax_phase=[];
relax_phase(:,1)=M(array_position_peak:last_time,1);
relax_phase(:,2)=smoothed_load(array_position_peak:last_time,1);

% Break up stress relaxation data into only 100 points to make code
more
% efficient with curve fitting

interval_analyzed_points=length(relax_phase)/101;
interval=round(interval_analyzed_points);

truncated_data_set=[];
data_point=1;
row_count=1;

for k=1:100
    truncated_data_set(row_count,:)=relax_phase(data_point,:);
    data_point=data_point+interval;
    row_count=row_count+1;
end

```

```

% Set bounds for each parameter in curve fitting

peak_truncated=max(truncated_data_set(:,2));
lb_peak_truncated=peak_truncated-0.01;
lb=[-inf 0 0 0 lb_peak_truncated];
ub=[inf inf inf inf peak_truncated];

% Curvefit Relaxation Data

% Parameters: param(1)=EqLd; param(2)=PercentFast; param(3)=KFast;
% param(4)=KSlow

xdata=truncated_data_set(:,1)-truncated_data_set(1,1);
ydata=truncated_data_set(:,2);

% Start with parameter guesses

% PercentFastInit=90;
% KFastInit=0.017;
% KSlowInit=0.003;
% init_EqLd=measured load;
% param=[EqLd PercentFast KFast KSlow];
%
% param0=[EqLdInit PercentFastInit KFastInit KSlowInit];
%
% [param, exitflat]=lsqcurvefit(fun_fit,Param0,xdata,ydata);

init_EqLd=eq_load;

init_param=[init_EqLd 90 0.0175 0.003 peak_truncated];

% Curve fit calling stress_relax_fun_fit and parameters

[fit_param]=lsqcurvefit(@stress_relax_fun_fit,init_param,xdata,ydata,
lb, ub);

% Visualize data that was curve fit with by plugging in all
% of the fit parameters and a longer time to see if it reaches
equilibrium

extended_time = linspace(0,3000,3001)';
fit_function=fit_param(1)+((fit_param(5)-
fit_param(1))*fit_param(2)*0.01)*exp(-
fit_param(3)*extended_time)+((fit_param(5)-fit_param(1))*(100-
fit_param(2))*0.01)*exp(-fit_param(4)*extended_time);

% Plot the original data (blue), the moving point averaged data (red),
and

```

```

% the stress relax fit data (green)
% Horizontal lines used to denote loads of interest: Initial (magenta);
Peak
% (orange); Unfit EqLoad (cyan); Fit EqLoad (purple)

plot(time, load, 'LineWidth', 2, 'Color','blue')
hold on
h = plot(time, smoothed_load,'LineWidth', 2, 'Color','red');
hold on

fit_eq_load=fit_param(1);

plot(extended_time+truncated_data_set(1,1), fit_function, 'LineWidth',
2, 'Color', [0.066, 0.7686, 0.0314]);

line([1,3400],[peak_load, peak_load], 'LineWidth', 2,'Color',[0.996,
0.3725, 0.0235]);
hold on
line([1,3400],[initial_load, initial_load],'LineWidth', 2,'Color',
'magenta');
hold on
line([1,3400],[eq_load, eq_load], 'LineWidth',2, 'Color','cyan');
hold on
line([1,3400],[fit_eq_load, fit_eq_load], 'LineWidth',2, 'Color',[0.4,
0, 0.8]);

% Output initial load values and fit parameters into an excel sheet

str4 = ['.dat'];
str5 = [];
str6 = ['_stress_relax_analyzed.png'];
img_out_name = char(strrep(stress_relax_file, str4, str5));
img_out_name = char(strrep(img_out_name, pathname, xls_pathname));
img_out_name = strcat(img_out_name, str6);
saveas(figure(1), img_out_name, 'png');

eq_diff=eq_load-fit_eq_load;
eq_minus_int=fit_eq_load-initial_load;

file_matrix(i, 1) = cellstr(stress_relax_file); %Name of image file
analyzed
data_out_matrix(i, 1) = initial_load;
data_out_matrix(i, 2)= peak_load;
data_out_matrix(i, 3)= eq_load;
data_out_matrix(i,4)=fit_param(5);
data_out_matrix(i,5)=fit_param(1);
data_out_matrix(i,6)=fit_param(2);
data_out_matrix(i,7)=fit_param(3);
data_out_matrix(i,8)=fit_param(4);
data_out_matrix(i,9)=eq_diff;
data_out_matrix(i,10)=eq_minus_int;

```

```

initial_load_matrix(out_row_count,1)=initial_load;
peak_load_matrix(out_row_count,1)=peak_load;

out_row_count = out_row_count + 1;

clear M starts load smoothed_load row_end zero_positions new_start
row_count lower_eq_ave higher_eq_ave eq_load peak_load initial_load
array_position_peak data_point extended_time
clear fit_eq_load fit_function fit_param init_EqLd init_param
inital_load_matrix interval interval_analyzed_points
initial_load_matrix last_time lb lb_peak_truncated peak_load_matrix
peak_smooth peak_truncated relax_phase time truncated_data_set xdata
ydata

close all
end

headers = {'Originating File', 'Intial Load(g)', 'Peak Load(g)', 'Eq
Load(g)', 'Fit_Peak Load', 'Fit_Eq Load', 'Fit_%Fast', 'Fit_KFast',
'Fit_KSlow', 'EqLd Diff', 'FitEq-Init'};
headers = cellstr(headers);

        xlswrite(xls_filename, headers, 'Sheet1', 'A1')
        xlswrite(xls_filename, file_matrix, 'Sheet1', 'A2')
        xlswrite(xls_filename, data_out_matrix, 'Sheet1', 'B2')
        disp(['Save complete. Your file can be viewed here: ',
xls_filename]);

```

APPENDIX 3: 2-DIMENSIONAL CELL DEFORMATION ANALYSIS MATLAB CODE

```
% Cell/Object Count Program - High Throughput
% Megan Farrell
% For inclusion in dissertation, September 2013

% Purpose: High throughput quantification of object parameters in 2D
images

% Runs automatically, reading in all subfolders in main directory.

clear all
close all
warning off MATLAB:strrep:InvalidInputType
warning off Images:initSize:adjustingMag

% Insert um to pixel resolution
um_to_pix=0.828;

%Call in directory with all subfolders
way_large_directory=dir;
way_large_directory_length=length(way_large_directory);

isub = [way_large_directory(:).isdir]; %# returns logical vector
nameFolds = {way_large_directory(isub).name}';
nameFolds(ismember(nameFolds,{'.','..'})) = [];

for z=1:length(nameFolds)

day_cell={nameFolds(z,1)};
day=day_cell{1,1}{1,1};

cd(day)

main_directory_names=dir;
main_directory_length=length(main_directory_names);

% Make new directories to save modified images in

mkdir('Analyzed Images')
mkdir('Binary')
mkdir('Edge Filter')
mkdir('Excel Files')
mkdir('Area Filter')

file_names = dir('*.tif');
```

```

    num_files=length(file_names);

    row_count = 1;

%-----

%Create empty matrices to hold output data and file names for all .jpg
files
data_out_matrix = [];
file_matrix = {};

%Loop through analysis for each image selected
for j = 1:num_files

img_name = file_names(j,1).name;

img_out_name = strrep(img_name, '.tif', '');

img = imread(img_name);
pictureSize=size(img);
pictureW=pictureSize(2);
pictureH=pictureSize(1);

% Convert to black and white

BW = im2bw(img,0.1);
BW=imfill(BW, 'holes');

figure(1)
imshow(BW);

saveas(figure(1) ,strcat(cd, '\Binary\', img_out_name, '_object
identification'), 'jpg');

%Remove cells at border

clear_image_border=bwlabel(BW,4);
indx=[clear_image_border(1,:),clear_image_border(pictureH,:),clear_imag
e_border(:,1),clear_image_border(:,pictureW)'];
indx=sort(indx, 'ascend');
indx=unique(indx);
analyze_im = ~ismember(clear_image_border,indx);

analyze_im=bwlabel(analyze_im);

Area0=regionprops(analyze_im, 'area');
indxb = find([Area0.Area] > 300);
analyze_im_2 = ismember(analyze_im,indxb);

figure(2)

```

```

imshow(analyze_im_2);
saveas(figure(2) ,strcat(cd, '\Edge Filter\', img_out_name,
'_filter_from_border'),'jpg');

% Identify objects in binary image
label_matrix = bwlabel(analyze_im_2,4);

% Get object parameters
h=regionprops(label_matrix, 'area');

Area=regionprops(label_matrix, 'Area');
BoundingBox1=regionprops(label_matrix, 'BoundingBox');
Length=regionprops(label_matrix, 'majoraxislength');
Width=regionprops(label_matrix, 'minoraxislength');
Eccentricity=regionprops(label_matrix, 'Eccentricity');
Orientation=regionprops(label_matrix, 'Orientation');

Area=[Area.Area]';
BoundingBox2=[BoundingBox1.BoundingBox]';
Length=[Length.MajorAxisLength]';
Width=[Width.MinorAxisLength]';
Eccentricity=[Eccentricity.Eccentricity]';
Orientation=[Orientation.Orientation]';
AspectRatio=Length./Width;

data_out_matrix = [];
row_count=1;
cells_found = numel(h);
for k = 1:cells_found
    data_out_matrix(row_count, 1) = k; %Which cell it is
    data_out_matrix(row_count, 2) = Area(row_count, 1);
    data_out_matrix(row_count,3) = Length(row_count, 1);
    data_out_matrix(row_count,4) = Width(row_count, 1);
    data_out_matrix(row_count,5) = Eccentricity(row_count, 1);
    data_out_matrix(row_count,6) = Orientation(row_count, 1);
    data_out_matrix(row_count,7) = AspectRatio(row_count, 1);

data_out_matrix(row_count,8:11)=BoundingBox1(row_count,1).BoundingBox;
    row_count = row_count + 1;
end

data_out_initial_cells=data_out_matrix(:,1);

BoundingBox_Ratio=data_out_matrix(:,11)./data_out_matrix(:,10);
data_out_matrix(:,12)=BoundingBox_Ratio(:,1);

%to get radius of circle fitting in bounding box, taking average of
bounding box lengths and dividing by 2
BoundingBox_radius=(data_out_matrix(:,11)+data_out_matrix(:,10))/4;
BoundingBox_circular_area=BoundingBox_radius.^2*pi;

%Back-calculating volume assuming volume is spherical and area is
circular
Area_radius_squared=data_out_matrix(:,2)/pi;

```

```

Area_radius=Area_radius_squared.^0.5;
Area_volume=Area_radius.^3*pi*(4/3);

BoundingBox_volume=BoundingBox_radius.^3*pi*(4/3);

Area_um=data_out_matrix(:,2)*um_to_pix^2;
BB_Area_um=BoundingBox_circular_area*um_to_pix^2;
Area_volume_um=Area_volume*um_to_pix^3;
BoundingBox_volume_um=BoundingBox_volume*um_to_pix^3;

data_out_matrix(:,13)=BoundingBox_circular_area(:,1);
data_out_matrix(:,14)=Area_volume(:,1);
data_out_matrix(:,15)=BoundingBox_volume(:,1);

data_out_matrix(:,16)=Area_um(:,1);
data_out_matrix(:,17)=BB_Area_um(:,1);
data_out_matrix(:,18)=Area_volume_um(:,1);
data_out_matrix(:,19)=BoundingBox_volume_um(:,1);

% Export figures with object numbers identified and bounding boxes
plotted

row2=1;
column2=1;
image=label_matrix(:,:,1);
figure(3)

imshow(image);
hold on
stop_row=1;
stop_matrix(1,1)=0;
for row2=1:pictureH
    for column2=1:pictureW
        if label_matrix(row2, column2, 1)~=0
            go=1;
        else
            go=0;
        end

        stop_row2=stop_row+1;
        for i=1:stop_row2
            if i<=numel(stop_matrix)
                z1=stop_matrix(i,1);
                z2=label_matrix(row2,column2, 1);
            else
                z1=0;
            end
            if z1==z2
                go=0;
            end
        end
    end
end

```

```

end

if go==1
    cell_num2=label_matrix(row2,column2,1);
    stop_row=stop_row+1;
    stop_matrix(stop_row,1)=cell_num2;
    str_cell_num=num2str(cell_num2);
    text(column2, row2, str_cell_num, 'Color', 'red');
end

    column2=column2+1;
end

    row2=row2+1;
end

stop_length=numel(stop_matrix);

for q=2:stop_length
    cell_in_matrix=stop_matrix(q,1);

x1=data_out_matrix(cell_in_matrix,8);
y1=data_out_matrix(cell_in_matrix,9);

x2=data_out_matrix(cell_in_matrix,8) +
data_out_matrix(cell_in_matrix,10);
y2=data_out_matrix(cell_in_matrix,9)+
data_out_matrix(cell_in_matrix,11);

x = [x1 x2 x2 x1 x1];
y = [y1 y1 y2 y2 y1];
plot(x, y, 'Color', 'red');
hold on
end

% Take inner 60% of the data

saveas(figure(3) ,strcat(cd, '\Analyzed Images\', img_out_name,
'_boundingbox'),'jpg');

data_out_matrix=data_out_matrix(data_out_matrix(:,2)>50,:);
data_out_matrix_averaged=data_out_matrix;
ave_row=length(data_out_matrix)+2;
st_dev_row=length(data_out_matrix)+3;

data_ave=mean(data_out_matrix_averaged(:,1:19));
data_stdev=std(data_out_matrix_averaged(:,1:19));
[numb_rows_orig, numb_col_orig]=size(data_out_matrix_averaged);

data_out_matrix_averaged(ave_row,:)=data_ave;
data_out_matrix_averaged(st_dev_row,:)=data_stdev;

```

```

    data_out_matrix_averaged(ave_row, 20)=numb_rows_orig;

data_out_matrix_sort1=sortrows(data_out_matrix,2);

[sort_rows, sort_columns]=size(data_out_matrix_sort1);

lower_limit_num=round(.2*sort_rows);
upper_limit_num=round(.8*sort_rows);
lower_cutoff=lower_limit_num;
upper_cutoff=upper_limit_num;

data_out_matrix_60_percent=data_out_matrix_sort1(lower_cutoff:upper_cu
off, :);

cell_nums_unsorted=data_out_matrix(:,1);
cell_nums_sorted=data_out_matrix_60_percent(:,1);

[object_filter_outside_60_percent,
filter_index]=setdiff(data_out_initial_cells, cell_nums_sorted);

% Remove objects from image that were removed from data

image_filter=image;
filter_indexes = find(ismember(image_filter,
object_filter_outside_60_percent));
image_filter(filter_indexes)=0;

figure(4)
imshow(image_filter);

saveas(figure(4) ,strcat(cd, '\Area Filter\', img_out_name,
'_40per_removed'),'jpg');

[numb_rows_filt, numb_col_filt]=size(data_out_matrix_60_percent);

% Save all data and data filtered to only include inner 60 percent
based on
% area into two different sheets

data_out_matrix_sort_averaged=data_out_matrix_60_percent;
sort_ave_row=length(data_out_matrix_sort_averaged)+2;
sort_st_dev_row=length(data_out_matrix_sort_averaged)+3;

data_sort_ave=mean(data_out_matrix_sort_averaged(:,1:19));
data_sort_stdev=std(data_out_matrix_sort_averaged(:,1:19));

data_out_matrix_sort_averaged(sort_ave_row,:)=data_sort_ave;
data_out_matrix_sort_averaged(sort_st_dev_row,:)=data_sort_stdev;

data_out_matrix_sort_averaged(sort_ave_row, 20)=numb_rows_filt;

```

```

headers = {'Cell Number', 'Area (pixels)', 'Length', 'Width',
'Eccentricity', 'Orientation', 'Aspect Ratio', 'BB X', 'BB Y', 'BB X
Length', 'BB Y Length', 'BB Ratio Y/X', 'BB CircArea', 'Vol_Area',
'Vol_BB', 'Area (um^2)', 'BB_Area (um^2)', 'AreaVol (um^3)',
'BB_Vol (um^3)'};
headers = cellstr(headers);

xls_filename = strcat(img_out_name, '.xls');

xlswrite(strcat(cd, '\Excel Files\', xls_filename), headers,
'Sheet1', 'A1')
xlswrite(strcat(cd, '\Excel Files\', xls_filename),
data_out_matrix_averaged, 'Sheet1', 'A2')
xlswrite(strcat(cd, '\Excel Files\', xls_filename), headers,
'Sheet2', 'A1')
xlswrite(strcat(cd, '\Excel Files\', xls_filename),
data_out_matrix_sort_averaged, 'Sheet2', 'A2')
xlswrite(strcat(cd, '\Excel Files\', xls_filename), data_out_matrix,
'Sheet3', 'A1')
xlswrite(strcat(cd, '\Excel Files\', xls_filename),
data_out_matrix_60_percent, 'Sheet4', 'A1')

%close all
imtool close all

clear pictureSize pictureW pictureH indx label_matrix image h Area
BoundingBox1 Length Width Eccentricity Orientation BoundingBox2
AspectRatio
clear data_out_matrix cells_found ave_row st_dev_row data_ave
data_stdev stop_matrix stop_row stop_row2 cell_num2 str_cell_num
column2
clear stop_length x1 y1 x2 y2 x y img_out_name xls_filename j k q
data_out_matrix_sort1 length_sorted_vector lower_limit_num
upper_limit_num lower_cutoff
clear upper_cutoff data_out_matrix_60_percent cell_nums_unsorted
cell_nums_sorted object_filter_outside_60_percent filter_index
image_filter
clear data_out_matrix_sort_averaged sort_ave_row sort_st_dev_row
data_sort_ave data_sort_st_dev
clear BoundingBox_radius BoundingBox_circular_area
Area_radius_squared Area_radius Area_volume BoundingBox_volume indxb
clear removed_indexes removed_cells image_filter filter_indexes
data_out_intial_cells data_out_matrix_60_percent
clear Area0 Area_um Area_volume_um BoundingBox_Ratio
BoundingBox_volume_um analyze_im analyze_im_2 cell_in_matrix
cell_nums_sorted cell_nums_unsorted clear_image_border
clear data_out_initial_cells data_out_matrix_averaged
data_sort_stdev row2 row_count BB_Area_um
clear numb_rows_orig numb_col_orig numb_rows_filt numb_col_filt
sort_rows sort_columns

end
cd ..
end

```

APPENDIX 4: 3-DIMENSIONAL CELL DEFORMATION ANALYSIS MATLAB CODE

```
% Megan Farrell
% Mauck Lab - Oct, 2011
% 3D Cell Analysis (Ghetto, yet better version of Volocity)

clear all;
close all;

% Purpose: High throughput quantification of object parameters in 3D
image
% stacks.

% -----

% Automatically loop through all of the directories
way_large_directory=dir;
way_large_directory_length=length(way_large_directory);

isub = [way_large_directory(:).isdir]; %# returns logical vector
nameFolds = {way_large_directory(isub).name}';
nameFolds(ismember(nameFolds,{'.','..'})) = [];

for z=1:length(nameFolds)

    day_cell={nameFolds(z,1)};
    day=day_cell{1,1}{1,1};

    cd(day)

    main_directory_names=dir;
    main_directory_length=length(main_directory_names);
    isub2 = [main_directory_names(:).isdir]; %# returns logical vector
    nameFolds_2 = {main_directory_names(isub2).name}';
    nameFolds_2(ismember(nameFolds_2,{'.','..'})) = [];

    for y=1:length(nameFolds_2)

        sub_dir_name={nameFolds_2(y,1)};
        sub_dir_name2=sub_dir_name{1,1}{1,1};

        cd(sub_dir_name2)

        % Pull jpegs from subdirectories into binary sequence matrix

        file_names_mat = dir('*.*.jpg');
        num_files=numel(file_names_mat);
```

```

file_names={file_names_mat.name}';
num_files=numel(file_names);

I = imread(file_names{1});

I_BW = im2bw(I,0.1);
I_BW_hole_fill=imfill(I_BW, 'holes');

direc=cd;

mkdir('Binary')
bw_file1=strcat(direc, '\Binary\', 'bw_1.jpg');
imwrite(I_BW_hole_fill, bw_file1, 'jpg');

% Preallocate the array
sequence = zeros([size(I_BW) num_files]);
sequence(:, :, 1) = I_BW_hole_fill;

% Create image sequence array
for p = 2:num_files

    I_seq=imread(file_names{p});
    I_seq_BW=im2bw(I_seq, 0.1);
    I_seq_BW_hole_fill= imfill(I_seq_BW, 'holes');

    filename2=sprintf('bw_%d.jpg',p);
    binary_file=strcat(direc, '\Binary\', filename2);
    imwrite(I_seq_BW_hole_fill,binary_file, 'jpg');

    sequence(:, :, p) = I_seq_BW_hole_fill;
end

pixels_x=size(image(I_seq_BW_hole_fill));
pixels_y=size(image(I_seq_BW_hole_fill));
num_slices=num_files;

% alibrate um to pixel scale

x_pixel_um_ratio = 0.828;
z_pixel_um_ratio= 2.34;

depth_factor=x_pixel_um_ratio/z_pixel_um_ratio;

%-----
----

% Begin first pass image analysis. Label ALL identified objects.

```

```

label_matrix=bwlabeln(sequence);

clear sequence

h=regionprops(label_matrix, 'area');

    %SUM(:,1)=h.BoundingBox;
Area=regionprops(label_matrix, 'Area');
BoundingBox1=regionprops(label_matrix, 'BoundingBox');
Area=[Area.Area]';
BoundingBox2=[BoundingBox1.BoundingBox]';

data_out_matrix = [];
row_count=1;
cells_found = numel(h);
for k = 1:cells_found
    data_out_matrix(row_count, 1) = k; %Which cell it is
    data_out_matrix(row_count, 2) = Area(row_count, 1);

data_out_matrix(row_count,3:8)=BoundingBox1(row_count,1).BoundingBox;
    row_count = row_count + 1;
end

xlswrite('cell_data_before_exclusion.xls', data_out_matrix, 'Sheet1',
'A2')

% Find position of objects in 3D array for exclusion purposes.

    position_matrix=[];

for i=1:cells_found

TULx=data_out_matrix(i,3);
TULy=data_out_matrix(i,4);
TULz=data_out_matrix(i,5);

TLRx=data_out_matrix(i,3) + data_out_matrix(i,6);
TLRy=data_out_matrix(i,4)+data_out_matrix(i,7);

BULz=data_out_matrix(i,5)+data_out_matrix(i,8);

position_matrix(i,1)=data_out_matrix(i,1);
position_matrix(i,2)=TULx;
position_matrix(i,3)=TULy;
position_matrix(i,4)=TULz;
position_matrix(i,5)=TLRx;
position_matrix(i,6)=TLRy;
position_matrix(i,7)=BULz;

end

row_count2=1;

```

```

% Identifies any object that touches the edges of 2D images or top and
bottom
% of 3D stack.

edge_matrix=[];
edge_matrix(cells_found,1)=0;

% The following commands are only valid if there is an object at all
% extrema of image cube. Otherwise, user will have to identify max x,
Y,
% and z position and change these values.

image_cube_maxx=max(position_matrix(:,5));
image_cube_maxy=max(position_matrix(:,6));
image_cube_maxz=max(position_matrix(:,7));
for i=1:cells_found

if position_matrix(i,2)==0.5
    edge_matrix(row_count2,1)=i;
end
if position_matrix(i,3)==0.5
    edge_matrix(row_count2,1)=i;
end
if position_matrix(i,4)==0.5
    edge_matrix(row_count2,1)=i;
end
if position_matrix(i,5)==image_cube_maxx
    edge_matrix(row_count2,1)=i;
    end
if position_matrix(i,6)==image_cube_maxy
    edge_matrix(row_count2,1)=i;
    end
    if position_matrix(i,7)==image_cube_maxz
        edge_matrix(row_count2,1)=i;
        end

    row_count2=row_count2+1;
end

exclusion_matrix=[];
row_count3=1;
for i=1:cells_found
    if (edge_matrix(i,1)>0)
        exclusion_matrix(row_count3,1)=edge_matrix(i,1);
        row_count3=row_count3+1;
    end
end

% Size Exclusion Criteria

for i=1:cells_found
    if data_out_matrix(i,2)<100
        exclusion_matrix(row_count3,1)=data_out_matrix(i,1);
        row_count3=row_count3+1;
    end
end

```

```

end

clear position_matrix data_out_matrix h I I2 I3

% Removes any object that meets edge and size exclusion criteria.
% Creates another 3D Matrix with objects that did not meet exclusion
% criteria.

% To exclude edge touching cells from label_matrix; find numbers in
% exclusion matrix corresponding to numbers in label matrix and make 0

row_count4=row_count3-1;
x_size=size(label_matrix,1);
y_size=size(label_matrix,2);
z_size=size(label_matrix,3);

binary_matrix_excluded=[];
binary_matrix_excluded=label_matrix;

bar=waitbar(0,'Excluding Cells....');

for j=1:x_size
    for k=1:y_size
        for m=1:z_size
            for i=1:row_count4
                if ((binary_matrix_excluded(j,k,m)==exclusion_matrix(i,1)))
                    binary_matrix_excluded(j,k,m)=0;
                end
            end
            for i=1:row_count4
                if ((binary_matrix_excluded(j,k,m)~=0))
                    binary_matrix_excluded(j,k,m)=1;
                end
            end
        end
    end
    waitbar(j/x_size);
end
close(bar)

clear exclusion_matrix label_matrix

% Erode to get surface area
erode_matrix=[];
bar2=waitbar(0,'Eroding Cells....');

for j=1:z_size

    image_original=binary_matrix_excluded(:, :, j);
    perimeter=bwperim(image_original);

    erode_matrix(:, :, j)=perimeter;

```

```

waitbar(j/z_size);
end

close (bar2)

% Once again, identify and label objects in new 3D matrix.

surface_area_label=bwlabeln(erode_matrix);
Surface_Area=regionprops(surface_area_label, 'Area');
Surface_Area2=[Surface_Area.Area]';

% Size Exclusion Criteria of Erode/Surface Area

reg_prop_surf_area=regionprops(surface_area_label);
cell_num_erode=numel(reg_prop_surf_area);
exclusion_matrix2=[];
row_count5=0;

for i=1:cell_num_erode
    if Surface_Area2(i,1)<70

        row_count5=row_count5+1;
        exclusion_matrix2(row_count5,1)=i;
    end
end

% Exclude Cells with small Surface Area
surface_area_matrix_excluded=[];
surface_area_matrix_excluded=surface_area_label;

clear surface_area erode_matrix surface_area_label

%Alternate code = bwperim
erode_images=surface_area_matrix_excluded;
label_erode_final=bwlabeln(surface_area_matrix_excluded);
clear surface_area_matrix_excluded Surface_Area Surface_Area2

Surface_Area_exclude=regionprops(label_erode_final, 'Area');
Surface_Area2_exclude=[Surface_Area_exclude.Area]';

label_matrix2=bwlabeln(binary_matrix_excluded);

h2=regionprops(label_matrix2);

Area2=regionprops(label_matrix2, 'Area');
BoundingBox3=regionprops(label_matrix2, 'BoundingBox');
Area3=[Area2.Area]';

% Output data into data matrix
data_out_matrix2 = [];
row_count_box2=1;

```

```

cells_found_2 = numel(h2);
for k = 1:cells_found_2
    data_out_matrix2(row_count_box2, 1) = k; %Which cell it is
    data_out_matrix2(row_count_box2, 2) = Area3(row_count_box2, 1);

data_out_matrix2(row_count_box2,3:8)=BoundingBox3(row_count_box2,1).Bou
ndingBox;
    row_count_box2 = row_count_box2 + 1;
end

% Export figure sequence with cells touching edge removed
mkdir('exclude cell')
for i=1:z_size
image=binary_matrix_excluded(:,:,i);

filename = sprintf('exclude_%d.jpg', i);
file=strcat(direc, '\exclude_cell\', filename);
imwrite(image, file, 'jpg');

end

% Export figures with object numbers identified and bounding boxes
plotted
mkdir('Label Cell')
for j=1:z_size
    clear stop_matrix
    row2=1;
    column2=1;
    image=binary_matrix_excluded(:,:,j);
    imshow(image);
    hold on
    stop_row=1;
    stop_matrix(1,1)=0;
    for row2=1:x_size
        for column2=1:y_size
            if label_matrix2(row2, column2, j)~=0
                go=1;
            else
                go=0;
            end

            stop_row2=stop_row+1;
            for i=1:stop_row2
                if i<=numel(stop_matrix)
                    z1=stop_matrix(i,1);
                    z2=label_matrix2(row2, column2, j);
                else
                    z1=0;
                end
                if z1==z2
                    go=0;
                end
            end
        end
    end
end
end

```

```

        if go==1
            cell_num2=label_matrix2(row2,column2,j);
            stop_row=stop_row+1;
            stop_matrix(stop_row,1)=cell_num2;
            str_cell_num=num2str(cell_num2);
            text(column2, row2, str_cell_num, 'Color', 'red');
        end

        column2=column2+1;
    end

    row2=row2+1;
end

stop_length=numel(stop_matrix);

for q=2:stop_length
    cell_in_matrix=stop_matrix(q,1);

    x1=data_out_matrix2(cell_in_matrix,3);
    y1=data_out_matrix2(cell_in_matrix,4);

    x2=data_out_matrix2(cell_in_matrix,3) +
    data_out_matrix2(cell_in_matrix,6);
    y2=data_out_matrix2(cell_in_matrix,4)+
    data_out_matrix2(cell_in_matrix,7);

    x = [x1 x2 x2 x1 x1];
    y = [y1 y1 y2 y2 y1];
    plot(x, y, 'Color', 'red');
    hold on
end

filename_label = sprintf('exclude_label_%d.jpg', j);
file=strcat(direc, '\Label Cell\', filename_label);
saveas(figure(1), file, 'jpg');

close all
end

mkdir('Cell Surface Area_Periphery')

% Export figures of periphery with cell number (i.e. surface area)
for j=1:z_size
    clear stop_matrix
    row2=1;
    column2=1;
    image=erode_images(:, :, j);
    imshow(image);
    hold on
    stop_row=1;
    stop_matrix(1,1)=0;
end

```

```

for row2=1:x_size
    for column2=1:y_size
        if label_erode_final(row2, column2, j)~=0
            go=1;
        else
            go=0;
        end

        stop_row2=stop_row+1;
        for i=1:stop_row2
            if i<=numel(stop_matrix)
                z1=stop_matrix(i,1);
                z2=label_erode_final(row2,column2, j);
            else
                z1=0;
            end
            if z1==z2
                go=0;
            end
        end

        if go==1
            cell_num2=label_erode_final(row2,column2,j);
            stop_row=stop_row+1;
            stop_matrix(stop_row,1)=cell_num2;
            str_cell_num=num2str(cell_num2);
            text(column2, row2, str_cell_num, 'Color', 'red');
        end

        column2=column2+1;
    end

    row2=row2+1;
end

filename_label = sprintf('perimeter_%d.jpg', j);
file=strcat(direc, '\Cell Surface Area_Periphery\', filename_label);
saveas(figure(1), file, 'jpg');

close all
end

% Output Data

final_data_out_matrix=[];

[data_out_row data_out_column]=size(data_out_matrix2);

for i=1:data_out_row

    numb_cell=i;

```

```

final_data_out_matrix(i,1)=data_out_matrix2(numb_cell,1);
final_data_out_matrix(i,2)= data_out_matrix2(numb_cell,2);

final_data_out_matrix(i,4)= data_out_matrix2(numb_cell,6);
final_data_out_matrix(i,5)= data_out_matrix2(numb_cell,7);
final_data_out_matrix(i,6)= data_out_matrix2(numb_cell,8);

final_data_out_matrix(i,7)=
(x_pixel_um_ratio^2)*z_pixel_um_ratio*data_out_matrix2(numb_cell,2);

final_data_out_matrix(i,9)=x_pixel_um_ratio*data_out_matrix2(numb_cell,
6);

final_data_out_matrix(i,10)=x_pixel_um_ratio*data_out_matrix2(numb_cell
,7);

final_data_out_matrix(i,11)=z_pixel_um_ratio*data_out_matrix2(numb_cell
,8);
end

Y_X_BB_Ratio=final_data_out_matrix(:,10)./final_data_out_matrix(:,9);
Z_X_BB_Ratio=final_data_out_matrix(:,11)./final_data_out_matrix(:,9);
Z_Y_BB_Ratio=final_data_out_matrix(:,11)./final_data_out_matrix(:,10);
X_Y_scaled_radius=(final_data_out_matrix(:,9)+final_data_out_matrix(:,1
0))/4;
Z_Y_X_Ave_BB_Ratio=final_data_out_matrix(:,11)./((final_data_out_matrix
(:,9)+final_data_out_matrix(:,10))/2);
BB_spherical_volume=X_Y_scaled_radius.^3*pi*(4/3);
BB_spherical_SA=X_Y_scaled_radius.^2*pi*4;

final_data_out_matrix(:,12)=Y_X_BB_Ratio;
final_data_out_matrix(:,13)=Z_X_BB_Ratio;
final_data_out_matrix(:,14)=Z_Y_BB_Ratio;
final_data_out_matrix(:,15)=Z_Y_X_Ave_BB_Ratio;
final_data_out_matrix(:,16)=BB_spherical_volume;
final_data_out_matrix(:,17)=BB_spherical_SA;

final_data_out_matrix_averaged=final_data_out_matrix;

[numb_rows_out numb_col_out]=size(final_data_out_matrix);

sample_number=numb_rows_out;
ave_row=numb_rows_out+2;
st_dev_row=numb_rows_out+3;

data_ave=mean(final_data_out_matrix_averaged(:,1:17));
data_stdev=std(final_data_out_matrix_averaged(:,1:17));

```

```

        final_data_out_matrix_averaged(ave_row,:)=data_ave;
        final_data_out_matrix_averaged(st_dev_row,:)=data_stdev;

final_data_out_matrix_averaged(ave_row,18)=sample_number;

xls_out_name = strrep(sub_dir_name2, '.jpg.frames', '');
xls_filename = strcat(xls_out_name, '.xls');

clear Y_X_BB_Ratio Z_X_BB_Ratio Z_Y_BB_Ratio X_Y_sclaed_radius
BB_spherical_volume BB_sperical_SA

% If there are greater than 3 cells that made it through image
processing,
% filter the inner 60 percent.

if numb_rows_out>4

data_out_matrix_sort1=sortrows(final_data_out_matrix,2);

[sort_rows, sort_columns]=size(data_out_matrix_sort1);

lower_limit_num=round(.2*sort_rows);
upper_limit_num=round(.8*sort_rows);
lower_cutoff=lower_limit_num;
upper_cutoff=upper_limit_num;

data_out_matrix_60_percent=data_out_matrix_sort1(lower_cutoff:upper_cut
off, :);

else
    data_out_matrix_60_percent=final_data_out_matrix;
end

[numb_rows_filt, numb_col_filt]=size(data_out_matrix_60_percent);

data_out_matrix_sort_averaged=data_out_matrix_60_percent;
sort_ave_row=numb_rows_filt+2;
sort_st_dev_row=numb_rows_filt+3;

data_sort_ave=mean(data_out_matrix_sort_averaged(:,1:17));
data_sort_stdev=std(data_out_matrix_sort_averaged(:,1:17));

data_out_matrix_sort_averaged(sort_ave_row,:)=data_sort_ave;

data_out_matrix_sort_averaged(sort_st_dev_row,:)=data_sort_stdev;

data_out_matrix_sort_averaged(sort_ave_row, 18)=numb_rows_filt;

```

```

% Write data to Excel spreadsheet

headers = {'Cell Number','Volume pix', 'Surface Area pix', 'BB X-Length
pix', 'BB Y-Length pix', 'BB Z-Length pix','Cell Volume (um^3)', 'Cell
Surface Area(um^2)', 'Cell Bounding Box X-Length', 'Cell Bounding Box
Y-Length', 'Cell Bounding Box Z-Length', 'Y/X', 'Z/X' 'Z/Y',
'Z/Y_X_Ave', 'BBr_Vol', 'BBr_SA','n'};
headers = cellstr(headers);
    xlswrite(xls_filename, headers, 'Sheet1', 'A1')
    xlswrite(xls_filename, final_data_out_matrix_averaged, 'Sheet1',
'A2')
    xlswrite(xls_filename, final_data_out_matrix, 'Sheet3', 'A1')
    xlswrite(xls_filename, headers, 'Sheet2', 'A1')
    xlswrite(xls_filename, data_out_matrix_sort_averaged, 'Sheet2',
'A2')
    xlswrite(xls_filename, data_out_matrix_60_percent, 'Sheet4', 'A1')

clear Area Area2 Area3 BULz BoudningBox1 BoundingBox2 BoundingBox3 I_BW
I_BW_hole_fill I_seq I_seq_BW I_seq_BW_hole_fill
clear Surface_Area2_exclude Surface_Area_exclude TLRx TLRy TULx TULy
TULz bar bar2 binary_file binary_matrix_excluded bw_file1
clear cell_num_erod cells_found cells_found_2 column2 data_out_matrix2
edge_matrix erode_images erode_matrix exclulsion_matrix2
clear filename_label go h2 i image image_cube_maxx image_cube_maxy
image_cube_maxz image_original isub isub2
clear j k label_erode_final label_matrix2 m perimeter q
reg_prop_surf_area row2 row_count row_count2 row_count3
clear row_count4 row_count5 row_count_box2 stop_length stop_matrix
stop_row stop_row2 surface_area_label x_size
clear y_size z_size x y z x1 y1 z1 x2 y2 z2 data_ave data_stdev
_final_data_out_matrix_averaged n st_dev_row ave_row Z_Y_X_Ave_BB_Ratio

clear numb_rows_out data_out_matrix_sort1 sort_rows sort_columns
final_data_out_matrix lower_limit_num upper_limit_num lower_cutoff
upper_cutoff
clear data_out_matrix_60_percent numb_rows_filt numb_col_filt
data_out_matrix_sort_averaged sort_ave_row sort_st_dev_row
data_sort_ave data_sort_stdev

cd ..
end
cd ..
end
% Export Data

```

BIBLIOGRAPHY

Adesida, A.B., Mulet-Sierra, A., Jomha, N.M., 2012. Hypoxia mediated isolation and expansion enhances the chondrogenic capacity of bone marrow mesenchymal stromal cells. *Stem Cell Res Ther* 3, 9.

Armstrong, C.G., Mow, V.C., 1982. Variations in the intrinsic mechanical properties of human articular cartilage with age, degeneration, and water content. *J Bone Joint Surg Am* 64, 88-94.

Ateshian, G.A., Chahine, N.O., Basalo, I.M., Hung, C.T., 2004. The correspondence between equilibrium biphasic and triphasic material properties in mixture models of articular cartilage. *J Biomech* 37, 391-400.

Athanasίου, K.A., Rosenwasser, M.P., Buckwalter, J.A., Malinin, T.I., Mow, V.C., 1991. Interspecies comparisons of in situ intrinsic mechanical properties of distal femoral cartilage. *J Orthop Res* 9, 330-340.

Barry, F., Boynton, R.E., Liu, B., Murphy, J.M., 2001. Chondrogenic differentiation of mesenchymal stem cells from bone marrow: differentiation-dependent gene expression of matrix components. *Exp Cell Res* 268, 189-200.

Bartov, E., Jerdan, J.A., Glaser, B.M., 1988. A simple technique for isolating pre cell populations from mixed primary cultures. *Journal of Tissue Culture Methods* 11, 181-183.

Basic, N., Basic, V., Bulic, K., Grgic, M., Kleinman, H.K., Luyten, F.P., Vukicevic, S., 1996. TGF-beta and basement membrane matrigel stimulate the chondrogenic phenotype in osteoblastic cells derived from fetal rat calvaria. *J Bone Miner Res* 11, 384-391.

Benya, P.D., Shaffer, J.D., 1982. Dedifferentiated chondrocytes reexpress the differentiated collagen phenotype when cultured in agarose gels. *Cell* 30, 215-224.

Berenbaum, F., 2013. Osteoarthritis as an inflammatory disease (osteoarthritis is not osteoarthrosis!). *Osteoarthritis Cartilage* 21, 16-21.

Bhardwaj, N., Nguyen, Q.T., Chen, A.C., Kaplan, D.L., Sah, R.L., Kundu, S.C., 2011. Potential of 3-D tissue constructs engineered from bovine chondrocytes/silk fibroin-chitosan for in vitro cartilage tissue engineering. *Biomaterials* 32, 5773-5781.

Bian, L., Angione, S.L., Ng, K.W., Lima, E.G., Williams, D.Y., Mao, D.Q., Ateshian, G.A., Hung, C.T., 2009. Influence of decreasing nutrient path length on the development of engineered cartilage. *Osteoarthritis Cartilage* 17, 677-685.

Bian, L., Guvendiren, M., Mauck, R.L., Burdick, J.A., 2013. Hydrogels that mimic developmentally relevant matrix and N-cadherin interactions enhance MSC chondrogenesis. *Proc Natl Acad Sci U S A* 110, 10117-10122.

- Bian, L., Zhai, D.Y., Mauck, R.L., Burdick, J.A., 2011a. Coculture of Human Mesenchymal Stem Cells and Articular Chondrocytes Reduces Hypertrophy and Enhances Functional Properties of Engineered Cartilage. *Tissue Engineering Part A* 17, 1137-1145.
- Bian, L., Zhai, D.Y., Tous, E., Rai, R., Mauck, R.L., Burdick, J.A., 2011b. Enhanced MSC chondrogenesis following delivery of TGF-beta3 from alginate microspheres within hyaluronic acid hydrogels in vitro and in vivo. *Biomaterials* 32, 6425-6434.
- Bian, L., Zhai, D.Y., Zhang, E.C., Mauck, R.L., Burdick, J.A., 2012. Dynamic compressive loading enhances cartilage matrix synthesis and distribution and suppresses hypertrophy in hMSC-laden hyaluronic acid hydrogels. *Tissue Eng Part A* 18, 715-724.
- Bianco, P., Cao, X., Frenette, P.S., Mao, J.J., Robey, P.G., Simmons, P.J., Wang, C.Y., 2013. The meaning, the sense and the significance: translating the science of mesenchymal stem cells into medicine. *Nat Med* 19, 35-42.
- Boeuf, S., Steck, E., Pelttari, K., Hennig, T., Buneb, A., Benz, K., Witte, D., Sultmann, H., Poustka, A., Richter, W., 2008. Subtractive gene expression profiling of articular cartilage and mesenchymal stem cells: serpins as cartilage-relevant differentiation markers. *Osteoarthritis Cartilage* 16, 48-60.
- Bradham, D.M., Passaniti, A., Horton, W.E., Jr., 1995. Mesenchymal cell chondrogenesis is stimulated by basement membrane matrix and inhibited by age-associated factors. *Matrix Biol* 14, 561-571.
- Brodin, H., 1955. Paths of nutrition in articular cartilage and intervertebral discs. *Acta Orthop Scand* 24, 177-183.
- Buckley, C.T., Meyer, E.G., Kelly, D.J., 2012. The influence of construct scale on the composition and functional properties of cartilaginous tissues engineered using bone marrow-derived mesenchymal stem cells. *Tissue Eng Part A* 18, 382-396.
- Buckley, C.T., Thorpe, S.D., Kelly, D.J., 2009. Engineering of large cartilaginous tissues through the use of microchanneled hydrogels and rotational culture. *Tissue Eng Part A* 15, 3213-3220.
- Burdick, J.A., Chung, C., Jia, X., Randolph, M.A., Langer, R., 2005. Controlled degradation and mechanical behavior of photopolymerized hyaluronic acid networks. *Biomacromolecules* 6, 386-391.
- Buschmann, M.D., Gluzband, Y.A., Grodzinsky, A.J., Kimura, J.H., Hunziker, E.B., 1992. Chondrocytes in agarose culture synthesize a mechanically functional extracellular matrix. *J Orthop Res* 10, 745-758.
- Buschmann, M.D., Grodzinsky, A.J., 1995. A molecular model of proteoglycan-associated electrostatic forces in cartilage mechanics. *J Biomech Eng* 117, 179-192.

- Cals, F.L., Hellingman, C.A., Koevoet, W., Baatenburg de Jong, R.J., van Osch, G.J., 2012. Effects of transforming growth factor-beta subtypes on in vitro cartilage production and mineralization of human bone marrow stromal-derived mesenchymal stem cells. *J Tissue Eng Regen Med* 6, 68-76.
- Carr, A.J., Robertsson, O., Graves, S., Price, A.J., Arden, N.K., Judge, A., Beard, D.J., 2012. Knee replacement. *Lancet* 379, 1331-1340.
- Cash, D.E., Bock, C.B., Schughart, K., Linney, E., Underhill, T.M., 1997. Retinoic acid receptor alpha function in vertebrate limb skeletogenesis: a modulator of chondrogenesis. *J Cell Biol* 136, 445-457.
- Chang, N.J., Jung, Y.R., Yao, C.K., Yeh, M.L., 2012. Hydrophilic gelatin and hyaluronic acid-treated PLGA scaffolds for cartilage tissue engineering. *J Appl Biomater Function Mater*, 0.
- Choi, J.B., Youn, I., Cao, L., Leddy, H.A., Gilchrist, C.L., Setton, L.A., Guilak, F., 2007. Zonal changes in the three-dimensional morphology of the chondron under compression: the relationship among cellular, pericellular, and extracellular deformation in articular cartilage. *J Biomech* 40, 2596-2603.
- Chung, C., Burdick, J.A., 2009. Influence of three-dimensional hyaluronic acid microenvironments on mesenchymal stem cell chondrogenesis. *Tissue Eng Part A* 15, 243-254.
- Chung, C., Erickson, I.E., Mauck, R.L., Burdick, J.A., 2008. Differential behavior of auricular and articular chondrocytes in hyaluronic acid hydrogels. *Tissue Eng Part A* 14, 1121-1131.
- Coates, E.E., Riggin, C.N., Fisher, J.P., 2012. Matrix molecule influence on chondrocyte phenotype and proteoglycan 4 expression by alginate-embedded zonal chondrocytes and mesenchymal stem cells. *J Orthop Res*.
- Cooke, M.E., Allon, A.A., Cheng, T., Kuo, A.C., Kim, H.T., Vail, T.P., Marcucio, R.S., Schneider, R.A., Lotz, J.C., Alliston, T., 2011. Structured three-dimensional co-culture of mesenchymal stem cells with chondrocytes promotes chondrogenic differentiation without hypertrophy. *Osteoarthritis and Cartilage* 19, 1210-1218.
- Custers, R.J., Dhert, W.J., Saris, D.B., Verbout, A.J., van Rijen, M.H., Mastbergen, S.C., Lafeber, F.P., Creemers, L.B., 2010. Cartilage degeneration in the goat knee caused by treating localized cartilage defects with metal implants. *Osteoarthritis Cartilage* 18, 377-388.
- Custers, R.J., Saris, D.B., Dhert, W.J., Verbout, A.J., van Rijen, M.H., Mastbergen, S.C., Lafeber, F.P., Creemers, L.B., 2009. Articular cartilage degeneration following the treatment of focal cartilage defects with ceramic metal implants and compared with microfracture. *J Bone Joint Surg Am* 91, 900-910.

- D'Lima, D.D., Fregly, B.J., Patil, S., Steklov, N., Colwell, C.W., Jr., 2012. Knee joint forces: prediction, measurement, and significance. *Proc Inst Mech Eng H* 226, 95-102.
- Davidson, D., Blanc, A., Fillion, D., Wang, H., Plut, P., Pfeffer, G., Buschmann, M.D., Henderson, J.E., 2005. Fibroblast growth factor (FGF) 18 signals through FGF receptor 3 to promote chondrogenesis. *J Biol Chem* 280, 20509-20515.
- Davies, M.R., Ribeiro, L.R., Downey-Jones, M., Needham, M.R., Oakley, C., Wardale, J., 2009. Ligands for retinoic acid receptors are elevated in osteoarthritis and may contribute to pathologic processes in the osteoarthritic joint. *Arthritis Rheum* 60, 1722-1732.
- Dechant, J.E., Symm, W.A., Nieto, J.E., 2011. Comparison of pH, lactate, and glucose analysis of equine synovial fluid using a portable clinical analyzer with a bench-top blood gas analyzer. *Vet Surg* 40, 811-816.
- Degala, S., Williams, R., Zipfel, W., Bonassar, L.J., 2012. Calcium signaling in response to fluid flow by chondrocytes in 3D alginate culture. *J Orthop Res* 30, 793-799.
- Denker, A.E., Nicoll, S.B., Tuan, R.S., 1995. Formation of cartilage-like spheroids by micromass cultures of murine C3H10T1/2 cells upon treatment with transforming growth factor-beta 1. *Differentiation* 59, 25-34.
- Deschepper, M., Oudina, K., David, B., Myrtil, V., Collet, C., Bensidhoum, M., Logeart-Avramoglou, D., Petite, H., 2011. Survival and function of mesenchymal stem cells (MSCs) depend on glucose to overcome exposure to long-term, severe and continuous hypoxia. *J Cell Mol Med*.
- Dickhut, A., Gottwald, E., Steck, E., Heisel, C., Richter, W., 2008. Chondrogenesis of mesenchymal stem cells in gel-like biomaterials in vitro and in vivo. *Front Biosci* 13, 4517-4528.
- Dolgin, E., 2011. Taking tissue engineering to heart. *Nat Med* 17, 1032-1035.
- Dominici, M., Le Blanc, K., Mueller, I., Slaper-Cortenbach, I., Marini, F., Krause, D., Deans, R., Keating, A., Prockop, D., Horwitz, E., 2006. Minimal criteria for defining multipotent mesenchymal stromal cells. The International Society for Cellular Therapy position statement. *Cytotherapy* 8, 315-317.
- Dorotka, R., Bindreiter, U., Vavken, P., Nehrer, S., 2005. Behavior of human articular chondrocytes derived from nonarthritic and osteoarthritic cartilage in a collagen matrix. *Tissue Eng* 11, 877-886.
- El Tamer, M.K., Reis, R.L., 2009. Progenitor and stem cells for bone and cartilage regeneration. *J Tissue Eng Regen Med* 3, 327-337.

- Erickson, I.E., Huang, A.H., Chung, C., Li, R.T., Burdick, J.A., Mauck, R.L., 2009a. Differential maturation and structure-function relationships in mesenchymal stem cell- and chondrocyte-seeded hydrogels. *Tissue Eng Part A* 15, 1041-1052.
- Erickson, I.E., Huang, A.H., Sengupta, S., Kestle, S., Burdick, J.A., Mauck, R.L., 2009b. Macromer density influences mesenchymal stem cell chondrogenesis and maturation in photocrosslinked hyaluronic acid hydrogels. *Osteoarthritis Cartilage* 17, 1639-1648.
- Erickson, I.E., Kestle, S.R., Zellars, K.H., Farrell, M.J., Kim, M., Burdick, J.A., Mauck, R.L., 2012. High mesenchymal stem cell seeding densities in hyaluronic acid hydrogels produce engineered cartilage with native tissue properties. *Acta Biomater* 8, 3027-3034.
- Estes, B.T., Diekman, B.O., Gimple, J.M., Guilak, F., Isolation of adipose-derived stem cells and their induction to a chondrogenic phenotype. *Nat Protoc* 5, 1294-1311.
- Estes, B.T., Diekman, B.O., Gimple, J.M., Guilak, F., 2010. Isolation of adipose-derived stem cells and their induction to a chondrogenic phenotype. *Nat Protoc* 5, 1294-1311.
- Farndale, R.W., Buttle, D.J., Barrett, A.J., 1986. Improved quantitation and discrimination of sulphated glycosaminoglycans by use of dimethylmethylene blue. *Biochim Biophys Acta* 883, 173-177.
- Farrell, M.J., Comeau, E.S., Mauck, R.L., 2012. Mesenchymal stem cells produce functional cartilage matrix in three-dimensional culture in regions of optimal nutrient supply. *Eur Cell Mater* 23, 425-440.
- Fell, H.B., 1925. The histogenesis of cartilage and bone in the long bones of the embryonic fowl. *Journal of Morphology* 40, 417-459.
- Fening, S.D., Mihnovets, J., Jones, M.H., Midura, R.J., Miniaci, A., 2011. The effect of storage medium tonicity on osteochondral autograft plug diameter. *Arthroscopy* 27, 188-193.
- Fischer, J., Dickhut, A., Rickert, M., Richter, W., 2010. Human articular chondrocytes secrete parathyroid hormone-related protein and inhibit hypertrophy of mesenchymal stem cells in coculture during chondrogenesis. *Arthritis Rheum* 62, 2696-2706.
- Flandry, F., Hommel, G., 2011. Normal anatomy and biomechanics of the knee. *Sports Med Arthrosc* 19, 82-92.
- Freeman, M.A.R., 1979. *Adult articular cartilage*, 2d ed. Pitman Medical, Tunbridge Wells, Eng.
- Freyria, A.M., Mallein-Gerin, F., 2012. Chondrocytes or adult stem cells for cartilage repair: the indisputable role of growth factors. *Injury* 43, 259-265.

- Friedenstein, A.J., Chailakhjan, R.K., Lalykina, K.S., 1970. The development of fibroblast colonies in monolayer cultures of guinea-pig bone marrow and spleen cells. *Cell Tissue Kinet* 3, 393-403.
- Friedenstein, A.J., Deriglasova, U.F., Kulagina, N.N., Panasuk, A.F., Rudakowa, S.F., Luria, E.A., Ruadkow, I.A., 1974. Precursors for fibroblasts in different populations of hematopoietic cells as detected by the in vitro colony assay method. *Exp Hematol* 2, 83-92.
- Friedenstein, A.J., Gorskaja, J.F., Kulagina, N.N., 1976. Fibroblast precursors in normal and irradiated mouse hematopoietic organs. *Exp Hematol* 4, 267-274.
- Friedenstein, A.J., Latzinik, N.W., Grosheva, A.G., Gorskaya, U.F., 1982. Marrow microenvironment transfer by heterotopic transplantation of freshly isolated and cultured cells in porous sponges. *Exp Hematol* 10, 217-227.
- Gilbert, P.M., Havenstrite, K.L., Magnusson, K.E., Sacco, A., Leonardi, N.A., Kraft, P., Nguyen, N.K., Thrun, S., Lutolf, M.P., Blau, H.M., 2010. Substrate elasticity regulates skeletal muscle stem cell self-renewal in culture. *Science* 329, 1078-1081.
- Goldring, M.B., Tsuchimochi, K., Ijiri, K., 2006. The control of chondrogenesis. *J Cell Biochem* 97, 33-44.
- Goldring, S.R., Goldring, M.B., 2006. Clinical aspects, pathology and pathophysiology of osteoarthritis. *J Musculoskelet Neuronal Interact* 6, 376-378.
- Gomoll, A.H., 2012. Microfracture and augments. *J Knee Surg* 25, 9-15.
- Gomoll, A.H., Minas, T., 2011. Debridement, Microfracture, and Osteochondral Autograft Transfer for Treatment of Cartilage Defects, in: Minas, T. (Ed.), *A Primer in Cartilage Repair and Joint Preservation of the Knee*. Saunders, Philadelphia, PA, pp. 48-53.
- Gong, J., Katsuyama, Y., Kurokawa, T., Osada, Y., 2003. Double-Network Hydrogels with Extremely High Mechanical Strength. *Advanced Materials* 15, 1155-1158.
- Gray, H., Goss, C.M., 1973. *Anatomy of the human body*, 29th American ed. Lea & Febiger, Philadelphia,.
- Grimshaw, M.J., Mason, R.M., 2000. Bovine articular chondrocyte function in vitro depends upon oxygen tension. *Osteoarthritis Cartilage* 8, 386-392.
- Gronthos, S., Zannettino, A.C., Hay, S.J., Shi, S., Graves, S.E., Kortessidis, A., Simmons, P.J., 2003. Molecular and cellular characterisation of highly purified stromal stem cells derived from human bone marrow. *J Cell Sci* 116, 1827-1835.

- Guenther, H.L., Guenther, H.E., Froesch, E.R., Fleisch, H., 1982. Effect of insulin-like growth factor on collagen and glycosaminoglycan synthesis by rabbit articular chondrocytes in culture. *Experientia* 38, 979-981.
- Guettler, J.H., Demetropoulos, C.K., Yang, K.H., Jurist, K.A., 2004. Osteochondral defects in the human knee: influence of defect size on cartilage rim stress and load redistribution to surrounding cartilage. *Am J Sports Med* 32, 1451-1458.
- Guilak, F., Alexopoulos, L.G., Upton, M.L., Youn, I., Choi, J.B., Cao, L., Setton, L.A., Haider, M.A., 2006. The pericellular matrix as a transducer of biomechanical and biochemical signals in articular cartilage. *Ann N Y Acad Sci* 1068, 498-512.
- Guo, X., Wang, C., Zhang, Y., Xia, R., Hu, M., Duan, C., Zhao, Q., Dong, L., Lu, J., Qing Song, Y., 2004. Repair of large articular cartilage defects with implants of autologous mesenchymal stem cells seeded into beta-tricalcium phosphate in a sheep model. *Tissue Eng* 10, 1818-1829.
- Halleux, C., Sottile, V., Gasser, J.A., Seuwen, K., 2001. Multi-lineage potential of human mesenchymal stem cells following clonal expansion. *J Musculoskelet Neuronal Interact* 2, 71-76.
- Hangody, L., Vasarhelyi, G., Hangody, L.R., Sukosd, Z., Tibay, G., Bartha, L., Bodo, G., 2008. Autologous osteochondral grafting--technique and long-term results. *Injury* 39 Suppl 1, S32-39.
- Harrington, E.K., Lunsford, L.E., Svoboda, K.K., 2004. Chondrocyte terminal differentiation, apoptosis, and type X collagen expression are downregulated by parathyroid hormone. *Anat Rec A Discov Mol Cell Evol Biol* 281, 1286-1295.
- Haviv, B., Bronak, S., Thein, R., 2013. The complexity of pain around the knee in patients with osteoarthritis. *Isr Med Assoc J* 15, 178-181.
- Heir, S., Nerhus, T.K., Rotterud, J.H., Loken, S., Ekeland, A., Engebretsen, L., Aroen, A., 2010. Focal cartilage defects in the knee impair quality of life as much as severe osteoarthritis: a comparison of knee injury and osteoarthritis outcome score in 4 patient categories scheduled for knee surgery. *Am J Sports Med* 38, 231-237.
- Hellingman, C.A., Koevoet, W., Kops, N., Farrell, E., Jahr, H., Liu, W., Baatenburg de Jong, R.J., Frenz, D.A., van Osch, G.J., 2010. Fibroblast growth factor receptors in in vitro and in vivo chondrogenesis: relating tissue engineering using adult mesenchymal stem cells to embryonic development. *Tissue Eng Part A* 16, 545-556.
- Henderson, S.E., Santangelo, K.S., Bertone, A.L., 2011. Chondrogenic effects of exogenous retinoic acid or a retinoic acid receptor antagonist (LE135) on equine chondrocytes and bone marrow-derived mesenchymal stem cells in monolayer culture. *Am J Vet Res* 72, 884-892.

- Heywood, H.K., Bader, D.L., Lee, D.A., 2006. Glucose concentration and medium volume influence cell viability and glycosaminoglycan synthesis in chondrocyte-seeded alginate constructs. *Tissue Eng* 12, 3487-3496.
- Heywood, H.K., Lee, D.A., 2008. Monolayer expansion induces an oxidative metabolism and ROS in chondrocytes. *Biochem Biophys Res Commun* 373, 224-229.
- Heywood, H.K., Lee, D.A., 2010. Low oxygen reduces the modulation to an oxidative phenotype in monolayer-expanded chondrocytes. *J Cell Physiol* 222, 248-253.
- Heywood, H.K., Sembi, P.K., Lee, D.A., Bader, D.L., 2004. Cellular utilization determines viability and matrix distribution profiles in chondrocyte-seeded alginate constructs. *Tissue Eng* 10, 1467-1479.
- Hinchliffe, J.R., 1994. Evolutionary developmental biology of the tetrapod limb. *Development. Supplement.*, 163-168.
- Hodge, J.A., McKibbin, B., 1969. The nutrition of mature and immature cartilage in rabbits. An autoradiographic study. *J Bone Joint Surg Br* 51, 140-147.
- Hoffman, L.M., Weston, A.D., Underhill, T.M., 2003. Molecular mechanisms regulating chondroblast differentiation. *J Bone Joint Surg Am* 85-A Suppl 2, 124-132.
- Holder, N., 1977. An experimental investigation into the early development of the chick elbow joint. *J Embryol Exp Morphol* 39, 115-127.
- Hsieh-Bonassera, N.D., Wu, I., Lin, J.K., Schumacher, B.L., Chen, A.C., Masuda, K., Bugbee, W.D., Sah, R.L., 2009. Expansion and redifferentiation of chondrocytes from osteoarthritic cartilage: cells for human cartilage tissue engineering. *Tissue Eng Part A* 15, 3513-3523.
- Hu, J.C., Athanasiou, K.A., 2006. Chondrocytes from different zones exhibit characteristic differences in high density culture. *Connect Tissue Res* 47, 133-140.
- Huang, A.H., Farrell, M.J., Kim, M., Mauck, R.L., 2010a. Long-term dynamic loading improves the mechanical properties of chondrogenic mesenchymal stem cell-laden hydrogel. *Eur Cell Mater* 19, 72-85.
- Huang, A.H., Farrell, M.J., Mauck, R.L., 2010b. Mechanics and mechanobiology of mesenchymal stem cell-based engineered cartilage. *J Biomech* 43, 128-136.
- Huang, A.H., Stein, A., Mauck, R.L., Evaluation of the complex transcriptional topography of mesenchymal stem cell chondrogenesis for cartilage tissue engineering. *Tissue Eng Part A* 16, 2699-2708.
- Huang, A.H., Stein, A., Mauck, R.L., 2010c. Evaluation of the complex transcriptional topography of mesenchymal stem cell chondrogenesis for cartilage tissue engineering. *Tissue Eng Part A* 16, 2699-2708.

- Huang, A.H., Stein, A., Tuan, R.S., Mauck, R.L., 2009. Transient exposure to transforming growth factor beta 3 improves the mechanical properties of mesenchymal stem cell-laden cartilage constructs in a density-dependent manner. *Tissue Eng Part A* 15, 3461-3472.
- Huang, C.Y., Stankiewicz, A., Ateshian, G.A., Mow, V.C., 2005. Anisotropy, inhomogeneity, and tension-compression nonlinearity of human glenohumeral cartilage in finite deformation. *J Biomech* 38, 799-809.
- Hui, A.Y., McCarty, W.J., Masuda, K., Firestein, G.S., Sah, R.L., 2012. A systems biology approach to synovial joint lubrication in health, injury, and disease. *Wiley Interdiscip Rev Syst Biol Med* 4, 15-37.
- Hunter, W., 1743. Of the structure and diseases of articulating cartilages. *Philosophical Transactions of the Royal Society of London* 42, 514-521.
- Huntley, J.S., Bush, P.G., McBirnie, J.M., Simpson, A.H., Hall, A.C., 2005. Chondrocyte death associated with human femoral osteochondral harvest as performed for mosaicplasty. *J Bone Joint Surg Am* 87, 351-360.
- Hwang, N.S., Varghese, S., Li, H., Elisseeff, J., 2011. Regulation of osteogenic and chondrogenic differentiation of mesenchymal stem cells in PEG-ECM hydrogels. *Cell Tissue Res* 344, 499-509.
- Imhof, H., Breitenseher, M., Kainberger, F., Rand, T., Trattnig, S., 1999. Importance of subchondral bone to articular cartilage in health and disease. *Top Magn Reson Imaging* 10, 180-192.
- Jiang, J., Tang, A., Ateshian, G.A., Guo, X.E., Hung, C.T., Lu, H.H., 2010. Bioactive stratified polymer ceramic-hydrogel scaffold for integrative osteochondral repair. *Ann Biomed Eng* 38, 2183-2196.
- Johnstone, B., Alini, M., Cucchiari, M., Dodge, G.R., Eglin, D., Guilak, F., Madry, H., Mata, A., Mauck, R.L., Semino, C.E., Stoddart, M.J., 2013. Tissue engineering for articular cartilage repair--the state of the art. *Eur Cell Mater* 25, 248-267.
- Johnstone, B., Hering, T.M., Caplan, A.I., Goldberg, V.M., Yoo, J.U., 1998. In vitro chondrogenesis of bone marrow-derived mesenchymal progenitor cells. *Exp Cell Res* 238, 265-272.
- Jones, B.A., Pei, M., 2012. Synovium-Derived Stem Cells: A Tissue-Specific Stem Cell for Cartilage Engineering and Regeneration. *Tissue Eng Part B Rev*.
- Jones, R.S., Keene, G.C., Learmonth, D.J., Bickerstaff, D., Nawana, N.S., Costi, J.J., Pearcy, M.J., 1996. Direct measurement of hoop strains in the intact and torn human medial meniscus. *Clin Biomech (Bristol, Avon)* 11, 295-300.

- Jurgens, W.J., Lu, Z., Zandieh-Doulabi, B., Kuik, D.J., Ritt, M.J., Helder, M.N., 2012. Hyperosmolarity and hypoxia induce chondrogenesis of adipose-derived stem cells in a collagen type 2 hydrogel. *J Tissue Eng Regen Med* 6, 570-578.
- Kafienah, W., Mistry, S., Perry, M.J., Politopoulou, G., Hollander, A.P., 2007. Pharmacological regulation of adult stem cells: chondrogenesis can be induced using a synthetic inhibitor of the retinoic acid receptor. *Stem Cells* 25, 2460-2468.
- Kandel, R.A., Grynblas, M., Pilliar, R., Lee, J., Wang, J., Waldman, S., Zalzal, P., Hurtig, M., 2006. Repair of osteochondral defects with biphasic cartilage-calcium polyphosphate constructs in a sheep model. *Biomaterials* 27, 4120-4131.
- Karagianes, M.T., Wheeler, K.R., Nilles, J.L., 1975. Cartilage repair over porous metal implants. *Arch Pathol* 99, 398-400.
- Kavalkovich, K.W., Boynton, R.E., Murphy, J.M., Barry, F., 2002. Chondrogenic differentiation of human mesenchymal stem cells within an alginate layer culture system. *In Vitro Cell Dev Biol Anim* 38, 457-466.
- Kelly, T.A., Ng, K.W., Wang, C.C., Ateshian, G.A., Hung, C.T., 2006. Spatial and temporal development of chondrocyte-seeded agarose constructs in free-swelling and dynamically loaded cultures. *J Biomech* 39, 1489-1497.
- Kielty, C.M., Kwan, A.P., Holmes, D.F., Schor, S.L., Grant, M.E., 1985. Type X collagen, a product of hypertrophic chondrocytes. *Biochem J* 227, 545-554.
- Kim, H.J., Im, G.I., 2009. Combination of transforming growth factor-beta2 and bone morphogenetic protein 7 enhances chondrogenesis from adipose tissue-derived mesenchymal stem cells. *Tissue Eng Part A* 15, 1543-1551.
- Kim, M., Erickson, I.E., Choudhury, M., Pleshko, N., Mauck, R.L., 2012. Transient exposure to TGF-beta3 improves the functional chondrogenesis of MSC-laden hyaluronic acid hydrogels. *J Mech Behav Biomed Mater* 11, 92-101.
- Kim, M., Kraft, J.J., Volk, A.C., Pugarelli, J., Pleshko, N., Dodge, G.R., 2011. Characterization of a cartilage-like engineered biomass using a self-aggregating suspension culture model: molecular composition using FT-IRIS. *J Orthop Res* 29, 1881-1887.
- Kim, T.K., Sharma, B., Williams, C.G., Ruffner, M.A., Malik, A., McFarland, E.G., Elisseeff, J.H., 2003. Experimental model for cartilage tissue engineering to regenerate the zonal organization of articular cartilage. *Osteoarthritis Cartilage* 11, 653-664.
- Kim, Y.J., Kim, H.J., Im, G.I., 2008. PTHrP promotes chondrogenesis and suppresses hypertrophy from both bone marrow-derived and adipose tissue-derived MSCs. *Biochem Biophys Res Commun* 373, 104-108.

Klein, T.J., Chaudhry, M., Bae, W.C., Sah, R.L., 2007. Depth-dependent biomechanical and biochemical properties of fetal, newborn, and tissue-engineered articular cartilage. *J Biomech* 40, 182-190.

Klein, T.J., Sah, R.L., 2007. Modulation of depth-dependent properties in tissue-engineered cartilage with a semi-permeable membrane and perfusion: a continuum model of matrix metabolism and transport. *Biomech Model Mechanobiol* 6, 21-32.

Knight, M.M., Lee, D.A., Bader, D.L., 1998. The influence of elaborated pericellular matrix on the deformation of isolated articular chondrocytes cultured in agarose. *Biochim Biophys Acta* 1405, 67-77.

Koyama, E., Golden, E.B., Kirsch, T., Adams, S.L., Chandraratna, R.A., Michaille, J.J., Pacifici, M., 1999. Retinoid signaling is required for chondrocyte maturation and endochondral bone formation during limb skeletogenesis. *Dev Biol* 208, 375-391.

Koyama, E., Shibukawa, Y., Nagayama, M., Sugito, H., Young, B., Yuasa, T., Okabe, T., Ochiai, T., Kamiya, N., Rountree, R.B., Kingsley, D.M., Iwamoto, M., Enomoto-Iwamoto, M., Pacifici, M., 2008. A distinct cohort of progenitor cells participates in synovial joint and articular cartilage formation during mouse limb skeletogenesis. *Dev Biol* 316, 62-73.

Koyama, E., Yasuda, T., Minugh-Purvis, N., Kinumatsu, T., Yallowitz, A.R., Wellik, D.M., Pacifici, M., 2010. Hox11 genes establish synovial joint organization and phylogenetic characteristics in developing mouse zeugopod skeletal elements. *Development* 137, 3795-3800.

Kris Kostanski, L., Huang, R., Filipe, C.D., Ghosh, R., 2009. Interpenetrating polymer networks as a route to tunable multi-responsive biomaterials: development of novel concepts. *J Biomater Sci Polym Ed* 20, 271-297.

Lahiji, A., Sohrabi, A., Hungerford, D.S., Frondoza, C.G., 2000. Chitosan supports the expression of extracellular matrix proteins in human osteoblasts and chondrocytes. *J Biomed Mater Res* 51, 586-595.

Lai, W.M., Hou, J.S., Mow, V.C., 1991. A triphasic theory for the swelling and deformation behaviors of articular cartilage. *J Biomech Eng* 113, 245-258.

Lane, J.M., Brighton, C.T., Menkowitz, B.J., 1977. Anaerobic and aerobic metabolism in articular cartilage. *J Rheumatol* 4, 334-342.

LaPrade, R.F., Bursch, L.S., Olson, E.J., Havlas, V., Carlson, C.S., 2008. Histologic and immunohistochemical characteristics of failed articular cartilage resurfacing procedures for osteochondritis of the knee: a case series. *Am J Sports Med* 36, 360-368.

Lee, C.H., Cook, J.L., Mendelson, A., Moioli, E.K., Yao, H., Mao, J.J., 2010. Regeneration of the articular surface of the rabbit synovial joint by cell homing: a proof of concept study. *Lancet* 376, 440-448.

- Lee, D.A., Bader, D.L., 1995. The development and characterization of an in vitro system to study strain-induced cell deformation in isolated chondrocytes. *In Vitro Cell Dev Biol Anim* 31, 828-835.
- Lee, D.A., Knight, M.M., Bolton, J.F., Idowu, B.D., Kayser, M.V., Bader, D.L., 2000. Chondrocyte deformation within compressed agarose constructs at the cellular and sub-cellular levels. *J Biomech* 33, 81-95.
- Lefkoe, T.P., Trafton, P.G., Ehrlich, M.G., Walsh, W.R., Dennehy, D.T., Barrach, H.J., Akelman, E., 1993. An experimental model of femoral condylar defect leading to osteoarthritis. *J Orthop Trauma* 7, 458-467.
- Leidy, J., 1849. On the intimate structure and history of the articular cartilages. *The American Journal of the Medical Sciences* 34, 277-294.
- Li, X.A., Iyer, S., Cross, M.B., Figgie, M.P., 2012. Total joint replacement in adolescents: literature review and case examples. *Curr Opin Pediatr* 24, 57-63.
- Li, Z., Yao, S.J., Alini, M., Stoddart, M.J., 2011. The role of retinoic acid receptor inhibitor LE135 on the osteochondral differentiation of human bone marrow mesenchymal stem cells. *J Cell Biochem* 112, 963-970.
- Lima, E.G., Bian, L., Ng, K.W., Mauck, R.L., Byers, B.A., Tuan, R.S., Ateshian, G.A., Hung, C.T., 2007. The beneficial effect of delayed compressive loading on tissue-engineered cartilage constructs cultured with TGF-beta3. *Osteoarthritis Cartilage* 15, 1025-1033.
- Liu, X., Jin, X., Ma, P.X., 2011. Nanofibrous hollow microspheres self-assembled from star-shaped polymers as injectable cell carriers for knee repair. *Nat Mater* 10, 398-406.
- Macchiarini, P., Jungebluth, P., Go, T., Asnaghi, M.A., Rees, L.E., Cogan, T.A., Dodson, A., Martorell, J., Bellini, S., Parnigotto, P.P., Dickinson, S.C., Hollander, A.P., Mantero, S., Conconi, M.T., Birchall, M.A., 2008. Clinical transplantation of a tissue-engineered airway. *Lancet* 372, 2023-2030.
- Mackay, A.M., Beck, S.C., Murphy, J.M., Barry, F.P., Chichester, C.O., Pittenger, M.F., 1998. Chondrogenic differentiation of cultured human mesenchymal stem cells from marrow. *Tissue Eng* 4, 415-428.
- Maher, S.A., Mauck, R.L., Rackwitz, L., Tuan, R.S., 2010. A nanofibrous cell-seeded hydrogel promotes integration in a cartilage gap model. *J Tissue Eng Regen Med* 4, 25-29.
- Makris, E.A., Hadidi, P., Athanasiou, K.A., 2011. The knee meniscus: structure-function, pathophysiology, current repair techniques, and prospects for regeneration. *Biomaterials* 32, 7411-7431.

- Malda, J., Martens, D.E., Tramper, J., van Blitterswijk, C.A., Riesle, J., 2003. Cartilage tissue engineering: controversy in the effect of oxygen. *Crit Rev Biotechnol* 23, 175-194.
- Malinin, T., Ouellette, E.A., 2000. Articular cartilage nutrition is mediated by subchondral bone: a long-term autograft study in baboons. *Osteoarthritis Cartilage* 8, 483-491.
- Marcus, R.E., 1973. The effect of low oxygen concentration on growth, glycolysis, and sulfate incorporation by articular chondrocytes in monolayer culture. *Arthritis Rheum* 16, 646-656.
- Mardones, R.M., Reinholz, G.G., Fitzsimmons, J.S., Zobitz, M.E., An, K.N., Lewallen, D.G., Yaszemski, M.J., O'Driscoll, S.W., 2005. Development of a biologic prosthetic composite for cartilage repair. *Tissue Eng* 11, 1368-1378.
- Mareddy, S., Crawford, R., Brooke, G., Xiao, Y., 2007. Clonal isolation and characterization of bone marrow stromal cells from patients with osteoarthritis. *Tissue Eng* 13, 819-829.
- Markway, B.D., Tan, G.K., Brooke, G., Hudson, J.E., Cooper-White, J.J., Doran, M.R., 2010. Enhanced chondrogenic differentiation of human bone marrow-derived mesenchymal stem cells in low oxygen environment micropellet cultures. *Cell Transplant* 19, 29-42.
- Matricali, G.A., Dereymaeker, G.P., Luyten, F.P., 2010. Donor site morbidity after articular cartilage repair procedures: a review. *Acta Orthop Belg* 76, 669-674.
- Mauck, R.L., Hung, C.T., Ateshian, G.A., 2003a. Modeling of neutral solute transport in a dynamically loaded porous permeable gel: implications for articular cartilage biosynthesis and tissue engineering. *J Biomech Eng* 125, 602-614.
- Mauck, R.L., Soltz, M.A., Wang, C.C., Wong, D.D., Chao, P.H., Valhmu, W.B., Hung, C.T., Ateshian, G.A., 2000. Functional tissue engineering of articular cartilage through dynamic loading of chondrocyte-seeded agarose gels. *J Biomech Eng* 122, 252-260.
- Mauck, R.L., Wang, C.C., Oswald, E.S., Ateshian, G.A., Hung, C.T., 2003b. The role of cell seeding density and nutrient supply for articular cartilage tissue engineering with deformational loading. *Osteoarthritis Cartilage* 11, 879-890.
- Mauck, R.L., Yuan, X., Tuan, R.S., 2006. Chondrogenic differentiation and functional maturation of bovine mesenchymal stem cells in long-term agarose culture. *Osteoarthritis Cartilage* 14, 179-189.
- Mease, P.J., Hanna, S., Frakes, E.P., Altman, R.D., 2011. Pain mechanisms in osteoarthritis: understanding the role of central pain and current approaches to its treatment. *J Rheumatol* 38, 1546-1551.

- Melrose, J., Smith, S., Ghosh, P., 2004. Cartilage and osteoarthritis, in: Sabatini, M., Pastoureau, P., De Ceuninck, F. (Eds.), *Methods in molecular medicine* 100-101. Humana Press, Totowa, N.J., pp. 39-63.
- Mendez-Ferrer, S., Michurina, T.V., Ferraro, F., Mazloom, A.R., Macarthur, B.D., Lira, S.A., Scadden, D.T., Ma'ayan, A., Enikolopov, G.N., Frenette, P.S., 2010. Mesenchymal and haematopoietic stem cells form a unique bone marrow niche. *Nature* 466, 829-834.
- Meretoja, V.V., Dahlin, R.L., Wright, S., Kasper, F.K., Mikos, A.G., 2013. The effect of hypoxia on the chondrogenic differentiation of co-cultured articular chondrocytes and mesenchymal stem cells in scaffolds. *Biomaterials* 34, 4266-4273.
- Meyer, E.G., Buckley, C.T., Steward, A.J., Kelly, D.J., 2011. The effect of cyclic hydrostatic pressure on the functional development of cartilaginous tissues engineered using bone marrow derived mesenchymal stem cells. *J Mech Behav Biomed Mater* 4, 1257-1265.
- Minas, T., 2001. Autologous chondrocyte implantation for focal chondral defects of the knee. *Clin Orthop Relat Res*, S349-361.
- Minas, T., 2011. Autologous Chondrocyte Implantation, in: Minas, T. (Ed.), *A Primer in Cartilage Repair and Joint Preservation of the Knee*. Saunders, Philadelphia, PA, pp. 65-119.
- Mithoefer, K., McAdams, T., Williams, R.J., Kreuz, P.C., Mandelbaum, B.R., 2009. Clinical efficacy of the microfracture technique for articular cartilage repair in the knee: an evidence-based systematic analysis. *Am J Sports Med* 37, 2053-2063.
- Mitrovic, D., 1978. Development of the diarthrodial joints in the rat embryo. *Am J Anat* 151, 475-485.
- Mobasheri, A., Richardson, S., Mobasheri, R., Shakibaei, M., Hoyland, J.A., 2005. Hypoxia inducible factor-1 and facilitative glucose transporters GLUT1 and GLUT3: putative molecular components of the oxygen and glucose sensing apparatus in articular chondrocytes. *Histol Histopathol* 20, 1327-1338.
- Mouw, J.K., Connelly, J.T., Wilson, C.G., Michael, K.E., Levenston, M.E., 2007. Dynamic compression regulates the expression and synthesis of chondrocyte-specific matrix molecules in bone marrow stromal cells. *Stem Cells* 25, 655-663.
- Mow, V.C., Huiskes, R., 2005. *Basic orthopaedic biomechanics & mechano-biology*, 3rd ed. Lippincott Williams & Wilkins, Philadelphia, PA.
- Mow, V.C., Kuei, S.C., Lai, W.M., Armstrong, C.G., 1980. Biphasic creep and stress relaxation of articular cartilage in compression? Theory and experiments. *J Biomech Eng* 102, 73-84.

- Mrosek, E.H., Schagemann, J.C., Chung, H.W., Fitzsimmons, J.S., Yaszemski, M.J., Mardones, R.M., O'Driscoll, S.W., Reinholz, G.G., 2010. Porous tantalum and poly-epsilon-caprolactone biocomposites for osteochondral defect repair: preliminary studies in rabbits. *J Orthop Res* 28, 141-148.
- Mueller, M.B., Fischer, M., Zellner, J., Berner, A., Dienstknecht, T., Kujat, R., Prantl, L., Nerlich, M., Tuan, R.S., Angele, P., 2013. Effect of parathyroid hormone-related protein in an in vitro hypertrophy model for mesenchymal stem cell chondrogenesis. *Int Orthop* 37, 945-951.
- Mueller, M.B., Fischer, M., Zellner, J., Berner, A., Dienstknecht, T., Prantl, L., Kujat, R., Nerlich, M., Tuan, R.S., Angele, P., 2010. Hypertrophy in mesenchymal stem cell chondrogenesis: effect of TGF-beta isoforms and chondrogenic conditioning. *Cells Tissues Organs* 192, 158-166.
- Mueller, M.B., Tuan, R.S., 2008. Functional characterization of hypertrophy in chondrogenesis of human mesenchymal stem cells. *Arthritis Rheum* 58, 1377-1388.
- Muir, H., Bullough, P., Maroudas, A., 1970. The distribution of collagen in human articular cartilage with some of its physiological implications. *J Bone Joint Surg Br* 52, 554-563.
- Mulhall, K.J., Ghomrawi, H.M., Scully, S., Callaghan, J.J., Saleh, K.J., 2006. Current etiologies and modes of failure in total knee arthroplasty revision. *Clin Orthop Relat Res* 446, 45-50.
- Muller, J., Benz, K., Ahlers, M., Gaissmaier, C., Mollenhauer, J., 2011. Hypoxic conditions during expansion culture prime human mesenchymal stromal precursor cells for chondrogenic differentiation in three-dimensional cultures. *Cell Transplant* 20, 1589-1602.
- Mwale, F., Yao, G., Ouellet, J.A., Petit, A., Antoniou, J., 2010. Effect of parathyroid hormone on type X and type II collagen expression in mesenchymal stem cells from osteoarthritic patients. *Tissue Eng Part A* 16, 3449-3455.
- Natoli, R.M., Revell, C.M., Athanasiou, K.A., 2009. Chondroitinase ABC treatment results in greater tensile properties of self-assembled tissue-engineered articular cartilage. *Tissue Eng Part A* 15, 3119-3128.
- Nehrer, S., Spector, M., Minas, T., 1999. Histologic analysis of tissue after failed cartilage repair procedures. *Clin Orthop Relat Res*, 149-162.
- Neuman, R.E., Logan, M.A., 1950. The determination of hydroxyproline. *J Biol Chem* 184, 299-306.
- Ng, K.W., Ateshian, G.A., Hung, C.T., 2009. Zonal chondrocytes seeded in a layered agarose hydrogel create engineered cartilage with depth-dependent cellular and mechanical inhomogeneity. *Tissue Eng Part A* 15, 2315-2324.

- Nguyen, Q.T., Hwang, Y., Chen, A.C., Varghese, S., Sah, R.L., 2012. Cartilage-like mechanical properties of poly (ethylene glycol)-diacrylate hydrogels. *Biomaterials* 33, 6682-6690.
- O'Hara, B.P., Urban, J.P., Maroudas, A., 1990. Influence of cyclic loading on the nutrition of articular cartilage. *Ann Rheum Dis* 49, 536-539.
- Ogston, A.G., Stanier, J.E., 1953. The physiological function of hyaluronic acid in synovial fluid; viscous, elastic and lubricant properties. *J Physiol* 119, 244-252.
- Okamoto, T., Aoyama, T., Nakayama, T., Nakamata, T., Hosaka, T., Nishijo, K., Nakamura, T., Kiyono, T., Toguchida, J., 2002. Clonal heterogeneity in differentiation potential of immortalized human mesenchymal stem cells. *Biochem Biophys Res Commun* 295, 354-361.
- Otte, P., 1991. Basic cell metabolism of articular cartilage. Manometric studies. *Z Rheumatol* 50, 304-312.
- Pacifici, M., Koyama, E., Iwamoto, M., 2005. Mechanisms of synovial joint and articular cartilage formation: recent advances, but many lingering mysteries. *Birth Defects Res C Embryo Today* 75, 237-248.
- Pacifici, M., Koyama, E., Shibukawa, Y., Wu, C., Tamamura, Y., Enomoto-Iwamoto, M., Iwamoto, M., 2006. Cellular and molecular mechanisms of synovial joint and articular cartilage formation. *Ann N Y Acad Sci* 1068, 74-86.
- Pallante, A.L., Bae, W.C., Chen, A.C., Gortz, S., Bugbee, W.D., Sah, R.L., 2009. Chondrocyte viability is higher after prolonged storage at 37 degrees C than at 4 degrees C for osteochondral grafts. *Am J Sports Med* 37 Suppl 1, 24S-32S.
- Pattappa, G., Heywood, H.K., de Bruijn, J.D., Lee, D.A., 2011. The metabolism of human mesenchymal stem cells during proliferation and differentiation. *J Cell Physiol* 226, 2562-2570.
- Pelttari, K., Winter, A., Steck, E., Goetzke, K., Hennig, T., Ochs, B.G., Aigner, T., Richter, W., 2006. Premature induction of hypertrophy during in vitro chondrogenesis of human mesenchymal stem cells correlates with calcification and vascular invasion after ectopic transplantation in SCID mice. *Arthritis Rheum* 54, 3254-3266.
- Pevsner-Fischer, M., Levin, S., Zipori, D., 2011. The origins of mesenchymal stromal cell heterogeneity. *Stem Cell Rev* 7, 560-568.
- Phinney, D.G., 2002. Building a consensus regarding the nature and origin of mesenchymal stem cells. *J Cell Biochem Suppl* 38, 7-12.
- Pittenger, M.F., Mackay, A.M., Beck, S.C., Jaiswal, R.K., Douglas, R., Mosca, J.D., Moorman, M.A., Simonetti, D.W., Craig, S., Marshak, D.R., 1999. Multilineage potential of adult human mesenchymal stem cells. *Science* 284, 143-147.

- Potier, E., Ferreira, E., Meunier, A., Sedel, L., Logeart-Avramoglou, D., Petite, H., 2007. Prolonged hypoxia concomitant with serum deprivation induces massive human mesenchymal stem cell death. *Tissue Eng* 13, 1325-1331.
- Raj, A., van den Bogaard, P., Rifkin, S.A., van Oudenaarden, A., Tyagi, S., 2008. Imaging individual mRNA molecules using multiple singly labeled probes. *Nat Methods* 5, 877-879.
- Ranera, B., Remacha, A.R., Alvarez-Arguedas, S., Castiella, T., Vazquez, F.J., Romero, A., Zaragoza, P., Martin-Burriel, I., Rodellar, C., 2013. Expansion under hypoxic conditions enhances the chondrogenic potential of equine bone marrow-derived mesenchymal stem cells. *Vet J* 195, 248-251.
- Redler, I., Mow, V.C., Zimny, M.L., Mansell, J., 1975. The ultrastructure and biomechanical significance of the tidemark of articular cartilage. *Clin Orthop Relat Res*, 357-362.
- Reimann, I., 1976. Pathological human synovial fluids. Viscosity and boundary lubricating properties. *Clin Orthop Relat Res*, 237-241.
- Ropes, M.W., Bennett, G.A., Bauer, W., 1939. The Origin and Nature of Normal Synovial Fluid. *J Clin Invest* 18, 351-372.
- Russell, K.C., Phinney, D.G., Lacey, M.R., Barrilleaux, B.L., Meyertholen, K.E., O'Connor, K.C., 2010. In vitro high-capacity assay to quantify the clonal heterogeneity in trilineage potential of mesenchymal stem cells reveals a complex hierarchy of lineage commitment. *Stem Cells* 28, 788-798.
- Schek, R.M., Taboas, J.M., Segvich, S.J., Hollister, S.J., Krebsbach, P.H., 2004. Engineered osteochondral grafts using biphasic composite solid free-form fabricated scaffolds. *Tissue Eng* 10, 1376-1385.
- Schiltz, J.R., Mayne, R., Holtzer, H., 1973. The Synthesis of Collagen and Glycosaminoglycans by Dedifferentiated Chondroblasts in Culture. *Differentiation* 1, 97-108.
- Schinagl, R.M., Gurskis, D., Chen, A.C., Sah, R.L., 1997. Depth-dependent confined compression modulus of full-thickness bovine articular cartilage. *J Orthop Res* 15, 499-506.
- Schipani, E., Ryan, H.E., Didrickson, S., Kobayashi, T., Knight, M., Johnson, R.S., 2001. Hypoxia in cartilage: HIF-1alpha is essential for chondrocyte growth arrest and survival. *Genes Dev* 15, 2865-2876.
- Schulz, R.M., Zscharnack, M., Hanisch, I., Geiling, M., Hepp, P., Bader, A., 2008. Cartilage tissue engineering by collagen matrix associated bone marrow derived mesenchymal stem cells. *Biomed Mater Eng* 18, S55-70.

Schumacher, B.L., Block, J.A., Schmid, T.M., Aydelotte, M.B., Kuettner, K.E., 1994. A novel proteoglycan synthesized and secreted by chondrocytes of the superficial zone of articular cartilage. *Arch Biochem Biophys* 311, 144-152.

Sechriest, V.F., Miao, Y.J., Niyibizi, C., Westerhausen-Larson, A., Matthew, H.W., Evans, C.H., Fu, F.H., Suh, J.K., 2000. GAG-augmented polysaccharide hydrogel: a novel biocompatible and biodegradable material to support chondrogenesis. *J Biomed Mater Res* 49, 534-541.

Sengers, B.G., Van Donkelaar, C.C., Oomens, C.W., Baaijens, F.P., 2004. The local matrix distribution and the functional development of tissue engineered cartilage, a finite element study. *Ann Biomed Eng* 32, 1718-1727.

Shahin, K., Doran, P.M., 2011. Improved seeding of chondrocytes into polyglycolic acid scaffolds using semi-static and alginate loading methods. *Biotechnol Prog* 27, 191-200.

Shimono, K., Tung, W.E., Macolino, C., Chi, A.H., Didizian, J.H., Mundy, C., Chandraratna, R.A., Mishina, Y., Enomoto-Iwamoto, M., Pacifici, M., Iwamoto, M., 2011. Potent inhibition of heterotopic ossification by nuclear retinoic acid receptor-gamma agonists. *Nat Med* 17, 454-460.

Silver, I.A., 1975. Measurement of pH and ionic composition of pericellular sites. *Philos Trans R Soc Lond B Biol Sci* 271, 261-272.

Sivasubramanian, K., Lehnen, D., Ghazanfari, R., Sobiesiak, M., Harichandan, A., Mortha, E., Petkova, N., Grimm, S., Cerabona, F., de Zwart, P., Abele, H., Aicher, W.K., Faul, C., Kanz, L., Buhning, H.J., 2012. Phenotypic and functional heterogeneity of human bone marrow- and amnion-derived MSC subsets. *Ann N Y Acad Sci* 1266, 94-106.

Skaalure, S.C., Milligan, I.L., Bryant, S.J., 2012. Age impacts extracellular matrix metabolism in chondrocytes encapsulated in degradable hydrogels. *Biomed Mater* 7, 024111.

Solorio, L.D., Vieregge, E.L., Dhami, C.D., Dang, P.N., Alsberg, E., 2012. Engineered cartilage via self-assembled hMSC sheets with incorporated biodegradable gelatin microspheres releasing transforming growth factor-beta1. *J Control Release* 158, 224-232.

Song, L., Tuan, R.S., 2004. Transdifferentiation potential of human mesenchymal stem cells derived from bone marrow. *FASEB J* 18, 980-982.

Spiller, K.L., Holloway, J.L., Gribb, M.E., Lowman, A.M., 2011. Design of semi-degradable hydrogels based on poly(vinyl alcohol) and poly(lactic-co-glycolic acid) for cartilage tissue engineering. *J Tissue Eng Regen Med* 5, 636-647.

- Spiller, K.L., Laurencin, S.J., Lowman, A.M., 2009. Characterization of the behavior of porous hydrogels in model osmotically-conditioned articular cartilage systems. *J Biomed Mater Res B Appl Biomater* 90, 752-759.
- Starkman, B.G., Cravero, J.D., Delcarlo, M., Loeser, R.F., 2005. IGF-I stimulation of proteoglycan synthesis by chondrocytes requires activation of the PI 3-kinase pathway but not ERK MAPK. *Biochem J* 389, 723-729.
- Stegemann, H., Stalder, K., 1967. Determination of hydroxyproline. *Clin Chim Acta* 18, 267-273.
- Strangeways, T.S., 1920. Observations ON THE NUTRITION OF ARTICULAR CARTILAGE. *Br Med J* 1, 661-663.
- Studer, D., Millan, C., Ozturk, E., Maniura-Weber, K., Zenobi-Wong, M., 2012. Molecular and biophysical mechanisms regulating hypertrophic differentiation in chondrocytes and mesenchymal stem cells. *Eur Cell Mater* 24, 118-135; discussion 135.
- Swann, D.A., Silver, F.H., Slayter, H.S., Stafford, W., Shore, E., 1985. The molecular structure and lubricating activity of lubricin isolated from bovine and human synovial fluids. *Biochem J* 225, 195-201.
- Tampieri, A., Sandri, M., Landi, E., Pressato, D., Francioli, S., Quarto, R., Martin, I., 2008. Design of graded biomimetic osteochondral composite scaffolds. *Biomaterials* 29, 3539-3546.
- Tanaka, T., Komaki, H., Chazono, M., Fujii, K., 2005. Use of a biphasic graft constructed with chondrocytes overlying a beta-tricalcium phosphate block in the treatment of rabbit osteochondral defects. *Tissue Eng* 11, 331-339.
- Terada, S., Yoshimoto, H., Fuchs, J.R., Sato, M., Pomerantseva, I., Selig, M.K., Hannouche, D., Vacanti, J.P., 2005. Hydrogel optimization for cultured elastic chondrocytes seeded onto a polyglycolic acid scaffold. *J Biomed Mater Res A* 75, 907-916.
- Thomopoulos, S., Williams, G.R., Gimbel, J.A., Favata, M., Soslowsky, L.J., 2003. Variation of biomechanical, structural, and compositional properties along the tendon to bone insertion site. *J Orthop Res* 21, 413-419.
- Thompson, G.R., Manshady, B.M., Weiss, J.J., 1978. Septic bursitis. *JAMA* 240, 2280-2281.
- Thorpe, S.D., Buckley, C.T., Vinardell, T., O'Brien, F.J., Campbell, V.A., Kelly, D.J., 2008. Dynamic compression can inhibit chondrogenesis of mesenchymal stem cells. *Biochem Biophys Res Commun* 377, 458-462.
- Tickle, C., Munsterberg, A., 2001. Vertebrate limb development--the early stages in chick and mouse. *Curr Opin Genet Dev* 11, 476-481.

- Toh, W.S., Lee, E.H., Cao, T., 2011. Potential of human embryonic stem cells in cartilage tissue engineering and regenerative medicine. *Stem Cell Rev* 7, 544-559.
- Toh, W.S., Lim, T.C., Kurisawa, M., Spector, M., 2012. Modulation of mesenchymal stem cell chondrogenesis in a tunable hyaluronic acid hydrogel microenvironment. *Biomaterials* 33, 3835-3845.
- Toynbee, J., 1837. Researches tending to prove the non-vascularity of certain animal tissues, and to demonstrate the peculiar uniform mode of their organization and nutrition. *philosophical Transactions of the Royal Society of London* 4, 307.
- Tran-Khanh, N., Hoemann, C.D., McKee, M.D., Henderson, J.E., Buschmann, M.D., 2005. Aged bovine chondrocytes display a diminished capacity to produce a collagen-rich, mechanically functional cartilage extracellular matrix. *J Orthop Res* 23, 1354-1362.
- Treppo, S., Koepp, H., Quan, E.C., Cole, A.A., Kuettner, K.E., Grodzinsky, A.J., 2000. Comparison of biomechanical and biochemical properties of cartilage from human knee and ankle pairs. *J Orthop Res* 18, 739-748.
- Tuan, R.S., 2003. Cellular signaling in developmental chondrogenesis: N-cadherin, Wnts, and BMP-2. *J Bone Joint Surg Am* 85-A Suppl 2, 137-141.
- Tumram, N.K., Bardale, R.V., Dongre, A.P., 2011. Postmortem analysis of synovial fluid and vitreous humour for determination of death interval: A comparative study. *Forensic Sci Int* 204, 186-190.
- Van Assche, D., Staes, F., Van Caspel, D., Vanlauwe, J., Bellemans, J., Saris, D.B., Luyten, F.P., 2010. Autologous chondrocyte implantation versus microfracture for knee cartilage injury: a prospective randomized trial, with 2-year follow-up. *Knee Surg Sports Traumatol Arthrosc* 18, 486-495.
- Vigfusdottir, A.T., Pasrija, C., Thakore, P.I., Schmidt, R.B., Hsieh, A.H., 2010. Role of pericellular matrix in mesenchymal stem cell deformation during chondrogenic differentiation. *Cellular and Molecular Bioengineering* 3, 387-397.
- Villavicencio-Lorini, P., Kuss, P., Friedrich, J., Haupt, J., Farooq, M., Turkmen, S., Duboule, D., Hecht, J., Mundlos, S., 2010. Homeobox genes d11-d13 and a13 control mouse autopod cortical bone and joint formation. *J Clin Invest* 120, 1994-2004.
- Vinardell, T., Sheehy, E.J., Buckley, C.T., Kelly, D.J., 2012. A comparison of the functionality and in vivo phenotypic stability of cartilaginous tissues engineered from different stem cell sources. *Tissue Eng Part A* 18, 1161-1170.
- Wang, C.C., Hung, C.T., Mow, V.C., 2001. An analysis of the effects of depth-dependent aggregate modulus on articular cartilage stress-relaxation behavior in compression. *J Biomech* 34, 75-84.

- Wang, Y., Wei, L., Zeng, L., He, D., Wei, X., 2013. Nutrition and degeneration of articular cartilage. *Knee Surg Sports Traumatol Arthrosc* 21, 1751-1762.
- Watanabe, H., de Caestecker, M.P., Yamada, Y., 2001. Transcriptional cross-talk between Smad, ERK1/2, and p38 mitogen-activated protein kinase pathways regulates transforming growth factor-beta-induced aggrecan gene expression in chondrogenic ATDC5 cells. *J Biol Chem* 276, 14466-14473.
- Weiss, S., Hennig, T., Bock, R., Steck, E., Richter, W., 2010. Impact of growth factors and PTHrP on early and late chondrogenic differentiation of human mesenchymal stem cells. *J Cell Physiol* 223, 84-93.
- Weston, A.D., Chandraratna, R.A., Torchia, J., Underhill, T.M., 2002. Requirement for RAR-mediated gene repression in skeletal progenitor differentiation. *J Cell Biol* 158, 39-51.
- Weston, A.D., Rosen, V., Chandraratna, R.A., Underhill, T.M., 2000. Regulation of skeletal progenitor differentiation by the BMP and retinoid signaling pathways. *J Cell Biol* 148, 679-690.
- Williamson, A.K., Chen, A.C., Sah, R.L., 2001. Compressive properties and function-composition relationships of developing bovine articular cartilage. *J Orthop Res* 19, 1113-1121.
- Wong, J.M., Khan, W.S., Chimutengwende-Gordon, M., Dowd, G.S., 2011. Recent advances in designs, approaches and materials in total knee replacement: literature review and evidence today. *J Perioper Pract* 21, 165-171.
- Ylostalo, J., Bazhanov, N., Prockop, D.J., 2008. Reversible commitment to differentiation by human multipotent stromal cells in single-cell-derived colonies. *Exp Hematol* 36, 1390-1402.
- Yodmuang, S., Gadjanski, I., Chao, P.H., Vunjak-Novakovic, G., 2013. Transient hypoxia improves matrix properties in tissue engineered cartilage. *J Orthop Res* 31, 544-553.
- Yokota, M., Yasuda, K., Kitamura, N., Arakaki, K., Onodera, S., Kurokawa, T., Gong, J.P., 2011. Spontaneous hyaline cartilage regeneration can be induced in an osteochondral defect created in the femoral condyle using a novel double-network hydrogel. *BMC Musculoskelet Disord* 12, 49.
- Youn, I., Choi, J.B., Cao, L., Setton, L.A., Guilak, F., 2006. Zonal variations in the three-dimensional morphology of the chondron measured in situ using confocal microscopy. *Osteoarthritis Cartilage* 14, 889-897.
- Yuan, T., Zhang, L., Feng, L., Fan, H., Zhang, X., 2010. Chondrogenic differentiation and immunological properties of mesenchymal stem cells in collagen type I hydrogel. *Biotechnol Prog* 26, 1749-1758.

Zhou, S., Cui, Z., Urban, J.P., 2004. Factors influencing the oxygen concentration gradient from the synovial surface of articular cartilage to the cartilage-bone interface: a modeling study. *Arthritis Rheum* 50, 3915-3924.

Zhou, S., Cui, Z., Urban, J.P., 2008. Nutrient gradients in engineered cartilage: metabolic kinetics measurement and mass transfer modeling. *Biotechnol Bioeng* 101, 408-421.